

Ocean Acidification in the Baltic Sea

Involved Processes, Metrology of pH in Brackish Waters, and
Calcification under Fluctuating Conditions

Kumulative Dissertation

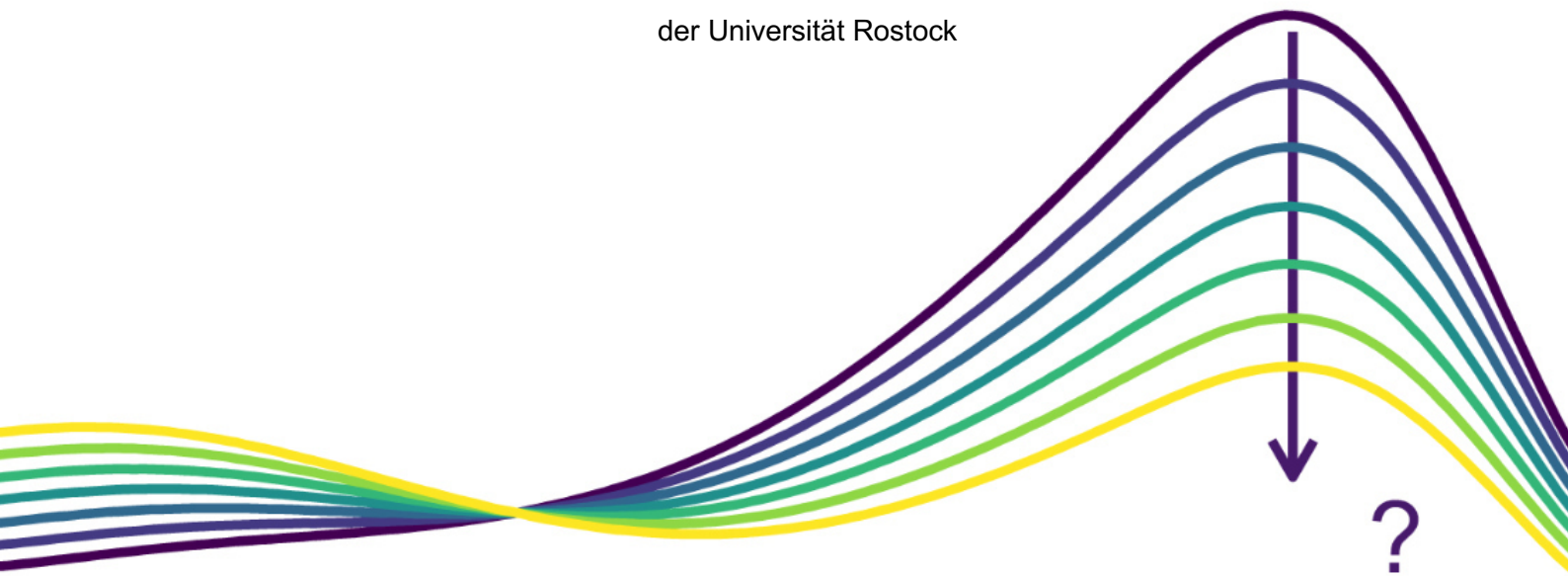
zur

Erlangung des akademischen Grades

doctor rerum naturalium (Dr. rer. nat.)

der Mathematisch-Naturwissenschaftlichen Fakultät

der Universität Rostock



vorgelegt von

Jens Daniel Müller

Geboren am 5. Februar 1986 in Berlin

-

Rostock, 2018

Die vorliegende Arbeit entstand in dem Zeitraum von Juni 2014 bis Januar 2018 am Leibniz Institut für Ostseeforschung Warnemünde und der Universität Rostock.

This thesis was produced in the period from June 2014 to January 2018 at the Leibniz Institute for Baltic Sea Research Warnemünde and the University of Rostock.

Gutachter / Referees

Prof. Dr. Gregor Rehder | Leibniz Institut für Ostseeforschung Warnemünde

Prof. Dr. Arne Körtzinger | GEOMAR - Helmholtz-Zentrum für Ozeanforschung Kiel

Prof. Dr. Dieter Wolf-Gladrow | Alfred-Wegener-Institut Helmholtz-Zentrum für Polar- und Meeresforschung

Einreichungsdatum / date of submission: 26th of January 2018

Verteidigungsdatum / date of defense: 8th of May 2018

Table of contents

Table of contents.....	V
Abstract.....	VII
Zusammenfassung.....	IX
Publications.....	XI
Articles in peer-reviewed scientific journals.....	XI
Published articles.....	XI
Submitted articles.....	XII
Monographs.....	XIII
Conference and workshop presentations.....	XIII
Acknowledgement.....	XV
List of abbreviations, symbols and variables.....	XVII
Introduction.....	1
Significance of pH.....	1
Comparison of pH in the open ocean and the Baltic Sea.....	1
Objectives of this thesis.....	3
The marine CO ₂ system.....	4
Equilibrium reactions.....	4
Measureable parameters and their characteristics.....	6
Internal consistency and the ocean acidification paradigm.....	8
Marine organisms in a changing CO ₂ world.....	9
The Baltic Sea.....	10
Hydrography.....	10
Biogeochemical peculiarities.....	12
Focus 1: Long-term changes and variability of the Baltic Sea CO ₂ system.....	15
Background.....	15
Scope.....	15
Approach and results.....	15
Long-term alkalinity trends.....	15
Combined impact of changes in seawater alkalinity and atmospheric CO ₂	18
Drivers for alkalinity trends.....	19

Variability caused by primary production and remineralization	20
Conclusion	21
Focus 2: pH measurements in brackish waters	23
Background	23
Scope	24
Theory	24
Harned cells as a primary method for pH determination	24
Spectrophotometric pH measurements	26
Potential disturbance of spectrophotometric pH measurements	28
Approach and results	28
pH _T of TRIS buffered ASW solutions	28
Characterization of the pH indicator dye m-Cresol Purple	30
Spectrophotometric pH measurements in the presence of hydrogen sulfide and dissolved organic matter	33
Conclusion	35
Focus 3: Impact of acidification and fluctuating pH conditions on calcification	37
Background	37
Scope	37
Approach and results	38
pH variability in benthic coastal ecosystems	38
Relevance of pH fluctuations for calcifying organisms	39
Conclusion	40
Summary and outlook	41
References	43
Appendix	48
Curriculum vitae	49
Eigenständigkeitserklärung	51
Publications	52

Abstract

The pH value is an invaluable quantity to determine the state and change of numerous acid-base equilibria, biogeochemical transformations and physiological conditions in natural waters. The CO₂ system dominates the acid-base reactions in seawater and has gained increasing attention in times of climate change, because the world's oceans take up a large share of anthropogenic CO₂ emissions. The oceanic CO₂ uptake is controlled by the alkalinity, which is a measure for the buffer capacity of seawater. If the alkalinity remains unchanged, the dissolution of CO₂ in seawater results in a predictable decrease of pH and the calcium carbonate saturation state. This process was termed ocean acidification and threatens the stability of marine ecosystems. In the Baltic Sea, however, it is currently impossible to directly assess the acidification process, because reliable pH measurement techniques and observations are lacking and pronounced pH fluctuations superimpose long-term trends. This thesis aims to improve our understanding of ocean acidification in the Baltic Sea by evaluating past acidification scenarios, improving pH measurement procedures for brackish waters, and investigating the impact of pH fluctuations on calcifiers.

In the first focus of this thesis, a regional alkalinity trend analysis was performed. In contrast to the open ocean, increasing alkalinity levels were detected throughout the Baltic Sea over the past two decades. It was found that the rise in alkalinity significantly counteracted the CO₂-induced acidification. It increased the CO₂ uptake capacity and promoted stable calcium carbonate saturation states. Further, the pronounced variability of the Baltic Sea CO₂ system was investigated in the first focus, and processes that superimpose the partly counter-balancing long-term trends in atmospheric CO₂ and seawater alkalinity were identified. In view of this complexity of the CO₂ system, the results of the first focus suggest that a meaningful acidification monitoring requires accurate and precise pH measurements with a high spatio-temporal coverage.

Spectrophotometric measurements with pH indicator dyes are currently the most reliable method to determine seawater pH. The second focus provides the scientific basis for the application of the method in brackish waters like the Baltic Sea. This was achieved by a coordinated series of characterization experiments that covered (i) the pH determination of low-saline TRIS buffer solutions by Harned cell measurements in cooperation with the Physikalische-Technische Bundesanstalt and (ii) the characterization of a suitable pH indicator dye, m-Cresol Purple, in those buffer solutions. For the first time, the results allow traceability of pH measurements to a primary pH standard in brackish waters, as well as

the unambiguous determination of the hydrogen ion concentration on the total scale. Furthermore, the robustness of the spectrophotometric method to dissolved organic matter and hydrogen sulfide was verified for the entire concentration range of both substances in the Baltic Sea. To fill the spatio-temporal gap in environmental pH measurements, an automated spectrophotometric pH measurement system was developed in cooperation with an industry partner.

The third focus of this thesis addresses the potential impact of acidification on calcifying organisms in the Baltic Sea. The studies, performed under the lead of benthic ecologists at Geomar in Kiel, focused on the quantification of immense diurnal CO₂ system fluctuations created by the photosynthetic activity of macroalgae in coastal benthic habitats. It was found that pH fluctuations offer time windows of favorable conditions during daytime, in which calcifiers in close proximity are able to maintain high calcification rates, even under acidified conditions. Macrophyte meadows could therefore represent important acidification refugia worth protecting in times of ocean acidification.

In summary, this thesis highlights the complexity of ocean acidification in land-influenced seas, exemplified by processes occurring in the Baltic Sea. It lays the foundation for a reliable pH monitoring in brackish waters worldwide, which is crucial for a meaningful assessment of changes in acidity.

Zusammenfassung

Der pH-Wert natürlicher Gewässer ist von besonderer Bedeutung, um den Zustand und die Veränderung von Säure-Base Gleichgewichten, biogeochemische Umsetzungsprozesse und physiologische Bedingungen für Organismen zu beschreiben. Im Meerwasser dominiert das CO₂-System die stattfindenden Säure-Base-Reaktionen. Die Untersuchung dieses marinen CO₂-Systems hat in Zeiten des Klimawandels an Bedeutung gewonnen, da die Ozeane einen Großteil der anthropogenen CO₂-Emissionen aufnehmen. Die CO₂-Aufnahmekapazität der Meere wird von der Alkalinität bestimmt, die ein Maß für die Pufferkapazität des Meerwassers darstellt. Bei unveränderter Alkalinität führt die CO₂-Aufnahme zu einer vorhersagbaren Verringerung sowohl des pH-Wertes als auch des Sättigungsgrades von Kalziumkarbonat. Dieser Prozess wird als Ozeanversauerung bezeichnet und gefährdet weltweit die Stabilität mariner Ökosysteme. Für die Ostsee ist es derzeit nicht möglich die Versauerung zu quantifizieren, da es an adäquater pH-Messtechnik und ausreichenden pH-Messungen in der Vergangenheit mangelt. Außerdem erschweren ausgeprägte pH-Fluktuationen die Bestimmung langfristiger Trends. Diese Arbeit soll das Verständnis möglicher Versauerungsprozesse in der Ostsee verbessern. Dafür wurden zurückliegende Versauerungsszenarien bewertet, die Grundlagen für hochgenaue pH-Messungen im Brackwasser gelegt und der Einfluss von pH-Fluktuationen auf Kalzifizierer untersucht.

Im ersten Schwerpunkt dieser Arbeit wurde eine regionale Trendanalyse der Alkalinität durchgeführt. Anders als im offenen Ozean wurde in großen Teil der Ostsee über die letzten 20 Jahre ein deutlicher Alkalinitätsanstieg festgestellt. Dieser Alkalinitätsanstieg wirkte der Versauerung durch die Aufnahme von CO₂ deutlich entgegen. Er erhöhte außerdem die Aufnahmekapazität für CO₂ und stabilisierte den Sättigungsgrad von Kalziumkarbonat. Neben den sich teilweise ausgleichenden, langfristigen Trends des atmosphärischen CO₂-Gehaltes und der Alkalinität, wurden im ersten Schwerpunkt Prozesse identifiziert, welche die ausgeprägte Variabilität des pH-Wertes in der Ostsee verursachen. In Hinblick auf die Komplexität dieser Prozesse belegen die Ergebnisse des ersten Schwerpunktes, dass es für eine verlässliche Beschreibung des Versauerungsgeschehens unumgänglich ist genaue und präzise pH-Messungen mit großer zeitlicher und räumlicher Auflösung zu etablieren.

Spektrophotometrische Messungen mit pH-Indikatorfarbstoffen stellen derzeit die verlässlichste Methode zur pH-Bestimmung in Meerwasser dar. Im zweiten Schwerpunkt dieser Arbeit wurde daher die wissenschaftliche Grundlage für die Anwendung dieser

Methode in Brackwassergebieten wie der Ostsee geschaffen. Dafür wurden eine Reihe koordinierte Experimente durchgeführt. Diese umfassten sowohl (i) die pH-Bestimmung von niedrig-salinen TRIS-Pufferlösungen in Kooperation mit der Physikalisch-Technischen Bundesanstalt in Braunschweig, als auch (ii) die Charakterisierung des pH-Indikatorfarbstoffes meta-Kresolpurpur anhand dieser Pufferlösungen. Die umfangreichen Arbeiten erlauben erstmals die Rückführbarkeit von pH-Messungen im Brackwasser auf einen primären pH Standard, sowie eine eindeutige Bestimmung der Protonenkonzentration auf der sogenannten totalen Skala. Weiterhin wurde sichergestellt, dass spektrophotometrische pH-Messungen durch das Auftreten von Schwefelwasserstoff und gelöstem organischem Material selbst bei hohen, ostseetypischen Konzentration nicht beeinträchtigt werden. Um die räumlich-zeitliche Abdeckung mit pH-Messungen im Ostseeraum zu erhöhen, wurde in Kooperation mit einem Industriepartner ein automatisiertes spektrophotometrisches pH-Messsystem entwickelt.

Abschließend behandelt diese Arbeit im dritten Schwerpunkt die potentiellen Auswirkungen von Ozeanversauerung auf kalkbildende Organismen in der Ostsee. Die unter der Leitung von Benthosökologen am Geomar in Kiel durchgeführten Studien quantifizieren ausgeprägte tageszeitlicher Fluktuationen im CO₂-System, die durch die Photosyntheseaktivität benthischer Makroalgen verursacht werden. Es wurde festgestellt, dass assoziiert lebende Kalkbildner in der Lage sind die tagsüber vorherrschenden, guten Kalzifizierungsbedingungen zu nutzen, um selbst unter versauerten Bedingungen hohe Kalzifizierungsraten aufrecht zu erhalten. Makroalgenhabitate könnten demnach besonders schützenswerte Lebensräume für Kalkbildner in Zeiten globaler Ozeanversauerung darstellen.

Zusammenfassend beleuchtet diese Arbeit am Beispiel der Ostsee die Komplexität des Ozeanversauerungsgeschehens in Meeresgebieten, die von landbasierten Prozessen beeinflusst sind und legt die wissenschaftlichen Grundlagen für ein zuverlässiges Versauerungsmonitoring in Brackwassergebieten weltweit, ohne das eine aussagekräftige Bewertung von Änderungen in deren Säure-Base-Haushalt nicht möglich ist.

Publications

*Included in the appendix of this thesis

Articles in peer-reviewed scientific journals

Published articles

***Müller, J. D.**, Schneider, B., and Rehder, G. (2016)

Long-term alkalinity trends in the Baltic Sea and their implications for CO₂-induced acidification

Limnol. Oceanogr., 61: 1984–2002 | doi:10.1002/lno.10349.

Contribution: Data compilation, data analysis and interpretation, majority of manuscript writing

***Müller, J. D.**, Schneider, B., Aßmann, S., and Rehder, G. (2017)

Spectrophotometric pH measurements in the presence of dissolved organic matter and hydrogen sulfide

Limnol. Oceanogr. Methods. | doi:10.1002/lom3.10227.

Contribution: Approach and concept of the study, practical work, data analysis and interpretation, manuscript writing

*Wahl, M., Schneider Covachã, S., Saderne, V., Hiebenthal, C., **Müller, J. D.**, Pansch, C., et al. (2018)

Macroalgae may mitigate ocean acidification effects on mussel calcification by increasing pH and its fluctuations

Limnol. Oceanogr., 63: 3-21 | doi:10.1002/lno.10608.

Contribution: Involved in study design and field work, written contributions to the manuscript focusing on pH-related issues, discussion of results, approval of manuscript

Fritzsche, E., Gruber, P., Schutting, S., Fischer, J. P., Strobl, M., **Müller, J. D.**, et al. (2017)

Highly sensitive poisoning-resistant optical carbon dioxide sensors for environmental monitoring

Anal. Methods, 9: 55–65 | doi:10.1039/C6AY02949C.

Contribution: Comparison measurements for CO₂ system determination during research cruise, writing respective parts of manuscript, discussion of CO₂ and Baltic Sea specific contents, approval of manuscript

Wahl, M., Buchholz, B., Winde, V., Golomb, D., Guy-Haim, T., **Müller, J.**, et al. (2015)

A mesocosm concept for the simulation of near-natural shallow underwater climates: The Kiel Outdoor Benthocosms (KOB)

Limnol. Oceanogr. Methods, 13: 651–663. | doi:10.1002/lom3.10055.

Contribution: pCO₂ measurements in benthocosms, preparation of a first draft of the manuscript, approval of manuscript

Submitted articles

***Müller, J. D.**, Bastkowski, F., Sander, B., Seitz, S., Turner, D.R., Dickson, A.G., and Rehder, G. (subm.)

pH Measurements in Brackish Waters: Extending the Electrochemical pH_T Determination of TRIS buffers to Salinities 5 – 20

Contribution: Initiation and concept of the study, solution composition concept and computation, data analysis, communication with co-authors, ~50% of manuscript writing, shared first-authorship with FB

***Müller, J. D.** and Rehder, G. (subm.)

pH Measurements in Brackish Waters: Experimental Characterization of Purified m-Cresol Purple for Spectrophotometric pH_T Measurements

Contribution: Approach and concept of the study, laboratory work, data analysis and interpretation, manuscript writing

Saderne, V., Fietzek, P., **Müller, J. D.**, Körtzinger, A., and Hiebenthal, C. (2017)

Intense pCO₂ and [O₂] Oscillations in a Mussel-Seagrass Habitat: Implications for Calcification

Biogeosciences Discuss. | doi:10.5194/bg-2017-351.

Contribution: Involved in field work, development of a model to estimate organic alkalinity contributions and writing of the respective chapter, discussion of CO₂ and Baltic Sea specific contents, approval of manuscript

Monographs

Schneider, B., and **Müller, J. D.** (2017)

Biogeochemical Transformations in the Baltic Sea: Observations Through Carbon Dioxide Glasses

Springer International Publishing | doi:10.1007/978-3-319-61699-5.

Contribution: Data handling and analysis, figure preparation, proof reading, writing chapter on surface water pCO₂ trends

Conference and workshop presentations

Müller J.D., Bastkowski F., Schneider B., Rehder G.

Updating pH measurements in brackish waters: Characterization of the indicator dye m-Cresol purple based on newly available TRIS buffers

Poster | Baltic Sea Science Congress | Rostock | 17.06.2017

Müller J.D., Schneider B.

High-resolution pCO₂ measurements on a cargo ship in the Baltic Sea: Patterns and trends derived from a synoptic look at 13 years of observations,

Poster | Baltic Sea Science Congress | Rostock | 17.06.2017.

Müller J.D., Schneider B., Rehder G.

Long-term alkalinity trends in the Baltic Sea and their implications for CO₂-induced acidification

Talk and Poster | 1st Baltic Earth Conference | Nida | 17.06.2016

Müller J.D., Aßmann S., Turner D., Schneider B., Rehder G.

PINBAL: Development of a spectrophotometric pH-measurement system for monitoring in the Baltic Sea

Talk | Quasimeme Ocean Acidification Workshop | Southampton | 04.02.2016

Müller J., Schneider B., Rehder G.

Long-term alkalinity trends in the Baltic Sea and their implications for CO₂-induced acidification

Talk | IOW symposium "Little salts and many protons: Acid-Base System Studies in the Baltic Sea" | 04.12.2015

Müller J., Schneider B., Aßmann S., Hammer K., Rehder G.

Spectrophotometric pH measurements in the Baltic Sea: necessity, challenges and solutions

Talk | Wasser 2015 - Jahrestagung der Wasserchemischen Gesellschaft (GdCH) | Schwerin | 11.05.2015

Müller J., Schneider B., Aßmann S., Hammer K., Rehder G.

Spectrophotometric pH measurements in the Baltic Sea: necessity, challenges and solutions

Talk | ASLO 2015 - Aquatic Sciences Meeting | Grenada | 23.02.2015

Acknowledgement

The outcome of this thesis could not have been achieved without the extensive supervision of Gregor Rehder and Bernd Schneider. I appreciated very much your openness to new perspectives, the collegial atmosphere you created and your patience during hours of discussions.

I acknowledge the support of all participants of the EU BONUS project PINBAL, in particular David Turner (University of Gothenburg), who did not hesitate to discuss hundreds of questions concerning the fundamentals of acid-base chemistry in seawater.

The successful characterization of pH buffer solutions is the merit of colleagues at the Physikalisch-Technische Bundesanstalt (PTB), Beatrice Sander, Frank Bastkowski, and Steffen Seitz. I am grateful for the visit of Andrew Dickson (Scripps Institution of Oceanography) in December 2015, which helped to initiate this project with PTB.

The extensive monitoring activities of the Swedish Meteorological and Hydrological Institute provided an important data base interpreted in this thesis. I was happy to continue working with the benthic ecologists of the working group of Martin Wahl at Geomar in Kiel. Arne Körtzinger (Geomar) provided excellent reviews that improved presentation of results in publications that are part of this cumulative thesis and organized an outstanding summer school on ocean observation technologies that I enjoyed in Tjärnö 2014.

I thank my parents, Karin and Andreas Müller, who supported my scientific education from the beginning. The contact improvisation group of Rostock and Tanzland e.V. were an extraordinary source of inspiration and relaxation. Friederike Saathoff did an incredible job keeping me motivated and balanced during the demanding final work on this dissertation.

Thanks to all of you!

The research leading to this thesis has received funding from BONUS, the joint Baltic Sea research and development programme (Art 185), funded jointly from the European Union's Seventh Programme for research, technological development and demonstration and from the German Federal Ministry of Education and Research through Grant No. 03F0689A (BONUS PINBAL).

List of abbreviations, symbols and variables

$[\]$	Concentration in moles per kg-solution
A	Absorption
Ag AgCl	Silver silver-chloride
ASW	Artificial seawater
A_T	Total alkalinity
b	Molality in moles per kg water
Ca²⁺	Calcium ion
CO₂	Carbon dioxide
CO_{2, aq}	CO ₂ physically dissolved in seawater
CO₂[*]	Sum of CO _{2, aq} and carbonic acid H ₂ CO ₃
CO₃²⁻	Carbonate ion
C_T	Total amount of dissolved inorganic carbon
d	Cuvette length
DOM	Dissolved organic matter
ϵ	Molar extinction coefficient
E	Electric potential
E[°]	Standard potential of the Ag AgCl electrode in pure ASW
e₁₋₃	Molar absorptivity ratios of mCP
F	Faraday constant
fCO₂	Fugacity of CO ₂
FIA	Flow injection analysis
H⁺	Hydrogen ion
H₂	Hydrogen gas
HCO₃⁻	Hydrogen carbonate ion
H₂CO₃	Carbonic acid
H₂S	Hydrogen sulfide
HELCOM	Baltic Marine Environment Protection Commission
HI⁻	mCP monoprotinated species
I²⁻	mCP deprotonated species
IOW	Leibniz Institute for Baltic Sea Research Warnemünde
K₁	First dissociation constant of the marine CO ₂ system
K₂	Second dissociation constant of the marine CO ₂ system
K_{CaCO₃}	Solubility product of calcium carbonate

$K_{\text{HSO}_4^-}$	Dissociation constant of hydrogen sulfate
mCP	pH indicator dye m-Cresol Purple
Ω	Saturation state of calcium carbonate minerals
pCO₂	Partial pressure of CO ₂
pH_T	pH on the total scale
pK₂	Negative decadic logarithm of the second dissociation constant of mCP
Pt	Platinum
R	Gas constant
R_A	Absorption ratio of mCP
S	Salinity
SMHI	Swedish Meteorological and Hydrological Institute
[SO₄²⁻]_T	Total concentration of sulfate
T	Temperature
TRIS	2-amino-2-hydroxymethyl-1,3-propanediol
$\omega_{\text{H}_2\text{O}}$	Water content defined as mass water per mass solution

Introduction

Significance of pH

The pH value is without doubt a quantity of overriding importance for the understanding of processes occurring in aqueous solutions, as it allows determining the state and change of acid-base equilibria. The acidity of natural waters regulates many chemical reactions including those important to living organisms. In seawater, the equilibrium reactions of carbon dioxide, CO₂, are of particular importance. Any increase in the CO₂ content of seawater results in a decrease of pH and vice versa, assuming other conditions remain unchanged (Zeebe and Wolf-Gladrow, 2001). This coupling between the amount of dissolved CO₂ and pH allows using pH to track two processes with significance to the global carbon cycle and the functioning of marine ecosystems:

- (1) **Ocean acidification:** The oceanic uptake of anthropogenic CO₂ counteracts rising atmospheric CO₂ concentrations and therefore mitigates climate change (Le Quéré et al., 2016). However, the CO₂ uptake results in the formation of carbonic acid and a decrease in seawater pH. This process, termed ocean acidification (Bates et al., 2012; Doney et al., 2009), shifts acid-base equilibria in seawater. The alteration in physiological conditions affects the performance of marine organisms, which might result in currently unpredictable changes in species interactions and ecosystem functioning (Kroeker et al., 2010). pH is by definition the most direct measure to track ocean acidification.
- (2) **Biogeochemical transformations:** The primary production (Schneider et al., 2006) and remineralization of organic matter (Schneider et al., 2010) are inevitably coupled to the uptake and release of CO₂ (Schneider and Müller, 2017). Seasonal and diurnal variability in those processes is therefore reflected in pH fluctuations (Hofmann et al., 2011) that superimpose long-term trends (Wahl et al., 2016). Accordingly, the magnitude and timing of primary production and remineralization can be determined from pH measurements.

Comparison of pH in the open ocean and the Baltic Sea

The simultaneous control of pH by (1) anthropogenic CO₂ emissions and (2) biogeochemical transformations in seawater suggests that the detection of long-term pH

trends is complicated by the presence of fluctuations. In the **surface water of the Baltic Sea such pH variability is higher than in the open ocean**, because of high productivity in combination with a lower buffer capacity (alkalinity) in most regions. The latter causes high pH changes per change in CO₂ concentration. Figure 1 displays the contrasting pH conditions in the Baltic Sea (SMHI monitoring data) and the North Atlantic Ocean (Bates et al., 2012). In the latter, ocean acidification occurs at a rate of around -0.002 per year, which could unambiguously be detected due to the comparably low amplitude of pH fluctuations (Bates et al., 2012) and the advanced technology for the determination of CO₂ system parameters in seawater (Byrne, 2014). Very similar acidification rates were identified in the surface water of other open ocean regions (Bates et al., 2014; Byrne et al., 2010). The observed pH trends agree well with theoretical predictions based on the atmospheric CO₂ forcing (Caldeira and Wickett, 2003). The underlying reason for this strict correlation is the constancy of seawater composition - in particular the **constancy of oceanic alkalinity as the “backbone” of the marine CO₂ system** – on time scales of ocean acidification, i.e. decades to centuries (Archer, 2005; Bates et al., 2012). In contrast, pH trends in the Baltic Sea remain understudied and few regional trend analysis reveal high uncertainty in trend detection (Almén et al., 2017).

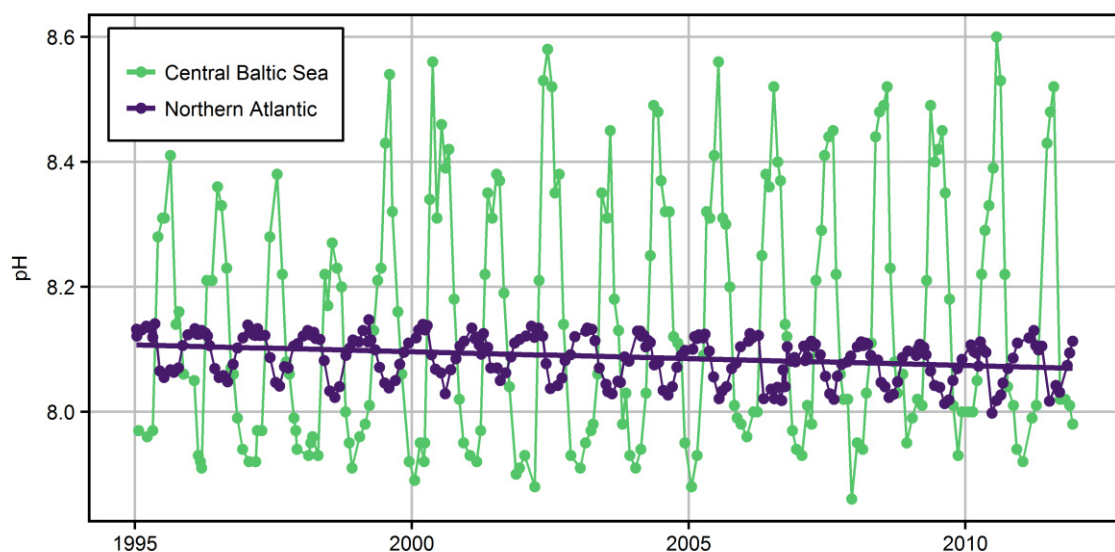


Fig. 1: pH time series for the Baltic Sea (Station BY-15, 57°19'N 020°05'E, SMHI monitoring data) and the North Atlantic Ocean surface water (Bermuda Atlantic Time-series Study, 31°40'N 64°10'W, Bates et al., 2012).

The absence of significant pH trends in the Baltic Sea may have three reasons: (i) pH trends may be masked by the **interannual variability of pH amplitudes**. If this is the case, even perfect (i.e., continuous and error-free) knowledge on pH would not allow detecting significant trends. (ii) The **pH measurement quality** may be too poor to resolve trends. Poor quality in this respect refers to the analytical quality (i.e., accuracy and

precision) but also to the data coverage (i.e., the spatio-temporal resolution). Indeed, the pH monitoring data displayed in Figure 1 have to be considered poor quality with respect to the detection of acidification trends, because they were obtained with questionable glass electrode measurements and less than monthly resolution. (iii) Acidification driven by the rise in atmospheric CO₂ might be counteracted by other **simultaneous changes in seawater chemistry**, e.g., an increase in the buffer capacity. Such simultaneous changes are plausible for the Baltic Sea due to the large influence of river water discharge on seawater composition.

Objectives of this thesis

Motivated by those shortcomings in the understanding of long-term changes in the acid-base system of the Baltic Sea, this thesis emphasizes three foci:

Focus 1 unravels the acidification potential of the Baltic Sea without having access to pH data of sufficient quality. This is achieved by quantifying alkalinity trends over the past decades and by putting those into perspective with the atmospheric CO₂ forcing. The derived acidification scenarios are discussed in the light of CO₂ system fluctuations caused by the production and remineralization of organic matter. Based on those insights, analytical requirements for pH determinations are derived that have to be met if ocean acidification in the Baltic Sea is to be tracked.

Focus 2 forms the scientific basis for pH measurements in brackish waters that fulfill the quality criteria for a meaningful acidification monitoring. It introduces a series of experiments to establish traceability for pH measurements, which means the relation of results to an accepted primary reference by an unbroken chain of comparison measurements. The established traceability chain covers the characterization of primary pH standards by Harned cell measurements and the determination of molecular properties of the pH indicator dye m-Cresol Purple, which is required to perform spectrophotometric pH measurements. Furthermore, perturbation experiments of the latter method with two common substances in the Baltic Sea - dissolved organic matter and hydrogen sulfide – are presented. The fundamental chemical characterization work was performed in parallel and with substantial mutual support to the ambitions of an industry partner to develop a marked-ready spectrophotometric pH instrument that allows tracking ocean acidification in the Baltic Sea over the largest range of conditions. Those efforts were embedded in the EU BONUS project PINBAL.

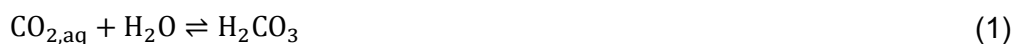
Focus 3 investigates the impact of acidification on benthic calcifiers under fluctuating pH conditions. The vast majority of previous experiments addressing the consequences of ocean acidification for marine organisms was performed under lowered, but stable pH levels. Focus 3 resolves those methodological shortcomings by quantifying the seawater CO₂ chemistry fluctuations induced by the metabolic activity of macroalgae in shallow benthic ecosystems. The diurnal fluctuations imply periodically improved conditions for calcifications. It is presented to which degree calcifying organisms are capable to shift calcification into those time windows of favorable conditions under current and future CO₂ levels.

The following two chapters briefly introduce the peculiarities of the marine CO₂ system and the Baltic Sea hydrochemistry essential for the understanding of foci 1-3.

The marine CO₂ system

Equilibrium reactions

The equilibrium reactions of CO₂ dominate the acid-base systems in seawater and link the atmospheric, oceanic and solid phase carbon reservoirs. The hydration of CO₂, once physically dissolved in seawater (CO_{2,aq}), results in the formation of carbonic acid:



The sum of physically dissolved CO₂ and carbonic acid is referred to as CO₂^{*}:



The dissociation of carbonic acid into bicarbonate (eq. 3) and carbonate ions (eq. 4) transfers protons, H⁺, to water molecules and other proton acceptors in seawater:



The equilibrium conditions of those dissociation reactions are described by the equilibrium constants K₁ and K₂ (e.g. Millero, 2010):

$$K_1 = \frac{[\text{H}^+] \cdot [\text{HCO}_3^-]}{[\text{CO}_2^*]} \quad (5)$$

$$K_2 = \frac{[\text{H}^+] \cdot [\text{CO}_3^{2-}]}{[\text{HCO}_3^-]} \quad (6)$$

where brackets denote concentrations. The **conventional expression of seawater equilibrium reactions in terms of concentrations** – instead of activities – results in a dependency of the equilibrium constants on salinity, in addition to temperature and pressure, because the equilibrium constants implicitly include the salinity-dependent activity coefficients.

The concentration of CO_2^* (eq. 2) is directly related to the fugacity of CO_2 in seawater, $f\text{CO}_2$, by

$$f\text{CO}_2 = \frac{[\text{CO}_2^*]}{K_0} \quad (7)$$

where K_0 is the solubility constant. The direction of CO_2 gas exchange between atmosphere and seawater is exclusively controlled by differences in the CO_2 fugacity in both compartments, whereas gas fluxes also depend on the state of the sea surface, typically approximated by wind speed (Wanninkhof, 2014). The **increase of atmospheric $f\text{CO}_2$ by anthropogenic CO_2 emissions drives the net CO_2 uptake by the world's oceans.**

The oceanic CO_2 uptake results in the transfer of protons to proton acceptors in seawater (eqs. 3, 4, 9), causing a shift of respective acid-base equilibria towards the protonated species. This process was termed ocean acidification (Doney et al., 2009). With respect to CO_2 equilibria, the resulting changes in speciation can be illustrated by dividing eq. 5 by eq. 6, which gives:

$$\frac{[\text{HCO}_3^-]}{[\text{CO}_2^*] \cdot [\text{CO}_3^{2-}]} = \frac{K_1}{K_2} \quad (8)$$

The equilibrium condition in eq. 8 formally refers to the so-called **buffer reaction** in seawater:



The buffer equation highlights two peculiarities of ocean acidification: (i) the **oceanic CO_2 uptake capacity is controlled by the amount of carbonate ions** available to buffer the release of protons and (ii) the **carbonate ion concentration decreases with increasing CO_2 levels**. The largest share of the protons released by the dissociation of an additional amount of carbonic acid is actually transferred to carbonate ions.

Due to almost constant concentration of calcium ions (Ca^{2+}) in the ocean, changes in the carbonate ion concentration are directly reflected in changes in **the saturation state of calcium carbonate**, which is defined as the product of the carbonate and calcium ion concentration, divided by the solubility product of calcium carbonate, K_{CaCO_3} :

$$\Omega_{\text{CaCO}_3} = \frac{[\text{CO}_3^{2-}] \cdot [\text{Ca}^{2+}]}{K_{\text{CaCO}_3}} \quad (10)$$

Different forms of CaCO_3 minerals exists that differ in solubility and therefore have different saturation states at identical carbonate and calcium ion concentration. Organism typically precipitate two mineral forms: calcite and the more soluble aragonite.

Measureable parameters and their characteristics

The state of the marine CO_2 system is characterized by four measurable variables (Dickson et al., 2007). Those are the total concentration of dissolved inorganic carbon (C_T), total alkalinity (A_T), the partial pressure of carbon dioxide ($p\text{CO}_2$) and the negative decadic logarithm of protons (pH), which refers to H^+ activities or concentrations dependent on the chosen pH-scale (see below).

C_T accounts for the sum of all inorganic CO_2 species dissolved in seawater and is defined as:

$$C_T = [\text{CO}_2^*] + [\text{HCO}_3^-] + [\text{CO}_3^{2-}] \quad (11)$$

As carbon is the major constituent of living biomass, growing phytoplankton organisms take up CO_2 from seawater. Due to the re-equilibration of the CO_2 system, the **primary production of every unit of organic matter is directly reflected in an equivalent decrease of C_T** , irrespective of the CO_2 species used as carbon source. Vice versa, the remineralization of organic matter results in an increase of C_T .

A_T is defined as the excess of proton acceptors over donors with respect to the chosen zero level of protons (Dickson, 1981; Wolf-Gladrow et al., 2007). Focusing only on the dominant carbonate contributions to A_T , a simplified¹ expression is:

$$A_T = [\text{OH}^-] + [\text{HCO}_3^-] + 2[\text{CO}_3^{2-}] - [\text{H}^+] + [\text{minor bases} - \text{minor acids}] \quad (12)$$

¹A more complete definition taking into account other major acid-base systems relevant in oxic, open ocean seawater is:

$$A_T = [\text{HCO}_3^-] + 2[\text{CO}_3^{2-}] + [\text{B}(\text{OH})_4^-] + [\text{OH}^-] + [\text{HPO}_4^{2-}] + 2[\text{PO}_4^{3-}] + [\text{SiO}(\text{OH})_3^-] + [\text{NH}_3] + [\text{HS}^-] - [\text{H}^+]_F \\ - [\text{HF}] - [\text{HSO}_4^-] - [\text{H}_3\text{PO}_4] + [\text{minor bases} - \text{minor acids}]$$

On a global scale, A_T in seawater originates from continental weathering processes and is delivered to the sea by riverine input. The major oceanic A_T sink is the sedimentation of calcium carbonate formed by marine organism. **A_T controls the rate of ocean acidification**, because $\Delta\text{pH}/\Delta\text{pCO}_2$ decreases towards higher A_T . Furthermore, **A_T controls C_T** , because under the prevailing conditions equilibrium is achieved when seawater dissolved as much CO_2 as required to protonate most of the carbonate ions to hydrogen carbonate (eq. 8). This results in an $A_T:C_T$ ratio in the order of 1, with HCO_3^- representing the major contribution to both.

Both, C_T and A_T are so called **conservative variables** of the marine CO_2 system, which means that, being determined in moles per kg solution, they do not change as a function of temperature or pressure. Like salinity, C_T and A_T also behave conservatively upon mixing of water masses. The conservative behavior of A_T and salinity during mixing of river and seawater typically results in region-specific **linear A_T -S relationships** in coastal areas (Friis et al., 2003), with an A_T intercept at zero salinity that corresponds to the mean A_T of the river water. In contrast, pH and pCO_2 depend on temperature and pressure and do not behave conservatively during mixing of water masses.

pCO_2 is closely related to the $f\text{CO}_2$ (eq. 7). Both quantities differ only by few μatm because $f\text{CO}_2$ takes into account the non-ideal behavior of the CO_2 gas.

pH is defined as the negative decadic logarithm of the H^+ activity. However, such a single ion quantity is immeasurable by any thermodynamically valid method (Buck et al., 2002). Therefore, pH determination requires conventions. For low ionic strength solutions, IUPAC recommends determination of pH on the activity scale. The required estimate of activity coefficients relies on the Bates-Guggenheim convention, which applies only for solutions with ionic strength $\leq 0.1 \text{ mol}\cdot\text{kg}^{-1}$. However, the ionic strength of oceanic seawater samples with a salinity of 35 is around $0.7 \text{ mol}\cdot\text{kg}^{-1}$. For measurements in seawater it is therefore convenient to determine **pH on concentration scales**, which requires the definition of a standard composition of the seawater matrix for pH buffer solutions, because hydrogen ions are in equilibrium with other acid-base components in seawater. The so called pH_T scale became a widely accepted convention within the scientific community. The index T denotes the **total hydrogen ion concentration**, which includes the amount of “free” hydrogen ions (H^+) referring to the sum of protonated water molecules (H_3O^+) or water molecule clusters, and the protonated form of the sulfate ion, HSO_4^{2-} . Accordingly, pH_T is defined as:

$$\text{pH}_T = -\log_{10} \left\{ [\text{H}^+] \left(1 + \frac{[\text{SO}_4^{2-}]_T}{K_{\text{HSO}_4^-}} \right) \right\} \quad (13)$$

where $[\text{SO}_4^{2-}]_T$ is the total concentration of sulfate and $K_{\text{HSO}_4^-}$ is the dissociation constant of hydrogen sulfate (Dickson, 1990). The determination of pH_T requires the calibration of instruments in buffer solutions that match the ionic composition of the analyte. The pH of such buffer solutions should be **traceable to a primary method, i.e., Harned cell measurements** (Buck et al., 2002). For seawater with salinity 20-40 this was previously achieved, but no adequate buffers were available for brackish waters (Dickson et al., 2015). Brackish waters are a mixture of seawater and freshwater but only loosely defined in terms of upper and lower salinity thresholds. In this study we consider brackish waters operationally as those with a salinity between 5 and 20, for which pH buffer solutions were investigated. The lack of buffer solutions made it impossible to correctly calibrate any pH instrument for brackish water conditions. The calibration at the salinity of the sample to be analyzed is required for example for pH glass electrodes, because the liquid junction potential depends on salinity. Likewise, the dissociation constant of pH indicator dyes used for spectrophotometric pH determinations needs to be characterized as a function of salinity (See Focus 2: Theory).

Internal consistency and the ocean acidification paradigm

A fundamental characteristic of CO_2 equilibrium reactions in seawater is that the **CO_2 system is fully determined when two out of four parameters** introduced above (C_T , A_T , pH, pCO_2) are given. This is a consequence of (i) of the two degrees of freedom of the coupled system of equilibrium reactions (eqs. 5-7) and (ii) the constancy in seawater composition that includes constant proportions of the various acid-base systems contributing to A_T . Provided that the equilibrium constants of all involved acid-base systems are known, any CO_2 system parameter can be calculated from two others. This constraint can be used to test the consistency of individually determined parameters by an overdetermination of the CO_2 system (Byrne, 2014). However, in coastal waters with unquantified contributions to alkalinity - like organic matter that carries acidic functional groups - A_T may not be suitable to derive other CO_2 system parameters (Kuliński et al., 2014).

The constraint in degrees of freedom of the CO_2 system has an important implication for the understanding of the **ocean acidification paradigm**, which states that an increase in pCO_2 is directly coupled to a decrease in seawater pH (Doney et al., 2009). This strict

relationship only holds true when another variable remains unchanged. For open ocean conditions with water residence times $\sim 10^5$ years this criterion is indeed fulfilled, because A_T concentrations are largely constant on the decadal to centennial timescales of ocean acidification (Archer and Brovkin, 2008; Bates et al., 2012). However, for enclosed sea areas influenced by land, this is not necessarily the case.

Marine organisms in a changing CO₂ world

A major concern of ocean acidification is its impact on marine ecosystems. It was shown that many living organism in the sea are vulnerable to changes in the CO₂ system (Kroeker et al., 2010). A general believe was that calcifying organism are particularly threatened, because the reduction in the saturation state of calcium carbonates increases the metabolic costs for calcification. However, the mechanistic control of calcification rates is still under debate. Recent studies suggest that calcification is rather controlled by the ratio of [HCO₃⁻] to [H⁺], because HCO₃⁻ serves as inorganic carbon substrate and H⁺ inhibits calcification (Bach, 2015; Thomsen et al., 2015). The determination of the controlling factors for calcification is complicated by the proportionality between the saturation state and the [HCO₃⁻] to [H⁺] ratio, which is obvious from a rearranged version of eq. 6:

$$\frac{[\text{HCO}_3^-]}{[\text{H}^+]} = \frac{1}{K_2} \cdot [\text{CO}_3^{2-}] \quad (14)$$

Although the mechanistic control remains a subject of ongoing discussions, there is little doubt about the generally impaired calcification conditions at low pH. However, most studies that investigated the impact of ocean acidifications on organisms compared stable current and future pH levels. but did not take pH fluctuations into account (Wahl et al., 2016). This is a severe limitation, because many calcifying organisms experience strong pH and respective CO₂ system fluctuations in their specific habitat (Hofmann et al., 2011). Such fluctuations are often the consequence of intense metabolic activity of primary producers. Macroalgae in benthic habitats for example take up CO₂ during daytime and thereby create pronounced diurnal fluctuations that are by orders of magnitude larger than expected annual changes in pH (Saderne et al., 2013). Many sessile benthic calcifiers live on, in between or nearby those macroalgae stands and therefore experience CO₂ system conditions completely different from open ocean surface waters. However, only few studies investigate how calcifiers react upon such large pH fluctuations and associated changes in calcification conditions.

The Baltic Sea

Hydrography

The semi-enclosed Baltic Sea is **one of the world's largest estuaries**. The sea is divided into five major sub-regions: the Baltic Proper (BP), the adjacent Gulfs of Bothnia (GB), Finland (GF) and Riga (GR), and the Kattegat (KA), which includes the transition area to the North Sea and the Belt Sea (Fig. 2A). The topography features a succession of sills and basins (Fig. 2B).

The **water budget** is characterized by strong inputs of river water and saltwater inflow from the North Sea that enter through the narrow belts and sounds in the Kattegat. Sporadic Major Baltic Inflow events (Mohrholz et al., 2015) transport dense, high-saline waters from the North Sea into the deep basins of the Baltic Sea, whereas the low-saline river water contributions form the surface water layers. Consequently, a permanent halocline establishes in the Baltic Proper at a depth of around 60 m (Fig. 2B). The surplus of freshwater input triggers an estuarine circulation. However, before being exported to the Kattegat, the low-saline surface waters mix with inflowing North Sea waters and thereby close the salt budget. The mean salinity of the Baltic Sea shows decadal, large-scale variations of up to 1 salinity unit, but no long-term trend was found during the past century (Winsor et al. 2001, 2003). The surface salinity increases from a mean in the Gulf of Bothnia ~3 to ~10 in the south-western part of the Baltic Proper. A strong gradient to the oceanic salinity of ~35 exists in the Kattegat region. The constancy of ionic composition of seawater known from the open ocean (Millero et al., 2008) vanishes towards low salinity and is known as **salinity anomaly** (Feistel et al., 2009). Regional differences of the salinity anomaly result from the variety of river water compositions determined by the weathering processes in the specific drainage basin.

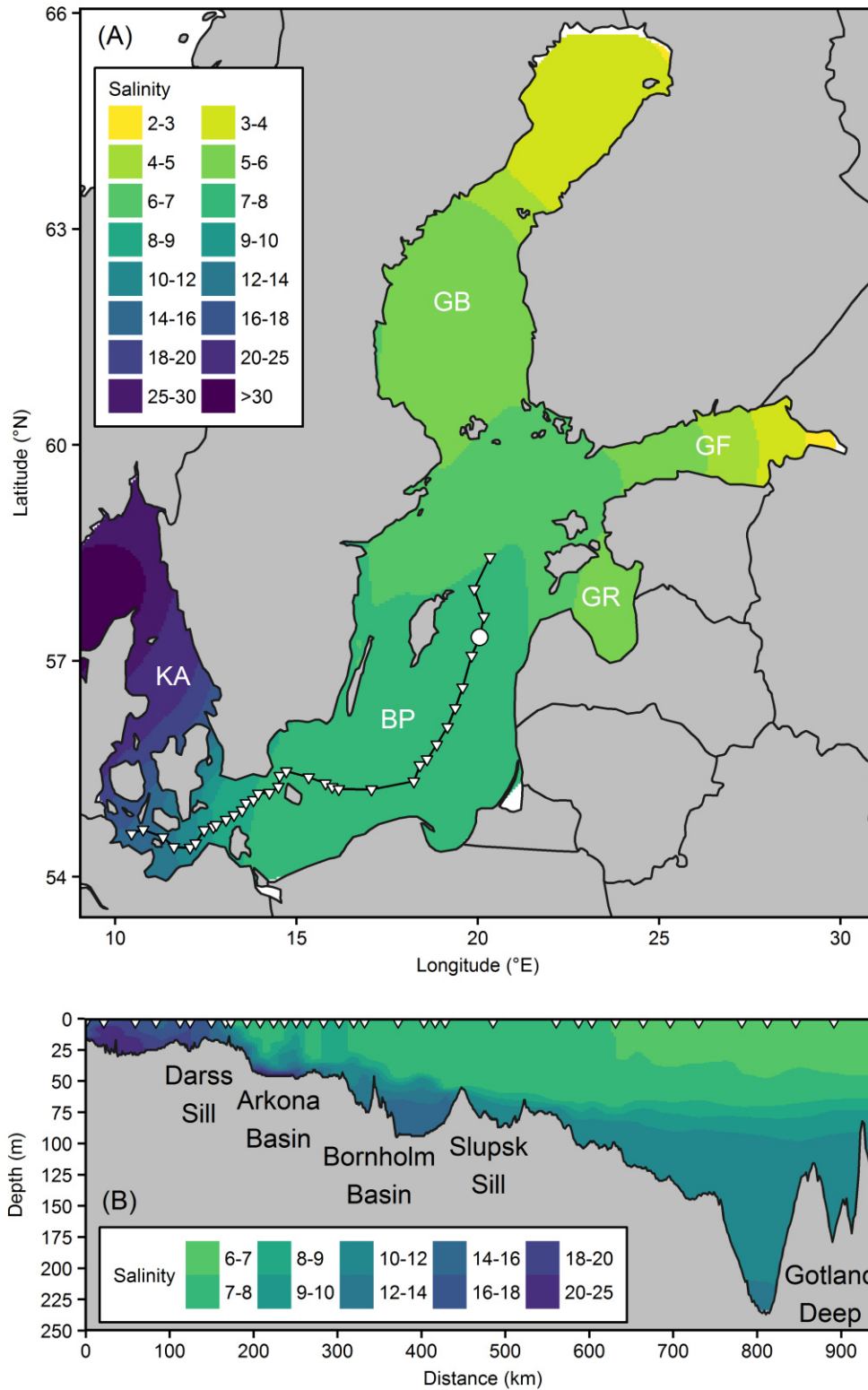


Fig. 2: Baltic Sea: (A) Surface salinity distribution and major sub-regions (KA: Kattegat, BP: Baltic Proper, GB: Gulf of Bothnia, GF: Gulf of Finland, GR: Gulf of Riga). The circle indicates the monitoring station BY-15 (57°19'N 020°05'E) at the Gotland deep. Triangles mark locations for vertical salinity profiles displayed below as (B) interpolated cross section (IOW monitoring data, 2013). Redrawn from Schneider and Müller (2017).

Biogeochemical peculiarities

The majority of the processes discussed in this thesis refer to the surface waters of the Baltic Sea, where intense primary production of organic matter takes place. The majority of this organic material is only remineralized after sinking to deep waters (Schneider and Müller, 2017), where stagnant conditions favor the occurrence of anoxia. Under anoxic conditions, when sulfate is used as electron acceptor for the oxidation of organic matter, hydrogen sulfide accumulates in the deep basins and reaches concentrations of up to $100 \mu\text{mol}\cdot\text{kg}^{-1}$ (Fonselius and Valderrama, 2003). Apart from the stratification of the water body that largely separates primary production and remineralization, the freshwater input also causes comparable high dissolved organic matter concentrations of $300\text{-}400 \mu\text{mol}\cdot\text{kg}^{-1}$ in the Baltic Sea surface waters (Kuliński et al., 2014).

Similar, but more pronounced than the salinity anomaly, the alkalinity patterns in the Baltic Sea are a consequence of the region-specific **terrestrial weathering** processes. The Baltic Sea drainage basin can be divided into a northern and southern part that intersect at the easternmost end of the Gulf of Finland (Håkanson et al., 2003). The bedrock of the northern part mainly consists of granite, which has low weathering rates and causes low A_T levels of Scandinavian rivers. The bedrock of the southern part consists of limestone, clay and sandstone and produces high-alkaline river water. The surface water A_T -S pattern in the Baltic Sea (Fig. 3) results from the mixing of various river water sources and North Sea water, during which S and A_T behave conservatively. As a consequence, the surface A_T decreases with decreasing salinity, except in the Gulf of Riga. **Linear A_T -S regimes** exist in the three gulfs (GB, GF, GR) and the Kattegat region, whereas the Baltic Proper is the “mixing chamber” of waters from the other areas and consequently shows no strictly linear A_T -S relation (Beldowski et al., 2010). The intercepts of the linear A_T -S relationships represent the river water A_T signatures of the respective basin. The C_T -S pattern closely follows that of A_T , highlighting the strong control of A_T over C_T (see: Measureable parameters and their characteristics).

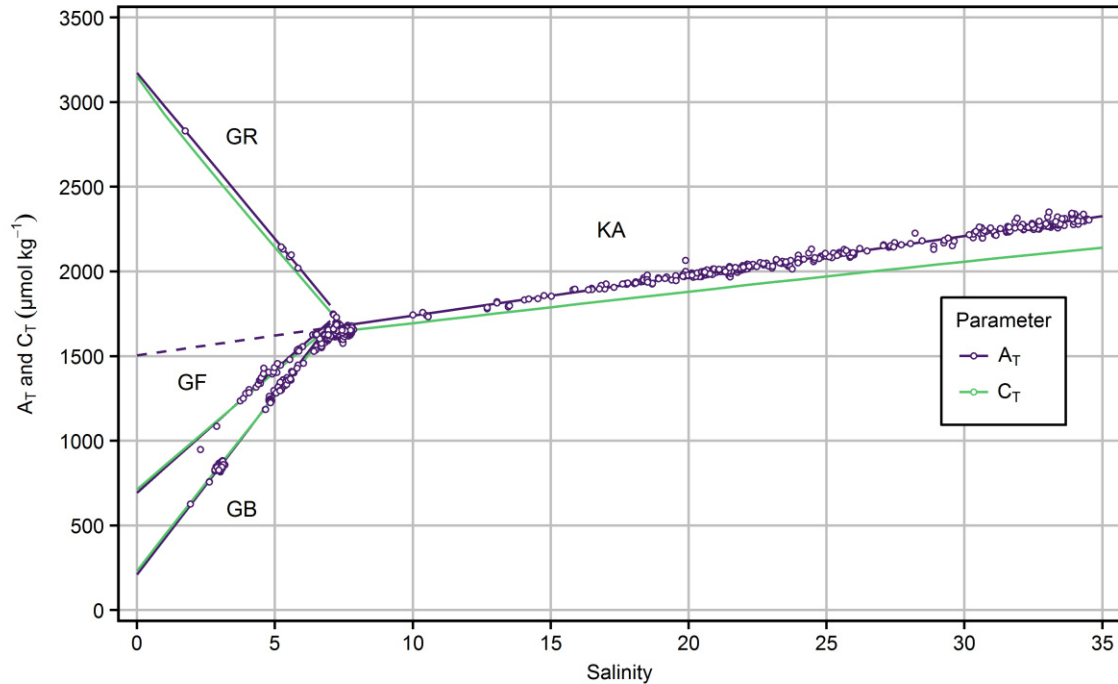


Fig. 3: Alkalinity (A_T) and dissolved inorganic carbon (C_T) as a function of salinity in the Baltic Sea. C_T data are calculated from linear A_T - S relationships in the four sub-regions and $pCO_2 = 400 \mu\text{atm}$. Redrawn from Schneider and Müller (2017).

Due to its generally lower alkalinity (except in the Gulf of Riga) the Baltic Sea is believed to be especially vulnerable to CO_2 -induced acidification. Indeed, for the current atmospheric pCO_2 increase of around $+2 \mu\text{atm yr}^{-1}$ a slightly lower mean pH trend of -0.0019 yr^{-1} can be expected for the open ocean ($S=35$, $T=10^\circ\text{C}$, $A_T=2300 \mu\text{mol}\cdot\text{kg}^{-1}$) compared to -0.0021 yr^{-1} in the Baltic Proper ($S=7$, $T=10^\circ\text{C}$, $A_T=1650 \mu\text{mol}\cdot\text{kg}^{-1}$). However, the direct link to riverine A_T input and the short water residence time of around 30 years (Helcom, 1993) suggest that significant A_T changes may occur in the Baltic Sea on timescales similar to that of anthropogenic atmospheric pCO_2 perturbations (10–100 yr), e.g., if changes in weathering processes occur (Archer, 2005; Lenton and Britton, 2006). This implies that a reliable acidification estimate cannot solely be based on the atmospheric pCO_2 evolution.

Focus 1: Long-term changes and variability of the Baltic Sea CO₂ system

Background

Open ocean acidification is almost exclusively controlled by the uptake of anthropogenic CO₂ due to constant alkalinity levels on timescale of decades to centuries (Bates et al., 2012; Byrne et al., 2010). The **Baltic Sea alkalinity is controlled by the river endmember A_T** signature (Fig. 3, Beldowski et al., 2010). The low water residence time therefore suggests that the alkalinity might change on ocean acidification timescales, if the riverine A_T input changes. Indications for changes in riverine A_T source were previously reported (Hjalmarsson et al., 2008). Accordingly, ΔpH in the Baltic Sea cannot be predicted from ΔpCO₂ in the atmosphere. Furthermore, the data quality achieved by past pH monitoring efforts does not allow for a reliable trend assessment (Almén et al., 2017). However, extensive A_T measurements were performed in the Baltic Sea region dating back to the early 20th century (Buch 1945; Hjalmarsson et al. 2008). Preliminary studies indeed suggested that the alkalinity in the eastern Gotland Sea increased by around 100 μmol·kg⁻¹ from 1930 to 2010 (Schneider et al., 2015). Nevertheless, a comprehensive analysis of the A_T evolution in the Baltic Sea had not been performed.

Scope

Focus 1 aims at evaluating the acidification potential of the Baltic Sea by putting the atmospheric CO₂ forcing into the context of long-term A_T dynamics in the various sub-regions. Resulting changes in other CO₂ system parameters, such as the saturation state of calcium carbonate, are presented. Results of this approach are discussed in the light of the pH variability caused by primary production and mineralization and requirements for a reasonable acidification monitoring in the Baltic Sea are derived.

Approach and results

Long-term alkalinity trends

Müller et al. (2016) compiled a comprehensive data set that consists - to the best knowledge of the authors - of **all A_T observation available from the Baltic Sea** at the

date of compilation in April 2015. The majority of the data originated from SMHI monitoring efforts. The analysis was restricted to water depths <20 m to avoid temporary A_T contributions from sulfide (S^{2-}) that is formed in stagnant anoxic bottom waters, but re-oxidized to sulfate under oxic conditions in surface waters. The analysed data set comprised 31436 observations. The data quality was found to be high since 1995, when Certified Reference Materials (Dickson et al., 2003) were introduced to the Swedish monitoring. Therefore, the summary information given here **focus on the 1995-2014 period**.

Taking the complex A_T -S distribution of the Baltic Sea into account, two types of sub-regions were investigated differently: (i) Sub-regions with linear A_T -S relationship (KA, GB, GF, GR; Fig. 3) and (ii) the Baltic Proper, which - as a mixing chamber for waters from the adjacent gulfs and the North Sea - reveals no distinct A_T -S relation.

For sub-regions with linear A_T -S relationships, three-dimensional statistical models - expressing changes of the slope and intercept of the A_T -S relationship with time - were developed and fitted to the data. The models included the dependency of A_T on salinity, time, as well as an interaction term of both parameters. Applying the models to the time period 1995-2014, it was found that **A_T rates of change increased consistently towards lower salinity**: In the Kattegat region (Fig. 4) constant A_T was found at high salinities around 30. In contrast, at salinity 15, A_T increased from 1812 to 1880 $\mu\text{mol}\cdot\text{kg}^{-1}$, which corresponds to a rate of +3.4 $\mu\text{mol}\cdot\text{kg}^{-1}\cdot\text{yr}^{-1}$.

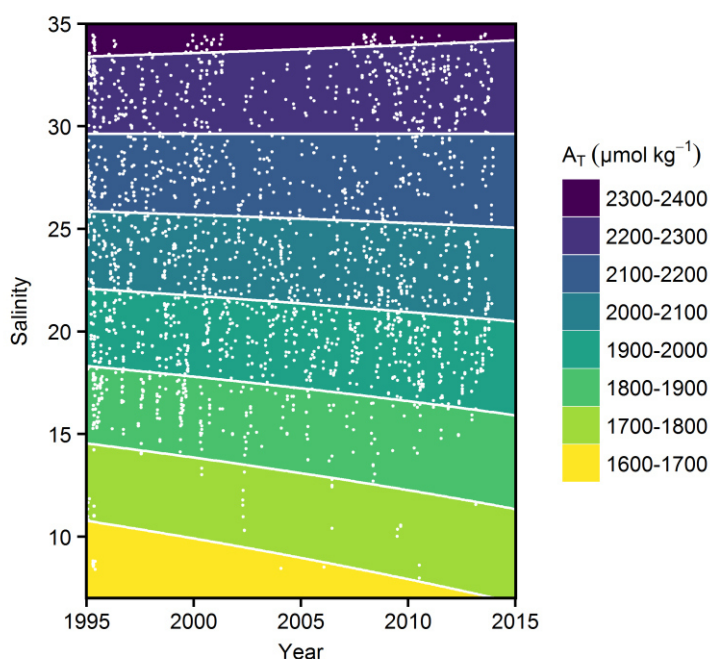


Fig. 4: Surface water alkalinity as a function of salinity and time in the Kattegat from 1995 to 2014. Colours display A_T levels as derived from the best fitting three-dimensional models. White dots represent observations. Redrawn from Müller et al. (2016)

Much higher rates were determined for the Gulf of Bothnia, e.g., $+7.4 \mu\text{mol}\cdot\text{kg}^{-1} \text{yr}^{-1}$ at a salinity of 3. Results for the Gulf of Finland indicated similar trends, however, associated with a higher degree of uncertainty. In the Gulf of Riga the data coverage was too poor for a reasonable application of the model.

For the Baltic Proper A_T trends were analysed after grouping the data covering the salinity range 6.5-7.7 into salinity intervals of 0.2. The deviations (ΔA_T) of the individual values from the mean A_T were computed separately for each salinity interval. Afterwards, the ΔA_T values from all salinity intervals were pooled and temporal trends were investigated by linear regression analysis. A significant positive A_T trend was found in the Baltic Proper that amounted to $+3.4 \mu\text{mol}\cdot\text{kg}^{-1} \text{yr}^{-1}$ for the 1995-2014 period (Fig. 5A). This is similar to the trends found at lowest and highest salinity in the Kattegat and Gulf of Bothnia, respectively.

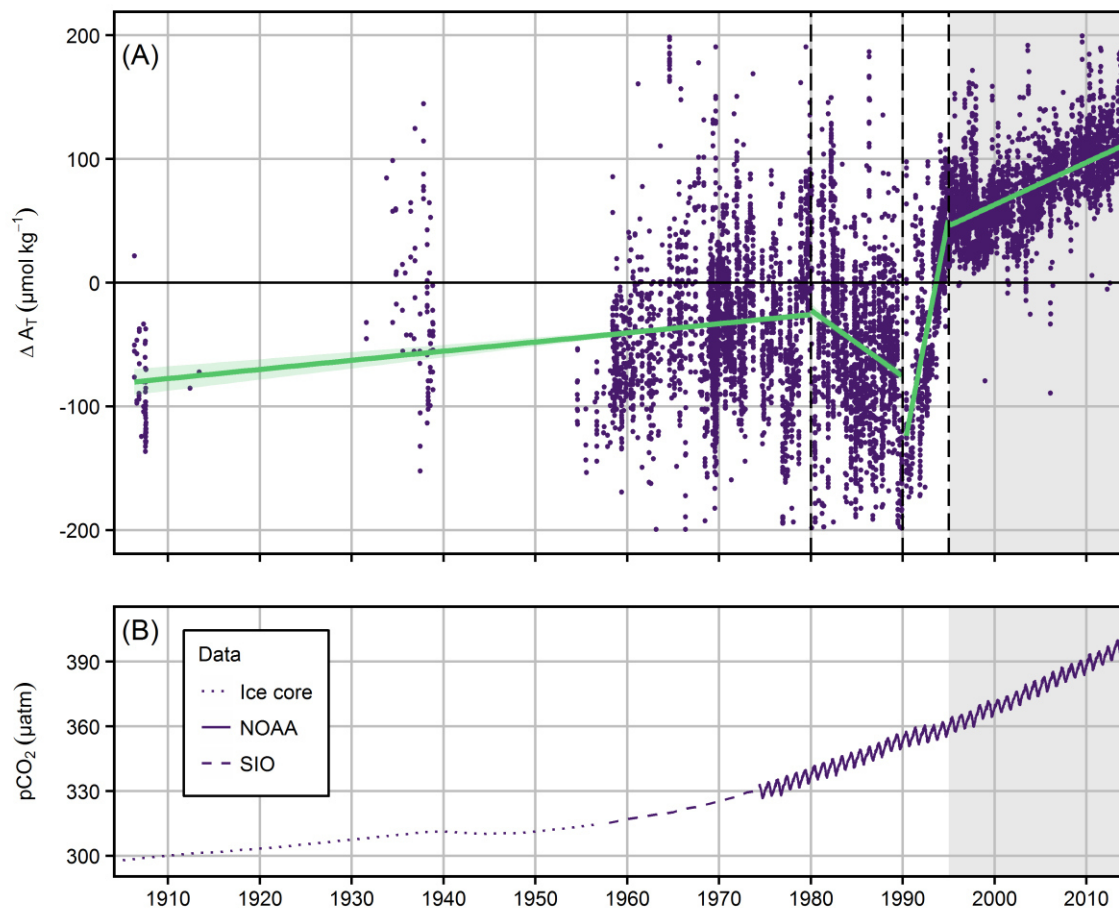


Fig. 5: (A) Alkalinity trends in the Baltic Proper displayed as deviations from the long-term mean (ΔA_T). Linear regression models were fitted separately within the four time frames indicated by the vertical dashed lines. Redrawn from Müller et al. (2016). (B) Atmospheric $p\text{CO}_2$ trajectories (source: NASA, including ice core data and measurement from Mauna Loa performed by Scripps Institution for Oceanographic (SIO) and the National Oceanic and Atmospheric Administrations (NOAA)). The combined impact of A_T and $p\text{CO}_2$ trends shown in Fig. 6 was computed for the 1995-2014 period (highlighted grey).

Combined impact of changes in seawater alkalinity and atmospheric CO₂

In the absence of reliable pH data, Müller et al. (2016) computed the acidification potential for the Baltic Sea from increasing atmospheric pCO₂ and observed seawater A_T trends for the time period 1995-2014 (grey periods in Fig. 5). The estimates are based on a pCO₂ trend of +2 μatm yr⁻¹ (IPCC, 2013). For comparison, the changes in the seawater CO₂ system were also computed for the same increase in pCO₂ but constant A_T levels. It was found that in the **Baltic Proper, the A_T increase mitigates CO₂-induced acidification by around 50%** (Fig. 6). In the low saline areas of the Bothnian Sea the alkalinity increase fully compensated the acidification potential during the last two decades.

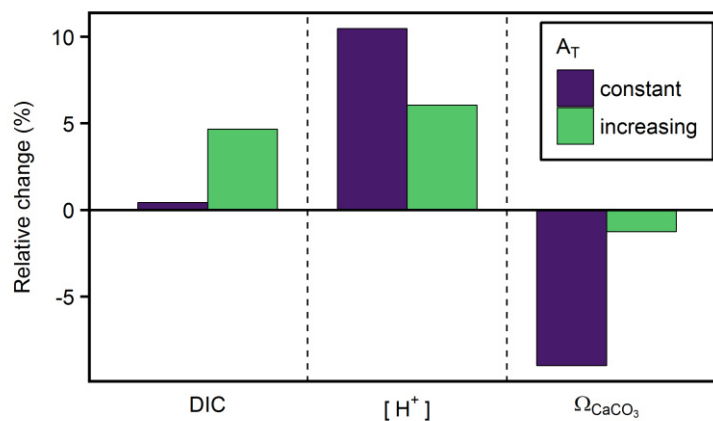


Fig. 6: Combined influence of simultaneous changes in atmospheric pCO₂ and seawater A_T on dissolved inorganic carbon (DIC), proton concentration [H⁺], and calcium carbonate saturation (Ω_{CaCO₃}) in the Baltic Proper from 1995 to 2014 (grey periods in Fig. 5). Relative changes were computed for two A_T scenarios: The observed A_T trend of +3.4 μmol kg⁻¹ yr⁻¹ was taken into account (green) and the A_T was assumed to be constant at mean A_T (purple). (conditions: S = 7, T = 10°C, dissociation constants from Millero (2010)). Redrawn from Müller et al. (2016).

Focusing on the Baltic Proper and the 1995-2014 period, the mean salinity and mean A_T were 7 and 1587 μmol·kg⁻¹, respectively. Taking the positive A_T trend into account, the A_T rose from around 1550 to 1620 μmol·kg⁻¹. Assuming equilibrium with the atmosphere, the simultaneous pCO₂ increase would have raised the dissolved inorganic carbon C_T in the Baltic Proper only by ~6 μmol·kg⁻¹ under a constant mean A_T background (Fig. 6). However, with A_T and pCO₂ rising in parallel, **C_T increased by ~70 μmol·kg⁻¹ (~5%)** from 1522 to 1593 μmol·kg⁻¹. This is very similar to the absolute change in A_T and reflects the tight control of A_T on the CO₂ storage capacity of seawater (compare Fig. 3).

The A_T increase observed in the Baltic Proper over the past two decades also stabilized the carbonate ion concentration. At constant mean A_T levels the pCO₂ increase would have caused a drop in carbonate concentration from 42.7 to 38.8 μmol·kg⁻¹, but with A_T

increasing simultaneously the carbonate concentration decreased only from 40.9 to 40.4 $\mu\text{mol}\cdot\text{kg}^{-1}$. Assuming a constant calcium concentration of 2.7 $\text{mmol}\cdot\text{kg}^{-1}$ (Dyrssen, 1993), changes in the carbonate concentration were directly reflected in the saturation state of calcium carbonate (Ω_{CaCO_3}). With respect to the solubility product of calcite (Mucci, 1983), the **increasing A_T stabilized Ω_{CaCO_3}** at a level of around 1.5. In contrast, the non-mitigated CO_2 uptake would have decreased the saturation state by around 0.2, corresponding to relative change of -9% (Fig. 6). The observed A_T increase might thus be twofold beneficial to calcifying organisms, because it helps to stabilize both, pH and the CaCO_3 saturation state.

Drivers for alkalinity trends

An interesting question asks what drives the observed positive A_T trends in the Baltic Sea. Based on a semi-quantitative plausibility assessment, Müller et al. (2016) suggested that these trends might be **driven by an interplay of acidic precipitation, increasing atmospheric CO_2 and liming activities**. All of these drivers act upon weathering processes and the riverine A_T input, whereas significant contributions from changes in the internal A_T formation, recently proposed as another major A_T source to the Baltic Sea (Gustafsson et al., 2014), were considered unlikely. In agreement with the conclusion of Müller et al. (2016), Sun et al. (2017) indeed found increasing weathering rates by 10–20% in the pristine boreal northern drainage basin by analysing a 40-year record of river water chemistry data. Sun et al. (2017) argued that, among others, an important factor affecting weathering could be an increase of available soil organic matter, as an intermediate phase between atmospheric and soil CO_2 .

Müller et al. (2016) and Sun et al. (2017) agree that increased CO_2 consumption by weathering and the resulting elevated A_T delivery to the ocean might act as a **negative feedback between atmospheric CO_2 increase and ocean acidification**. However, the still very limited mechanistic understanding of A_T dynamics in the Baltic Sea region limits the prediction of future trends. Müller et al. (2016) emphasized that their findings should not be misinterpreted as a permanent protection against CO_2 -induced acidification and related processes. However, a comprehensive monitoring of large estuarine systems like the Baltic Sea would not only be beneficial for the understanding of the particular ecosystem itself, but could also serve as valuable **early indicator for changes, e.g., in weathering processes, that might affect the global carbon cycle** on much longer timescales. The required continued monitoring of coastal seawater chemistry should ideally be harmonized globally, as increasing alkalinity trends were also observed in other

large rivers and coastal systems (Kapsenberg et al., 2017; Raymond and Cole, 2003) and recently on continental scales (Kaushal et al., 2018).

Variability caused by primary production and remineralization

The assessment of simultaneous changes in atmospheric CO₂ and seawater A_T by Müller et al. (2016) served to compare the impact of both drivers on the seawater acid-base system and to highlight the complexity of ocean acidification processes in coastal environments. The **derived acidification scenarios do not refer to real changes in mean pH** that occurred over the past two decades. The reason for this limitation is the **spatio-temporal variability in primary production and mineralization processes** in the Baltic Sea. Schneider and Müller (2017) entangled those processes by summarizing and re-analyzing 15 years of automated pCO₂ measurements on a cargo ship (Schneider et al., 2009, 2014) and bimonthly C_T measurements in the Gotland deep (Schneider et al., 2010). Though acidification detection was not a focus, two implications can be derived from their findings: (i) The **seasonality in the Baltic Sea surface water CO₂ system** is dominated by primary production processes (Fig. 7). The resulting pH variability (Fig. 1) is by far larger than annual changes expected from atmospheric CO₂ forcing. The control of primary production by an interplay of the radiation dose and nutrient availability suggests that such seasonal patterns might change over time, e.g. due to the reduction of nutrient concentrations targeted by HELCOM or the aim of the EU's Marine Framework Strategy Directive to establish a good ecological status of the Baltic Sea. Such changes could override pH trends induced by the atmospheric forcing. A shorter productive period with high pH conditions could for example cause a lower annual mean pH. (ii) CO₂ formed by mineralization of organic matter was found to accumulate in stagnant deep waters of the Gotland deep. **Over the course of a stagnation period the increase in C_T might result in an increasing C_T flux across the halocline.** Such an increased flux of previously accumulated CO₂ could favor increasing pCO₂ and decreasing pH in the surface water. This could superimpose the atmospheric pCO₂ forcing with trends related to sporadic deep water renewal events (Mohrholz et al., 2015). Indeed, Schneider and Müller (2017) found an increase in surface water pCO₂ larger than the atmospheric trend, ranging from +4.6 to +6.1 μatm yr⁻¹ in various investigated areas for the period 2008-2015 (Fig. 7). The first 7 years of this period were part of a deep water stagnation period that lasted from 2004 to 2014.

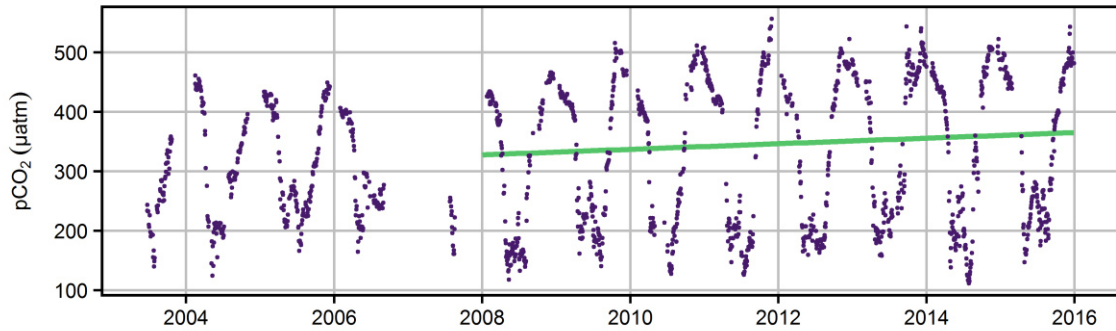


Fig. 7: pCO₂ time series in the Northern Gotland Sea obtained from autonomous measurements on a cargo ship. The green line represents a linear regression analysis for the period 2008–2015 based on daily interpolated data. Redrawn from Schneider and Müller (2017).

The complexity of the Baltic Sea CO₂ system – exemplified in this focus by alkalinity trends and region-specific patterns in the pronounced production and remineralization processes – has two implications for a reliable assessment of ocean acidification processes. First, the acidification assessment should be based on pH observations as the most direct measure for seawater acidity and changes in atmospheric pCO₂ are not a reliable predictor. Second, a **meaningful pH monitoring not only requires highly accurate and precise measurements, but also high spatial and temporal resolution**. Otherwise, there is a high risk of overlooking important, short-lasting processes in this highly variable system.

Conclusion

The observed A_T trends and the importance of primary production and mineralization processes highlight the complexity of the CO₂ system in the Baltic Sea. As a consequence, the simplified ocean acidification paradigm – ΔpH in seawater is a direct consequence of atmospheric ΔpCO₂ – though valid for open ocean regions, cannot be applied for enclosed sea areas influenced by land. In the light of the variability of the system, a reliable acidification assessment is not possible without a direct pH monitoring that achieves a high analytical quality and spatio-temporal resolution.

Focus 2: pH measurements in brackish waters

Background

The CO₂ system of the Baltic Sea is extremely variable and complex. Potential changes of pH due to ocean acidification are small compared to seasonal and other fluctuations. As concluded in Focus 1, a reliable acidification monitoring places highest demands on the pH determination. Measurements not only need to be of highest **analytical quality** in terms of accuracy and precision, further a high **spatio-temporal resolution** is indispensable. Among the scientific platforms currently operated in the Baltic Sea those requirements could be achieved with automated pH measurements on board of voluntary observing cargo ships (Schneider and Müller, 2017), which visit large areas of the Baltic Sea sufficiently often to resolve the seasonality of the CO₂ system. Deployed pH instruments must cope with salinities covering almost the full range from marine to freshwater conditions (Fig 2A), as well as large pH amplitudes spreading more than one order of magnitude in terms of proton concentration (Fig. 1).

Within the open ocean community **spectrophotometric pH measurements** became a widely accepted standard for pH determination (Dickson et al., 2015; Martz et al., 2015). The method relies on absorption measurements of a pH-sensitive indicator like m-Cresol Purple (Clayton and Byrne, 1993). The required characterization of the molecular properties of the dye includes absorption measurements in pH buffer solutions (Liu et al., 2011). Such buffer solutions, with pH assigned by an accepted primary method like **Harned cell measurements**, that achieves the highest level of accuracy (Buck et al., 2002), were not available for brackish waters with salinities below 20. Consequently, it was **not possible to correctly calibrate any pH instrument for applications in major parts of the Baltic Sea** (Fig 2A). An interim solution was provided by Mosley et al. (2004), who interpolated the pH of TRIS buffer solutions between salinity 5 and 20 and determined the dissociation constant of mCP in those solutions. Douglas and Byrne (2017b) corrected the results of Mosley et al. (2004) for dye impurities and fitted a model for mCP properties to a combined data set including previous characterizations at salinities 20-40 (Liu et al., 2011) and 0 (Lai et al., 2016, 2017). However, other uncertainties associated to Mosley's characterization remained unaccounted, namely the (i) interpolation of unknown TRIS buffer pH values, (ii) the interpretation of TRIS/HCl ionic strength as salinity in the salinity range 0.06-2, and (iii) the restriction of experimental data to 298.15 K. Due to a lack of more reliable experimental data, it was previously impossible to estimate the accuracy of

the mCP model by Douglas and Byrne (2017b), which covers the full salinity (0-40) and temperature (278.15 – 308.15 K) range.

Another uncertainty associated to spectrophotometric pH measurements in the Baltic Sea arose from high loads of **dissolved organic matter (DOM) and hydrogen sulfide (H₂S)** that might disturb the method (see Theory: Disturbance of spectrophotometric pH determination), but have never been included in any testing.

Scope

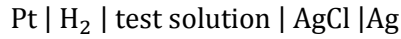
Focus 2 aims at establishing the scientific basis for traceable pH measurements in brackish waters. This includes the characterization of TRIS buffer solutions in artificial seawater (ASW) for salinities 5 to 20 by Harned cell measurements, as well as a consistent determination of the dissociation behavior of mCP in those buffers. Further, tests for the robustness of spectrophotometric pH measurements to DOM and H₂S are introduced. Implications of this fundamental chemical characterization work for the development of an automated spectrophotometric pH measurement system, based on a flow injection analysis (FIA) approach, are addressed.

Theory

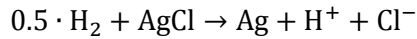
Electrochemical pH measurements with so called hydrogen electrodes or Harned cells (cells without liquid junction) represent a primary method for pH determination according to current IUPAC recommendations (Buck et al., 2002). Primary pH standards (buffer solutions) can be determined from measurements with such cells. However, Harned cell measurements are not suitable for the direct analysis of seawater samples, because the bubbling with pure hydrogen (H₂) gas would purge CO₂ out of the sample and thereby increase its pH. Furthermore, Harned cell measurements are laborious and require several days for a single measurement run. Therefore, the calibration of secondary methods by the use of primary standards is required, which establishes traceability to the primary method by an unbroken chain of comparisons.

Harned cells as a primary method for pH determination

Harned cells contain a platinum (Pt) electrode in contact with constantly bubbled pure hydrogen gas and a silver silver-chloride (Ag|AgCl) reference electrode. The cells are defined by (Buck et al., 2002; Dickson et al., 2015):



The cell reaction is:



The application of the Nernst equation to this cell reaction yields the electromotive force E:

$$E = E^\circ - \frac{RT}{F} \cdot \ln \left(\frac{b_{\text{H}^+} \cdot b_{\text{Cl}^-}}{(b^\circ)^2} \right) - 2 \frac{RT}{F} \ln(\gamma_{\pm, \text{HCl}}) \quad (15)$$

where E° is the standard electrode potential, b_{Cl^-} and b_{H^+} are the molalities of chloride and hydrogen ions, b° is the standard molality ($1 \text{ mol} \cdot \text{kg}^{-1}$), $\gamma_{\pm, \text{HCl}}$ is the mean activity coefficient of HCl, T is the temperature in K, R is the gas constant ($8.314 \text{ J} \cdot \text{mol}^{-1} \cdot \text{K}^{-1}$), and F is the Faraday constant ($96485.333 \text{ A} \cdot \text{s} \cdot \text{mol}^{-1}$).

To derive some kind of pH information from eq. 15, measurements are performed on two types of test solutions:

- (1) A dilution series of HCl solutions to estimate the standard potential E°
- (2) Buffer/HCl solutions to estimate E

For measurements of test solutions (1) and (2) prepared in artificial seawater (ASW) media two complications arise: First, it is not possible to estimate activity coefficients according to the Bates-Guggenheim convention, because of the high ionic strength of seawater. Secondly, Hydrogen ions react with sulfate ions in seawater to form hydrogen sulfate ions. To circumvent those limitations, it is convenient to **define pH in seawater based on the total hydrogen ion molality ($b_{\text{H}^+}^*$)**, rather than based on activities:

$$b_{\text{H}^+}^* = b_{\text{H}^+} + b_{\text{HSO}_4^-} \quad (16)$$

For the determination of $b_{\text{H}^+}^*$, test solutions (1) and (2) are prepared in ASW solutions of identical ionic strength (nominal salinity), which is achieved by replacing an equivalent amount of the ASW salts (NaCl, KCl, CaCl_2 , MgCl_2 , Na_2SO_4) by HCl or buffer/HCl, respectively. This procedure finally allows to determine pH_T defined on an amount content basis (moles per kilogram solution) according to:

$$\text{pH}_T = \frac{E_{\text{ASW}/\text{buffer}} - E^{*\circ}}{\frac{RT \ln 10}{F}} + \log_{10} \left(\frac{b_{\text{Cl}^-}}{b^\circ} \right) - \log_{10}(\omega_{\text{H}_2\text{O}}) \quad (17)$$

where $E_{\text{ASW}/\text{buffer}}$ is the electric Harned cell potential of the buffered seawater solution (test solution 2), $E^{*\circ}$ is the standard potential of the Ag|AgCl electrode in pure seawater

medium, and $\omega_{\text{H}_2\text{O}}$ is the specific water content of the ASW solution defined as mass water per mass solution. The $\omega_{\text{H}_2\text{O}}$ -term in eq. 17 converts the concentration scale from moles per kg water to moles per kg solution. An excellent summary of the derivation of eq. 17 from eq. 15 including required assumptions is given in Dickson et al. (2015).

$E^{*\circ}$ in eq. 17 needs to be determined at each salinity by measuring the cell potential $E_{\text{ASW/HCl}}$ of ASW solutions with varying HCl molalities (test solution 2) and extrapolating to zero HCl molality:

$$E^{*\circ} = \lim_{\text{HCl} \rightarrow 0} \left(E_{\text{ASW/HCl}} + \frac{RT \ln 10}{F} \cdot \log_{10} \left(\frac{b_{\text{HCl}} \cdot b_{\text{Cl}^-}}{(b^\circ)^2} \right) \right) \quad (18)$$

A fundamental shortcoming of Harned cell pH measurements in ASW solutions is the **unaccounted change in $\gamma_{\pm, \text{HCl}}$** (eq. 15) between test solutions (1) and (2), due to differences in the solution composition. Though the effect is assumed to be in the order of only a few thousandths of pH (Nemzer and Dickson, 2005), correct pH_T values can only be assigned after correction of the activity changes with results from seawater speciation models (Dickson et al., 2015; Turner et al., 2016), which do not yet meet the required quality criteria. However, when buffer pH_T values are determined at different buffer concentrations, calibration quantities determined in those buffers can be extrapolated to zero buffer concentration. In this case, the extrapolated quantity refers exactly to the hydrogen ion concentration scale defined for the specific composition of the ASW solution. This procedure has been recommended, but not been performed for any pH measurement technique. One calibration quantity to which this refers is the dissociation behavior of pH indicator dyes for spectrophotometric measurements.

Spectrophotometric pH measurements

Spectrophotometric pH measurements rely on the addition of a pH-sensitive indicator dye to a water sample. A suitable dye for seawater applications is the diprotic acid **meta-Cresol purple (mCP)**, because the negative decadic logarithm of the second dissociation constant, $\text{p}K_2$, is in the pH range typical for seawater (Clayton and Byrne, 1993). The sample pH relates to the ratio of the concentrations of the deprotonated (I^{2-}) and the monoprotinated (HI^-) species of mCP, according to:

$$\text{pH} = \text{p}K_2 + \log_{10} \left(\frac{[\text{I}^{2-}]}{[\text{HI}^-]} \right) \quad (19)$$

The concentration ratio $[\text{I}^{2-}] / [\text{HI}^-]$ can be determined by absorbance measurements, because HI^- and I^{2-} have two clearly distinguishable absorbance maxima (Fig. 8) at wavelength $\lambda_1 = 434 \text{ nm}$ and $\lambda_2 = 578 \text{ nm}$, respectively (Clayton and Byrne, 1993). Due to

overlapping absorbance spectra of both species, the total absorbance A_λ at both wavelengths needs to be expressed as the added absorbance contributions, $A_\lambda(I^{2-}) + A_\lambda(HI^-)$, according to the Lambert-Beer law:

$$A_\lambda = \{\varepsilon_\lambda(HI^-) \cdot [HI^-] + \varepsilon_\lambda(I^{2-}) \cdot [I^{2-}]\} \cdot d \quad (20)$$

where $\varepsilon_\lambda(X)$ are the molar extinction coefficients of the indicator species X at wavelength λ , and d is the cuvette length.

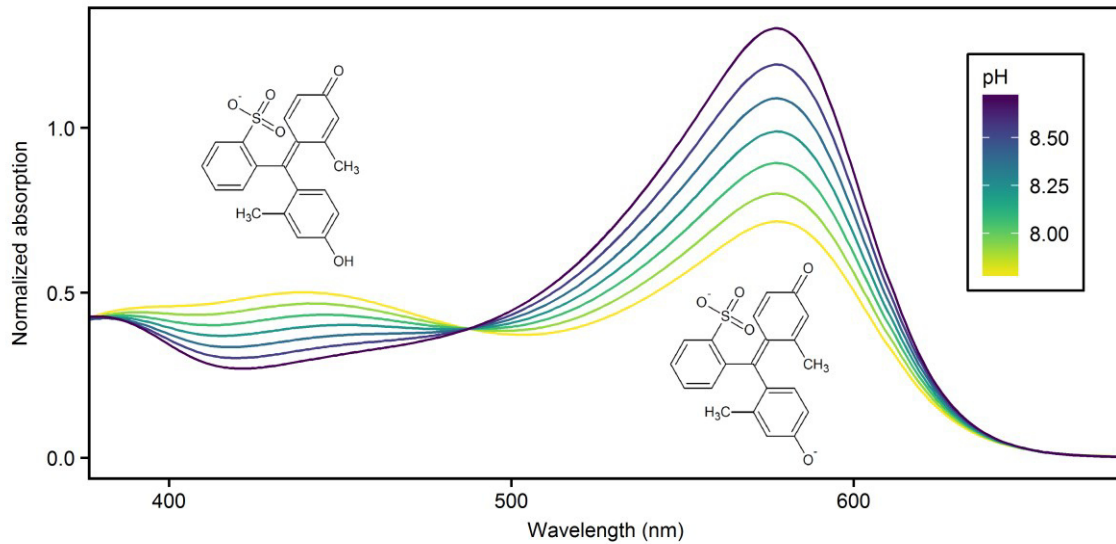


Fig. 8: Absorbance spectra of mCP as a function of pH at salinity 20. Spectra are normalized to the absorption at the isosbestic wavelength (488nm). The peak absorbances of HI^- and I^{2-} occur at 434 and 578 nm, respectively. Molecular structures of both protonation species are shown next to the respective absorbance peaks.

The pH of the solution can be expressed from a combination of eqs. 19 and 20 as:

$$pH = pK_2 + \log_{10} \left(\frac{R_A - e_1}{e_2 - e_3 \times R_A} \right) \quad (21)$$

where $R_A = A_{578} / A_{434}$ is the ratio of the absorbance measured at the two peak wavelengths and $e_1 = \varepsilon_{578}(HI^-) / \varepsilon_{434}(HI^-)$, $e_2 = \varepsilon_{578}(I^{2-}) / \varepsilon_{434}(HI^-)$ and $e_3 = \varepsilon_{434}(I^{2-}) / \varepsilon_{434}(HI^-)$ are the molar absorptivity ratios (Clayton and Byrne, 1993; Mosley et al., 2004).

The molar absorptivity ratio e_2 and e_3 includes molar extinction coefficients of both mCP species, HI^- and I^{2-} . Therefore, their determination would require the combination of separate measurements obtained in high and low pH solutions. Liu et al. (2011) avoided this by rearranging eq. 21 to:

$$pH = pK_2 e_2 + \log_{10} \left(\frac{R_A - e_1}{1 - \frac{e_3}{e_2} \times R_A} \right) \quad (22)$$

The salinity and temperature dependence of the term pK_{2e_2} can be determined from measurements in buffer solutions with a known pH, provided that e_1 and e_3/e_2 are known. The determined pK_{2e_2} term refers to the same pH scale assigned to the buffer, i.e., the total scale.

It was demonstrated that it is essential to use chromatographically **purified indicator dye** to achieve pH measurements of highest analytical quality (Liu et al., 2011). Purified mCP is currently only available in small quantities from a few research groups and not commercially produced. For measurements with non-purified dye spectral corrections are required (Douglas and Byrne, 2017a, 2017b), which have not yet been tested for the conditions in the Baltic Sea.

Potential disturbance of spectrophotometric pH measurements

Disturbance of spectrophotometric pH determinations could result from any difference in the solution composition between the buffered ASW solutions used for the pK_{2e_2} determination and the real seawater sample. One such difference is the **absence of the buffer component in the real seawater sample**. However, this difference is taken into account by extrapolating determined pK_{2e_2} values to zero buffer concentration. This requires that well-characterized dilution series of buffer solutions are available, which was previously the case only at salinity 35.

Another source of uncertainty is the occurrence of substances in natural seawater that are not included in the buffered ASW solutions. In regard to the **presence of DOM and H₂S** (which refers also to its dissociation products HS⁻, S²⁻, and polysulfides), spectral disturbances need to be expected from chromophoric dissolved organic matter (CDOM), the fraction of DOM that absorbs light in the UV and visible spectrum (Coble, 2007). Furthermore, molecular interactions between DOM/H₂S and mCP could alter the behavior of the dye.

Approach and results

pH_T of TRIS buffered ASW solutions

Müller et al. (subm.) performed Harned cell measurements on 2-amino-2-hydroxymethyl-1,3-propanediol (TRIS) buffered artificial seawater solutions in cooperation with the national metrological institute Physikalische-Technische Bundesanstalt (PTB), Braunschweig, Germany. Buffer solutions were prepared at salinities 5, 10, 15, 20, and 35 with TRIS/TRIS·H⁺ molalities of 0.01, 0.025, and 0.04 mol·kg-H₂O⁻¹. HCl solutions in ASW

with identical salinities were produced in the molality range of 0.005 - 0.05 mol·kg-H₂O⁻¹ to determine the standard potential of the Harned cell, E^{*°}. Measurements were performed in the temperature range 273.15 – 318.15 K.

At each target salinity, all solutions had to be prepared with identical ionic strength to achieve comparability between the potentials measured in the buffer solutions and the determined standard potential. This required reducing the total amount of ASW salts, by the amount of TRIS/HCl added. In previous experiments at higher salinities this was achieved by replacing only NaCl. However, at low salinities this would result in solution compositions with very little to zero NaCl content. To circumvent this, Müller et al. (subm.) achieved constant ionic strength by a **proportional reduction of all seawater salts**. This achieved constant cation ratios, but came at the expense of variable concentrations of total sulfate, $b_{\text{SO}_4^{2-},T}$. The resulting difference in $b_{\text{SO}_4^{2-},T}$ between the pure ASW solutions, for which E^{*°} is determined, and the TRIS containing solutions was corrected according to:

$$\Delta\text{pH}_T = \log_{10} \left(1 + \frac{b_{\text{SO}_4^{2-},T}(\text{HCl})}{K_{\text{HSO}_4^-}} \right) - \log_{10} \left(1 + \frac{b_{\text{SO}_4^{2-},T}(\text{TRIS})}{K_{\text{HSO}_4^-}} \right) \quad (23)$$

where $K_{\text{HSO}_4^-}$ is the dissociation constant of hydrogen sulfate calculated as a function of temperature and salinity according to Dickson (1990).

Obtained pH_T data were combined with results from a previous study covering salinities from 20 to 40 (DeValls and Dickson, 1998). Excellent agreement of both data sets with deviations <0.003 was found at salinity 20 and 35, which is within the extended measurement uncertainty of the method. A model expressing pH_T as a function of salinity, TRIS/TRIS·H⁺ molality and temperature was fitted to the combined data set:

$$\text{pH}_T = f \left\{ \left[(1 + S + S^2 + S^3) \cdot \left(1 + T + \ln(T) + \frac{1}{T} \right) \right] + \left[(b_{\text{TRIS}/\text{TRIS}\cdot\text{H}^+} + b_{\text{TRIS}/\text{TRIS}\cdot\text{H}^+}^2) \cdot (1 + S + T + S \cdot T) \right] \right\} \quad (24)$$

The first part of eq. 24 includes a third order salinity polynomial and the physico-chemical expression of the temperature dependence of dissociation constants. The second part of eq. 24 accounts for the dependence of pH_T on the TRIS/TRIS·H⁺ molality. The fit was obtained by generalized linear modeling and insignificant terms were removed by stepwise variable selection. The resulting model and fitted coefficients are given in Müller et al. (subm.). The pH_T model (Fig. 9) differs from the observed pH_T data by not more than 0.004. Deviations from this pH_T model and that of DeValls and Dickson (1998), which covers the salinity range 20-40, are within 0.001. As this is within the expanded measurement

uncertainty of the method (~ 0.004), both models describe TRIS buffer pH_T equally well in the high salinity range.

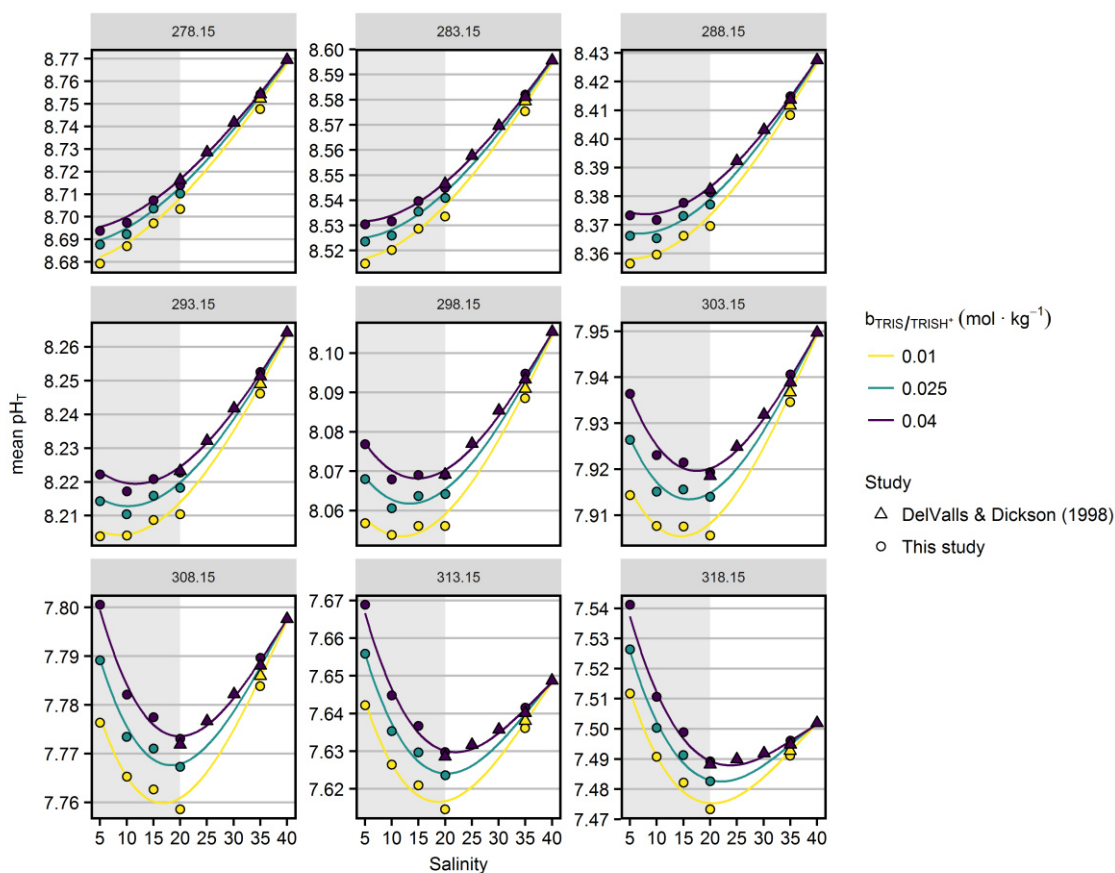


Fig. 9: Mean pH_T of TRIS buffer ASW solutions as a function of salinity, temperature in K (panels) and $\text{TRIS}/\text{TRIS}\cdot\text{H}^+$ molality according to Müller et al. (subm.). Lines indicate the pH_T model fitted to the combined data set including results from this study (circles, salinity range highlighted grey) and DelValls and Dickson (1998) (triangles).

The pH_T model of TRIS-buffered ASW solutions provided by Müller et al. (subm.) can be used to reliably calibrate pH instruments in the salinity range 5-40. At salinities 5-20 and 35, the reported dependency of TRIS pH_T on the buffer concentration allows extrapolation of calibration results to pure synthetic seawater conditions and thereby define a true hydrogen ion concentration scale in seawater media.

Characterization of the pH indicator dye m-Cresol Purple

Müller and Rehder (subm.) recorded absorption spectra of purified mCP in all TRIS buffered ASW solutions reported in the previous chapter. The buffer solutions were prepared and bottled by PTB in parallel to the solutions used for Harned cell

measurements. This concerted approach is the first of its kind and reduces pH uncertainty resulting from the preparation of buffer solutions (Nemzer and Dickson, 2005).

Measurements were performed at temperatures ranging from 278.15 – 308.15 K with a **spectrophotometric pH measurement system according to Carter et al. (2013)**. The system consisted of an Agilent 8453 diode array spectrophotometer (Santa Clara, US). The 10 cm, cylindrical, jacketed, flow-through cuvette (custom made by Hellma Analytics, Müllheim, Germany) was temperature-controlled by flushing the mantle with water supplied from a Julabo F30 heating circulator (Seelbach, Germany).

The determined pK_{2e_2} values were linearly extrapolated to zero TRIS/TRIS·H⁺ molality and therefore represent the first ever reported determination referring to an **exact definition of the hydrogen ion concentration scale without constraints**. The impact of TRIS/TRIS·H⁺ on pK_{2e_2} was found to depend on salinity and ranged from -0.004 at salinity 35 to 0.0012 at salinity 5 for the correction of values obtained in buffer solutions with a molality of 0.04 mol·kg-H₂O⁻¹.

The pK_{2e_2} results obtained by Müller and Rehder (subm.) were combined with previous results at higher and lower salinity reported by Douglas and Byrne (2017), Lai et al. (2016, 2017), and Liu et al. (2011). A pK_{2e_2} model similar to that for TRIS buffer pH_T values given in eq. 24, but without dependence on the TRIS/TRIS·H⁺ molality was fitted to the combined data set (Fig. 10). In the salinity range 5-20, the largest offset between the model fitted by Douglas and Byrne (2017) and that by Müller and Rehder (subm.) amounts to 0.013 at salinity 5 and 308.15 K. This agreement is surprisingly good, taking into account that the model of Douglas and Byrne (2017) relied on questionable data restricted to 298.15 K. It should be noted that the accuracy of the previous results could not have been assessed without the traceability to a primary pH standard achieved by the combined results of Müller et al. (subm.) and Müller and Rehder (subm.).

The results presented by Müller and Rehder (subm.) allow well-defined, traceable spectrophotometric pH measurements in the salinity range 5-40, without loss of quality in the salinity range 20-40. The salinity range that had to be bridged with the results of Mosley et al. (2004) to establish a full salinity pK_{2e_2} model was reduced from 0-20 (Douglas and Byrne, 2017b) to 0-5. However, at salinities <5 the model by Müller and Rehder (subm.) remains associated to the same uncertainties (see chapter: Background) as the model by Douglas and Byrne (2017b).

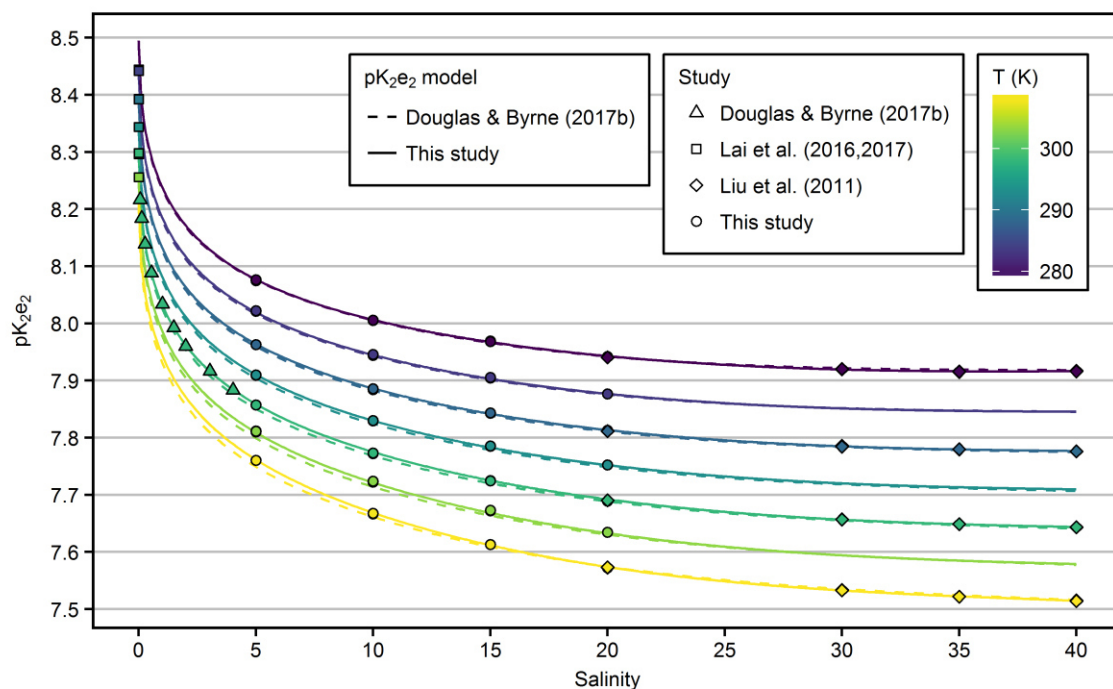


Fig. 10: pK_{2e_2} of mCP as a function of salinity and temperature. Results from this study (salinity: 5-20) were combined with previous results and fitted to a common pK_{2e_2} model (solid lines). Dashed lines represent the pK_{2e_2} model by Douglas and Byrne (2017b). Redrawn from Müller and Rehder (subm.).

A general limitation remains the unknown impact of **changes in the ionic composition of natural waters** on the molecular behavior of mCP. Such changes in ionic composition are small in ocean water, which was recognized as a prerequisite for spectrophotometric pH measurements by Clayton and Byrne (1993), who stated that “*the relative constancy of seawater composition throughout the world's ocean basins ... produce only small medium-induced changes in the physical-chemical characteristics of the indicator dyes*”. However, the constancy in composition decreases towards low salinity as a result of the variety of natural river water compositions (see Introduction: Baltic Sea). Taking this salinity anomaly (Feistel et al., 2009) and the strong dependence of pK_{2e_2} on salinity (Fig. 10) into account, it remains to be tested whether spectrophotometric pH measurement are the best method to determine pH in very low-saline waters. Approaches to approximate the sensitivity of the molecular properties of mCP on solution composition at constant ionic strength involve speciation models (Gallego-Urrea and Turner, 2017) and buffer experiments performed in variable ionic matrices.

The achieved extension of a traceable mCP characterization in brackish waters from a single temperature (Mosley et al., 2004) to the temperature range 278.15 – 308.15K (Müller and Rehder, subm.) allows performing **spectrophotometric pH measurements**

near in-situ temperature, which has two advantages: (i) The temperature correction required to calculate pH at in-situ temperature is small, thereby reducing the uncertainty associated to the CO₂ equilibrium constants (eqs. 5,6,7). This uncertainty related to the choice of equilibrium constants can exceed 0.01 for a temperature correction of 20 K, which is significantly larger than the uncertainty of spectrophotometric pH measurements at in-situ conditions. (ii) **Spectrophotometric pH measurement systems based on flow injection analysis (FIA)** determine pH in a constant flow of seawater. This requires measurements at in-situ temperature, because the equilibration time of the CO₂ system after warming a seawater sample by 20 K requires ~1 min. Such long equilibration times can hardly be realized in a flow-through approach due to difficulties to establish the temperature control. Accordingly, the temperature dependency of pK_{2e2} reported by Müller and Rehder (subm.) is a prerequisite for the successful application of the FIA spectrophotometric pH measurement system HydroFIA® (Kongsberg Maritime Contros) developed in the framework of EU BONUS PINBAL in the brackish waters of the Baltic Sea. More information concerning the development of this system, including the precision of the method, the correction of the dye pH-perturbation, and field testing results are available at the project homepage (www.io-warnemuende.de/pinbal-home.html).

Spectrophotometric pH measurements in the presence of hydrogen sulfide and dissolved organic matter

Müller et al. (2017) tested potential perturbations of spectrophotometric pH measurements with mCP by spike experiments performed with the pH measurement system according to Carter et al. (2013). Both tested substances, DOM and H₂S, represent acid-base systems and their addition to a seawater sample changes the pH of the solution. Therefore, the spike experiments were performed on two types of solutions:

- (1) Strongly buffered ASW solution, which did not change pH significantly upon spiking with the DOM containing stock solutions (pH stability within 0.005 was verified by potentiometric measurements).
- (2) Poorly buffered ASW solutions that changed pH upon spiking with DOM or H₂S stock solutions. Those measurements required comparison measurements with glass electrodes that were assumed to be undisturbed.

Müller et al. (2017) found no perturbations of spectrophotometric measurements for **H₂S** concentrations up to 400 µmol·kg⁻¹, which reflect high levels such as those reported from the Baltic and the Black Sea. Likewise, natural **DOM**, represented in this study by humic and fulvic acids extracted from the Suwannee river in the United States, did not interfere with the method at concentrations typical for oceanic environments and large estuarine

systems. However, high-DOM concentrations representing conditions like in black water rivers of the South American rain forest, caused pH values that were up to tenths of pH units too low. The reason for those deviations, which were found only for the Carter system equipped with a 10 cm cuvette, were spectral disturbances (Fig. 11). The spectral disturbances were due to low light intensities at the detector, caused by the added absorption of DOM. DOM absorbs light primarily in the low wavelength range of the visible spectrum. The observed overestimation of the absorbance therefore affected the absorbance of the acidic species of mCP at 434 nm. The spectral disturbance was less pronounced when operating the instrument with a strong light source (deuterium lamp) in the short wavelength range. The finding must thus be considered instrument-specific. Molecular interactions were excluded as a cause, because no perturbations were observed for measurements with the HydroFIA® pH measurement system (Aßmann et al., 2011), which has a cuvette length of 1 cm and a proportionally higher ratio of dye absorbance to DOM absorbance.

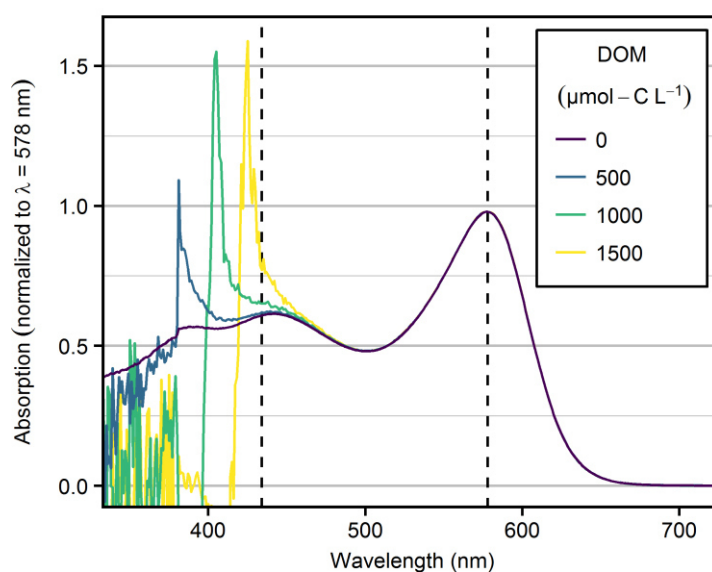


Fig. 11: Normalized absorption spectra of m-Cresol purple in TRIS buffer solutions as a function of the DOM concentration (color, 0-1500 $\mu\text{mol-C L}^{-1}$). The spectral disturbance at high DOM concentration are instrument-specific and occur when light intensities at the detector are very low.

Furthermore, Müller et al. (2017) found that the pH disturbance can be eliminated by switching to undisturbed wavelengths and calculate pH from the absorbances at 488 and 578 nm. Although this approach represents interesting options to circumvent also spectral perturbations by dye impurities, which affect the absorption at 434 nm (Douglas and Byrne, 2017a), the mCP absorption properties at 488 nm remain poorly characterized and can therefore currently not be used to compute accurate pH values. Müller et al. (2017)

therefore recommended to use strong light sources or short cuvette lengths when performing measurements on strongly absorbing solutions.

Conclusion

The traceability of spectrophotometric pH measurements to a primary pH standard was extended to brackish waters with salinities as low as 5. This was achieved by calibration experiments directly linking Harned cell and spectrophotometric measurements. The reported temperature dependence of the dissociation behavior of mCP allows determining pH near in-situ conditions, which is essential for measurements performed with a FIA approach. Combination with previous results allows for spectrophotometric pH measurements over the full salinity range from 0 to 40, without discontinuity and compromise compared to previous results at salinities higher 20. However, uncertainties remain due to uninvestigated changes of the ionic composition of natural waters occurring at very low ionic strength. The most suitable method to determine pH at salinities well below 5 needs to be identified.

The achieved molecular characterization of mCP forms the foundation for pH measurements in most parts of the Baltic Sea, irrespective of the presence of DOM or H₂S. This opens the road towards the implementation of a regular acidification monitoring in brackish waters. A spectrophotometric pH measurement system (HydroFIA®) was developed in cooperation with an industry partner and will be launched in 2018.

Remaining practical tasks include the rigorous comparison of commercial systems available at the market and ensuring the access to sufficient amounts of purified dye or a validated correction procedure for impurities.

Focus 3: Impact of acidification and fluctuating pH conditions on calcification

Background

Ocean acidification impairs physiological conditions for marine calcifying organisms on a global average (Kroeker et al., 2010). Although alkalinity changes counteracted the CO₂-induced acidification in the Baltic Sea over the past 20 years (Müller et al., 2016), this trend may stop or even reverse in future times (Focus 1). Accordingly, it is important to understand the response of marine organisms and ecosystems to ocean acidification in order to anticipate potential changes. Many studies investigated organism performance under current and future pH levels. However, the vast majority of these studies did not take into account that pH and other **CO₂ system parameter fluctuate on shorter time scales**, e.g., with seasonal (Fig. 1) and diurnal frequencies (Hofmann et al., 2011; Wahl et al., 2016). Such regular pH fluctuations can result from the metabolic activity of organisms, e.g., the switch between net photosynthesis and respiration during day- and nighttime, respectively. Photosynthesis improves calcification conditions by removing CO₂ from seawater. In coastal benthic ecosystems primary producers like macroalgae often form dense meadows with high biomass and induce intense diurnal pH fluctuations. Many calcifying organisms like mussels are located directly in or nearby these macroalgae stands. However, little was known about the amplitude of those CO₂ system fluctuations in typical benthic habitats of the Baltic Sea and the **capability of calcifiers to shift calcification activity to time windows of more favorable conditions**.

Scope

Focus 3 aims at the quantification of CO₂ system fluctuations in coastal benthic ecosystems of Kiel fjord in the Baltic Sea. Furthermore, the impact of such fluctuations on calcification rates of benthic calcifiers was investigated at three experimental scales and under current and future CO₂ scenarios.

Approach and results

pH variability in benthic coastal ecosystems

Saderne et al. (2017) placed state-of-the-art $p\text{CO}_2$ sensors on a mussel patch located in the middle of a seagrass meadow (*Zostera marina*) to obtain a high-resolution time series of CO_2 system parameters over a two-month period in late summer 2013. A site-specific alkalinity-salinity relationship was derived from discrete water samples. This A_T -S relation allowed the reconstruction of an A_T time series from continuous salinity data, also taking into account A_T contributions from dissolved organic material (Kuliński et al., 2014). From the $p\text{CO}_2$ and A_T time series, in combination with salinity and temperature data, other CO_2 system parameters were computed with high temporal resolution for the entire study period (Fig. 12).

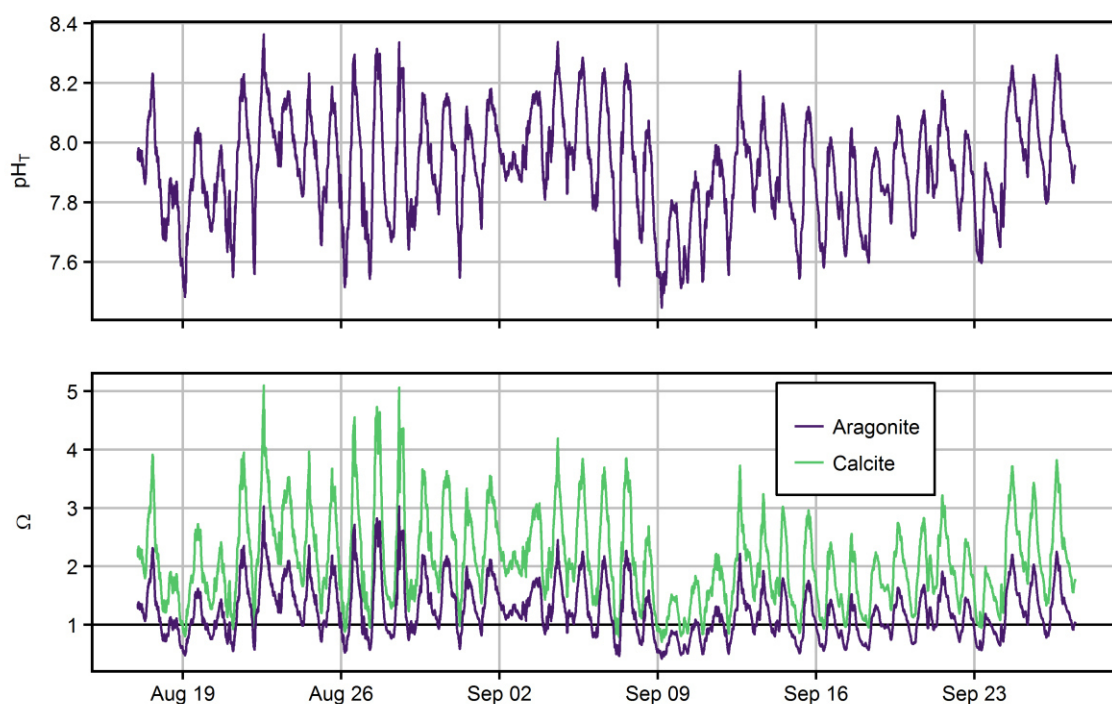


Fig. 12: Time series of CO_2 system parameters in a seagrass habitat in Kiel fjord in August/September 2013: (A) pH_T and (B) saturation states for aragonite and calcite with the dissolution threshold $\Omega = 1$ highlighted by a horizontal line. Redrawn from Saderne et al. (2017).

The authors found **pH_T amplitudes of up to 0.8 day^{-1}** within the seagrass meadow (Fig. 12). Corrosive conditions for calcium carbonates ($\Omega < 1$) centered on sunrise. Undersaturation for calcite occurred only sporadically, but amounted to 5.7 - 8.8 h per day for aragonite. In addition, Saderne et al. (2017) estimated that mussels experience conditions limiting calcification for 12 - 15 h per day, based on a carbonate ion

concentration threshold of $80 \mu\text{mol}\cdot\text{kg}^{-1}$ below which biomineralization rates were found to decline rapidly (Thomsen et al., 2015). However, whether undersaturation or another threshold value is the most appropriate descriptor for adverse calcification conditions remains a subject of ongoing discussions and research.

Above stands of another macrophyte species, the brownalgae *Fucus spec.*, Saderne et al. (2013) and Wahl et al. (2018) found slightly higher diurnal pH_T amplitudes (>1) compared to seagrass meadows. In addition to fluctuations, Wahl et al. (2018) reported an increase of the overall mean pH in macrophyte habitats by up to 0.3, but highlighted that the impact of macrophytes on the seawater CO_2 system is sensitive to the ratio of biomass to the volume of the affected water body, and therefore depends on weather and current conditions.

Relevance of pH fluctuations for calcifying organisms

Wahl et al. (2018) focused on the relevance of diurnal fluctuations for the calcification of the blue mussel *Mytilus edulis*. Therefore, calcification rates were determined by **laboratory, mesocosm and field studies**. With increasing experimental scale, natural conditions are better reflected, however, at the cost of less experimental control, e.g., food supply. In the laboratory experiments individual macroalgae were placed in a sequence of five aquaria connected in a flow through system. Preconditioned water sampled from those aquaria represented conditions from the outside to the inside of a macroalgae meadow. The 12 mesocosm units permanently installed at the Geomar pier in Kiel fjord have a volume of 1500 L each and can host entire groups of species to rebuild benthic ecosystems. Details of the mesocosm set-up are given in Wahl et al. (2015). In both experiments, laboratory and mesocosms, the background CO_2 content was manipulated to establish current and future CO_2 conditions. Diurnal pH amplitudes were created by the macrophytes. From both experimental set-ups water samples were taken at the end of day and night periods, respectively. Mussels were incubated in those water samples and the calcification was determined from the decrease in alkalinity during incubation. In both set-ups, Wahl et al. (2018) found that biogenic pH modulation allowed mussels to maintain high calcification rates during daytime, even under acidified conditions, whereas calcification decreased significantly during night time and acidified conditions (Fig. 13). Improved calcification conditions by macrophyte activity during daytime can therefore be considered temporal acidification refugia for calcifiers.

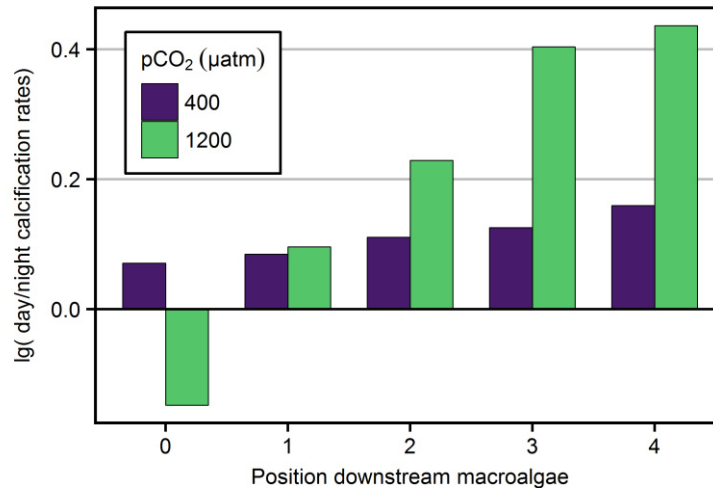


Fig. 13: Differences between calcification rates at day and night time under acidified (green) and non-acidified (purple) conditions in a laboratory experiment. The ratio of day-to-night calcification is expressed as log response ratio where a value of 1 means that calcification is 10 times stronger during daytime. It should be noted that the trends under high pCO₂ conditions are mainly due to a decrease of absolute calcification rates at night. Redrawn from Wahl et al. (2018).

In the field experiments, 35-days growth rates of mussel were determined as the increase in shell length and compared between macroalgae and sandy habitats. Background CO₂ concentrations were not manipulated. During the survey period, neither mean pH nor pH amplitudes differed among habitats, likely because the selected habitat patches with a size of only 1-2 m² were too small to achieve a sufficient biomass to water volume ratio. Accordingly, mussel growth rates did not differ inside and outside the macroalgae meadows. These findings indicate that the importance of calcification time windows created by macrophytes in natural habitats requires more investigations to better understand the importance of site-specific properties, like currents and the density and size of the macroalgae meadows.

Conclusion

In dense algae or seagrass habitats, macrophytes may reduce the impact of ocean acidification on mussel calcification by raising mean pH and providing temporal refuge from acidification stress. Therefore, the protection of coastal macroalgal habitats - which are increasingly endangered by various pressures such as coastal construction or eutrophication - might be considered as an additional measure to mitigate negative impacts of ocean acidification on marine benthic calcifiers, apart from the required reduction of anthropogenic CO₂ emissions as its primary cause.

Summary and outlook

This thesis highlights that the ocean acidification paradigm, though valid for the surface waters of the open ocean, cannot be applied to coastal areas like the Baltic Sea. Two major differences of the functioning of the Baltic Sea CO₂ system were presented: (i) The alkalinity increased over the past two decades, at rates high enough to significantly buffer changes in the CO₂ system anticipated for the uptake of anthropogenic CO₂. (ii) The magnitude of pH fluctuations on several spatio-temporal scales was found to be orders of magnitude larger than potential long-term ocean acidifications trends. It was shown that such pH fluctuations caused by macroalgae in shallow benthic habitats can create temporal acidification refugia with improved conditions for nearby calcifiers.

The limited understanding of the processes controlling alkalinity trends and pH fluctuations prevents a reliable prediction of the combined impact of such drivers on the acid-base system of the Baltic Sea. Those shortcomings make a case for a high-quality pH monitoring with good spatio-temporal coverage, if we are to reliably track pH changes. The required quality criteria can currently only be achieved by automated spectrophotometric pH measurements. This study lays the foundation for the application of this method in brackish waters, which was achieved by a series of experiments including the characterization of primary pH buffer standards in the salinity range 5-20 by Harned cell measurements and the subsequent determination of the dissociation behavior of the pH indicator dye m-Cresol Purple. Experiments were performed at variable buffer concentrations, which allowed extrapolating the dissociation constant of mCP to pure artificial seawater conditions and represents the first access to measurements on a true total hydrogen ion concentration scale in seawater. Combination with previous results enables spectrophotometric pH measurements from river to ocean water and a large range of temperatures. Furthermore, the robustness of spectrophotometric pH measurements against hydrogen sulfide and dissolved organic matter was verified for the entire concentration range occurring in the Baltic Sea. In parallel to this fundamental chemical characterization effort, an automated spectrophotometric pH measurement system was developed in cooperation with an industry partner and will be launched in 2018.

The achievements of this thesis mean a reliable and meaningful pH monitoring in the Baltic Sea can start now. Aiming at the implementation of a monitoring networking, few remaining practical tasks should be tackled. Those include ensuring access to sufficient amounts of purified dye or providing an alternative correction procedure for impurities, and performing unbiased tests between the measurement systems available at the market. Finally, it

should be noted that the achievements of this study are strictly valid only for salinities as low as five. An unambiguous concept for pH determination, including the choice of the most appropriate pH scale, at lower ionic strength, or at least a comprehensive assessment of uncertainty, remains to be completed.

References

- Almén, A. K., Glippa, O., Pettersson, H., Alenius, P., and Engström-Öst, J. (2017). Changes in wintertime pH and hydrography of the Gulf of Finland (Baltic Sea) with focus on depth layers. *Environ. Monit. Assess.* 189. doi:10.1007/s10661-017-5840-7.
- Archer, D. (2005). Fate of fossil fuel CO₂ in geologic time. *J. Geophys. Res. C Ocean.* 110, 1–6. doi:10.1029/2004JC002625.
- Archer, D., and Brovkin, V. (2008). The millennial atmospheric lifetime of anthropogenic CO₂. *Clim. Change* 90, 283–297. doi:10.1007/s10584-008-9413-1.
- Aßmann, S., Frank, C., and Körtzinger, A. (2011). Spectrophotometric high-precision seawater pH determination for use in underway measuring systems. *Ocean Sci.* 7, 597–607. doi:10.5194/os-7-597-2011.
- Bach, L. T. (2015). Reconsidering the role of carbonate ion concentration in calcification by marine organisms. *Biogeosciences* 12, 4939–4951. doi:10.5194/bg-12-4939-2015.
- Bates, N. R., Astor, Y. M., Church, M. J., Currie, K., Dore, J. E., González-Dávila, M., et al. (2014). A time-series view of changing surface ocean chemistry due to ocean uptake of anthropogenic CO₂ and ocean acidification. *Oceanography* 27, 126–141. doi:http://dx.doi.org/10.5670/oceanog.2014.16.
- Bates, N. R., Best, M. H. P., Neely, K., Garley, R., Dickson, A. G., and Johnson, R. J. (2012). Detecting anthropogenic carbon dioxide uptake and ocean acidification in the North Atlantic Ocean. *Biogeosciences* 9, 2509–2522. doi:10.5194/bg-9-2509-2012.
- Beldowski, J., Löffler, A., Schneider, B., and Joensuu, L. (2010). Distribution and biogeochemical control of total CO₂ and total alkalinity in the Baltic Sea. *J. Mar. Syst.* 81, 252–259. doi:10.1016/j.jmarsys.2009.12.020.
- Buck, R. P., Rondinini, S., Covington, A. K., Baucke, F. G. K., Brett, C. M. A., Camoes, M. F., et al. (2002). Measurement of pH. Definition, standards, and procedures (IUPAC Recommendations 2002). *Pure Appl. Chem.* 74, 2169–2200. Available at: <http://www.degruyter.com/view/j/pac.2002.74.issue-11/pac200274112169/pac200274112169.xml> [Accessed October 2, 2014].
- Byrne, R. H. (2014). Measuring ocean acidification: new technology for a new era of ocean chemistry. *Environ. Sci. Technol.* 48, 5352–60. doi:10.1021/es405819p.
- Byrne, R. H., Mecking, S., Feely, R. a., and Liu, X. (2010). Direct observations of basin-wide acidification of the North Pacific Ocean. *Geophys. Res. Lett.* 37. doi:10.1029/2009GL040999.
- Caldeira, K., and Wickett, M. E. (2003). Anthropogenic carbon and ocean pH. *Nature* 425, 365.
- Carter, B. R., Radich, J. a., Doyle, H. L., and Dickson, a. G. (2013). An automated system for spectrophotometric seawater pH measurements. *Limnol. Oceanogr. Methods* 11, 16–27. doi:10.4319/lom.2013.11.16.
- Clayton, T. D., and Byrne, R. H. (1993). Spectrophotometric seawater pH measurements: total hydrogen results. *Deep Sea Res. Part I Oceanogr. Res. Pap.* 40, 2115–2129.

- Coble, P. G. (2007). Marine optical biogeochemistry: The chemistry of ocean color. *Chem. Rev.* 107, 402–418. doi:10.1021/cr050350+.
- DelValls, T. A., and Dickson, A. G. (1998). The pH of buffers based on 2-amino-2-hydroxymethyl-1,3-propanediol (“tris”) in synthetic sea water. *Deep Sea Res. Part I Oceanogr. Res. Pap.* 45, 1541–1554. doi:10.1016/S0967-0637(98)00019-3.
- Dickson, A. G. (1981). An exact definition of total alkalinity and a procedure for the estimation of alkalinity and total inorganic carbon from titration data. *Deep Sea Res. Part A. Oceanogr. Res. Pap.* 28, 609–623. doi:10.1016/0198-0149(81)90121-7.
- Dickson, A. G. (1990). Standard potential of the reaction $\text{AgCl(s)} + 1/2 \text{H}_2(\text{g}) = \text{Ag(s)} + \text{HCl(aq)}$, and the standard acidity constant of the ion HSO_4^- in synthetic sea water from 273.15 to 318.15 K. *J. Chem. Thermodyn.* 22, 113–127. doi:10.1016/0021-9614(90)90074-Z.
- Dickson, A. G., Afghan, J. D., and Anderson, G. C. (2003). Reference materials for oceanic CO₂ analysis: a method for the certification of total alkalinity. *Mar. Chem.* 80, 185–197. doi:10.1016/S0304-4203(02)00133-0.
- Dickson, A. G., Cam, M. F., Spitzer, P., Fisticaro, P., Stoica, D., Pawlowicz, R., et al. (2015). Metrological challenges for measurements of key climatological observables. Part 3: seawater pH. *Metrologica*.
- Dickson, A. G., Sabine, C. L., and Christian, J. R. (2007). *Guide to best practices for ocean CO₂ measurements*. PICES Special Publication 3.
- Doney, S. C., Fabry, V. J., Feely, R. A., and Kleypas, J. A. (2009). Ocean Acidification: The Other CO₂ Problem. *Ann. Rev. Mar. Sci.* 1, 169–192. doi:10.1146/annurev.marine.010908.163834.
- Douglas, N. K., and Byrne, R. H. (2017a). Achieving accurate spectrophotometric pH measurements using unpurified meta-cresol purple. *Mar. Chem.* 190, 66–72. doi:10.1016/j.marchem.2017.02.004.
- Douglas, N. K., and Byrne, R. H. (2017b). Spectrophotometric pH measurements from river to sea: Calibration of mCP for $0 \leq S \leq 40$ and $278.15 \leq T \leq 308.15$ K. *Mar. Chem.*, 1–6. doi:10.1016/j.marchem.2017.10.001.
- Dyrssen, D. (1993). The Baltic-Kattegat-Skagerrak Estuarine System. *Estuaries* 16, 446–452. doi:10.2307/1352592.
- Feistel, R., Weinreben, S., Wolf, H., Seitz, S., Spitzer, P., Adel, B., et al. (2009). Density and Absolute Salinity of the Baltic Sea 2006–2009. *Ocean Sci.* 6, 3–24. doi:10.5194/osd-6-1757-2009.
- Fonselius, S., and Valderrama, J. (2003). One hundred years of hydrographic measurements in the Baltic Sea. *J. Sea Res.* 49, 229–241. doi:10.1016/S1385-1101(03)00035-2.
- Friis, K., Körtzinger, A., and Wallace, D. W. R. (2003). The salinity normalization of marine inorganic carbon chemistry data. *Geophys. Res. Lett.* 30, 1–4. doi:10.1029/2002GL015898.
- Gallego-Urrea, J. A., and Turner, D. R. (2017). Determination of pH in estuarine and brackish waters: Pitzer parameters for Tris buffers and dissociation constants for m-cresol purple at 298.15 K. *Mar. Chem.*, 1–6. doi:10.1016/j.marchem.2017.07.004.
- Gustafsson, E., Wällstedt, T., Humborg, C., Mörth, M., and Gustafsson, B. G. (2014). External total alkalinity loads versus internal generation: The influence of nonriverine alkalinity sources in the Baltic Sea. *Global*

- Biogeochem. Cycles* 28, 1358–1370. doi:10.1002/2014GB004888.
- Håkanson, L., Andersson, M., and Rydén, L. (2003). "The Baltic Sea Basin: Nature, History, and Economy," in *Environmental Science: Understanding, protecting and managing the environment in the Baltic Sea Region*, eds. L. Rydén, P. Migula, and M. Andersson (Uppsala: Baltic University Press), 92–119.
- Helcom (1993). First assessment of the state of the coastal waters of the Baltic Sea. *Baltic Sea Environment Proceedings No. 54*. 1–160.
- Hjalmarsson, S., Wesslander, K., Anderson, L. G., Omstedt, A., Perttilä, M., and Mintrop, L. (2008). Distribution, long-term development and mass balance calculation of total alkalinity in the Baltic Sea. *Cont. Shelf Res.* 28, 593–601. doi:10.1016/j.csr.2007.11.010.
- Hofmann, G. E., Smith, J. E., Johnson, K. S., Send, U., Levin, L. a, Micheli, F., et al. (2011). High-frequency dynamics of ocean pH: a multi-ecosystem comparison. *PLoS One* 6, e28983. doi:10.1371/journal.pone.0028983.
- IPCC (2013). "Summary for Policymakers," in *Climate Change 2013: The Physical Science Basis. Contribution of Working Group I to the Fifth Assessment Report of the Intergovernmental Panel on Climate Change*, eds. T. F. Stocker, D. Qin, G. K. Plattner, M. Tignor, S. K. Allen, J. Boschung, et al. (Cambridge and New York: Cambridge University Press), 27.
- Kapsenberg, L., Alliouane, S., Gazeau, F., Mousseau, L., and Gattuso, J. P. (2017). Coastal ocean acidification and increasing total alkalinity in the northwestern Mediterranean Sea. *Ocean Sci.* 13, 411–426. doi:10.5194/os-13-411-2017.
- Kaushal, S. S., Likens, G. E., Pace, M. L., Utz, R. M., Haq, S., Gorman, J., et al. (2018). Freshwater salinization syndrome on a continental scale. *Proc. Natl. Acad. Sci.* doi:10.1073/pnas.1711234115.
- Kroeker, K. J., Kordas, R. L., Crim, R. N., and Singh, G. G. (2010). Meta-analysis reveals negative yet variable effects of ocean acidification on marine organisms. *Ecol. Lett.* 13, 1419–34. doi:10.1111/j.1461-0248.2010.01518.x.
- Kuliński, K., Schneider, B., Hammer, K., Machulik, U., and Schulz-Bull, D. (2014). The influence of dissolved organic matter on the acid–base system of the Baltic Sea. *J. Mar. Syst.* 132, 106–115. doi:10.1016/j.jmarsys.2014.01.011.
- Lai, C., DeGrandpre, M. D., Wasser, B. D., Brandon, T. A., Clucas, D. S., Jaqueth, E. J., et al. (2016). Spectrophotometric measurement of freshwater pH with purified meta-cresol purple and phenol red. *Limnol. Oceanogr. Methods* 14, 864–873. doi:10.1002/lom3.10137.
- Lai, C. Z., DeGrandpre, M. D., Wasser, B. D., Brandon, T. A., Clucas, D. S., Jaqueth, E. J., et al. (2017). Corrigendum to: Spectrophotometric measurement of freshwater pH with purified meta-cresol purple and phenol red: Freshwater pH with purified indicators (*Limnology and Oceanography: Methods*, (2016), 14, 12, (864-873), 10.1002/lom3.10137). *Limnol. Oceanogr. Methods* 15, 903. doi:10.1002/lom3.10210.
- Le Quéré, C., Andrew, R. M., Canadell, J. G., Sitch, S., Ivar Korsbakken, J., Peters, G. P., et al. (2016). Global Carbon Budget 2016. *Earth Syst. Sci. Data* 8, 605–649. doi:10.5194/essd-8-605-2016.
- Lenton, T. M., and Britton, C. (2006). Enhanced carbonate and silicate weathering accelerates recovery from fossil fuel CO₂ perturbations. *Global Biogeochem. Cycles* 20. doi:10.1029/2005GB002678.

- Liu, X., Patsavas, M. C., and Byrne, R. H. (2011). Purification and characterization of meta-cresol purple for spectrophotometric seawater pH measurements. *Environ. Sci. Technol.* 45, 4862–8. doi:10.1021/es200665d.
- Martz, T. R., Daly, K., Byrne, R., Stillman, J., and Turk, D. (2015). Technology for Ocean Acidification Research: Needs and Availability. *Oceanography* 25, 40–47. doi:10.5670/oceanog.2015.30.
- Millero, F. J. (2010). Carbonate constants for estuarine waters. *Mar. Freshw. Res.* 61, 139. doi:10.1071/MF09254.
- Millero, F. J., Feistel, R., Wright, D. G., and McDougall, T. J. (2008). The composition of Standard Seawater and the definition of the Reference-Composition Salinity Scale. *Deep Sea Res. Part I Oceanogr. Res. Pap.* 55, 50–72. doi:10.1016/j.dsr.2007.10.001.
- Mohrholz, V., Naumann, M., Nausch, G., Krüger, S., and Gräwe, U. (2015). Fresh oxygen for the Baltic Sea - An exceptional saline inflow after a decade of stagnation. *J. Mar. Syst.* 148, 152–166. doi:10.1016/j.jmarsys.2015.03.005.
- Mosley, L. M., Husheer, S. L. G., and Hunter, K. a. (2004). Spectrophotometric pH measurement in estuaries using thymol blue and m-cresol purple. *Mar. Chem.* 91, 175–186. doi:10.1016/j.marchem.2004.06.008.
- Mucci, A. (1983). The solubility of calcite and aragonite in seawater at various salinities, temperatures and one atmosphere total pressure. *Am. J. Sci.* 283, 780–799.
- Müller, J. D., Schneider, B., Aßmann, S., and Rehder, G. (2017). Spectrophotometric pH measurements in the presence of dissolved organic matter and hydrogen sulfide. *Limnol. Oceanogr. Methods.* doi:10.1002/lom3.10227.
- Müller, J. D., Schneider, B., and Rehder, G. (2016). Long-term alkalinity trends in the Baltic Sea and their implications for CO₂-induced acidification. *Limnol. Oceanogr.* 61, 1984–2002. doi:10.1002/lno.10349.
- Nemzer, B. V., and Dickson, A. G. (2005). The stability and reproducibility of Tris buffers in synthetic seawater. *Mar. Chem.* 96, 237–242. doi:10.1016/j.marchem.2005.01.004.
- Raymond, P. A., and Cole, J. J. (2003). Increase in the Export of Alkalinity from North America's Largest River. *Science* 301, 88–91. doi:10.1126/science.1083788.
- Saderne, V., Fietzek, P., and Herman, P. M. J. (2013). Extreme variations of pCO₂ and pH in a macrophyte meadow of the Baltic Sea in summer: evidence of the effect of photosynthesis and local upwelling. *PLoS One* 8, e62689. doi:10.1371/journal.pone.0062689.
- Saderne, V., Fietzek, P., Müller, J. D., Körtzinger, A., and Hiebenthal, C. (2017). Intense pCO₂ and [O₂] Oscillations in a Mussel-Seagrass Habitat: Implications for Calcification. *Biogeosciences Discuss.* doi:10.5194/bg-2017-351.
- Schneider, B., Eilola, K., Lukkari, K., Müller-Karulis, B., and Neumann, T. (2015). "Environmental Impacts — Marine Biogeochemistry," in *Second Assessment of Climate Change for the Baltic Sea Basin*, ed. The BACC II Author Team (Springer International Publishing), 337–361.
- Schneider, B., Gustafsson, E., and Sadkowiak, B. (2014). Control of the mid-summer net community production and nitrogen fixation in the central Baltic Sea: An approach based on pCO₂ measurements on a cargo ship. *J. Mar. Syst.* 136, 1–9. doi:10.1016/j.jmarsys.2014.03.007.

- Schneider, B., Kaitala, S., and Maunula, P. (2006). Identification and quantification of plankton bloom events in the Baltic Sea by continuous pCO₂ and chlorophyll a measurements on a cargo ship. *J. Mar. Syst.* 59, 238–248. doi:10.1016/j.jmarsys.2005.11.003.
- Schneider, B., Kaitala, S., Raateoja, M., and Sadkowiak, B. (2009). A nitrogen fixation estimate for the Baltic Sea based on continuous pCO₂ measurements on a cargo ship and total nitrogen data. *Cont. Shelf Res.* 29, 1535–1540. doi:10.1016/j.csr.2009.04.001.
- Schneider, B., and Müller, J. D. (2017). *Biogeochemical Transformations in the Baltic Sea: Observations Through Carbon Dioxide Glasses*. Springer International Publishing doi:10.1007/978-3-319-61699-5.
- Schneider, B., Nausch, G., and Pohl, C. (2010). Mineralization of organic matter and nitrogen transformations in the Gotland Sea deep water. *Mar. Chem.* 119, 153–161. doi:10.1016/j.marchem.2010.02.004.
- Sun, X., Mörrth, C., Humborg, C., and Gustafsson, B. (2017). Temporal and spatial variations of rock weathering and CO₂ consumption in the Baltic Sea catchment. *Chem. Geol.* doi:10.1016/j.chemgeo.2017.04.028.
- Thomsen, J., Haynert, K., Wegner, K. M., and Melzner, F. (2015). Impact of seawater carbonate chemistry on the calcification of marine bivalves. *Biogeosciences* 12, 4209–4220. doi:10.5194/bg-12-4209-2015.
- Turner, D. R., Achterberg, E. P., Chen, C.-T. A., Clegg, S. L., Hatje, V., Maldonado, M. T., et al. (2016). Toward a Quality-Controlled and Accessible Pitzer Model for Seawater and Related Systems. *Front. Mar. Sci.* 3, 139. doi:10.3389/fmars.2016.00139.
- Wahl, M., Buchholz, B., Winde, V., Golomb, D., Guy-Haim, T., Müller, J., et al. (2015). A mesocosm concept for the simulation of near-natural shallow underwater climates: The Kiel Outdoor Benthocosms (KOB). *Limnol. Oceanogr. Methods* 13. doi:10.1002/lom3.10055.
- Wahl, M., Saderne, V., and Sawall, Y. (2016). How good are we at assessing the impact of ocean acidification in coastal systems? Limitations, omissions and strengths of commonly used experimental approaches with special emphasis on the neglected role of fluctuations. *Mar. Freshw. Res.* 67, 25–36. doi:10.1071/MF14154.
- Wahl, M., Schneider Covachã, S., Saderne, V., Hiebenthal, C., Müller, J. D., Pansch, C., et al. (2018). Macroalgae may mitigate ocean acidification effects on mussel calcification by increasing pH and its fluctuations. *Limnol. Oceanogr.* 63, 3–21. doi:10.1002/lno.10608.
- Wanninkhof, R. (2014). Relationship between wind speed and gas exchange over the ocean revisited. *Limnol. Oceanogr. Methods* 12, 351–362. doi:10.4319/lom.2014.12.351.
- Wolf-Gladrow, D. A., Zeebe, R. E., Klaas, C., Körtzinger, A., and Dickson, A. G. (2007). Total alkalinity: The explicit conservative expression and its application to biogeochemical processes. *Mar. Chem.* 106, 287–300. doi:10.1016/j.marchem.2007.01.006.
- Zeebe, R. E., and Wolf-Gladrow, D. A. (2001). CO₂ in seawater: equilibrium, kinetics, isotopes. *Elsevier Oceanogr. Ser.* doi:10.1016/S0924-7963(02)00179-3.

Appendix

Curriculum vitae

Name Jens Daniel Müller
 Date of birth 5. Februar 1986, Berlin
 E-Mail jens.mueller@io-warnemuende.de
 www www.io-warnemuende.de/jens-mueller-en.html
 ORCID 0000-0003-3137-0883
 Twitter @Jens_D_Mueller



Education

Since 07 / 2014 PhD student
 Leibniz-Institute for Baltic Sea Research Warnemünde (IOW)
 Working group: Trace gas biogeochemistry and marine CO₂ system
 Supervisor: Prof. Dr. Gregor Rehder

09 / 2010 – 08 / 2012 M.Sc. Biological Oceanography
 GEOMAR Helmholtz Centre for Ocean Research Kiel
 Final grade: 1.2
 Masterthesis: Ecology of Chilean Mytilids
 Alfred-Wegener-Institut Bremerhaven
 Incl. 3 month dive expedition: Huinay Scientific Field Station, Patagonia, Chile

09 / 2009 – 08 / 2010 Biology (preparation for Master programme)
 Christian-Albrechts-Universität zu Kiel
 Average grade: 1.2

09 / 2008 – 08 / 2009 B.Sc. Chemistry
 Phillips-Universität Marburg
 Final grade: 1.7

09 / 2006 – 08 / 2008 Chemistry (Intermediate diploma)
 Humboldt-Universität zu Berlin
 Grade: 2.0

Skills and practical experience

Since 03 / 2011 Certified Scientific Diver
 >200 logged dives, dive mission leader, Nitrox-diver

09 / 2014 Summer Field Course
Cutting Edge Observational Technology in Marine Biogeochemistry
 Sven Lovén Centre for Marine Sciences, Tjärnö; Schweden

01 – 03 / 2014 Off-shore mesocosm experiment
 Led by GEOMAR Helmholtz Centre for Ocean Research Kiel
 Gran Canaria, Spain

09 – 10 / 2010 Summer School Benthic Ecology
 HCMR Heraklion, Crete, Greece

2010 – 2013 Numerous Cruises on Research Vessel and voluntary observing ships:

2010 – 2013	Numerous Cruises on Research Vessel and voluntary observing ships: Poseidon, Alkor, Heincke, Littorina, Polarfuchs, Elisabeth Mann-Borgese, VOS Finnmaid
03 / 2009	Internship German Research Centre for Geosciences (GFZ), Potsdam

Work experience

10 / 2013 – 03 / 2014	Scientific Employee GEOMAR Helmholtz Centre for Ocean Research Kiel Research Unit Benthic Ecology, Prof. Dr. M. Wahl & Research Unit Marine Biogeochemistry, Prof. Dr. U. Riebesell
07 – 10 / 2013	Sailing Instructor Kiel Marketing GmbH, Camp 24/7
01 – 03 / 2013	Divemaster Al Dive dive centre, Loubiere, Dominica
05 – 08 / 2010	Research Assistant GEOMAR Helmholtz Centre for Ocean Research Kiel Research Unit Evolutionary Ecology of Marine Fishes, Prof. Dr. T. Reusch

Scholarships and Awards

06 / 2017	Best poster presentation by newcomers, Baltic Sea Science Congress
02 / 2007 – 06 / 2012	Support from the Studienstiftung des Deutschen Volkes: Full Scholarship
01 – 03 / 2012	Short-term grant for masterthesis field work Patagonia, Chile
03 / 2010	Language course (english, advanced) Bath, England
09 / 2010	Sommerakademie (The Invisible Hand: Self-interest and Common Welfare) San Giovanni, Italy
07 / 2005	Book-price for extraordinary achievements during the Abitur

Additional Information

Language skills	German (native speaker) English (advanced) French (advanced) Spanish (beginner)
-----------------	--

Eigenständigkeitserklärung

Doktorandinnen/Doktoranden-Erklärung gemäß § 4 Absatz 1 Buchstaben g und h der Promotionsordnung der Mathematisch-Naturwissenschaftlichen Fakultät der Universität Rostock

Name: **Jens Daniel Müller**

Ich habe eine Dissertation zum Thema

Ocean Acidification in the Baltic Sea

Involved Processes, Metrology of pH in Brackish Waters, and Calcification under Fluctuating Conditions

an der Mathematisch-Naturwissenschaftlichen Fakultät der Universität Rostock angefertigt.

Dabei wurde ich von Herrn **Prof. Gregor Rehder** betreut.

Ich gebe folgende Erklärung ab:

1. Die Gelegenheit zum vorliegenden Promotionsvorhaben ist mir nicht kommerziell vermittelt worden. Insbesondere habe ich keine Organisation eingeschaltet, die gegen Entgelt Betreuerinnen/Betreuer für die Anfertigung von Dissertationen sucht oder die mir obliegenden Pflichten hinsichtlich der Prüfungsleistungen für mich ganz oder teilweise erledigt.
2. Ich versichere hiermit an Eides statt, dass ich die vorliegende Arbeit selbstständig angefertigt und ohne fremde Hilfe verfasst habe. Dazu habe ich keine außer den von mir angegebenen Hilfsmitteln und Quellen verwendet und die den benutzten Werken inhaltlich und wörtlich entnommenen Stellen habe ich als solche kenntlich gemacht.

Rostock, den 26.01.2018

Publications

The following publications are included in the appendix in the order of appearance:

Müller et al. (2016): Long-term alkalinity trends in the Baltic Sea and their implications for CO₂-induced acidification

Supplementary information are available at:

<http://onlinelibrary.wiley.com/doi/10.1002/lno.10349/full>

Müller et al. (subm.): pH Measurements in Brackish Waters: Extending the Electrochemical pH_T Determination of TRIS Buffers to Salinities 5 – 20

Supplementary information are attached

Müller and Rehder (subm.): pH Measurements in Brackish Waters: Experimental Characterization of Purified m-Cresol Purple for Spectrophotometric pHT Measurements

Supplementary information are attached

Müller et al. (2017): Spectrophotometric pH measurements in the presence of dissolved organic matter and hydrogen sulfide

Supplementary information are available at:

<http://onlinelibrary.wiley.com/doi/10.1002/lom3.10227/full>

Wahl et al. (2018): Macroalgae may mitigate ocean acidification effects on mussel calcification by increasing pH and its fluctuations

Long-term alkalinity trends in the Baltic Sea and their implications for CO₂-induced acidification

Jens Daniel Müller,* Bernd Schneider, Gregor Rehder

Department of Marine Chemistry, Leibniz Institute for Baltic Sea Research, Warnemünde, Germany

Abstract

Anthropogenic CO₂ emissions currently decrease open ocean pH, but on multi-millennial time scales intensified continental weathering is expected to contribute to increasing oceanic alkalinity (A_T) and thus mitigate the acidification signal. The Baltic Sea is an ideal study site for such A_T dynamics, due to its direct link to terrestrial processes, short water residence time and long history of A_T measurements dating back to the early 20th century. We compiled an extensive A_T data set that revealed the highest data quality and coverage for the past two decades. Within that period, surface water A_T levels increased throughout the Baltic Sea. The rates of change were highest in the low-saline, northern areas and decreased gradually toward constant levels in the North Sea. The A_T increase observed in the Central Baltic Sea ($+3.4 \mu\text{mol kg}^{-1} \text{yr}^{-1}$) and the Gulf of Bothnia ($+7 \mu\text{mol kg}^{-1} \text{yr}^{-1}$) has compensated CO₂-induced acidification by almost 50% and 100%, respectively. Further, the A_T trends enhanced the CO₂ storage capacity and stabilized the CaCO₃ saturation state of the Baltic Sea over the past two decades. We discuss the attribution of the A_T trends to potential changes in precipitation patterns, continental weathering driven by acidic rain and increasing atmospheric CO₂, agricultural liming and internal A_T sources.

Introduction

Alkalinity: global relevance and characteristics

Total alkalinity (A_T) is a measure of the acid-binding capacity of seawater. As one of four measurable parameters of the marine CO₂ system, A_T has gained increasing attention within the field of climate change research. The importance of A_T for the carbon cycle can be exemplified by its control over the CO₂ uptake and the pH of seawater. Currently, the oceans absorb around ~30% of the anthropogenic CO₂ released into the atmosphere (Khatiwala et al. 2013; Le Quéré et al. 2015), mainly due to equilibration between the atmosphere and the surface ocean mixed layer. The penetration of anthropogenic CO₂ into the ocean interior is controlled by the ocean circulation and today the ongoing process can be observed at locations where deep

water is formed, e.g. in the high latitudes of the North Atlantic (Lee et al. 2003). When the fossil fuel derived CO₂ will invade the entire ocean interior on millennial time scales, the share of the oceanic uptake will increase to around 80% (Archer and Brovkin 2008). The oceanic uptake of CO₂ is beneficial, because it counteracts the rising atmospheric CO₂ levels and thus mitigates global warming. However, it comes at the expense of decreasing seawater pH. This process, termed ocean acidification (Doney et al. 2009), is expected to have global and potentially detrimental impacts on marine ecosystems (Hofmann et al. 2010; Kroeker et al. 2010). When CO₂ dissolves in water, carbonic acid is formed and protons are released. The alkalinity of seawater determines the share of these protons that are neutralized and thereby controls the CO₂ uptake and the degree of acidification. For a given increase in atmospheric pCO₂, more anthropogenic CO₂ can be stored in seawater with higher A_T . Although more CO₂ could be taken up by high- A_T seawater, the degree of acidification would be smaller than at lower A_T . Knowledge about spatio-temporal A_T dynamics is thus crucial for a comprehensive understanding of the global carbon cycle and the impact of anthropogenic CO₂ emissions on the marine CO₂ system.

The exact definition of A_T , as the excess of proton acceptors over proton donors (Dickson et al. 2007), is expressed by:

*Correspondence: Jens.Mueller@io-warnemuende.de

Additional Supporting Information may be found in the online version of this article.

This is an open access article under the terms of the Creative Commons Attribution License, which permits use, distribution and reproduction in any medium, provided the original work is properly cited.

$$A_T = [\text{HCO}_3^-] + 2[\text{CO}_3^{2-}] + [\text{B}(\text{OH})_4^-] + [\text{OH}^-] + [\text{HPO}_4^{2-}] \\ + 2[\text{PO}_4^{3-}] + [\text{SiO}(\text{OH})_3^-] + [\text{NH}_3] + [\text{HS}^-] - [\text{H}^+]_F - [\text{HF}] \quad (1) \\ - [\text{HSO}_4^-] - [\text{H}_3\text{PO}_4] + [\text{minor bases} - \text{minor acids}]$$

where $[\text{H}^+]_F$ is the free concentration of hydrogen ions. This definition implies that A_T is a conservative quantity with respect to changes in temperature and pressure, although the share of the various alkalinity components can vary. As a conservative quantity, A_T behaves exactly like salinity (S) when two water parcels are mixed (Wolf-Gladrow et al. 2007). This is not the case for non-conservative parameters of the marine CO_2 system, like pCO_2 and pH , which do not necessarily obey linear mixing relationships. Further, A_T is not affected by the release or dissolution of CO_2 , because the A_T loss caused by the release of protons (H^+) from the dissociation of carbonic acid (H_2CO_3) is balanced by the gain from produced bicarbonate (HCO_3^-) and carbonate (CO_3^{2-}) ions. Among the components that contribute to A_T according to Eq. 1, the major share can be attributed to HCO_3^- and CO_3^{2-} that originate not from the A_T -neutral dissolution of CO_2 , but from riverine input of continentally weathered carbonate and silicate minerals. On oceanic scales this input is currently balanced by CaCO_3 formation, sedimentation and burial as ultimate sinks (Sarmiento and Gruber 2006).

Zooming in from oceanic to coastal systems

The open ocean surface A_T is surprisingly stable, which reflects the long water residence time of $\sim 10^5$ yr (Sundquist 1991; Sarmiento and Gruber 2006). Most of the variation in surface alkalinity can be attributed to precipitation and evaporation patterns (Millero et al. 1998; Jiang et al. 2014; Fry et al. 2015). Because A_T and salinity are affected similarly by these processes, the salinity normalized alkalinity ($nA_T = A_T \times 35/S$) shows remarkably little spatial variability in the subtropical gyres of the major ocean basins, e.g., $2291 \pm 4 \mu\text{mol kg}^{-1}$ (mean \pm SD) between 30°S and 30°N in the Atlantic (Millero et al. 1998; Friis et al. 2003). Likewise, the surface nA_T in the Northern Atlantic did not exhibit significant temporal changes over the past three decades (Bates et al. 2012). Based on this constant A_T background in the open ocean, acidification trends around $0.002 \text{ pH units yr}^{-1}$ can be predicted from future pCO_2 scenarios “without major uncertainties” (Doney et al. 2009). These predictions match well with the currently observed pH trends at seven globally distributed time-series stations (Bates et al. 2014).

However, on longer time scales the oceanic alkalinity is expected to increase. On millennial time scales (10^3 yr) anthropogenic CO_2 will acidify the ocean interior and thus lift the carbonate lysocline. The resulting dissolution of carbonate sediments is expected to increase oceanic A_T . On geological time scales (10^3 – 10^6 yr) increased terrestrial weathering rates may further contribute to rising oceanic A_T levels (Lenton and Britton 2006). This postulated alkalinity gain is expected to increase the share of anthropogenic CO_2

stored in the ocean to 90% (Archer and Brovkin 2008). However, it may not dampen ocean acidification occurring on shorter, centennial timescales.

In contrast to the subtropical open ocean, A_T – S relations in marginal seas are much more variable because processes like riverine alkalinity input, CaCO_3 formation and denitrification (Cai et al. 2010; Gustafsson et al. 2014; Jiang et al. 2014) superimpose on evaporation and precipitation effects. The dominant effect of riverine A_T input in marginal seas is typically reflected in linear A_T – S relationships:

$$A_T = A_{T,0} + a \times S \quad (2)$$

where $A_{T,0}$ corresponds to the river end-member alkalinity at $S = 0$, and a is the slope representing the alkalinity change per salinity unit. The direct link of coastal alkalinity to the riverine A_T input (which is in turn often impacted by anthropogenic activities) and the shorter residence time of alkalinity in coastal environments (which is basically equal to the water residence time) suggest that temporal changes in A_T – S relationships may occur on timescales similar to that of CO_2 -induced ocean acidification. A more comprehensive understanding of alkalinity dynamics in such systems is thus essential to extent climate change research into the coastal zone.

Focus on the Baltic Sea

The semi-enclosed Baltic Sea can be considered as one of the world’s largest estuaries. The brackish water system is an ideal study site for the investigation of alkalinity dynamics, due to the long history of biogeochemical studies including decades of alkalinity and salinity monitoring, a diverse, but well-defined bedrock structure in different parts of its large drainage basin and a variety of existing biogeochemical models. For this study we divide the Baltic Sea into five subareas, which accounts for the patterns of the surface A_T – S distribution (Beldowski et al. 2010). The geographical borders of the five subareas, which are the narrow Belt Sea and Kattegat region (Kat), Central Baltic Sea (Cen), Gulf of Bothnia (Bot), Gulf of Finland (Fin) and Gulf of Riga (Rig), are displayed in Fig. 1. The hydrography of the Baltic Sea is characterized by inflowing, high saline water from the North Sea that enters the deep basins of the Baltic Sea and generates a permanent halocline. The outflow of low-saline surface waters, caused by river-runoff and positive net precipitation, slightly exceeds the inflow. The mean salinity of the Baltic Sea shows decadal, large-scale variations of up to 1 salinity unit, but no long-term trend was found during the past century (Winsor et al. 2001, 2003). The surface salinity is controlled by the mixing of oceanic and river water and increases from a mean surface salinity around 3 in the northern-most part of the Gulf of Bothnia to around 10 in the south-western part of the Central Baltic (Fig. 1). A strong gradient to the oceanic salinity of ~ 35 exists in the Kattegat region. With exception of the Gulf of Riga, the

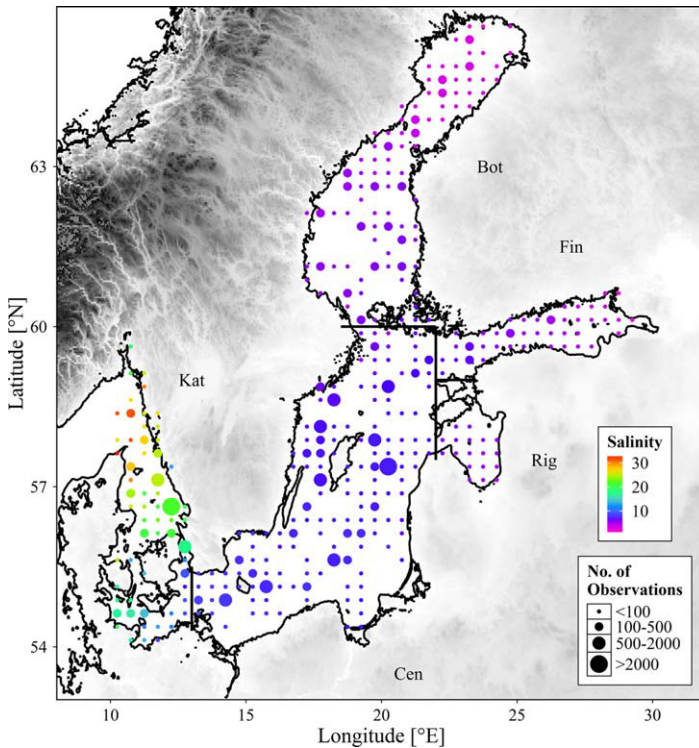


Fig. 1. Map of the Baltic Sea showing the spatial distribution of associated salinity and alkalinity observations. The geographical borders of the subareas Kattogat (Kat), Central Baltic Sea (Cen), Gulf of Bothnia (Bot), Gulf of Finland (Fin), and Gulf of Riga (Rig) that were assigned according to the hydrographical mixing regimes are indicated. The color scale represents the mean salinity and the point size the number of observations, both on a grid of 0.5° Lon and 0.25° Lat. The grey shading indicates the elevation of land above sea level.

surface A_T decreases with decreasing salinity (Fig. 2). However, different A_T - S signatures can be found in the surface waters of the various subareas, because the drainage basin composition – dominated by limestone in the south and granite in the northern parts – controls the $A_{T,0}$ levels in the river water. Linear A_T - S regimes exist in the three gulfs (Bot, Fin and Rig) and the Kattogat region (Fig. 2a), whereas the Central Baltic Sea is the “mixing chamber” of waters from the other areas and consequently shows no strictly linear A_T - S relation (Beldowski et al. 2010). During stagnation periods, A_T increases temporarily when anoxic conditions prevail below the halocline (Edman and Omstedt 2013). In anoxic bottom waters sulfate (SO_4^{2-}) is used as electron acceptor for the oxidation of organic material. This reaction produces sulfide (S^{2-}) that contributes two moles of A_T per mole of sulfate oxidized (Eq. 1), independent on the subsequent protonation of S^{2-} . However, under oxic conditions in the surface water, S^{2-} is reoxidized to SO_4^{2-} and the A_T increase is reversed. In addition to this reversible A_T contribution, recent modelling studies suggest that other significant internal A_T sources (e.g., denitrification) may exist in the Baltic Sea (Edman and Omstedt 2013; Gustafsson et al. 2014). Fur-

ther, it should be noted that planktonic calcifiers, which constitute the most important alkalinity sink in the oceanic environment, do not exist in the Baltic Sea (Tyrrell et al. 2008) except in the Kattogat area.

Due to its generally lower alkalinity the Baltic Sea is believed to be especially vulnerable to CO_2 -induced acidification. Indeed, for the current atmospheric pCO_2 increase ($+2 \mu\text{atm yr}^{-1}$) a slightly lower mean pH trend of -0.0019 yr^{-1} can be expected for the open ocean ($S = 35$, $T = 10^\circ\text{C}$, $A_T = 2300 \mu\text{mol kg}^{-1}$) compared to -0.0021 yr^{-1} in the Central Baltic Sea ($S = 7$, $T = 10^\circ\text{C}$, $A_T = 1650 \mu\text{mol kg}^{-1}$). However, the direct link to riverine A_T input (Hjalmarsson et al. 2008) and the short water residence time of around 20 yr (Helcom 1993) suggest that in the Baltic Sea significant A_T changes may occur on timescales similar to that of anthropogenic atmospheric pCO_2 perturbations (10–100 yr). This implies that a reliable acidification estimate cannot solely be based on the atmospheric pCO_2 evolution. Previous studies indeed suggested that the alkalinity in the eastern Gotland Sea increased by around $100 \mu\text{mol kg}^{-1}$ ($\sim 6\%$) from 1930 to 2010 (Schneider et al. 2015). Extensive A_T measurements were performed in the Baltic Sea region with investigations dating back to the early 20th century (Buch 1945; Hjalmarsson et al. 2008). Nevertheless, a comprehensive analysis of the A_T evolution in the Baltic Sea has not yet been performed. More detailed knowledge about past A_T changes in Baltic Sea is essential, e.g., to assess the anthropogenic, CO_2 -based acidification potential (Melzner et al. 2012), to validate modelling approaches of alkalinity dynamics (Kuznetsov and Neumann 2013; Gustafsson et al. 2014) and to obtain more reliable estimates for the Baltic carbon budget (Kuliński and Pempkowiak 2011; Gustafsson et al. 2015).

This work thus aims at:

- Detecting temporal A_T trends reflected in changes of the A_T - S relationship
- Quantifying the implications for CO_2 -induced acidification
- Attributing the detected A_T trends to biogeochemical drivers

Material and methods

The data handling, quality control, statistical analysis, and data visualization described in the following were performed with the statistical computing language R Version 3.1.1 (R Core Team 2014). The CO_2 system calculations were performed with the seacarb package (Lavigne et al. 2011), using the carbonate constants for estuarine waters (Millero 2010), K_W from Dickson and Riley (1979) and K_S from Dickson (1990).

Data compilation

To compile the most comprehensive data set of A_T observations from the Baltic Sea, we combined data from the following sources:

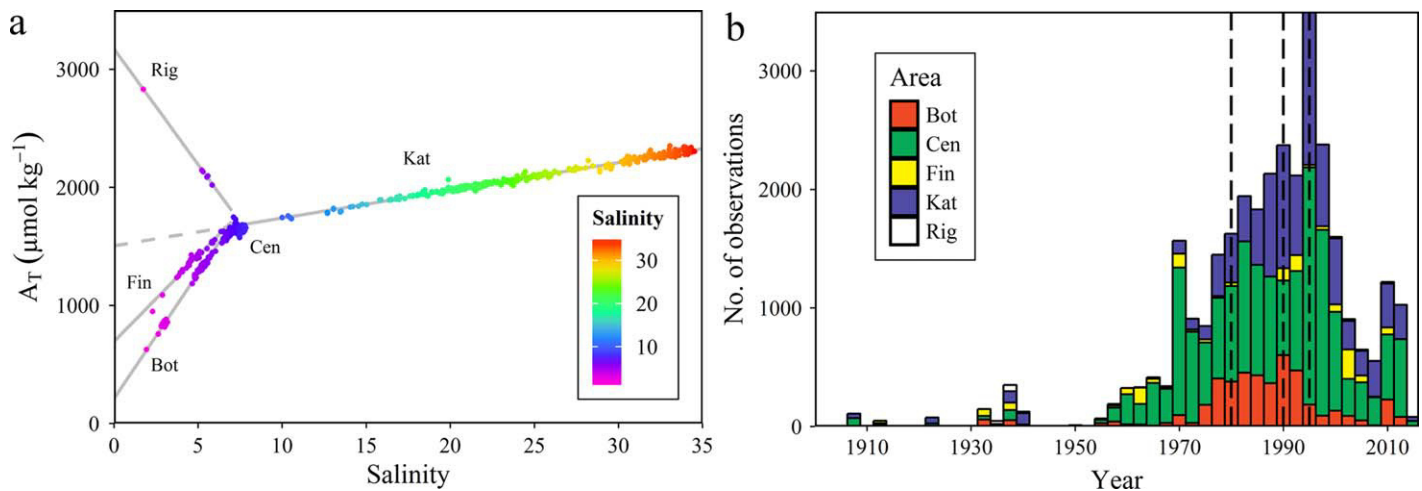


Fig. 2. (a) Exemplary A_T - S relationship in the Baltic Sea for observations from 2008/2009 with linear regression lines for the subareas Kat, Bot, Fin and Rig and (b) temporal distribution of available data over the past century (binwidth = 2.5 yr) with colors coding for the investigated subareas. The vertical dashed lines mark the periods (<1980, 1980–1990, 1990–1995, >1995) that were analysed separately.

- CANIBAL data set (Hjalmarsson et al. 2008 and references therein)
- SMHI monitoring data (extracted from SHARK data base: http://produkter.smhi.se/pshark/datamap_nationell.php?language=s)
- Baltic-C project (BALTEX Phase II (BONUS+), available at: <https://ecds.se/>)
- FMI monitoring data (provided by M. Perttala pers. comm.)

The data set was compiled in April 2015. Identical data points appearing in more than one of the data bases were removed prior to analysis. The analysis was restricted to water depths < 20 m to avoid temporary A_T contributions from sulfide (S^{2-}) formed in stagnant bottom waters. The analysed data set comprises 31436 single observations. The spatio-temporal coverage of the data is presented in Figs. 1, 2b.

Quality control

The applied quality control focuses on the homogeneity of the A_T measurements as well as the accuracy and precision of the available data.

The homogeneity of the measurement method is a critical aspect, because the data used for our trend analysis originate from different sources and time periods. The oldest observations date back to the beginning of the 20th century when for the first time intense theoretical and experimental work including comprehensive field studies concerning the marine CO_2 system was performed (Buch 1945). A review of the analytical methods for the determination of alkalinity – termed commonly “excess base” at that time – was given by Gripenberg (1936). For the back titration method that became the standard procedure for many decades, Gripenberg (1936) reported a precision of only a few $\mu\text{mol kg}^{-1}$. However, a systematic bias may have been associated with the choice of the indicator for the detection of the titration end-point and could amount up to 10 $\mu\text{mol kg}^{-1}$ according to the data presented

by Gripenberg (1936). The alkalinity data from the Swedish Monitoring Programme, which constitute the bulk of the more recent data used in our study, were based on the back titration method until 1995 and after that based on the direct titration. No significant bias was caused by this change in method, which was demonstrated for an extensive number of samples measured in parallel (M. Krysell pers. comm.). In combination with the use of certified carbon reference material (CRM, Dickson et al. 2007) the back titration facilitates an overall range of bias of $\pm 5 \mu\text{mol kg}^{-1}$ (Dickson et al. 2007) and is currently state of the art. It was also the basis for the data collected within the Baltic-C project.

In addition to available information about the analytical accuracy and precision for the alkalinity determination, one may use the characteristics of A_T - S relationships to identify data that are obviously biased by analytical shortcomings. The precision of A_T observations can be estimated from the residuals when performing linear regression analysis for the A_T - S relation (Fig. 2a) in the subareas Kat, Bot, Fin and Rig (Fig. 1). Observations with low precision can be excluded, when the residual exceeds a predefined threshold. This analysis was performed separately for data from each cruise within the CANIBAL data set, which contributes the most questionable historic data. However, applying a threshold for the various subareas led to the exclusion of observations primarily from the period 1975–1995, whereas no precision deficiency could be identified for the past two decades. Accordingly, Swedish scientists reported unidentified sources of error for the observation period 1975–1995 (K. Wesslander and M. Krysell pers. comm.). However, apparently low precision can also reflect increased natural variability of the investigated parameter. By largely removing A_T observations from the critical 1975–1995 period we risked to discard important information and thus decided to analyse the critical time

frames separately, comprehensively report the observed variability and interpret the respective findings with great care.

In contrast to the precision control described above, it is not possible to retrospectively test the accuracy of A_T observations. Since CRMs were introduced for monitoring purposes around 1995, an accuracy of better than $5 \mu\text{mol kg}^{-1}$ can be assumed (Dickson et al. 2007; Hjalmarsen et al. 2008). With respect to historic observations from before 1995, somewhat larger uncertainties are to be expected. However, even when assuming an inaccuracy twice as large as the current level, the detected trends are almost an order of magnitude larger than the potential bias.

Alkalinity trend analysis

The analysis of oceanic A_T trends is typically based on alkalinities normalized to a salinity of 35 ($nA_T = A_T \times 35/S$) to account for local evaporation, precipitation and circulation patterns (Millero et al. 1998). Friis et al. (2003) highlighted that this approach has its limitations already in oceanic environments influenced by riverine input of alkalinity or the dissolution of biogenic carbonates. For a comprehensive analysis of A_T trends in estuarine systems, which receive significant amounts of A_T from freshwater end-members and thus cover a large range of variable A_T - S conditions, the classical alkalinity normalization is by no means adequate.

Taking the complex A_T - S distribution of the Baltic Sea into account, two types of subareas had to be investigated differently: (1) The Central Baltic Sea, which – as a mixing chamber for waters from the adjacent gulfs and the North Sea – reveals no distinct A_T - S relation and (2) the other subareas (Kat, Bot, Fin, Rig), which feature a linear A_T - S relationship (Fig. 2a).

Central Baltic Sea: no defined A_T - S relation

A simple regression analysis of A_T trends at a given station in Central Baltic Sea is not meaningful, because changes in circulation patterns could alter A_T . To identify potential A_T changes driven by biogeochemical processes, it is thus more informative to analyse A_T trends at specific salinity levels. Therefore, all observations were grouped into salinity intervals of 0.2 (range: 6.5–7.7). The interval width was chosen as narrow as necessary to avoid significant salinity dependence of A_T within the groups, but as wide as possible to increase the number of observations within each interval. The deviations (dA_T) of the individual val-

ues from the mean A_T were computed separately for each salinity interval. The dA_T values from the various salinity intervals were pooled and plotted as a function of time (Fig. 3). Based on the pooled dA_T values temporal trends were investigated by linear regression analysis. For the trend analysis the whole observation period was divided into four distinct periods. This division into up to four periods reduced the mean squared error (MSE), whereas a larger number of distinct periods did not further reduce the MSE significantly. The exact breakpoint between two adjacent time periods was determined with an iterative procedure (Crawley 2007) that we applied to identify the breakpoints resulting in the lowest MSE. The iterative procedure was repetitively applied to all breakpoints until no change in breakpoint position occurred. The three breakpoints 1980, 1990, and 1995 were identified with this iterative procedure.

Subareas with linear A_T - S relationship

For subareas with linear A_T - S relationships (Kat, Bot, Fin) a three dimensional (3d) statistical model was applied. The 3d model includes the dependency of A_T on salinity (S), time (t) and an interaction term of both parameters ($S \times t$), that accounts for the change of the A_T - S -slope with time, but can also be interpreted as the dependency of the temporal A_T trend on salinity. The applied linear 3d model is:

$$A_T(S, t) = A_{T(S_0, t_0)} + \left(\frac{\Delta A_T}{\Delta S} \right)_{t_0} \times (S - S_0) + \left(\frac{\Delta A_T}{\Delta t} \right)_{S_0} \times (t - t_0) + \frac{\Delta \left(\frac{\Delta A_T}{\Delta S} \right)}{\Delta t} \times (S - S_0) \times (t - t_0) \quad (3)$$

where t_0 and S_0 are the assigned reference year and salinity, respectively. The fitted coefficients and their interpretation are summarized in Table 1.

The 3d models were applied only to the time period 1995–2014, reflecting the usage of CRMs in the monitoring programs, the last breakpoint found in the Central Baltic Sea and a high spatio-temporal data coverage. Accordingly, the beginning of the observation period t_0 was set to 1995. The reference salinity S_0 was set to 7, allowing a direct comparison of the coefficient $(\Delta A_T / \Delta t)_{S_0}$ to the slope found in the Central Baltic Sea (Table 2). It should be noted that the values assigned to S_0 and t_0 do change the specific coefficients obtained from the model, but have no impact on the general

Table 1. Summary and interpretation of the coefficients that characterize the applied 3d model.

Coefficient	Unit	Interpretation
$A_{T(S_0, t_0)}$	$\mu\text{mol kg}^{-1}$	A_T intercept, (at the beginning of the observation period and reference salinity)
$\left(\frac{\Delta A_T}{\Delta S} \right)_{(t_0)}$	$\mu\text{mol kg}^{-1}$	Slope $A_T \sim$ salinity (at the beginning of the observation period t_0)
$\left(\frac{\Delta A_T}{\Delta t} \right)_{(S_0)}$	$\mu\text{mol kg}^{-1} \text{ yr}^{-1}$	Slope $A_T \sim$ time (at the reference salinity S_0)
$\frac{\Delta \left(\frac{\Delta A_T}{\Delta S} \right)}{\Delta t}$	$\mu\text{mol kg}^{-1} \text{ yr}^{-1}$	Interaction term: (change of slope $A_t \sim$ salinity, if time increases by 1 yr, or change of slope $A_t \sim$ time, if salinity increases by one unit)

outcome of the model, i.e., the predicted A_T at any given S and t . The fitted 3d models and residuals are displayed in Figs. 4, 5, respectively.

To test the outcome of the 3d models described above, a more simplistic and less universal trend analysis was performed for the same time period after 1995. Therefore, linear regression models ($A_T = f(t)$) were applied for salinity intervals of 1 unit separately for each subarea. The slopes derived from these 2d linear regression models are compared to the slope obtained from the 3d models at the same salinity and subarea (Fig. 7a, Supporting Information Figs. S2, S3).

Due to insufficient spatio-temporal data records from before 1995 the 3d model could not be applied. The available historic data for the regions Bot, Fin, and Kat had thus to be presented according to the same principle as applied in the Central Baltic Sea: For area-specific salinity intervals we computed the deviations from mean A_T . In contrast to the Central Baltic Sea we did not pool the computed deviations thereafter, because different rates of change were expected at differing salinity intervals. We thus display the deviations as boxplots grouped by salinity intervals and decades for the subareas Kat, Bot, Fin and Rig (Fig. 6).

Calculation of acidification trends

The annual acidification trend caused by increasing atmospheric CO_2 was computed from pCO_2 and A_T for the time period 1995–2014. The acidification estimates are based on a pCO_2 trend of $+2 \mu\text{atm yr}^{-1}$ (IPCC 2013). Calculations were performed for an increase from $\text{pCO}_{2,t0} = 380 \mu\text{atm}$ to $\text{pCO}_{2,t1} = 382 \mu\text{atm}$, reflecting the annual increase in the northern-hemisphere pCO_2 roughly in the middle of the investigated period. Two A_T scenarios were analysed:

1. Alkalinity was assumed to be constant. For this scenario the mean A_T (mA_T) of the observation period was computed for each salinity interval. Based on this mA_T , the pH trend was computed according to:

$$dpH_{(A_T=\text{constant})} = pH(mA_T, pCO_{2,t1}) - pH(mA_T, pCO_{2,t0}) \quad (4)$$

2. The alkalinity trend ($\Delta A_T/\Delta t$) was taken into account and the pH trend was computed as:

$$dpH_{(A_T=\text{variable})} = pH\left(\left(mA_T + \frac{\Delta A_T}{\Delta t} \times 1\text{yr}\right), pCO_{2,t1}\right) - pH(mA_T, pCO_{2,t0}) \quad (5)$$

The alkalinity trend for the second scenario was derived from the 3d models for the Kattegat region and the Gulf of Bothnia, and from the 2d model for the Central Baltic Sea (Table 2). The estimated pH trends for a constant and an increasing A_T background are displayed in Fig. 7b.

Results

Within this chapter we first present A_T trends for the time period 1995–2014 (Figs. 3, 4), for which we found the smallest mean residual ($\sim 20 \mu\text{mol kg}^{-1}$, Table 2) and a homogenous spatial and temporal data coverage (Fig. 5). Further, we present A_T changes before 1995 (Figs. 3, 6). Data from that period revealed much higher variability (mean residual $\sim 50 \mu\text{mol kg}^{-1}$, Table 2) and the spatio-temporal data coverage is more fragmentary compared to the recent two decades. Results from before 1995 should thus be interpreted with greater care. We therefore focus the following estimation of CO_2 -induced acidification trends on the time period after 1995 (Fig. 7b). The chapter concludes with an evaluation of the applied models and uncertainties associated to our findings.

Time period 1995–2014

In the Central Baltic Sea we found an increase of the alkalinity deviations (dA_T) by $+70 \mu\text{mol kg}^{-1}$ for the time period 1995–2014, corresponding to a rate of $+3.4 \mu\text{mol kg}^{-1} \text{yr}^{-1}$ (Fig. 3; Table 2). The deviations of the dA_T values from the applied linear model are evenly distributed over time (Fig. 5) and the mean residual is below $20 \mu\text{mol kg}^{-1}$ (Table 1).

In the Kattegat region at salinity 15, A_T increased from 1812 to 1880 $\mu\text{mol kg}^{-1}$ over the time period 1995–2014. This corresponds to a trend of $+3.4 \mu\text{mol kg}^{-1} \text{yr}^{-1}$ (Fig. 4; Table 2) and matches the A_T increase observed in the Central Baltic Sea at salinities around 7. The positive A_T trend continuously decreases toward the high saline waters of the North Sea and levels off at salinity 30. At salinities higher 30, we found a minor decrease of A_T over time (Fig. 4), which is smaller than the mean residual of the observed A_T values from the fitted 3d model ($16 \mu\text{mol kg}^{-1}$, Table 2). The observations in the Kattegat region are evenly distributed over the salinity range from 15 to 35. Fewer observations cover the salinity range below 15, reflecting the steep salinity gradient and the small number of monitoring stations in the Belt Sea. Residuals are evenly distributed over time (Fig. 5).

In the Gulf of Bothnia we found an A_T increase from 730 to 870 $\mu\text{mol kg}^{-1}$ at salinity 3 ($+7.4 \mu\text{mol kg}^{-1} \text{yr}^{-1}$), which is slightly higher than the increase from 1170 to 1290 $\mu\text{mol kg}^{-1}$ ($+6.2 \mu\text{mol kg}^{-1} \text{yr}^{-1}$) observed at salinity 5 (Fig. 4; Table 2). Most of the observations available from the Gulf of Bothnia fall within the two salinity intervals 2.5–3.5 and 4.5–6 (Fig. 4), indicating the prevailing surface salinity in the northern Bothnian Bay and the southern Bothnian Sea, respectively (Winsor et al. 2001, 2003). However, the A_T trend is similar for both predominant salinity levels and should thus also hold true for the narrow transition zone.

In the Gulf of Finland, most of the available data are restricted to the salinity range 4–6.5 (Fig. 4) and only in 2001 extensive investigations covered lower salinities down to 2. The temporal A_T changes in the Gulf of Finland outside the salinity range 4–6.5 thus remain speculative. However, at

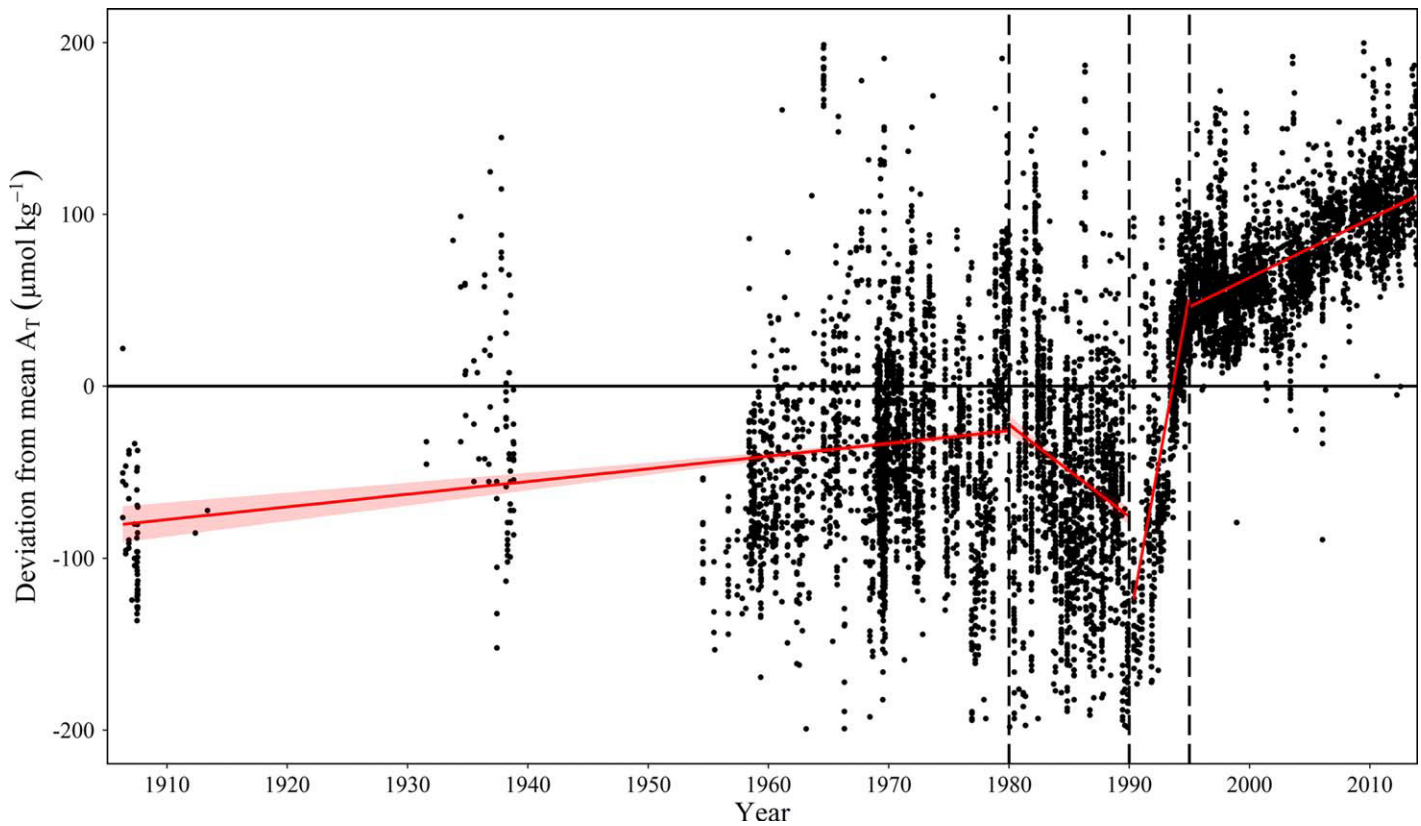


Fig. 3. Temporal alkalinity trends in the Central Baltic Sea from 1900 to 2015. Displayed are deviations (dA_T) of observed A_T from mean A_T . Linear regression models (red line + 95% confidence interval (red area)) were fitted separately within the four time frames indicated by the vertical dashed lines. For the coefficients of the regression analysis please refer to Table 2.

salinity 5 we found an A_T increase from 1340 to 1440 $\mu\text{mol kg}^{-1}$ ($+5.6 \mu\text{mol kg}^{-1} \text{yr}^{-1}$).

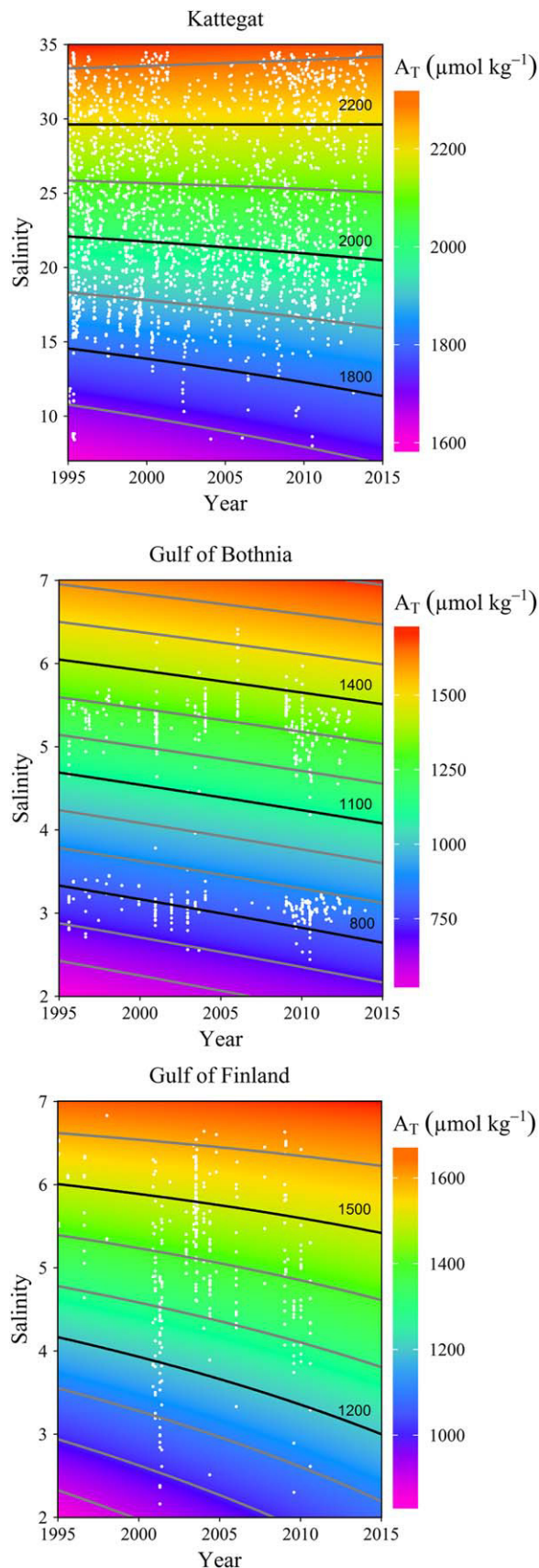
In the Gulf of Riga, the data coverage is not extensive enough for a reasonable application of the statistical 3d model. However, for the salinity range 5–6 and the limited time period 2000–2011, linear regression of A_T as function of time indicates a rate of change around $+8 \mu\text{mol kg}^{-1} \text{yr}^{-1}$ (Supporting Information Fig. S1).

Time period before 1995

In the Central Baltic Sea, we found that the increasing alkalinity trend observed over the past two decades, may have persisted for the entire past century. The alkalinity deviations increase by about 200 $\mu\text{mol kg}^{-1}$ from early 1900 to the current levels, corresponding to an overall rate of change of about $+2 \mu\text{mol kg}^{-1} \text{yr}^{-1}$ (Fig. 3). However, this overall trend observed in the Central Baltic Sea should be interpreted with

Table 2. Summary of the statistical parameters obtained from the application of the 2d and 3d models to the Central Baltic Sea and subareas with linear A_T - S relations (Kat, Bot, Fin), respectively.

Area	Model	Time period	$A_{T(S_0, t_0)}$	$\left(\frac{\Delta A_T}{\Delta S}\right)_{(t_0)}$	$\left(\frac{\Delta A_T}{\Delta t}\right)_{(S_0)}$	$\frac{\Delta\left(\frac{\Delta A_T}{\Delta S}\right)}{\Delta t}$	R^2	Mean residual	No of observations
Cen	$dA_T = f(t)$	1900–1980	-	-	0.7	-	0.02	44	3876
		1980–1990	-	-	-5.2	-	0.04	51	2591
		1990–1995	-	-	38.4	-	0.61	27	1713
		1995–2014	-	-	3.4	-	0.33	20	4080
Kat	$A_T = f(S, t)$		1600	26.5	5.3	-0.2	0.98	16	3333
Bot		1995–2014	1610	220.9	5.1	-0.6	0.98	24	738
Fin			1662	163.0	1.7	-1.9	0.87	34	476



care, because the spread of the observations from before 1995 is much larger (mean residual $> 40 \mu\text{mol kg}^{-1}$) than for the last two decades (mean residual $< 20 \mu\text{mol kg}^{-1}$, Table 1). Despite the large scatter of the earlier observations, we detected a break in the overall increasing A_T trend: A_T anomalies seem to have decreased ($-5 \mu\text{mol kg}^{-1} \text{yr}^{-1}$) from around 1980–1990, and recovered more rapidly ($+38 \mu\text{mol kg}^{-1} \text{yr}^{-1}$) thereafter from 1990 to 1995 (Table 2).

In the Kattegat and the Gulf of Finland, the majority of A_T observations before 1935 are around $50\text{--}100 \mu\text{mol kg}^{-1}$ below the long-term average (Fig. 6). A_T levels similar to the long-term mean were first observed in the 1940 decade and around 1970 respectively for the Kattegat and Gulf of Finland region. In the Gulf of Bothnia, the historic A_T evolution follows a contrasting trend. A_T residuals in the 1910 decade are almost entirely positive, but decrease thereafter and become consistently negative at all salinity levels around 1950 (Fig. 6). From the few observations available from Gulf of Riga it can be assumed that A_T was considerably lower in the 1925–1945 period, than in the recent decades.

For around three decades from 1965 to 1995 the A_T observations show remarkably lower precision in all three subareas discussed above (Kat, Bot, Fin) and we thus refrain from interpreting any temporal changes during that time (Fig. 6). The recent observations from the last decade reveal positive A_T residuals for the Gulfs of Bothnia and Finland around $+100 \mu\text{mol kg}^{-1}$ throughout all salinity intervals. In the Kattegat such positive evolution was only found at the lowest salinity (Fig. 6), which is in good agreement with the results from the applied 3d model (Fig. 4).

Implications for CO_2 -induced acidification trends

When assuming constant alkalinity levels in the Baltic Sea over the past two decades, the computed mean acidification trend (i.e., decrease in pH over time) caused by an increasing atmospheric pCO_2 is in a similar order of magnitude as in oceanic environments and increases only slightly from $-0.0020 \text{ pH units yr}^{-1}$ at salinity 35 to $-0.0022 \text{ pH units yr}^{-1}$ at salinity 5 (Fig. 7b). In contrast, if the observed positive A_T trends are taken into account, the estimated acidification is generally lower. In the Kattegat region, increasing A_T levels mitigate the acidification trend to around $-0.0015 \text{ pH units yr}^{-1}$ at salinity 15. Slightly higher mitigation effects of around 50% were found for the Central Baltic Sea (Fig. 7b). In the low saline areas of the Bothnian Sea, the alkalinity increase fully compensated the CO_2 -induced acidification signal during the last two decades (Fig. 7b).

Fig. 4. Surface water alkalinity as a function of salinity and time in the Kattegat, Gulf of Bothnia and Gulf of Finland from 1995 to 2014. The colors and black contour lines display A_T levels as derived from the best fitting 3d models. White dots represent the observations included in the analysis. For the fitting coefficients please refer to Table 2.

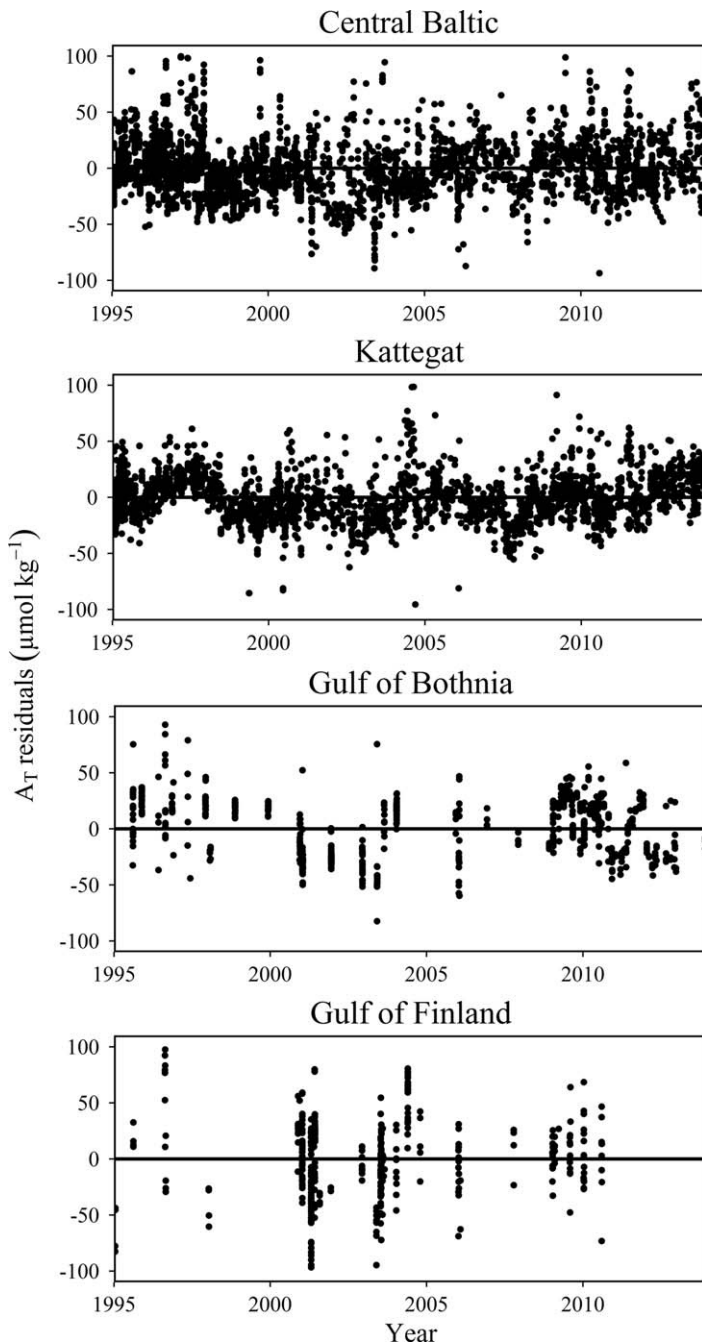


Fig. 5. Residuals of observed surface water alkalinity from the statistical models over the time period 1995–2014. In the Central Baltic Sea, the residuals correspond to the 2d linear regression model applied to the A_T deviations. In the Kattegat, Gulf of Bothnia and Gulf of Finland the residuals correspond to the statistical 3d models. Due to the scaling of the y -axis 38 (0.9%), 14 (0.4%), 10 (1.4%), and 15 (3.2%) observations are not displayed for Cen, Kat, Bot and Fin area, respectively.

3d model advantages and uncertainties

The applied 3d models have several advantages, compared to the simple regression analysis of A_T as a function of time within specific salinity intervals: (1) The 3d models are more

robust against outliers, due to the high number of observations contributing to each fit. (2) The 3d models require only four fitted coefficients per subarea, whereas simple linear regression requires 2 coefficients per salinity interval and area. (3) The 3d models do not group the A_T observations into salinity intervals as it is required for 2d regression analysis. Thus, each observation is included into the fitting procedure with the exact corresponding salinity. This difference explains the slight deviations between 3d and 2d models (Fig. 7a), which can best be exemplified for the salinity range 3 ± 0.5 in the Bothnian Sea: Within that salinity interval the 2d model underestimates the slope by around $1\text{--}2 \mu\text{mol kg}^{-1} \text{yr}^{-1}$, due to a larger number of observations with high salinities and thus higher A_T at the beginning of the period (visualized in Supporting Information Fig. S3). This limitation of the 2d model also applies in the Kattegat region (Supporting Information Fig. S2), but is less pronounced than in the gulfs, because the A_T - S slope is about fivefold less steep. In conclusion we found the 3d models to be more reliable to analyse A_T trends in estuarine systems covering large salinity ranges.

Fitting the statistical 3d models ($A_T = f(S, t)$) to A_T observations from the past two decades revealed trends ($50\text{--}150 \mu\text{mol kg}^{-1} \text{yr}^{-1}$) that were – in the typical salinity range of the Baltic Sea – by an order of magnitude larger than the measurement uncertainties.

In the Kattegat, we derived a slightly negative A_T trend for the North Sea end member, which is around $-15 \mu\text{mol kg}^{-1}$ for the time period 1995–2014 at salinity 33. Because this estimate is in the same order of magnitude as the mean residual it was considered to be not significant.

When extrapolating the 3d models for the Kattegat and Bothnian Sea to the mean salinity 7 of the Central Baltic Sea an alkalinity trend of $+5.2 \mu\text{mol kg}^{-1} \text{yr}^{-1}$ at salinity 7 was derived for both areas. This is somewhat higher than the rate ($+3.4 \mu\text{mol kg}^{-1} \text{yr}^{-1}$) found by direct observations from the Central Baltic Sea. The deviation can potentially be attributed to the increasing uncertainty generally associated to the extrapolation of regression analysis.

Discussion

We found a consistent increase of surface water A_T in the Baltic Sea over the past two decades (1995–2014), with increasing rates of change from the North Sea toward the low-saline areas in most northern parts. In the Central Baltic Sea, the A_T trend amounts to $+3.4 \mu\text{mol kg}^{-1} \text{yr}^{-1}$ for the past two decades. In contrast to this consistent positive trend, the evaluation of historic A_T data (1900–1995) suggests regional differences. The A_T increase in the Central Baltic Sea, Kattegat and Gulf of Finland seems to be a persistent long-term trend, whereas A_T levels in the Gulf of Bothnia have dropped during the first half of the century and increased only over the last two decades. The perception of the historic data is in agreement with previous studies (Ohlson and Anderson 1990; Kremling and Wilhelm 1997; Hjalmarsson et al. 2008).

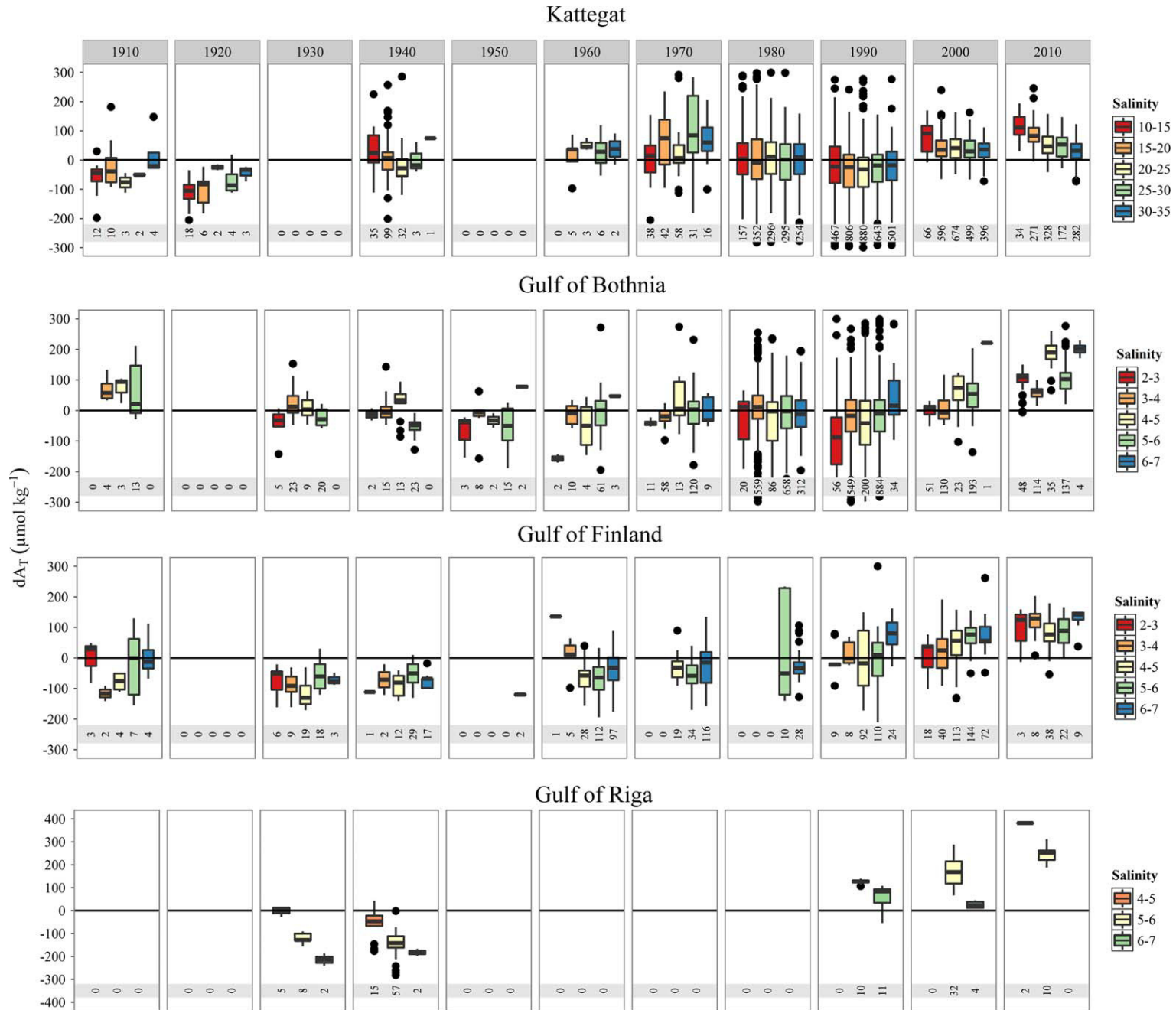


Fig. 6. Surface water alkalinity trends in the Kattegat and the three Gulfs of Bothnia, Finland and Riga from 1905 to 2015. The boxplots represent the deviations (dA_T) of observed A_T from mean A_T per salinity interval and decade. The number in the grey box on top of the panels indicates the middle of the decades, which cover ± 5 yr. The salinity intervals are indicated by color. Within the grey bar below each plot the number of observations is given.

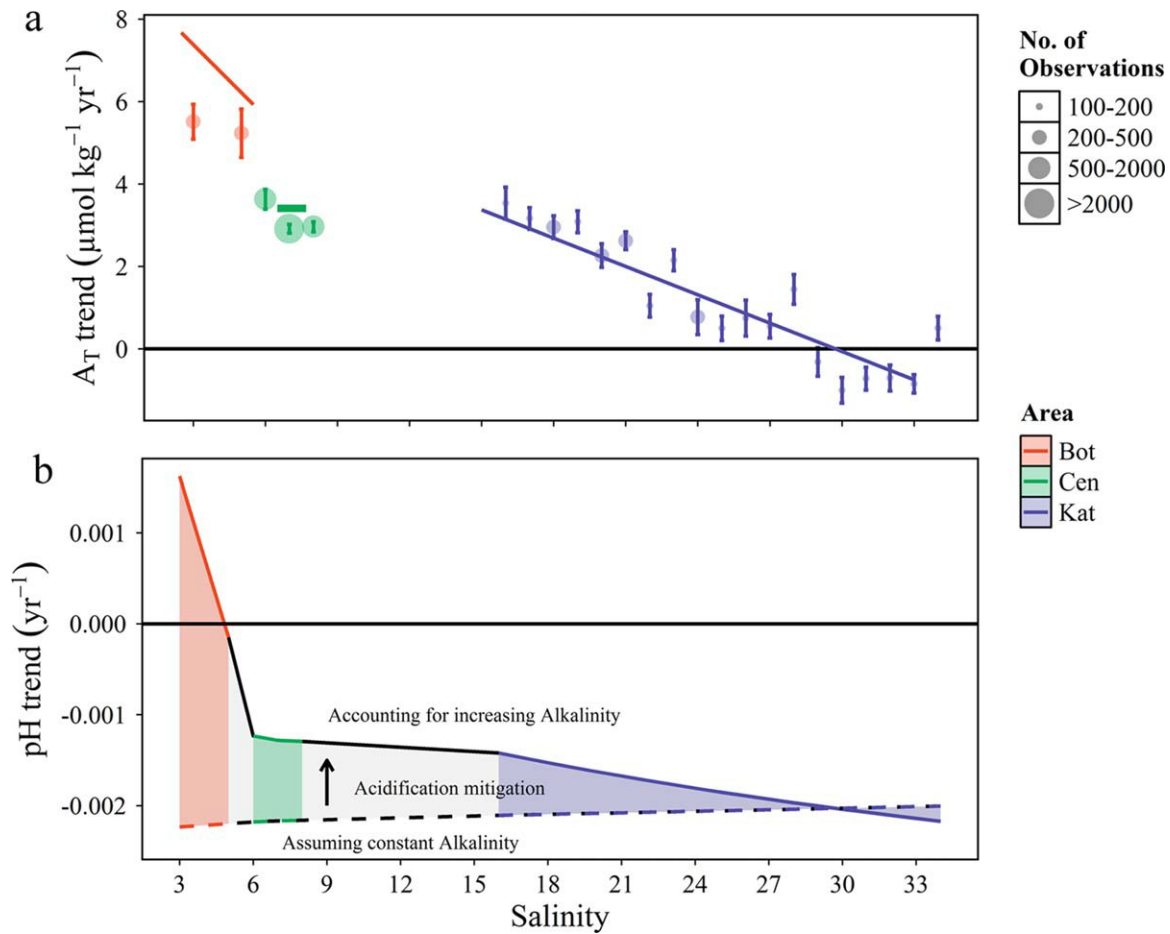


Fig. 7. Mean surface water alkalinity trends (a) and acidification mitigation (b) in the Kattegat, Central Baltic Sea and Gulf of Bothnia for the time period 1995–2014. (a) A_T trends displayed as points (\pm SE) correspond to the slope of linear regression models fitted separately at each salinity interval (given value \pm 0.5), whereas the lines represent the A_T slopes derived from the 3d models. The point size depicts the number of observations. (b) Mean annual acidification trend assuming an atmospheric pCO_2 increase of $2 \mu atm yr^{-1}$. The dashed line represents the acidification trend assuming that the mean A_T was constant, whereas the solid line depicts a mean annual pH decrease taking the observed A_T changes into account. The filled area corresponds to the acidification mitigation that increases toward lower salinity.

In the following discussion, we will first focus on the attribution of the detected surface water A_T trends to biogeochemical processes and subsequently address their implications for the evolution of the Baltic Sea CO_2 system.

Attribution of the detected A_T trends

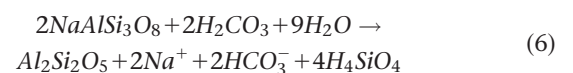
Within the following chapters the potential drivers for the observed trends are discussed, but a quantitative attribution to the numerous possible biogeochemical processes and anthropogenic impacts is beyond the scope of this study. The qualitative discussion covers processes that affect terrestrial weathering rates (changes in precipitation patterns, acidic rain deposition, and atmospheric CO_2 increase), liming activities and finally internal alkalinity generation.

Weathering in the Baltic drainage basin

With respect to terrestrial weathering processes the Baltic Sea drainage basin can be divided into a northern and south-

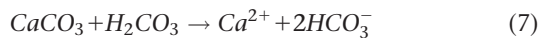
ern part that intersect at the easternmost end of the Gulf of Finland [for details see e.g., Håkanson et al. (2003)]. The Gulf of Bothnia and the Gulf of Riga are thus drained exclusively from the northern and southern part, respectively. All other subareas receive freshwater input from both drainage areas.

The bedrock of the northern part mainly consists of granite and is covered only with a thin layer of soil. Boreal forests are the predominant vegetation. The terrestrial weathering process in the northern catchment can be exemplified by the reaction of albite with carbonic acid (Berner and Berner 1987), which produces the secondary mineral kaolinite, dissolved silica, sodium ions and bicarbonate:



The bedrock of the southern part consists of limestone, clay and sandstone, covered with a thick soil layer that forms the

foundation for intense agricultural activities. The dominant weathering process in the southern part is the reaction of carbonate minerals with carbonic acid, which produces calcium ions and bicarbonate:



The weathering reactions exemplified in Eqs. 6 and 7 are driven by carbonic acid. That carbonic acid is produced by soil respiration processes, and thus ultimately originates from photosynthetically fixed atmospheric CO_2 . The fundamental difference in both weathering reactions with respect to the formation of alkalinity is that bicarbonate produced by the weathering of granite (Eq. 6) is entirely derived from carbonic acid. In contrast, roughly half of the alkalinity produced by the weathering of carbonate minerals (Eq. 7) originates from carbonic acid and the carbonate mineral, respectively. If the weathering is driven by a strong acid (e.g., H_2SO_4) instead of by carbonic acid, the weathering of carbonate minerals produces bicarbonate and the anion of the strong acid (e.g., sulfate), whereas the weathering of granite produces only the anion of the strong acid. In contrast to bicarbonate ions, the anions of the strong acids do not contribute to alkalinity. Thus, the weathering of carbonate minerals with a strong acid produces alkalinity, whereas the weathering of granite with a strong acid does not produce alkalinity, but neutralizes the delivered protons [for details see e.g., Berner and Berner (1987)]. This difference in the weathering processes is essential to understand the potential impacts of acidic rain on riverine alkalinity in the Baltic Sea drainage basin.

Precipitation patterns

Increasing precipitation and run-off were found to affect riverine alkalinity ($A_{T,0}$) in two counteracting ways: The lower contact time of water with the soil and bedrock reduces the concentration of weathering products and as such $A_{T,0}$. However, this effect is generally overcompensated by an increase in river discharge, which results in an increasing A_T flux (Berner and Berner 1987; Cai et al. 2008). In a classical estuarine system consisting of an unchanged marine- and one variable freshwater endmember, increasing precipitation should thus directly increase the slope and decrease the intercept of the A_T - S relationship, as both are controlled by $A_{T,0}$ but independent of the A_T flux. In contrast, the Baltic Sea has a complex and diverse drainage basin structure, and the surface water A_T - S distribution (Fig. 2a) also depends on the mixing ratio and thus the A_T flux of the various discharging rivers.

The precipitation and total river run-off in the Baltic Sea area do not show a significant long-term trend over the past 100 years, but the recent two decades were relatively wet and the total runoff increased (The BACC II Author Team 2015). This recent increase in run-off was pronounced in the Nordic

countries (Wilson et al. 2010), whereas the southern catchment revealed a contrasting tendency for a decrease in run-off (Gailiūšis et al. 2011; The BACC II Author Team 2015). Due to the increased run-off in the Nordic countries we would expect a decrease of $A_{T,0}$ in the Gulf of Bothnia. Likewise, the northward shift in run-off should favor decreasing A_T levels in the Central Baltic Sea, as it reduces the contribution from the A_T -rich rivers draining the southern catchment area. Both expected trends are in contrast to our observations and we thus do not expect a significant impact of changes in precipitation patterns on the observed A_T trends.

Hansson et al. (2011) report that runoff to the Baltic Sea is strongly linked to temperature and therefore suggest that southern regions will become drier and that the northern- and Gulf of Finland area will experience higher runoff with rising temperature. It can thus not be ruled out that changes in precipitation patterns (The BACC II Author Team 2015) will influence the future A_T - S distribution in the Baltic Sea.

Impacts of acidic rain

Anthropogenic emissions of sulphur oxides (SO_x) and nitrogen oxides (NO_x) cause acidic rain, because both react with water and form strong sulphuric acid (H_2SO_4) and nitric acid (HNO_3). European SO_2 emissions steadily increased to peak emissions of $> 50 \text{ Mt SO}_2 \text{ yr}^{-1}$ around 1980. Emissions decreased thereafter to today's $< 10 \text{ Mt SO}_2 \text{ yr}^{-1}$ with highest reduction rates in the 1990–2000 period (Vestreng et al. 2007). NO_x emissions showed a much lower decrease rate (Granier et al. 2011). The decrease of SO_x and NO_x emissions is reflected by an increased precipitation pH, e.g., in Germany from 4.3 during 1978–1990 to 4.8 in 1990–2010 (Lajtha and Jones 2013). A recent modelling study revealed that the history of SO_x and NO_x emissions is well-mirrored in the direct atmospheric deposition of acids in the Baltic Sea basin (Omstedt et al. 2015).

According to the peculiarities of the weathering processes described above, we expect that increasing acidic precipitation until 1980 enhanced the dissolution of carbonate minerals and thus the riverine A_T input from the southern drainage basin. In contrast, we expect a decreasing A_T input from the northern drainage basin until 1980 that reflects the direct removal of alkalinity by acidic precipitation. After 1980, the recovery from acid deposition should have an inverse effect (Stets et al. 2014). Superimposed on the potentially delayed signals from terrestrial weathering processes, the direct input of acidic precipitation into the Baltic Sea can be considered an immediate A_T sink that peaked around 1980 (Omstedt et al. 2015). In the following, we estimate the upper limits for acidic rain induced A_T changes for two simplified processes: (1) The potential A_T increase in rivers from the southern, limestone-dominated drainage basin and (2) the potential A_T removal by direct acidic precipitation into the Gulf of Bothnia.

1. To quantify the relationship between acidic precipitation and alkalinity generation in the southern, limestone-rich catchment area, we first considered the weathering without any acidic precipitation and attributed the reference A_T formation solely to the weathering with carbonic acid. Subsequently, we computed the additional dissolution of calcium carbonate due to acidic rain that causes higher A_T levels (for a detailed description of the calculation procedure see the Supporting Information). We performed the respective calculations for various precipitation pH levels, temperatures and reference A_T concentrations (Supporting Information Fig. S4). Assuming a reference river water A_T of $3000 \mu\text{mol kg}^{-1}$, $T = 10 \text{ }^\circ\text{C}$ and precipitation pH values of 3, 4, and 5 we estimated an A_T increase of 410, 47 and $5 \mu\text{mol kg}^{-1}$, respectively. Comparing these estimates with the temporal trends in A_T as detected in the Central Baltic Sea and Gulf of Finland, a decline of the precipitation pH to values below 4 would be required. However, according to Winkler (1983), who analysed precipitation pH data going back to the late 1930s, such low pH have not been observed. Hence, increased weathering due to acidic precipitation might have contributed to the A_T increase observed over the first half of the 20th century in subareas receiving river water from the southern drainage basin, but it is questionable that this is the major driver.
2. Acidic precipitation has the reverse effect on A_T when the weathering in the northern, granite-dominated drainage basin and the direct input into seawater are considered. In this case, A_T is reduced directly by the excess of proton donors over proton acceptors in rain water, approximated by the precipitation pH. The following estimate constitutes an upper limit, because we neglected that protons may partially be neutralized by increased weathering of granite rocks, which does however not produce additional alkalinity. For a precipitation pH of 4, the input of hydrogen ions into the Gulf of Bothnia and its drainage basin was estimated. Based on a precipitation rate of 600 mm yr^{-1} and a surface area of $490,000 \text{ km}^2$ (The BACC Author Team 2008), the annual A_T removal amounts to $\sim 29 \text{ Gmol yr}^{-1}$. This removal of A_T is in the same order of magnitude as the mean input of A_T by river water into the Gulf of Bothnia (43 Gmol yr^{-1} , Hjalmarsson et al. 2008) and indicates that the observed A_T loss in the Gulf of Bothnia during the first half of the 20th century (Fig. 6) may indeed be attributed to acidic precipitation. Reversely, the increasing A_T in the Gulf of Bothnia over the past two decades (Fig. 4) may constitute a relaxation effect from acidic precipitation.

In summary, our estimates support the concept of acidic rain impacts on the A_T system of the Baltic Sea, as suggested by previous studies (Ohlson and Anderson 1990; Kremling and Wilhelm 1997; Hjalmarsson et al. 2008). Hjalmarsson et al. (2008) compiled the Canibal data set – which contains

observations from 1911 to 2003 and was also included in our analysis – and investigated the A_T signature of the rivers entering the Baltic Sea. They derived the flow-weighted $A_{T,0}$ in rivers entering a specific region from the intercept at $S = 0$, when extrapolating a regression analysis of A_T vs. salinity. Hjalmarsson et al. (2008) found an increase in A_T in rivers entering the Gulf of Finland ($+2.6 \mu\text{mol L}^{-1} \text{ yr}^{-1}$) and a decrease in A_T in rivers entering the Gulf of Bothnia ($-2.7 \mu\text{mol L}^{-1} \text{ yr}^{-1}$). These rates of change estimated for river water A_T and the trends we observed in the Baltic Sea are of similar magnitude. However, it should be noted that the extrapolated river water alkalinity analysed by Hjalmarsson et al. (2008) suffers from at least the same uncertainty as the historic data included in our study. Ohlson and Anderson (1990) applied a similar principle to the Kattegat region and derived the flow-weighted calcium and A_T concentrations of all rivers entering the Baltic Sea. They found that the Ca- A_T ratio increased from around 0.4 (1938 and 1967) to 0.7 in 1986. This was attributed to an increase in weathering driven by acidic rain, which increases the ratio of weathered calcium to produced alkalinity compared to CO_2 -driven weathering (Eq. 7). An according trend was found by Kremling and Wilhelm (1997), who reported a mean Ca concentration increase of about 4% from 1970 to 1995 in the Central Baltic Sea.

A recent modelling study that focused on the direct deposition of acids into the Baltic Sea indicated that most pronounced A_T changes ($-30 \mu\text{mol kg}^{-1}$) may have occurred in the south-western Baltic Sea around 1990 (Omstedt et al. 2015). This proposed direct acid deposition signal coincides with the A_T drop that we observed – although with a high degree of uncertainty – in the Central Baltic Sea around 1990.

Atmospheric CO_2 impacts on weathering

In contrast to acidic precipitation – that peaked around 1980 – atmospheric CO_2 concentrations continuously increased over the whole observation period from $\sim 300 \mu\text{atm}$ at the beginning of the 20th century (MacFarling Meure et al. 2006) to today's $400 \mu\text{atm}$ (IPCC 2013). Increasing pCO_2 decreases the pH of a water mass, but has itself no direct effect on the alkalinity. Likewise, atmospheric pCO_2 should have only a minor direct effect on terrestrial weathering processes, because the high groundwater pCO_2 levels and thus the weathering rates are controlled by soil respiration processes, rather than directly by atmospheric pCO_2 . However, there is growing evidence that increasing atmospheric pCO_2 stimulates plant growth and soil respiration and thus indirectly raises soil pCO_2 (Andrews and Schlesinger 2001; Oh et al. 2007). Increased soil pCO_2 finally accelerates mineral weathering, which increases A_T irrespective of the weathered mineral (Eqs. 6, 7).

Free-Air CO_2 Enrichment (FACE) experiments were performed to investigate this effect. In a pine plantation area, where the bedrock consists mainly of feldspar and should

thus be comparable to conditions in the northern drainage basin of the Baltic Sea, Andrews and Schlesinger (2001) found that under elevated atmospheric $p\text{CO}_2$ (+200 μatm) the soil respiration increased by 27%. This in turn accelerated mineral weathering and increased alkalinity by 162%. Likewise, Macpherson et al. (2008) observed steadily increasing A_T levels in limestone-hosted groundwaters in the mid-continental North American grassland, which is rather comparable to the southern drainage basin of the Baltic Sea. The pronounced alkalinity increase from around 5400 to 6100 $\mu\text{mol kg}^{-1}$ ($\sim 47 \mu\text{mol kg}^{-1} \text{yr}^{-1}$) over the study period 1991–2005 was attributed to a 20% increase in groundwater CO_2 and enhanced weathering rates.

This positive feedback chain – increased atmospheric $p\text{CO}_2$, enhanced plant growth, elevated soil $p\text{CO}_2$ and finally raised groundwater A_T – can potentially be amplified by atmospheric warming. Indeed, the surface air temperatures in the Baltic Sea region increased during the past 100 yr, with the strongest warming trend taking place during spring season (The BACC II Author Team 2015). As the duration of the cold season has decreased and the duration of the growing season increased (The BACC II Author Team 2015), it can be speculated that warming and increasing $p\text{CO}_2$ favored primary production on land in concert and act in the same direction with respect to A_T changes in the Baltic Sea.

Although a quantitative assessment of the CO_2 -driven A_T contribution is currently impossible for the Baltic Sea, due to various types of landscapes and the lack of experimental work performed, we suggest that a positive feedback between atmospheric $p\text{CO}_2$ and weathering rates might have also contributed to the long-term increasing A_T trends in our study area.

Liming activities

In Sweden, a large scale liming programme was implemented to counteract the acidification of sensitive freshwater systems caused by acidic rain. Around 0.2 Mt yr^{-1} of limestone were introduced to Swedish freshwater systems from 1985 to 1995 (Svenson et al. 1995). Converting this to an alkalinity equivalent (twice the amount of $[\text{CO}_3^{2-}]$) reveals a potential A_T source of around 4 Gmol yr^{-1} . This anthropogenic A_T source might have mitigated acidification in Swedish lakes, but it is an order of magnitude smaller than the riverine input of A_T into the Baltic Proper (43 Gmol yr^{-1} , Hjalmarsson et al. 2008) and should thus have contributed only marginally to the observed A_T changes in the Baltic Sea.

Limestone is also applied for agricultural purposes mainly in the southern drainage area to improve soil pH and facilitate the nutrient uptake by plants. We could not compile a complete overview on agricultural liming statistics for the whole Baltic Sea drainage basin. However, liming rates in Germany – of which only a minor portion drains into the Baltic Sea – could be approximated by marketing of CaCO_3

(Supporting Information Fig. S5). The amount of marketed limestone rose from around 2 Mt yr^{-1} in 1950 to $>5 \text{Mt yr}^{-1}$ in 2014 (Statistisches Bundesamt 2015, www.destatis.de), with a pronounced drop after the reunification of Germany in 1990. Similar trends in liming are reported from Eastern Europe and Russia. At present, the amount of limestone marketed in Germany is equal to 50 Gmol yr^{-1} of CaCO_3 . In relation to the annual run-off from this area ($\sim 100 \text{km}^3 \text{yr}^{-1}$), the complete dissolution of the applied CaCO_3 would be equivalent to an alkalinity contribution of roughly 1000 $\mu\text{mol kg}^{-1}$. This estimate constitutes an upper limit, because it neglects the interdependency to the subsequent weathering of bedrock minerals, but it highlights the potentially immense contribution of agricultural liming on riverine A_T concentrations. We hypothesize that the overall increase in liming rates over the second half of the 20th century significantly contributed to the observed A_T trends in the Central Baltic Sea. This hypothesis is in agreement with findings from the intensively agricultural-used watersheds of the Ohio river basin, where Oh and Raymond (2006) estimated that 29% of the total riverine bicarbonate export could be attributed to liming activities. Likewise, Raymond and Cole (2003) reported an alkalinity increase from ~ 380 to $\sim 440 \mu\text{mol kg}^{-1}$ in the Mississippi river from 1953 to 2002 and attributed it to changes in land-use. The increase rate ($\sim 1.3 \mu\text{mol kg}^{-1} \text{yr}^{-1}$) estimated for the Mississippi river is in the same order of magnitude but lower than the trends we found in the Baltic Sea. Recently, Stets et al. (2014) extended the analysis and concluded that A_T increase was a widespread phenomenon in large rivers of the conterminous U.S. Among the diverse drivers that were investigated, Stets et al. (2014) highlighted that recovery from acidification and agricultural liming are important contributions that act in concert on river water A_T concentrations.

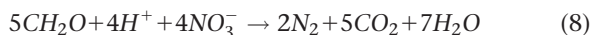
Internal alkalinity generation

In addition to the external A_T sources discussed so far, recent modelling studies suggest that biogeochemical processes can act as significant internal alkalinity sources in the Baltic Sea (Edman and Omstedt 2013; Gustafsson et al. 2014). With respect to A_T trends in the surface water over the past two decades, we discuss potential changes in A_T contributions from (1) primary production, (2) denitrification, and (3) net sulfate reduction.

1. Primary production increases A_T , mainly because the uptake of nitrate (NO_3^-) has to be balanced by H^+ uptake (Wolf-Gladrow et al. 2007). This A_T source is reversed when the produced organic material is remineralized. Pelagic primary production can however contribute to surface water A_T , when the organic matter is exported. With respect to alkalinity trends in the Baltic Sea surface water, it is reasonable to assume that nitrate based primary production and thus the A_T contribution increased along with nutrient inputs that peaked around 1980 (Gustafsson

et al. 2012; Schneider et al. 2015). However, recent modelling studies suggest that the previously increasing nitrogen uptake by phytoplankton levelled off around 1990 (Gustafsson et al. 2012). Thus, we do not assume that changes in primary production contributed significantly to the observed A_T trends since 1995.

- Denitrification increases A_T by 1 mole per mole of nitrate converted (Wolf-Gladrow et al. 2007) and is described by the reaction:



Denitrification is an irreversible process and can consequently contribute to surface water A_T changes irrespective of where it occurs in the water column. However, the denitrification of nitrate that was originally introduced to the system by nitrogen fixation and nitrification has no net effect on A_T . Since the 1980s the nitrogen input to the Baltic Sea was continuously reduced, which is reflected in decreasing winter nitrate concentrations in the surface water (Helcom 2015). It is therefore plausible to assume that rates of denitrification not compensated by nitrogen fixation have rather decreased than increased and thus not contributed to the positive A_T trend since 1995.

- Oxygen deficiency in the bottom waters results in sulfate reduction, when all nitrate is depleted as alternative electron acceptor. The reaction produces sulfide, which contributes to alkalinity:



However, sulfate reduction is reversed under oxic conditions and does therefore not contribute directly to surface water A_T , which was the focus of this study. However, the process can act as a permanent alkalinity source, if the reduced sulfide is buried as FeS_2 . In this case, the removal of iron – which represents a negative A_T contribution when oxidized to Fe_2O_3 – constitutes the permanent A_T source. Unfortunately, no reliable estimate of this removal processes and its relation to organic matter sedimentation is available by now and it is thus premature to speculate about the potential contribution to A_T trends.

Acidification mitigation

In the Central Baltic Sea, almost 50% of the CO_2 -induced acidification trend was mitigated by increasing alkalinities over the past two decades (Fig. 7b). In terms of proton concentration this corresponds to an increase of 6% instead of 10.5% (Fig. 8). Toward the low-saline and low-alkaline Gulf of Bothnia – where pH levels are generally lower – the alkalinity increase fully compensated the CO_2 -induced acidification.

In addition to the mitigation of CO_2 -induced acidification, the observed alkalinity increase has further implications for the CO_2 system. Focusing on the Central Baltic Sea from 1995 to

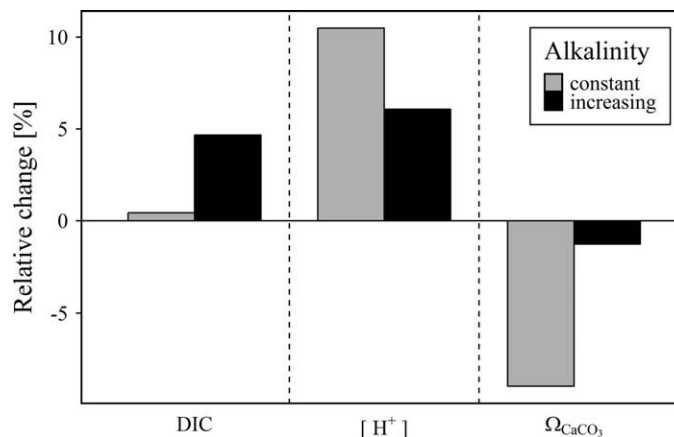


Fig. 8. Combined influence of simultaneous changes in atmospheric pCO_2 and seawater A_T on dissolved inorganic carbon (DIC), proton concentration $[\text{H}^+]$, and calcium carbonate saturation (Ω_{CaCO_3}) in the Central Baltic Sea from 1995 to 2014. Based on an atmospheric pCO_2 increase from 360 to 400 μatm , the relative changes in DIC, $[\text{H}^+]$, and Ω_{CaCO_3} were computed for two A_T scenarios: The observed A_T trend of $+3.4 \mu\text{mol kg}^{-1} \text{yr}^{-1}$ was taken into account (black bars) and the A_T was assumed to be constant at mean A_T (grey bars). Computations were performed for $S = 7$, $T = 10 \text{ }^\circ\text{C}$ and with the dissociation constants from Millero (2010).

2014 the mean salinity and A_T were 7 and 1587 $\mu\text{mol kg}^{-1}$, respectively. Taking the positive A_T trend of $+3.4 \mu\text{mol kg}^{-1} \text{yr}^{-1}$ into account, the A_T rose from around 1550 to 1620 $\mu\text{mol kg}^{-1}$. Over the same time period atmospheric pCO_2 increased from roughly 360 to 400 μatm . Assuming equilibrium with the atmosphere, this pCO_2 increase would raise the dissolved inorganic carbon (DIC) in the Central Baltic Sea only marginally from 1554 to 1560 $\mu\text{mol kg}^{-1}$ under a constant mean A_T background (Fig. 8). However, with A_T and pCO_2 rising in parallel, the DIC increased from 1522 to 1593 $\mu\text{mol kg}^{-1}$, which corresponds to a relative change of 5% (Fig. 8). The DIC gain of around 70 $\mu\text{mol kg}^{-1}$ is very similar to the change in A_T and reflects the tight control of A_T on the CO_2 storage capacity of seawater.

The potentially harmful effect of decreasing seawater pH on marine organisms has been reported extensively (Kroeker et al. 2010 and references therein). Consequently, increasing A_T levels and the mitigation of CO_2 -induced acidification can be judged beneficial to individual organisms and ecosystem stability. Specific concerns were raised about calcifying organisms, because they are believed to be sensitive not only to decreasing pH but also to decreasing carbonate concentrations, which may hinder the calcification process (Thomsen et al. 2015). The A_T increase we observed in the Central Baltic Sea over the past two decades not only mitigated acidification by 50%, but also stabilized the carbonate concentration. At constant mean A_T levels the pCO_2 increase from 1995 to 2014 would have caused a drop in carbonate concentration from 42.7 to 38.8 $\mu\text{mol kg}^{-1}$, but with A_T increasing in parallel this is reduced to a marginal change from

40.9 to 40.4 $\mu\text{mol kg}^{-1}$. Assuming a constant calcium concentration of 2.7 mmol kg^{-1} (Dyrssen 1993), the changes in the carbonate concentration are directly reflected in the saturation state of calcium carbonate (Ω_{CaCO_3}), which is defined as the solubility product divided by the product of $[\text{Ca}^{2+}]$ and $[\text{CO}_3^{2-}]$. With respect to the solubility product of calcite (Mucci 1983), the increasing A_T kept the saturation state stable at 1.5. In contrast, the non-mitigated CO_2 uptake would have decreased the saturation state by around 0.2, corresponding to relative change of -9% (Fig. 8). The observed A_T increase can thus be judged twofold beneficial to calcifying organisms, because it helps to stabilize both, pH and the CaCO_3 saturation state.

Conclusion

We found a consistent A_T increase in the Baltic Sea over the last two decades. Historic observations indicate that this positive A_T evolution might have persisted for extended periods of the 20th century, except for the Gulf of Bothnia.

We suggest that these trends were driven by an interplay of acidic precipitation, increasing atmospheric CO_2 and liming activities. The fundamental difference between those drivers is that acidic precipitation decreases the A_T input from the northern catchment and increase the A_T input from the southern catchment area, whereas increasing atmospheric CO_2 and liming activities are entirely positive drivers. Further, the temporal development of the drivers differs: Acidic precipitation peaked in the 1980s, atmospheric pCO_2 increased steadily since the onset of industrialization and liming rates, at least in Germany, have increased since the 1950s, with a drop after 1990. Finally, all three drivers have in common that they act on the Baltic Sea alkalinity by changing the freshwater-derived A_T contributions. Because this freshwater A_T input is delayed by the groundwater residence time, disentangling the various processes in time and space will be a future challenge for holistic biogeochemical models taking the land-sea interaction into account.

Irrespective of the difficulties in attributing the Baltic Sea A_T trends, we put them into context with increasing atmospheric pCO_2 and estimated the combined effect of both parameters on the seawater CO_2 -system. For the Central Baltic Sea, we estimated that the A_T increase over the past two decades compensated the CO_2 -induced acidification by 50%, stabilized the saturation state of calcium carbonate, and increased the CO_2 storage capacity. However, we emphasize that our findings should not be misinterpreted as suggesting a permanent protection against CO_2 -induced acidification and related processes in coastal seas. As discussed above, only a portion of the observed alkalinity trend might be driven by processes that have a positive feedback to atmospheric CO_2 and can thus be expected to proceed in the course of future CO_2 emissions.

We conclude that the predictability of future acidification processes in coastal seas is limited by the variability of CO_2 system constituents, especially the alkalinity, which forms the backbone of the CO_2 -pH-interdependency. The continued monitoring of the carbonate system and the introduction of automated, high-quality observation techniques are thus essential requirements for the detection and understanding of future changes in the CO_2 system of estuarine environments like the Baltic Sea. A comprehensive monitoring of such large estuarine systems would not only be beneficial for the understanding of the particular ecosystem itself, but could also serve as valuable indicators for expected changes in the open ocean on geological time scales.

References

- Andrews, J. A., and W. H. Schlesinger. 2001. Soil CO_2 dynamics, acidification, and chemical weathering in a temperate forest with experimental CO_2 enrichment. *Global Biogeochem. Cycles* **15**: 149–162. doi:10.1029/2000GB001278
- Archer, D., and V. Brovkin. 2008. The millennial atmospheric lifetime of anthropogenic CO_2 . *Clim. Change* **90**: 283–297. doi:10.1007/s10584-008-9413-1
- Bates, N. R., M. H. P. Best, K. Neely, R. Garley, A. G. Dickson, and R. J. Johnson. 2012. Detecting anthropogenic carbon dioxide uptake and ocean acidification in the North Atlantic Ocean. *Biogeosciences* **9**: 2509–2522. doi:10.5194/bg-9-2509-2012
- Bates, N. R., and others. 2014. A time-series view of changing surface ocean chemistry due to ocean uptake of anthropogenic CO_2 and ocean acidification. *Oceanography* **27**: 126–141. doi:10.5670/oceanog.2014.16
- Beldowski, J., A. Löffler, B. Schneider, and L. Joensuu. 2010. Distribution and biogeochemical control of total CO_2 and total alkalinity in the Baltic Sea. *J. Mar. Syst.* **81**: 252–259. doi:10.1016/j.jmarsys.2009.12.020
- Berner, E. K., and R. A. Berner. 1987. *The global water cycle*. Prentice-Hall.
- Buch, K. 1945. Kolsyrejämvikten i Baltiska Havet. *Fennia* **68**: 29–81.
- Cai, W., and others. 2008. A comparative overview of weathering intensity and HCO_3^- -flux in the world's major rivers with emphasis on the Changjiang, Huanghe, Zhujiang (Pearl) and Mississippi Rivers. *Cont. Shelf Res.* **28**: 1538–1549. doi:10.1016/j.csr.2007.10.014
- Cai, W. J., X. Hu, W. J. Huang, L. Q. Jiang, Y. Wang, T. H. Peng, and X. Zhang. 2010. Alkalinity distribution in the western North Atlantic Ocean margins. *J. Geophys. Res. Ocean.* **115**: 1–15. doi:10.1029/2009JC005482
- Crawley, M. J. 2007. *The R Book*. Wiley-VCH.
- Dickson, A. G. 1990. Standard potential of the reaction $\text{AgCl(s)} + 1/2 \text{H}_2(\text{g}) = \text{Ag(s)} + \text{HCl(aq)}$, and the standard acidity constant of the ion HSO_4^- in synthetic sea

- water from 273.15 to 318.15 K. *J. Chem. Thermodyn.* **22**: 113–127. doi:10.1016/0021-9614(90)90074-Z
- Dickson, A., and J. Riley. 1979. The estimation of acid dissociation constants in seawater media from potentiometric titrations with strong base. I. The ionic product of water — Kw. *Mar. Chem.* **7**: 89–99. doi:10.1016/0304-4203(79)90001-X
- Dickson, A. G., C. L. Sabine, and J. R. Christian. 2007. Guide to best practices for ocean CO₂ measurements, PICES Special Publication 3, North Pacific Marine Science Organization, Sidney, British Columbia.
- Doney, S. C., V. J. Fabry, R. A. Feely, and J. A. Kleypas. 2009. Ocean acidification: The other CO₂ problem. *Ann. Rev. Mar. Sci.* **1**: 169–192. doi:10.1146/annurev.marine.010908.163834
- Dyrssen, D. 1993. The Baltic-Kattegat-Skagerrak estuarine system. *Estuaries* **16**: 446–452. doi:10.2307/1352592
- Edman, M., and A. Omstedt. 2013. Modeling the dissolved CO₂ system in the redox environment of the Baltic Sea. *Limnol. Oceanogr.* **58**: 74–92. doi:10.4319/lo.2013.58.1.0074
- Friis, K., A. Körtzinger, and D. W. R. Wallace. 2003. The salinity normalization of marine inorganic carbon chemistry data. *Geophys. Res. Lett.* **30**: 1–4. doi:10.1029/2002GL015898
- Fry, C. H., T. Tyrrell, M. P. Hain, N. R. Bates, and E. P. Achterberg. 2015. Analysis of global surface ocean alkalinity to determine controlling processes. *Mar. Chem.* **174**: 46–57. doi:10.1016/j.marchem.2015.05.003
- Gailiušis, B., J. Kriaučiūnienė, D. Jakimavičius, and D. Šarauskienė. 2011. The variability of long-term runoff series in the Baltic Sea drainage basin. *BALTICA* **24**: 45–54. ISSN 0067-3064.
- Granier, C., and others. 2011. Evolution of anthropogenic and biomass burning emissions of air pollutants at global and regional scales during the 1980–2010 period. *Clim. Change* **109**: 163–190. doi:10.1007/s10584-011-0154-1
- Gripenberg, S. 1936. On the determination of excess base in seawater. *Vth Hydrol. Conf. Balt. States*.
- Gustafsson, B. G., and others. 2012. Reconstructing the development of baltic sea eutrophication 1850–2006. *Ambio* **41**: 534–548. doi:10.1007/s13280-012-0318-x
- Gustafsson, E., T. Wällstedt, C. Humborg, M. Mörth, and B. G. Gustafsson. 2014. External total alkalinity loads versus internal generation: The influence of nonriverine alkalinity sources in the Baltic Sea. *Global Biogeochem. Cycles* **28**: 1358–1370. doi:10.1002/2014GB004888
- Gustafsson, E., A. Omstedt, and B. G. Gustafsson. 2015. The air-water CO₂ exchange of a coastal sea—A sensitivity study on factors that influence the absorption and outgassing of CO₂ in the Baltic Sea. *J. Geophys. Res. Ocean.* **210**: 5342–5357 doi:10.1002/2015JC010832
- Håkanson, L., M. Andersson, and L. Rydén. 2003. The Baltic Sea Basin: Nature, history, and economy, p. 92–119. *In* L. Rydén, P. Migula and M. Andersson [eds.], *Environmental science: Understanding, protecting and managing the environment in the Baltic Sea Region*. Baltic Univ. Press.
- Hansson, D., C. Eriksson, A. Omstedt, and D. Chen. 2011. Reconstruction of river runoff to the Baltic Sea, AD 1500–1995. *Int. J. Climatol.* **31**: 696–703. doi:10.1002/joc.2097
- Helcom. 1993. First assessment of the state of the coastal waters of the Baltic Sea. *Baltic Sea Environment Proceedings* No. 54. 1–160.
- Helcom. 2015. Updated Fifth Baltic Sea pollution load compilation (PLC-5.5). *Baltic Sea Environment Proceedings* No. 145. 143.
- Hjalmarsson, S., K. Wesslander, L. G. Anderson, A. Omstedt, M. Perttilä, and L. Mintrop. 2008. Distribution, long-term development and mass balance calculation of total alkalinity in the Baltic Sea. *Cont. Shelf Res.* **28**: 593–601. doi:10.1016/j.csr.2007.11.010
- Hofmann, G. E., J. P. Barry, P. J. Edmunds, R. D. Gates, D. A. Hutchins, T. Klinger, and M. A. Sewell. 2010. The effect of ocean acidification on calcifying organisms in marine ecosystems: An organism-to-ecosystem perspective. *Annu. Rev. Ecol. Evol. Syst.* **41**: 127–147. doi:10.1146/annurev.ecolsys.110308.120227
- IPCC. 2013. Summary for policymakers, p. 27. *In* T. F. Stocker and others [eds.], *Climate Change 2013: The Physical Science Basis. Contribution of Working Group I to the Fifth Assessment Report of the Intergovernmental Panel on Climate Change*. Cambridge Univ. Press.
- Jiang, Z., T. Tyrrell, D. J. Hydes, M. Dai, and S. E. Hartman. 2014. Variability of alkalinity and the alkalinity-salinity relationship in the tropical and subtropical surface ocean. *Global Biogeochem. Cycles* **28**: 729–742. doi:10.1002/2013GB004678
- Khatiwala, S., and others. 2013. Global ocean storage of anthropogenic carbon. *Biogeosciences* **10**: 2169–2191. doi:10.5194/bg-10-2169-2013
- Kremling, K., and G. Wilhelm. 1997. Recent increase of the calcium concentrations in Baltic Sea waters. *Mar. Pollut. Bull.* **34**: 763–767. doi:10.1016/S0025-326X(97)00048-9
- Kroeker, K. J., R. L. Kordas, R. N. Crim, and G. G. Singh. 2010. Meta-analysis reveals negative yet variable effects of ocean acidification on marine organisms. *Ecol. Lett.* **13**: 1419–1434. doi:10.1111/j.1461-0248.2010.01518.x
- Kuliński, K., and J. Pempkowiak. 2011. The carbon budget of the Baltic Sea. *Biogeosciences* **8**: 3219–3230. doi:10.5194/bg-8-3219-2011
- Kuznetsov, I., and T. Neumann. 2013. Simulation of carbon dynamics in the Baltic Sea with a 3D model. *J. Mar. Syst.* **111–112**: 167–174. doi:10.1016/j.jmarsys.2012.10.011
- Lajtha, K., and J. Jones. 2013. Trends in cation, nitrogen, sulfate and hydrogen ion concentrations in precipitation in the United States and Europe from 1978 to 2010: A new look at an old problem. *Biogeochemistry* **116**: 303–334. doi:10.1007/s10533-013-9860-2

- Lavigne H., Epitalon, J.-M. & Gattuso J.-P., 2011. seacarb: seawater carbonate chemistry with R. R package version 3.0. <http://CRAN.R-project.org/package=seacarb>
- Le Quéré, C., and others. 2015. Global carbon budget 2015. *Earth Syst. Sci. Data* **7**: 349–396. doi:10.5194/essd-7-349-2015
- Lee, K., and others. 2003. An updated anthropogenic CO₂ inventory in the Atlantic Ocean. *Global Biogeochem. Cycles* **17**: 27/1–27/17. doi:10.1029/2003GB002067
- Lenton, T. M., and C. Britton. 2006. Enhanced carbonate and silicate weathering accelerates recovery from fossil fuel CO₂ perturbations. *Global Biogeochem. Cycles* **20**: GB3009/1–GB3009/12. doi:10.1029/2005GB002678
- MacFarling Meure, C., and others. 2006. Law Dome CO₂, CH₄ and N₂O ice core records extended to 2000 years BP. *Geophys. Res. Lett.* **33**: L14810. doi:10.1029/2006GL026152
- Macpherson, G. L., J. A. Roberts, J. M. Blair, M. A. Townsend, D. A. Fowle, and K. R. Beisner. 2008. Increasing shallow groundwater CO₂ and limestone weathering, Konza Prairie, USA. *Geochim. Cosmochim. Acta* **72**: 5581–5599. doi:10.1016/j.gca.2008.09.004
- Melzner, F., and others. 2012. Future ocean acidification will be amplified by hypoxia in coastal habitats. *Mar. Biol.* **160**: 1875–1888. doi:10.1007/s00227-012-1954-1
- Millero, F. J. 2010. Carbonate constants for estuarine waters. *Mar. Freshw. Res.* **61**: 139. doi:10.1071/MF09254
- Millero, F. J., K. Lee, and M. Roche. 1998. Distribution of alkalinity in the surface waters of the major oceans. *Mar. Chem.* **60**: 111–130. doi:10.1016/S0304-4203(97)00084-4
- Mucci, A. 1983. The solubility of calcite and aragonite in seawater at various salinities, temperatures and one atmosphere total pressure. *Am. J. Sci.* **283**: 780–799. doi:10.2475/ajs.283.7.780
- Oh, N.-H., and P. A. Raymond. 2006. Contribution of agricultural liming to riverine bicarbonate export and CO₂ sequestration in the Ohio River basin. *Global Biogeochem. Cycles* **20**: 1–17. doi:10.1029/2005GB002565
- Oh, N. H., M. Hofmockel, M. L. Lavigne, and D. D. Richter. 2007. Did elevated atmospheric CO₂ alter soil mineral weathering?: An analysis of 5-year soil water chemistry data at Duke FACE study. *Glob. Chang. Biol.* **13**: 2626–2641. doi:10.1111/j.1365-2486.2007.01452.x
- Ohlson, M., and L. Anderson. 1990. Recent investigation of total carbonate in the Baltic Sea: Changes from the past as a result of acid rain? *Mar. Chem.* **30**: 259–267. doi:10.1016/0304-4203(90)90075-N
- Omstedt, A., M. Edman, B. Claremar, and A. Rutgersson. 2015. Modelling the contributions to marine acidification from deposited SO_x, NO_x, and NH_x in the Baltic Sea: Past and present situations. *Cont. Shelf Res.* **111**: 234–249. doi:10.1016/j.csr.2015.08.024
- R Development Core Team (2014). R: A language and environment for statistical computing. R Foundation for Statistical Computing, Vienna, Austria. ISBN 3-900051-07-0, URL <http://www.R-project.org>.
- Raymond, P. A., and J. J. Cole. 2003. Increase in the export of alkalinity from North America's largest river. *Science* **301**: 88–91. doi:10.1126/science.1083788
- Sarmiento, J. L., and N. Gruber. 2006. Ocean biogeochemical dynamics. Princeton Univ. Press.
- Schneider, B., K. Eilola, K. Ukkari, B. Müller-Karulis, and T. Neumann. 2015. Environmental impacts—marine biogeochemistry, p. 337–361. *In* The BACC II Author Team [ed.], Second assessment of climate change for the Baltic Sea Basin. Springer International Publishing.
- Stets, E. G., V. J. Kelly, and C. G. Crawford. 2014. Long-term trends in alkalinity in large rivers of the conterminous US in relation to acidification, agriculture, and hydrologic modification. *Sci. Total Environ.* **488–489**: 280–289. doi:10.1016/j.scitotenv.2014.04.054
- Sundquist, E. T. 1991. Steady- and non-steady-state carbonate-silicate controls on atmospheric CO₂. *Quat. Sci. Rev.* **10**: 283–296. doi:10.1016/0277-3791(91)90026-Q
- Svenson, T., W. Dickson, J. Hellberg, G. Moberg, and N. Munthe. 1995. The Swedish liming programme. *Water Air Soil Pollut.* **85**: 1003–1008. doi:10.1007/BF00476961
- The BACC Author Team. 2008. Assessment of climate change for the Baltic Sea Basin. Springer.
- The BACC II Author Team. 2015. Second assessment of climate change for the Baltic Sea Basin. Springer International Publishing.
- Thomsen, J., K. Haynert, K. M. Wegner, and F. Melzner. 2015. Impact of seawater carbonate chemistry on the calcification of marine bivalves. *Biogeosciences* **12**: 4209–4220. doi:10.5194/bg-12-4209-2015
- Tyrrell, T., B. Schneider, A. Charalampopoulou, and U. Riebesell. 2008. Coccolithophores and calcite saturation state in the Baltic and Black Seas. *Biogeosciences* **5**: 485–494. doi:10.5194/bg-5-485-2008
- Vestreng, V., G. Myhre, H. Fagerli, S. Reis, and L. Tarrasón. 2007. Twenty-five years of continuous sulphur dioxide emission reduction in Europe. *Atmos. Chem. Phys.* **7**: 3663–3681. doi:10.5194/acp-7-3663-2007
- Wilson, D., H. Hisdal, and D. Lawrence. 2010. Has streamflow changed in the Nordic countries?—Recent trends and comparisons to hydrological projections. *J. Hydrol.* **394**: 334–346. doi:10.1016/j.jhydrol.2010.09.010
- Winkler, P. 1983. Trend Development of Precipitation-PH in Central Europe, p. 114–122. *In* S. Beilke and A.J. Elshout [eds.], Acid Deposition. Springer Netherlands. doi:10.1007/978-94-009-7139-4_10
- Winsor, P., J. Rodhe, and A. Omstedt. 2001. Baltic Sea ocean climate: An analysis of 100 yr of hydrographic data with focus on the freshwater budget. *Clim. Res.* **18**: 5–15. doi:10.3354/cr018005
- Winsor, P., J. Rodhe, and A. Omstedt. 2003. Erratum: Baltic Sea ocean climate: An analysis of 100 yr of hydrographical data with focus on the freshwater budget. *Climate Research*, **18**:5–15, 2001. *Clim. Res.* **25**: 183.

Wolf-Gladrow, D. A., R. E. Zeebe, C. Klaas, A. Körtzinger, and A. G. Dickson. 2007. Total alkalinity: The explicit conservative expression and its application to biogeochemical processes. *Mar. Chem.* **106**: 287–300. doi: [10.1016/j.marchem.2007.01.006](https://doi.org/10.1016/j.marchem.2007.01.006)

Acknowledgments

We greatly acknowledge the extensive monitoring work performed mainly by SMHI and FMI and the support for the data compilation and correct referencing by Leif Anderson, Matti Perttola, Antti Räsänen, Anders Omstedt and in particular Mikael Krysell, who in addition provided us with information to evaluate the quality of historic alkalinity observations. For an extensive revision of the manuscript and valuable comments we acknowledge David Kaiser, Friederike Saathoff and two anonymous reviewers. The research leading to this manuscript has

received funding from BONUS, the joint Baltic Sea research and development programme (Art 185), funded jointly from the European Union's Seventh Programme for research, technological development and demonstration and from the German Federal Ministry of Education and Research through Grant No. 03F0689A (BONUS PINBAL).

Conflict of Interest

None declared.

Submitted 9 March 2016

Revised 3 May 2016

Accepted 9 May 2016

Associate editor: James Falter

pH Measurements in Brackish Waters: Extending Electrochemical pH_T Measurements of TRIS buffers to Salinities 5 – 20

J.D. Müller¹, F. Bastkowski^{2,*}, B. Sander², S. Seitz², D.R. Turner³, A.G. Dickson⁴, G. Rehder¹

¹Department of Marine Chemistry, Leibniz Institute for Baltic Sea Research Warnemünde, Rostock, Germany

²Department of Physical Chemistry, Physikalisch-Technische Bundesanstalt, Braunschweig, Germany

³Department of Marine Sciences, University of Gothenburg, Gothenburg, Sweden

⁴Marine Physical Laboratory, Scripps Institution of Oceanography, University of California, San Diego, La Jolla, USA

*corresponding author: Frank Bastkowski, Frank.Bastkowski@ptb.de

Abstract

Harned cell pH_T measurements were performed on 2-amino-2-hydroxymethyl-1,3-propanediol (TRIS) buffered artificial seawater solutions in the salinity range 5-20, at three equimolar buffer concentrations (0.01, 0.025, 0.04 mol·kg-H₂O⁻¹), and in the temperature range 278.15 – 318.15 K. Measurement uncertainties were assigned to the pH_T values of the buffer solutions and ranged from 0.002 to 0.004 over the investigated salinity and temperature ranges. Obtained pH_T data were combined with previous results from literature covering salinities from 20 to 40. A model function expressing pH_T as a function of salinity, temperature and TRIS/TRIS·H⁺ molality was fitted to the combined data set. The results can be used to reliably calibrate pH instruments traceable to primary standards and over the salinity range 5 to 40, in particular, covering the low salinity range of brackish water for the first time. At salinities 5-20 and 35, the investigated dependency of pH_T on the TRIS/TRIS·H⁺ molality allows to extrapolate quantities calibrated against the pH_T values, e.g., the dissociation constants of pH indicator dyes, to zero TRIS molality. The extrapolated quantities refer to pure synthetic seawater conditions and define a true hydrogen ion concentration scale in seawater media without constraints.

Keywords

Harned cell, traceability, primary standard, TRIS, pH, total scale, buffer, brackish water, estuary, seawater.

Introduction

The change of seawater pH is linked to changes in the concentration of dissolved inorganic carbon and alkalinity. Precise and accurate pH measurements are therefore an ideal tool to investigate two processes of global importance: (i) Ocean acidification, caused by the

uptake of anthropogenic carbon dioxide (CO_2) from the atmosphere (Le Quéré et al., 2016), can directly be traced by pH measurements in open ocean environments (Byrne et al., 2010). (ii) The investigation of biogeochemical transformations can be supported by pH measurements, as any production or mineralization of organic matter is inevitably coupled to the uptake and release of CO_2 .

According to its definition on the activity scale, $\text{pH} = -\log_{10}(a_{\text{H}^+})$, pH involves a single ion quantity and is as such immeasurable by any thermodynamically valid method (Buck et al., 2002). Therefore, pH measurements according to the IUPAC recommendation require conventions which are only valid for ionic strength $\leq 0.1 \text{ mol}\cdot\text{kg}^{-1}$. For measurements in seawater with higher ionic strength it is convenient to measure pH on scales that refer to the hydrogen ion concentration. The definition of such concentration scales requires the definition of a standard composition of the seawater, because hydrogen ions are in equilibrium with other acid base components in seawater. The so called pH_T , where the index T denotes the total pH scale, became a widely accepted convention within the scientific community (Dickson et al., 2015). According to its definition, $\text{pH}_T = -\log_{10}\{[\text{H}^+] \cdot (1 + [\text{SO}_4^-]_T / K_{\text{HSO}_4^-})\}$, it accounts for the concentrations of both, the free hydrogen ions, $[\text{H}^+]$, and bisulfate ions, expressed as the total sulfate concentration $[\text{SO}_4^-]_T$ divided by the dissociation constant of bisulfate $K_{\text{HSO}_4^-}$. The latter contributes to the acidity of the solution by the potential to transfer further hydrogen ions to other proton acceptors.

In order to assure comparability of pH_T measurement results, internationally accepted primary pH_T standards are inevitable. Currently the de facto standards are TRIS (2-amino-2-hydroxymethyl-1,3-propanediol) buffered artificial seawater (ASW) solutions (DeValls and Dickson, 1998; Pratt, 2014) in the salinity (S) range 20-40, whose pH_T values have been measured using an electrochemical setup comprising so called Harned cells. This setup represents a primary method for pH measurements (Buck et al., 2012). In oceanographic practice, pH_T is typically measured by other methods such as spectrophotometric (Clayton and Byrne, 1993; Liu et al., 2011) and ISFET (Martz et al., 2010) measurements. The spectrophotometric pH_T measurement relies on pH indicator dyes such as m-Cresol Purple (mCP). Standard buffer solutions with well-defined, traceable pH_T values are required for the physico-chemical characterization of the purified dyes (Liu et al., 2011). Up to now, Harned cell measurements on TRIS buffered ASW solutions in the lower salinity range ($S < 20$) were missing. Consequently, spectrophotometrically obtained pH_T values in this salinity range were not traceable to a primary pH_T standard. Mosley et al. (2004) provided an interim solution by interpolating the pH_T values of TRIS buffered ASW solutions for the salinity range 0-20. The

interpolation was based on the results for $S=20-40$ of DelValls and Dickson (1998) and for TRIS in pure water by Bates and Hetzer (1961). The accuracy of the latter results is questionable, because measurements were performed on TRIS solutions in pure water and the buffer ionic strength was interpreted as salinity, although the solutions contained no other salts. Moreover, non-purified dye was used for the mCP characterization and measurements were conducted only at 298.15 K. Consequently, spectrophotometric pH_T measurements in brackish waters with salinity below 20 were not traceable to a primary pH_T standard and results were subject to an unknown degree of measurement uncertainty.

To fill this gap, we present Harned cell pH_T measurement results in the salinity range 5-20 and, in addition, at 35 for consistency assessment with previous results of DelValls and Dickson (1998) and Pratt (2014). In particular, we discuss issues of sample preparation in the low salinity range, which differs significantly from that in the upper salinity range and affects pH_T measurements. Measurements were performed in the temperature range 278.15 to 318.15 K. All buffer solutions were prepared at three equimolar amounts of TRIS/TRIS $\cdot\text{H}^+$, which allows extrapolating calibration parameters determined in these solutions to pure artificial seawater conditions as recommended by Nemzer and Dickson (2005). We combined our results with those of DelValls and Dickson (1998) to derive a consistent pH_T model for the salinity range 5-40, which is a prerequisite to compare pH_T values measured in ocean and brackish waters.

Materials and Methods

Scope and concept

We prepared and analyzed TRIS buffered ASW solutions (ASW/TRIS-HCl) with salinities $S = 5, 10, 15, 20,$ and 35 . Preparing low-saline buffer solutions for subsequent calibration of pH instruments includes a general problem: HCl and the buffer substance added contribute significantly to the ionic strength of the buffer solution. An equivalent amount of salt components of the ASW matrix has to be removed to ensure constant ionic strength. Consequently, the solution composition used for the calibration of any pH instrument differs from the seawater to be analyzed. For a classical equimolar TRIS/TRIS $\cdot\text{H}^+$ buffer with a molality of $0.04 \text{ mol}\cdot\text{kg}\cdot\text{H}_2\text{O}^{-1}$ (DelValls and Dickson, 1998), the ionic strength contribution ranges from 5-10% for salinities of 20-40. The impact of this ionic strength contribution on the determination of the dissociation constant of mCP was not yet assessed. Even though it might be negligible within the overall uncertainty of seawater pH_T measurements at salinities above 20, this assumption is critical at lower salinities since the contribution of the buffer substance increases with decreasing salinity. This problem is inevitable and counteracting it by reducing the concentration of the buffer component

comes at the cost of reduced buffer stability. To account for this problem, equimolal buffer consisting of TRIS and protonated TRIS ($\text{TRIS}\cdot\text{H}^+$) each at molalities of 0.04, 0.025 and 0.01 $\text{mol}\cdot\text{kg}\cdot\text{H}_2\text{O}^{-1}$ were prepared and individual pH_T values measured. This allows in subsequent calibration experiments to extrapolate quantities to zero TRIS/TRIS $\cdot\text{H}^+$ molality (Müller et al., *subm.*).

The relative composition of the salts (NaCl, MgCl_2 , Na_2SO_4 , CaCl_2 , and KCl) that form the ASW matrix is an associated problem. DelValls and Dickson (1998) computed the salt composition by first scaling a TRIS-free reference composition from $S=35$ to the target salinity. Afterwards, the amount of NaCl was reduced by the amount of HCl added to maintain the nominal ionic strength. If a specific HCl concentration, e.g. 0.04 mol kg^{-1} , is adjusted, this approach implies changing ratios between Na^+ and other cations at different salinities. For salinities of 20-40 those changes are small (Fig. 1A). However, toward lower salinities differences in the cation ratios become more pronounced. At a salinity of ~ 4 , NaCl would be entirely replaced by HCl when preparing solutions according to DelValls and Dickson (1998). Therefore, only our buffers at $S=35$ and the buffer at $S=20$ with equimolal TRIS/TRIS $\cdot\text{H}^+$ molality of 0.04 $\text{mol}\cdot\text{kg}\cdot\text{H}_2\text{O}^{-1}$ have been prepared according to the recipe of DelValls and Dickson (1998) in order to achieve best comparability to previous studies. The recipe was modified to achieve constant ratios between the ASW salts for all other buffer solutions.

Preparation of the TRIS-HCl and HCl solutions in artificial seawater

We have chosen the composition proposed by DelValls and Dickson (1998) for $S = 20$ and HCl molality $b_{\text{HCl}} = 0.04 \text{ mol}\cdot\text{kg}\cdot\text{H}_2\text{O}^{-1}$ as the reference composition of ASW (Table 1). Reported salinities therefore refer to the nominal scale according to DelValls and Dickson (1998). Based on the reference composition at $S=20$, the concentrations of all ASW salts were varied proportionally to compensate the HCl ionic strength contribution and achieve the target salinity.

This proportional variation of the molality b of any salt component x (NaCl, MgCl_2 , Na_2SO_4 , CaCl_2 and KCl) was computed as a function of S and b_{HCl} according to:

$$b_x(S, b_{\text{HCl}}) = \frac{I(S) - b_{\text{HCl}}}{I(20) - 0.04 \text{ mol}\cdot\text{kg}\cdot\text{H}_2\text{O}^{-1}} \cdot b_x(20, 0.04 \text{ mol}\cdot\text{kg}\cdot\text{H}_2\text{O}^{-1}) \quad (1)$$

where b_{HCl} is the target molality of HCl in $\text{mol}\cdot\text{kg}\cdot\text{H}_2\text{O}^{-1}$ (which is identical to $b_{\text{TRIS/TRIS}\cdot\text{H}^+}$), 0.04 $\text{mol}\cdot\text{kg}\cdot\text{H}_2\text{O}^{-1}$ refers to b_{HCl} in the reference solution, $b_x(20, 0.04 \text{ mol}\cdot\text{kg}\cdot\text{H}_2\text{O}^{-1})$ is the molality of salt x in the reference solution summarized in Table 1, and I is the ionic strength calculated from the target salinity S by:

$$I(S) = \frac{19.919 \cdot S}{1000 - 1.00192 \cdot S} \quad (2)$$

Based on the reference composition of ASW according to DelValls and Dickson (1998), equation (2) achieves proportional scaling of ionic strength in moles per kg solution with salinity (nominator) and conversion to ionic strength in moles per kg water (denominator). Coefficients in equation (2) are based on IUPAC 2013 atomic weights (Meija et al., 2016).

Table 1: Reference solution composition computed according to DelValls and Dickson (1998) for $S=20$ and $b_{\text{HCl}} = 0.04 \text{ mol} \cdot \text{kg} \cdot \text{H}_2\text{O}^{-1}$.

Component	Molality ($\text{mol} \cdot \text{kg} \cdot \text{H}_2\text{O}^{-1}$)
NaCl	0.20061
Na_2SO_4	0.01647
KCl	0.00595
MgCl_2	0.03080
CaCl_2	0.00605

For measurements of pH_T with Harned cells it is necessary to determine the standard potential of the silver-silver chloride ($\text{Ag}|\text{AgCl}$) electrodes. This can be achieved by measurements of a serial dilution of HCl in the respective solution (see chapter “Determination of pH_T ” below). Therefore, HCl solutions were prepared in ASW (ASW/HCl) at b_{HCl} of 0.0025, 0.005, 0.01, 0.02, 0.03, 0.04 and 0.05 $\text{mol} \cdot \text{kg} \cdot \text{H}_2\text{O}^{-1}$ at each target salinity according to equations (1) and (2) and table 1.

Our preparation method of ASW/TRIS-HCl and ASW/HCl solutions has the following implications at salinities ≤ 20 :

- Constant ratios of the ASW salt components at all salinities and HCl molalities, which is reflected in the $b_{\text{NaCl}} : b_{\text{MgCl}_2}$ ratio (Fig. 1A).
- Variable chloride and sulfate molality at a given salinity, because more sulfate is removed at higher HCl (Fig. 1B). This change in sulfate molality requires corrections (see “Sulfate correction for effective $E^{*\circ}$ values” below).

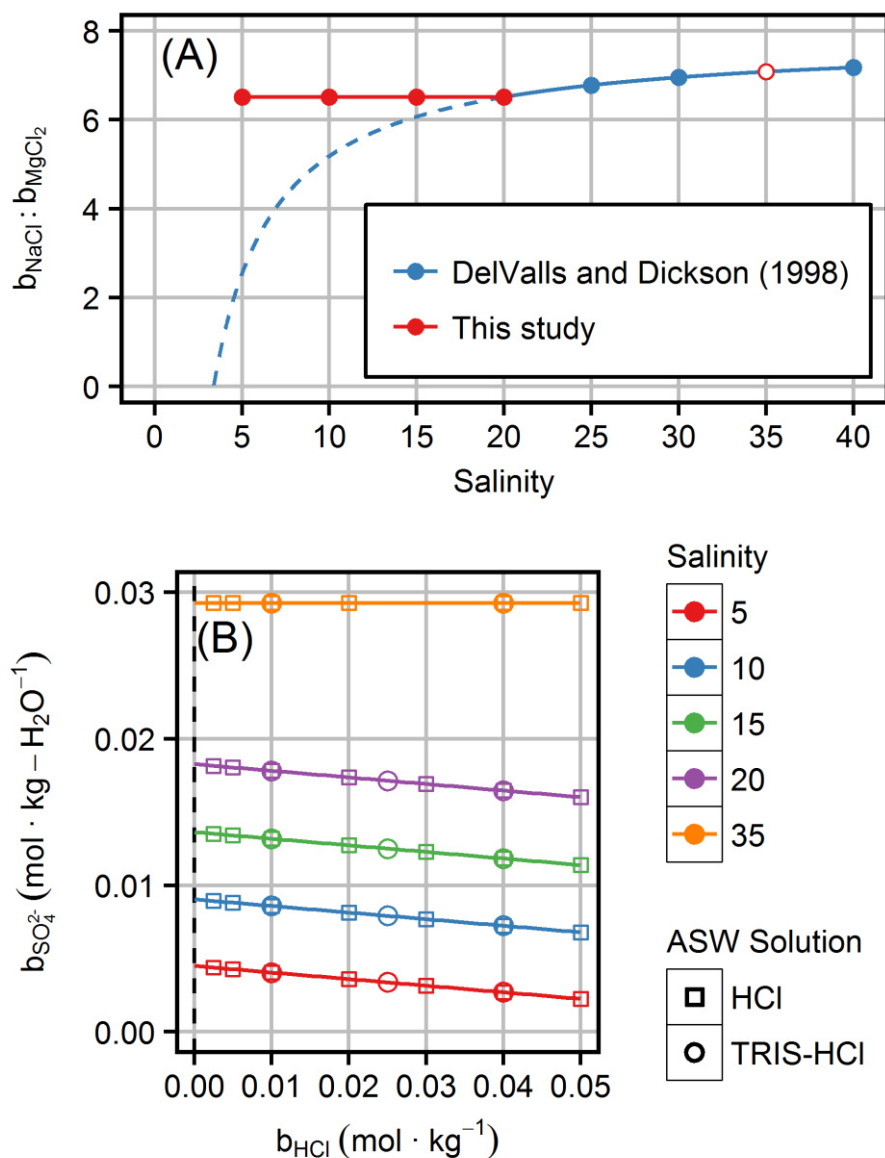


Fig. 1: Characteristics of artificial seawater solutions prepared in this study: (A) Cation composition represented by $b_{\text{NaCl}} : b_{\text{MgCl}_2}$ ratios for ASW solutions with a HCl molality of 0.04 mol·kg-H₂O⁻¹. The cation ratios as prepared in this study (red) are compared to those proposed by DeValls and Dickson (1998) - actually prepared: blue circles and solid line; recipe hypothetically applied for lower salinities: dashed blue line. (B) Sulfate molality, $b_{\text{SO}_4^{2-}}$, as a function of HCl molality and salinity. Squares represent HCl solutions in ASW to measure the standard potential of the Harned, E° . Circles indicate the three investigated TRIS/TRIS·H⁺ molalities.

All solutions were prepared from stock solutions of NaCl, KCl, CaCl₂, MgCl₂, Na₂SO₄, TRIS and HCl that have been gravimetrically prepared with ultrapure water (cf supplement). All weighings were performed using an analytical balance (Sartorius Genius) and were buoyancy corrected. The air density for buoyancy correction was calculated from the atmospheric conditions measured with a combined humidity and temperature sensor (Almemo) as well as a barometer (Setra Systems).

The various salts, NaCl, KCl, CaCl_2 , MgCl_2 (originating from MV laboratories Inc., Frenchtown, NJ, USA and kindly supplied from METAS, Switzerland), and Na_2SO_4 (originating from Merck), were characterized by coulometric measurements (cf supplement: Tab. S1 and S2.1). NaCl and KCl were dried at 383 K for 2 hours before use. CaCl_2 and MgCl_2 are hygroscopic. Hence, stock solutions were prepared and characterized using ion chromatography (cf supplement: Tab. S2.1). TRIS was purchased from NIST (SRM 723e). No losses of TRIS weight on drying over magnesium perchlorate could be detected in the range of weighing uncertainty. The HCl stock solution was prepared from Titrisol ampoules (Merck). The HCl stock solution molality was assayed by potentiometric titration against the stock solution of TRIS SRM 723e (cf supplement). The titration of the HCl- against the TRIS stock solution ensures equimolar TRIS/TRIS \cdot H⁺ ratios in the produced buffer solutions. All dilutions were carried out with ultrapure water obtained from a Milli-Q system. Actual salinities of the ASW/TRIS-HCl solutions were calculated from actual ionic strength based on weighings according to equation (2).

Harned cell measurements:

The pH_T values of the ASW/TRIS-HCl solutions have been calculated from measured potentials using Harned cells (Harned and Owen, 1958), which consist of a platinum hydrogen electrode and an Ag|AgCl reference electrode. Both electrodes are placed into a U-tube measurement cell. Both electrodes are in direct contact with the solution measured, i.e. there is no electrolyte bridge or a similar junction necessary to connect the electrodes electrically. The cells also comprise a unit for humidification of the hydrogen gas (see picture of the utilized Harned measurement cell in the supplement). The cell voltage was measured after temperature stabilization using a digital voltmeter (Agilent A3458) and corrected for the actual partial pressure of the hydrogen gas p_{H_2} (Hills and Ives 1951). Details of the Harned cell setup and the cell voltage correction are given in the supplement.

Measurements of the artificial seawater solutions containing TRIS-HCl were always measured in triplicate while artificial seawater solutions containing different HCl molalities were measured only once in most of the cases (cf. table S5.1 and S5.2 in the supplement).

Determination of pH_T :

pH_T is defined on an amount content basis (moles per kilogram solution). However, the electrochemical measurement of pH_T is established via the molality based expression of pH_b (DeValls and Dickson, 1998) according to:

$$\text{pH}_b = \frac{E_{\text{ASW/TRIS-HCl}} - E^{*\circ}}{\frac{RT \ln 10}{F}} + \log_{10} \left(\frac{b_{\text{Cl}^-}}{b^\circ} \right) \quad (3)$$

with the electric Harned cell potential $E_{\text{ASW/TRIS-HCl}}$ of the buffered artificial seawater solution, the standard potential $E^{*\circ}$ of the Ag|AgCl electrode in pure ASW of the same nominal salinity, the molality b_{Cl^-} of chloride in the solution and the standard molality $b^\circ = 1 \text{ mol} \cdot \text{kg} \cdot \text{H}_2\text{O}^{-1}$. The expression of pH_b in equation (3) assumes that the activity coefficient of HCl is the same in the buffer solution as its trace value in the pure artificial seawater (see discussion).

$E^{*\circ}$ was determined at each salinity and temperature from measured potentials $E_{\text{ASW/HCl}}$ of 7 ASW solutions with HCl molalities ranging from $0.0025 \text{ mol} \cdot \text{kg} \cdot \text{H}_2\text{O}^{-1}$ to $0.05 \text{ mol} \cdot \text{kg} \cdot \text{H}_2\text{O}^{-1}$. Therefore, E' values were calculated from measured $E_{\text{ASW/HCl}}$ according to equation (4):

$$E' = E_{\text{ASW/HCl}} + \frac{RT \ln 10}{F} \cdot \log_{10} \left(\frac{b_{\text{HCl}} \cdot b_{\text{Cl}^-}}{(b^\circ)^2} \right) \quad (4)$$

with b_{HCl} the molality of HCl. $E^{*\circ}$ was determined as the intercept at zero HCl molality of a second order polynomial fitted to E' as a function of b_{HCl} .

The pH_b value derived from equation (3) is molality based, while pH_T is defined in terms of the amount content (moles per kg solution). Therefore pH_T has to be calculated from pH_b (DeValls and Dickson, 1998) according to:

$$\text{pH}_T = \text{pH}_b - \log_{10}(1 - 0.00106 \cdot S) \quad (5)$$

where the term $1 - 0.00106 \cdot S$ expresses the relation between salinity and the water content of the pure ASW solution, $\omega_{\text{H}_2\text{O}}$. The latter is defined as mass water per mass solution (See discussion).

12 Harned cells have been used to measure the potential of 12 solutions synchronously to reduce measurement time. Measurements of ASW/HCl solution to determine $E^{*\circ}$ were not carried out in the same measurement run as the potential measurements of the ASW/TRIS-HCl solutions for practical reasons. To ensure that the electrochemical properties of the Ag|AgCl electrodes is, within the uncertainty limits, the same for all solutions, the potentials of these electrodes were measured against a master Ag|AgCl electrode. The master electrode was always stored in 0.005 M hydrochloric acid and was considered to be stable in potential with time. The comparison measurements of all electrodes against the master electrode were performed in the same HCl solution before each measurement run and found to differ not more than $85 \mu\text{V}$, corresponding to around 0.0015 in terms of pH.

The uncertainties of the measured pH_T values were determined for all temperatures, salinities and TRIS/TRIS·H⁺ molalities according to the Guide to the expression of uncertainty in measurement (<https://www.bipm.org/en/publications/guides/>) using a Monte Carlo method in Mathematica (for details see supplement).

Sulfate correction for effective E^{*°} values

E^{*°} of an Ag|AgCl electrode that is immersed in artificial seawater containing sulfate can be expressed as (DeValls and Dickson, 1998):

$$E^{*\circ} = E^{\circ} - \frac{2RT}{F} \ln \gamma_{\pm}(HCl) + \frac{RT}{F} \ln \left(1 + \frac{b_{SO_4^{2-},T}}{K_{HSO_4^-}} \right) \quad (6)$$

where E[°] is the potential of the Harned cell under standard conditions, $\gamma_{\pm}(HCl)$ is the trace activity coefficient of HCl in ASW, $b_{SO_4^{2-},T}$ is the total sulfate molality and $K_{HSO_4^-}$ is the limiting molality quotient for bisulfate in artificial seawater medium.

It is assumed that E^{*°}, determined at a particular salinity and temperature, remains unchanged if some of the artificial seawater salts are replaced with TRIS-HCl such that the ionic strength is unchanged. However, in this study the TRIS-HCl addition was compensated by a proportional reduction of all ASW salts to keep the ratios of cations constant. Consequently, the sulfate concentration was also reduced. The change in sulfate concentration requires a correction so that the effective E^{*°} corresponds to the respective ASW/TRIS-HCl solutions (E^{*°}(ASW/TRIS-HCl)) and not to the infinite dilution of HCl solutions to pure ASW condition (E^{*°}(ASW)). According to equation (3) the required correction can be expressed as:

$$\Delta pH_T = \frac{F}{RT \ln 10} (E^{*\circ}(ASW) - E^{*\circ}(ASW/TRIS-HCl)) \quad (7)$$

E^{*°}(ASW) and E^{*°}(ASW/TRIS-HCl) in equation (7) can be expressed by applying equation (6), where $b_{SO_4^{2-},T}$ is replaced by $b_{SO_4^{2-},T}(ASW)$ and $b_{SO_4^{2-},T}(ASW/TRIS-HCl)$, respectively. The former describes the sulfate molality in pure ASW and the latter describes the sulfate molality in ASW containing TRIS-HCl. $K_{HSO_4^-}$ is assumed constant for a given temperature and salinity according to Dickson (1990). Thus

$$\Delta pH_T = \log_{10} \left(1 + \frac{b_{SO_4^{2-},T}(ASW)}{K_{HSO_4^-}} \right) - \log_{10} \left(1 + \frac{b_{SO_4^{2-},T}(ASW/TRIS-HCl)}{K_{HSO_4^-}} \right) \quad (8)$$

The values of ΔpH_T calculated for the solution compositions of this study are displayed in Figure 2 and referred to as sulfate corrections hereafter. This correction does not account for any changes in the activity coefficients implicit in eq. 6 (see discussion).

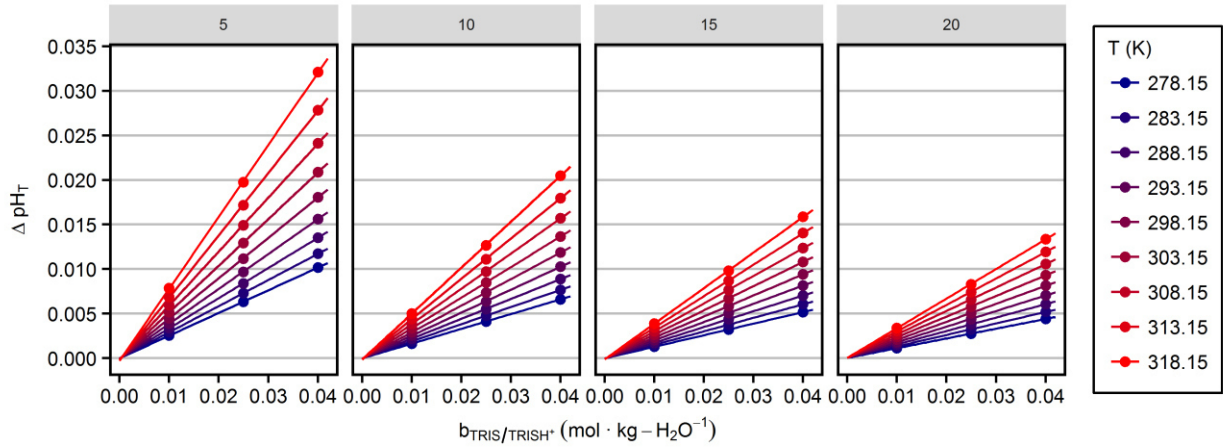


Fig. 2: Correction of pH_T terms due to changes in the total sulfate concentration as a function of TRIS/TRIS·H⁺ molality. Panels represent the four investigated salinities indicated at the top. Lines indicate the linear behavior at various temperatures.

Fitting combined pH_T results for the salinity range 5-40

In order to derive a common expression of pH_T as a function of salinity, temperature and TRIS/TRIS·H⁺ molality over the largest range of conditions, the sulfate corrected pH_T data from this study in the salinity range 5-20 were combined with previous pH_T data in the salinity range 20-40. The latter were calculated from potentials given in Table 2 of DelValls and Dickson (1998) and corresponding E^{*°} values from Dickson (1990) according to equations (3) and (5). Only measurements in the temperature range investigated in this study (278.15-318.15 K) were included in the combined data set.

The following expression of pH_T as a function (f) of S, T and $b_{TRIS/TRIS \cdot H^+}$ was specified as a full model and fitted to the combined data set:

$$\begin{aligned}
 \text{pH}_T = f \left\{ \left[(1 + S + S^2 + S^3) \cdot \left(1 + T + \ln(T) + \frac{1}{T} \right) \right] \right. \\
 \left. + \left[(b_{TRIS/TRIS \cdot H^+} + b_{TRIS/TRIS \cdot H^+}^2) \cdot (1 + S + T + S \cdot T) \right] \right\} \quad (9)
 \end{aligned}$$

The first part of this full model includes all combinations of the terms of a third order salinity polynomial with the terms of the physico-chemical expression of the temperature dependence of dissociation constants. This first part of equation (9) deviates from the model fitted by DelValls and Dickson in their equation (18) only by the higher order of the salinity polynomial. The second part of equation (9) accounts for the dependence of pH_T on the TRIS/TRIS·H⁺ molality. The total number of terms of the full model given in equation (9) is 24.

The fit of the full model was obtained by generalized linear modeling with the “stats” package of the statistical programming language “R” (R Core Team, 2014). The model was fitted to the mean pH_T values at each combination of target salinity, temperature, and TRIS/TRIS·H⁺ molality. Mean pH_T values were weighted by the respective standard measurement uncertainty (Tab S6) as $1/u(\text{pH}_T)^2$. The temperature dependency of measurement uncertainty found in this study at salinities 20 and 35 was fitted with a linear model and the same uncertainty was assigned to the data of DelValls and Dickson (1998). After fitting the full model (eq. 9), insignificant terms were removed by stepwise variable selection in both directions based on the Akaike information criterion. The removal of insignificant terms was performed with the “stepAIC” function from the R package “MASS”, and resulted in an expression with 19 terms given below in equation (10).

Results

pH_T of TRIS buffers

The pH_T values of the equimolal TRIS buffered ASW solutions at salinities 5, 10, 15, 20 and 35, temperatures from 278.15 to 318.15 K in intervals of 5 K, as well as equimolal TRIS/TRIS·H⁺ molalities 0.04, 0.025 and 0.01 mol·kg-H₂O⁻¹ are given in table S6, the corresponding electric potentials of all solutions measured are given in table S5.1 in the supplemental material.

Figure 3 shows mean pH_T values (triplicate measurements) of ASW/TRIS-HCl solutions as a function of temperature (278.15 – 318.15 K), for salinities 5, 10, 15 and 20 and at equimolal TRIS/TRIS·H⁺ molality 0.04 mol kg⁻¹.

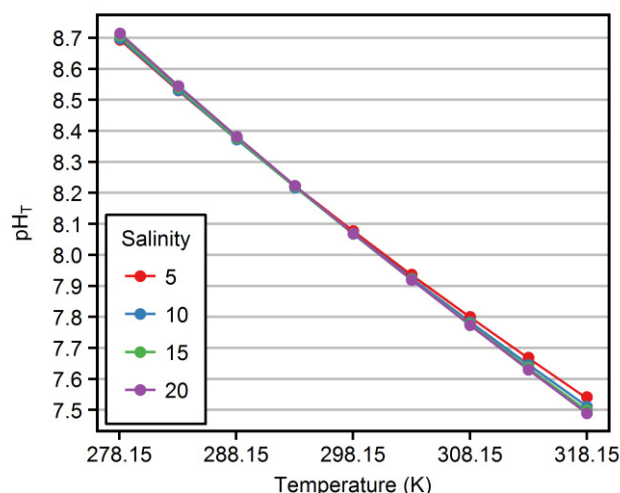


Fig. 3: pH_T values as a function of temperature. Circles represent mean measured pH_T for $b_{\text{TRIS}/\text{TRIS}\cdot\text{H}^+} = 0.04 \text{ mol} \cdot \text{kg}^{-1}$ and salinities 5-20 (color). Lines indicate the fitted pH_T model at respective conditions. Measurement uncertainties are <0.005 and cannot be visualized due to the scaling of the y-axis.

pH_T decreased almost linearly from around 8.7 to 7.5 with increasing temperature (around -0.03 K^{-1}). The investigation of the pH_T dependence on temperature at other TRIS/TRIS·H⁺ molalities showed no significant difference from the results shown in Figure 3.

Figure 4 displays in more detail the dependence of pH_T on salinity and TRIS/TRIS·H⁺ molality, including previous results from DelValls and Dickson (1998). pH_T values shown in Figure 4 were corrected for minor difference ($<0.06 \text{ K}$) between the actual measurement temperature (Tab. S6) and the target temperature indicated at the top of the panels to achieve a consistent presentation with the model results. At low temperatures pH_T decreased with decreasing salinity. Towards higher temperatures lowest pH_T values were found at intermediate salinities.

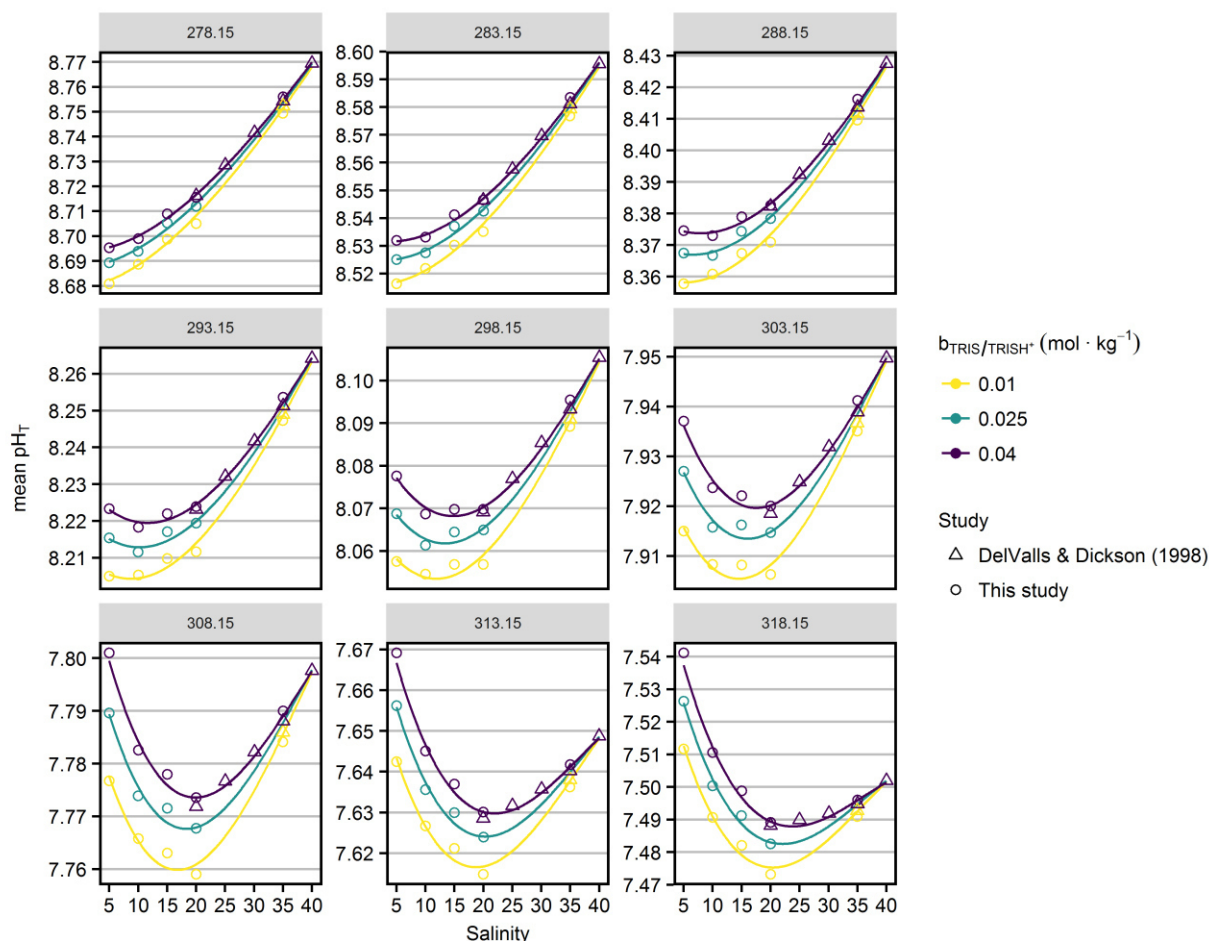


Fig. 4: Mean pH_T values as a function of salinity (x-axis), temperatures (in K, indicated at the top of the panels) and TRIS/TRIS·H⁺ molalities (color). Circles represent results from this study, triangles refer to DelValls and Dickson (1998). Lines represent the pH_T model (eq. 10) fitted to the combined data set.

The expanded measurement uncertainty (coverage factor $k=2$) of pH_T was found to range between 0.002 and 0.004, with the highest uncertainties at salinity 5 and 15 (Fig. 5). The

uncertainty of pH_T significantly increased with temperature at salinity 5 (Fig. S3), whereas the temperature dependence of the measurement uncertainty was much less pronounced at higher salinities.

It was found that the uncertainty of the pH_T values was dominated by the uncertainty contributions of the standard potential of the silver-silver chloride electrodes, $E^{*\circ}$, with relative contributions of 55-95% (Fig. S4). The determination of $E^{*\circ}$ was found to be sensitive to the extrapolation to zero HCl molality. The highest uncertainties of $E^{*\circ}$ were found at salinities 5 and 15 (Fig. S4) explaining the fact, that the highest pH_T uncertainties were found at these salinities (Fig. S3).

The second most important uncertainty contribution was that of the cell potential measured in the buffer solutions, $E_{\text{ASW/TRIS-HCl}}$, ranging between 5% and 35% (Fig. S4). The uncertainty of the measurement temperature T contributed 1% - 4% and the molalities of the NaCl, and MgCl_2 stock solutions contributed in sum 1% -7% to the pH_T measurement uncertainty. All other contributions to the measurement uncertainty were <1%.

pH_T model

The pH_T model fitted to the combined data set including results from this study and DeIvals and Dickson (1998) is expressed in equation (10). The parameters T and $b_{\text{TRIS}/\text{TRIS}\cdot\text{H}^+}$ in equation (10) were multiplied with $1/K$ and $1/\text{mol}\cdot\text{kg}\cdot\text{H}_2\text{O}^{-1}$, respectively, to derive unitless quantities. Corresponding unitless coefficients are given in Table 2.

pH_T values predicted by this model are displayed along with mean pH_T values in Figures 3 and 4. Residuals of triplicate pH_T measurements from the model are shown in Figure 5, along with expanded measurement uncertainties (coverage factor $k=2$). No uncertainties have been available for the results of DeIvals and Dickson (1998). Therefore, we interpolated our uncertainties determined at salinity 20 and 35 to roughly estimate the consistency between measurement results and residuals in the salinity range 20-40. The dependency of the measurement uncertainty on $b_{\text{TRIS}/\text{TRIS}\cdot\text{H}^+}$ is negligible (Fig. S3) and therefore not displayed in Figure 5. The residuals are within the range of the expanded measurement uncertainty, except for a few results at lowest TRIS/TRIS \cdot H $^+$ molality and salinities 15 and 20 (Fig. 5).

$$\begin{aligned}
 \text{pH}_T = & a + (b_1 \cdot S + b_2 \cdot S^2 + b_3 \cdot S^3) \\
 & + (c_1 \cdot T + c_2 \cdot S \cdot T + c_3 \cdot S^2 \cdot T + c_4 \cdot S^3 \cdot T) \\
 & + (d_1 \cdot \ln(T) + d_2 \cdot S \cdot \ln(T) + d_3 \cdot S^2 \cdot \ln(T) + d_4 \cdot S^3 \cdot \ln(T)) \\
 & + \left(e \cdot \frac{1}{T} \right) \\
 & + (f_1 \cdot b_{\text{TRIS/TRIS}\cdot\text{H}^+} + f_2 \cdot b_{\text{TRIS/TRIS}\cdot\text{H}^+} \cdot S + f_3 \cdot b_{\text{TRIS/TRIS}\cdot\text{H}^+} \\
 & \cdot T + f_4 \cdot b_{\text{TRIS/TRIS}\cdot\text{H}^+} \cdot S \cdot T) \\
 & + (g_1 \cdot b_{\text{TRIS/TRIS}\cdot\text{H}^+}^2 + g_2 \cdot b_{\text{TRIS/TRIS}\cdot\text{H}^+}^2 \cdot S)
 \end{aligned} \tag{10}$$

Table 2: Coefficients for the pH_T model (eq. 10). Test value: pH_T = 8.0703 at S=20, T=298.15 and $b_{\text{TRIS/TRIS}\cdot\text{H}^+}$ = 0.04.

Coefficient	Value
a	- 327.3307
b ₁	-2.400270
b ₂	8.124630·10 ⁻²
b ₃	-9.635344·10 ⁻⁴
c ₁	-9.103207·10 ⁻²
c ₂	-1.963311·10 ⁻³
c ₃	6.430229·10 ⁻⁵
c ₄	-7.510992·10 ⁻⁷
d ₁	56.92797
d ₂	5.235889·10 ⁻¹
d ₃	-1.7602·10 ⁻²
d ₄	2.082387·10 ⁻⁴
e	11382.97
f ₁	-2.417045
f ₂	7.645221·10 ⁻²
f ₃	1.122392·10 ⁻²
f ₄	-3.248381·10 ⁻⁴
g ₁	-4.161537
g ₂	6.143395·10 ⁻²

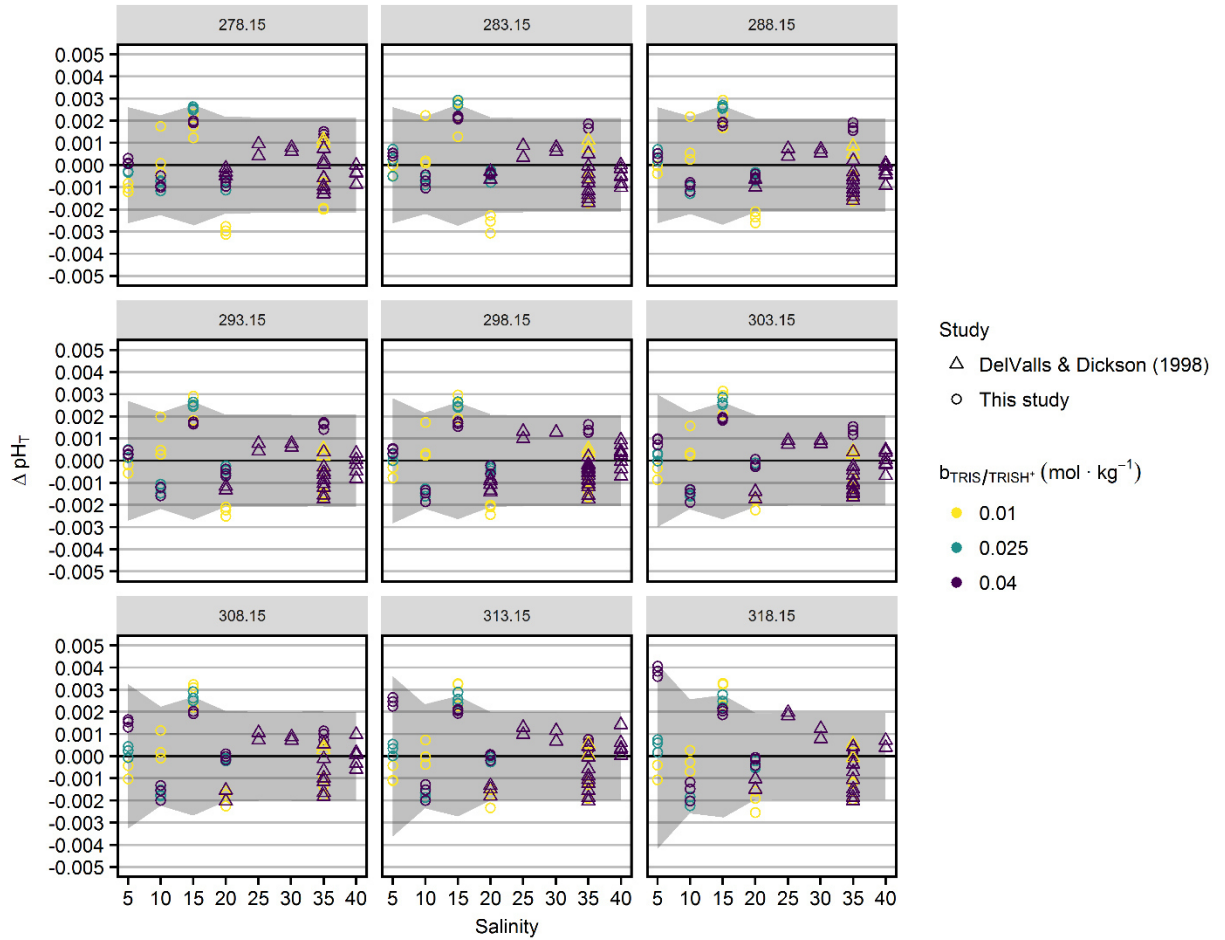


Fig. 5: Residuals of pH_T values from the model (eq. 10, Tab. 2, Fig. 4), $\Delta \text{pH}_T = \text{pH}_{T,\text{measured}} - \text{pH}_{T,\text{model}}$, as a function of salinity (x-axis), temperatures (in K, indicated at the top of the panels) and TRIS/TRIS·H⁺ molalities (color). Circles represent results from this study, triangles refer to DelValls and Dickson (1998). The grey areas indicate the expanded (coverage factor $k=2$) measurement uncertainty of pH_T .

Discussion

Measurement uncertainty and pH_T model

The deviations of measured pH_T values from the pH_T model (eq. 10, Tab. 2) agree well with the range of the expanded measurement uncertainty (Fig. 5), i.e., they are not significantly higher or lower. This indicates that the model represents the experimental results well, and does not overfit the data.

The deviations from the model reveal a minor salinity-dependent pattern. In the salinity range 5-20, there is a tendency towards positive offsets at $S=15$ and negative offsets at $S=20$. As this tendency exists for the pH_T of all TRIS/TRIS·H⁺ molalities and replicates, the patterns must have a common cause, which is the determination of the standard potential of the silver-silver chloride electrodes, E° . The determination of E° represents the major contribution to the measurement uncertainty (55-95%, Fig. S3) and was only performed

once for each combination of temperature and salinity. The uncertainty in the E° determination is presumably related to the extrapolation to pure ASW conditions, which is especially sensitive to the E' measurements (eq. 4) at lowest HCl molalities. The model deviations reveal slightly positive offsets at $S=25$ and 30 , which is very similar to the patterns displayed in Figure 2B of DelValls and Dickson (1998).

No pronounced temperature-dependence of the residuals exists, except at salinity 5 and $b_{\text{TRIS}/\text{TRIS}\cdot\text{H}^+} = 0.04 \text{ mol}\cdot\text{kg}\cdot\text{H}_2\text{O}^{-1}$, where a positive offset increases to a maximum of 0.004 at highest temperatures.

Comparison to previous studies

The highest deviation between pH_T values measured in this study and by DelValls and Dickson (1998) across all temperatures, at salinities 20 and 35, and $b_{\text{TRIS}/\text{TRIS}\cdot\text{H}^+} = 0.04 \text{ mol}\cdot\text{kg}^{-1}$ is 0.0025 at $S=35$ and $T=288.15\text{K}$. The deviations are therefore within the extended measurement uncertainty of the method.

At salinities ≥ 20 , excellent agreement was found between our pH_T model at $b_{\text{TRIS}/\text{TRIS}\cdot\text{H}^+} = 0.04 \text{ mol}\cdot\text{kg}^{-1}$ and the model defined in equation (18) of DelValls and Dickson (1998). Differences are <0.001 for the entire salinity range 20-40 and the temperature range 278.15-318.15K (Fig. S4). Within the range of the extended measurement uncertainty both models do not differ. The residuals from the model fitted in this study are larger than those presented in Figure 2 of DelValls and Dickson (1998), presumably a result of the larger range of salinities and the included dependency of pH_T on TRIS/TRIS $\cdot\text{H}^+$ molality in our model.

Our pH_T model at $b_{\text{TRIS}/\text{TRIS}\cdot\text{H}^+} = 0.04 \text{ mol}\cdot\text{kg}^{-1}$ and 298.15 K and the model by Mosley et al. (2004) agree within 0.002 in the salinity range 20-40, which is not surprising, because both models are based on the same results of DelValls and Dickson (1998). However, in the salinity range 5-20, where Mosley et al. (2004) interpolated the pH_T of TRIS buffer solutions between the results of DelValls and Dickson (1998) for $S>20$ and the results of Bates and Hetzer (1961) in pure water, deviations increase up to 0.009 and highlight the shortcomings of the interim solution.

Correction of E° for changes in sulfate concentration and activity coefficients

Changes in the sulfate concentration between pure ASW and ASW/TRIS-HCl solutions were corrected in this study according to equation (8) (Fig. 2). However, determined E° values do not exactly correspond to the values required for pH_T calculation in equation (3), because changes in activity coefficients between pure ASW and ASW/TRIS-HCl solutions remain unaccounted for, namely:

- (1) Changes in the value of $K_{\text{HSO}_4^-}$ arising from changes in the activity coefficients of H^+ , SO_4^{2-} and HSO_4^-
- (2) Changes in the activity coefficients of H^+ and Cl^-

This limitation was previously discussed (e.g., Dickson et al., 2015; Nemzer et al., 2005) and applies to all currently available experimental pH_T measurements of TRIS buffered ASW solutions. The activity changes can only be corrected with estimates from a speciation model. Gallego and Turner (2017) have recently developed optimized Pitzer coefficients for TRIS in artificial seawater at 298.15 K, using the artificial seawater model of Waters and Millero (2013). According to Gallego and Turner (2017), pH_T correction terms, addressing the above mentioned effects (1) and (2), were calculated for the results of this study at 298.15 K. Those $\square \text{pH}_T$ values from the speciation model differed from the applied sulfate corrections shown in Figure 2 by less than 0.002, indicating that changes in sulfate concentration dominate over the effect of changes in the activity coefficient.

However, the Pitzer coefficients for TRIS buffered ASW solutions are restricted to 298.15 K (Gallego and Turner, 2017) due to scarcity of experimental data for other temperatures and can therefore not be applied consistently to the full temperature range covered in this study. The development of accurate Pitzer models for TRIS in artificial seawater over an extended temperature range is a main focus of the SCOR Working Group 145 “Modelling Chemical Speciation in Seawater to Meet 21st Century Needs” (<http://marchemspec.org/>). It should be noted that the neglected effect of changes in activity coefficients does not impact the calibration of pH instruments, if those are performed at variable TRIS/TRIS⁺ molality and extrapolated to zero TRIS (see chapter: Calibration of pH instruments).

Conversion between pH_b and pH_T

The conversion of pH from the molality to the amount content scale (from pH_b to pH_T) was calculated as the negative decadic logarithm of

$$\omega_{\text{H}_2\text{O}} = 1 - 0.00106 \cdot S \quad (11)$$

according to DelValls and Dickson (1998). $\omega_{\text{H}_2\text{O}}$ represents the mass of water per mass solution and the given relationship between $\omega_{\text{H}_2\text{O}}$ and salinity refers to the composition of pure ASW. As pointed out by Pratt (2014), $\omega_{\text{H}_2\text{O}}$ in pure ASW is not exactly identical to $\omega_{\text{H}_2\text{O}}$ of the corresponding ASW/TRIS-HCl solution, due to the difference of the total mass of solution per amount of water after replacing some of the ASW salts with TRIS/HCl. As a result, for solutions with a TRIS molality of $0.04 \text{ mol}\cdot\text{kg}\cdot\text{H}_2\text{O}^{-1}$, the pH conversion based on the actually weighed buffer composition gives 0.003 and 0.004 higher pH_T values at

salinity 35 and 5, respectively, compared to those using equation (4). Obviously, the conversion error decreases towards lower TRIS molality. To be consistent with the pH_T results measured previously and to perform the pH_T -fit on a consistent data base we have also used equation (4) for the correction, even though we deem the conversion based on the actually weighed buffer composition more appropriate.

It should be noted that preliminary results obtained with the speciation model by Gallego and Turner (2017) indicate that the correction of changes in activity coefficients between pure ASW and ASW/TRIS-HCl solutions, which has been neglected in this study due to the restriction of model results to 298.15 K, is around -0.005 at $S=35$ and $b_{\text{TRIS}/\text{TRIS}\cdot\text{H}^+} = 0.04 \text{ mol}\cdot\text{kg}\cdot\text{H}_2\text{O}^{-1}$. This is in a similar order of magnitude, but with opposite direction compared to the effect of pH scale conversion according to equation (11). Therefore, if adequate activity coefficients will be available, superposition of the pH scale conversion using the actually weighed buffer composition and the correction of changes in activity coefficients will presumably provide pH_T values that are within the range of uncertainties of the pH_T value we have presented here.

In any case, the choice of the scale conversion does not impact the calibration of pH instruments, if they are performed at variable TRIS/TRIS H^+ molality and extrapolated to zero TRIS (see chapter: Calibration of pH instruments).

Calibration of pH instruments

We recommend to use TRIS buffered ASW solutions as prepared in this study as pH_T -standards for future calibration of pH instruments in the salinity range 5-20, with assigned pH_T values according to equation (10) and table 2. Moreover, this model also allows for a consistent assignment of pH_T values without discontinuity and significant differences to previous results in the salinity range 20-40 when buffer solutions are prepared according to DelValls and Dickson (1998).

As discussed in the previous two chapters, the composition of TRIS buffer solutions differs from that of pure ASW. The contribution of TRIS-HCl to the total ionic strength increases toward lower salinities and:

- (1) affects the pH_T values of the buffer solutions (Fig. 4),
- (2) requires corrections of the E° differences between pure ASW and ASW/TRIS-HCl,
- (3) affects $\omega_{\text{H}_2\text{O}}$ and therefore the scale conversion between pH_b and pH_T , and
- (4) impacts the calibration quantity of any pH instrument, such as the determination of dissociation constants of pH indicator dyes.

Uncertainties in (2) and (3) result in uncertainties of the assigned pH_T values of the buffer solutions. However, it must be emphasized that effects (1)-(4) do not affect the calibration of pH instruments, if they include the extrapolation of calibrated parameters, e.g., the dissociation constant of mCP (Müller et al., *subm.*), to pure ASW conditions. The extrapolated quantity refers to an exact definition of the total hydrogen ion concentration scale without constraints (Nemzer and Dickson, 2005; Dickson et al., 2015). Therefore, it is recommended to perform the calibration of pH instruments in the salinity range 5-20 at the three TRIS/TRIS·H⁺ molalities reported in this study and extrapolate the results to zero TRIS/TRIS·H⁺ molality. However, the dependence of pH_T on TRIS/TRIS·H⁺ in equation (10) is strictly valid only for salinities 5-20 and 35, due to the lack of experimental data at other salinities. It must further be noted that no uncertainties have been calculated for the coefficients listed in table 2, since no uncertainties have been available for the results of DelValls and Dickson (1998). We recommend to assign uncertainties to pH_T values corresponding to those given Table S6 if equation (10) is used to calculate pH_T values.

Recommendations for the preparation of TRIS buffer solutions

To replicate the TRIS buffer solutions characterized in this study, it is recommended to produce stock solutions for the salt components of the ASW matrix. The impact of salt impurities on buffer pH_T was not yet systematically studied. Therefore, we recommend to use salts of highest purity grade, although the contribution of ASW composition to the measurement uncertainty budget is assumed to be small. The stock solution of HCl should be titrated against the TRIS stock solution with potentiometric or colorimetric (e.g., methyl red) endpoint detection. This ensures an exact equimolar TRIS:TRIS·H⁺ ratio, which is essential to reproduce the pH_T value. Finally, all TRIS containing solutions should be handled in a way to avoid uptake of atmospheric CO₂. Ideally, the headspace of the containers should be flushed with humidified argon.

Solution composition concept and relevance to natural waters

Alternative strategies for the solution composition applied in this study would result in pronounced changes in cation ratios at low salinity (Fig. 1). Based on current knowledge it is impossible to quantify the effect of such changes of cation ratios on TRIS buffer pH_T , because information is missing about the sensitivity of the TRIS·H⁺ dissociation constant on the ionic composition of the matrix. An experimental approach to this open question might be the electrochemical pH_T measurement of TRIS buffered solutions in variable ASW matrices.

Characterized buffer solutions in various ASW matrices would further allow studying the impact of solution composition on the measurement signals of any other pH instruments,

including the dissociation behavior of mCP. Such experiments could shed light on the ultimate question of how representative pH_T measurements are for various natural brackish and freshwaters that differ in ionic composition (Feistel et al., 2010).

Conclusion

This study extends the characterization of TRIS buffer solutions by Harned cell measurements to brackish waters and provides a consistent pH_T model for the salinity range 5-40. It was emphasized that minor assumptions and uncertainties remain in the pH_T assignment and restrict the accuracy of all currently available TRIS buffer characterizations. However, these limitations do not affect the calibration of other pH instruments, if calibration results are extrapolated to zero buffer molality, which is especially important at low salinities. This study provides the required characterization of buffer solutions with variable TRIS molality in the salinity range 5-20. Measurements with pH instruments that have been calibrated against the buffer concentration represent currently the only access to the total hydrogen ion concentration without constraints.

Acknowledgements

We acknowledge the Swiss Federal Institute of Metrology (METAS) for providing characterized salts. The quality of this paper gained from scientific discussions with Bernd Schneider, Robert H. Byrne, Kenneth W. Pratt, Regina Easley and Michael DeGrandpre. We thank Franko Schmäling for valuable recommendations concerning appropriate fitting procedures.

The research leading to this manuscript has received funding from BONUS, the joint Baltic Sea research and development programme (Art 185), funded jointly from the European Union's Seventh Programme for research, technological development and demonstration and from the German Federal Ministry of Education and Research through Grant No. 03F0689A (BONUS PINBAL).

References

- Bates, R.G., Bower, V.E., (1954), Standard Potential of the Silver-Silver-Chloride Electrode from 0° to 95° C and the Thermodynamic Properties of Dilute Hydrochloric Acid Solutions, *J. Res. Natl. Bur. Stand.* 53 (5), 283–290.
- Bates, R.G., Hetzer, H.B. (1961), Dissociation constant of the protonated acid form of 2-amino-(hydroxymethyl)-1,3-propanediol [trihydroxymethyl]-aminomethane] and related thermodynamic quantities from 0 to 50°, *Journal of Physical Chemistry* 65(4), 667-671.
- Bates, R.G. (1973) *Determination of pH*. New York, Wiley.
- Buck, R.P., Rondinini, S., Covington, A.K., Baucke, F.G.K, Brett, C.M.A., Camoes, M.F. et al. (2002), Measurement of pH. Definition, standards, and procedures (IUPAC recommendations 2002), *Pure Applied Chemistry*, 74(11), 2169-2200.
- Byrne, R.H., Mecking, S., Feely, R.A. Liu, X et al (2010). Direct observations of basin-wide acidification of the North Pacific Ocean. *Geophys. Res. Lett.* 37. doi:10.1029/2009GL040999.
- Clayton, T.D., Byrne, R.H., 1993. Spectrophotometric seawater pH measurements — total hydrogen-ion concentration scale calibration of m-cresol purple and at-sea results. *Deep Sea Res. Part I Oceanogr. Res. Pap.* 40 (10), 2115–2129.
- DelValls, T.A., Dickson, A.G. (1998). The pH of buffers based on 2-amino-2-hydroxymethyl-1,3-propanediol ('tris') in synthetic sea water, *Deep-Sea Research Part I* 45, 1541-1554.
- Dickson, A.G. (1990), Standard potential of the reaction: $\text{AgCl(s)} + \frac{1}{2}\text{H}_2(\text{g}) = \text{Ag(s)} + \text{HCl(aq)}$, and the standard acidity constant of the ion HSO_4^- in synthetic sea water from 273.15 to 318.15 K, *J. Chem. Thermodynamics* 22, 113-127.
- Dickson, A. G., Cam, M. F., Spitzer, P., Fiscaro, P., Stoica, D., Pawlowicz, R., et al. (2015). Metrological challenges for measurements of key climatological observables. Part 3: seawater pH. *Metrologica*. Doi: 10.1088/0026-1394/53/1/R26

Feistel, R., Weinreben, S., Wolf, H., Seitz, S., Spitzer, P., Adel, B., Nausch, G., Schneider, B., and Wright, D. G.: Density and Absolute Salinity of the Baltic Sea 2006–2009, *Ocean Sci.*, 6, 3-24, <https://doi.org/10.5194/os-6-3-2010>, 2010.

Gallego-Urrea, J. A., and Turner, D. R. (2017). Determination of pH in estuarine and brackish waters: Pitzer parameters for Tris buffers and dissociation constants for m-cresol purple at 298.15 K. *Mar. Chem.*, 1–6. doi:10.1016/j.marchem.2017.07.004.

H. S. Harned and B. B. Owen. *The Physical Chemistry of Electrolytic Solutions*, Chap. 14, Reinhold, New York (1958).

ISO/IEC (2008) Guide to the expression of uncertainty in measurement (2008), Guide 98-3, Geneva, Switzerland

Le Quéré, C., Andrew, R.M., Canadell, J.G., Sitch, S., Korsbakken, J.I., Peters, G.P. et al (2016). Global Carbon Budget 2016, *Earth Syst. Sci. Data* 8, 605-649.

Liu, X., Patsavas, M. C., Byrne, R. H. (2011). Purification and characterization of meta-cresol purple for spectrophotometric seawater pH measurements. *Environ. Sci. Technol.* 45, 4862–4868. doi:10.1021/es200665d.

Martz, T. R., Connery, J. G., and Johnson, K. S. (2010). Testing the Honeywell Durafet for seawater pH applications. *Limnol. Oceanogr. Methods* 8, 172–184. doi:10.4319/lom.2010.8.172.

Meija J., Coplen T.B., Berglund M., Brand W.A., De Bièvre P., Gröning M., Holden N.E., Irrgeher J., Loss R.D., Walczyk T., and Prohaska T. (2016). *Pure Appl. Chem.* 88, 265-291.

Mosley, L.M., Husheer, S.L.G., Hunter, K.A. (2004), Spectrophotometric pH measurement in estuaries using thymol blue and m-cresol purple, *Marine Chemistry* 91, 175 – 186.

Nemzer, B. V., and Dickson, A. G. (2005). The stability and reproducibility of Tris buffers in synthetic seawater. *Mar. Chem.* 96, 237–242. doi:10.1016/j.marchem.2005.01.004.

Pratt, K. (2014). Measurement of pH_T values of Tris buffers in artificial seawater at varying mole ratios of Tris:Tris-HCl, *Marine Chemistry* 162, 89-95.

R Core Team (2014). R: A language and environment for statistical computing. Available at: <http://www.r-project.org/>.

Waters, J. F., and Millero, F. J. (2013). The free proton concentration scale for seawater pH. *Mar. Chem.* 149, 8–22. doi:10.1016/j.marchem.2012.11.003.

Supplementary Material to:
pH Measurements in Brackish Waters:
Extending the Electrochemical pH_T Determination of TRIS
Buffers to Salinities 5 – 20

J.D. Müller¹, F. Bastkowski^{2,*}, B. Sander², S. Seitz², D.R. Turner³, A.G. Dickson⁴, G. Rehder¹

¹Department of Marine Chemistry, Leibniz Institute for Baltic Sea Research Warnemünde, Rostock, Germany

²Department of Physical Chemistry, Physikalisch-Technische Bundesanstalt, Braunschweig, Germany

³Department of Marine Sciences, University of Gothenburg, Gothenburg, Sweden

⁴Marine Physical Laboratory, Scripps Institution of Oceanography, University of California, San Diego, La Jolla, USA

*corresponding author: Frank Bastkowski, Frank.Bastkowski@ptb.de

Purity of salts and molalities of the stock solutions

Table S1: Purities of reference salts and associated standard uncertainties (k=1) used for the preparation of the artificial seawater solutions.

Salt	Purity
NaCl*	0.9971 ± 0.0007
KCl*	0.9965 ± 0.0007
Na ₂ SO ₄	0.99997 ± 0.00014

* the bromide content was determined at METAS to be less than 50 mg·kg⁻¹

Table S2.1: Molalities of stock solutions used for the preparation of the measurement solutions.

Stock solution	Compound	b/ mol·kg-H ₂ O ⁻¹
1	HCl _{aq}	0.20050 ± 0.00007
2	NaCl _{aq}	2.54464 ± 0.00152
3	Na ₂ SO _{4aq}	0.466512 ± 0.000059
4	CaCl _{2aq}	0.14056 ± 0.00030 *0.13986 ± 0.00030
	MgCl _{2aq}	0.71603 ± 0.00149 *0.71248 ± 0.00148
	KCl _{aq}	0.138283 ± 0.000192 *0.137598 ± 0.000191
5	TRIS _{aq}	0.470973 ± 0.000240

* used only for the preparation of the 0.025 M TRIS buffers of salinity 10 and 15, and 0.01 M TRIS buffer of salinity 35

Table S2.2: Molalities of stock solutions used for the preparation of stock solution 4 (table S2.1).

Stock solution	b/ mol·kg-H ₂ O ⁻¹
CaCl _{2aq}	0.5642 ± 0.0012
MgCl _{2aq}	2.1677 ± 0.0045

Molalities of prepared solutions

Table S3: Overview of the molalities in mol·kg-H₂O⁻¹ of all hydrochloric acid in ASW solutions for the determination of the Ag|AgCl standard electrode potential.

S	b_{HCl}	b_{NaCl}	b_{KCl}	b_{Na2SO4}	b_{CaCl2}	b_{MgCl2}	
5	0.00250	0.05343	0.00158	0.00439	0.00161	0.00821	
	0.00500	0.05206	0.00155	0.00427	0.00157	0.00800	
	0.01000	0.04932	0.00146	0.00405	0.00149	0.00758	
	0.02000	0.04382	0.00130	0.00360	0.00132	0.00674	
	0.03000	0.03838	0.00114	0.00315	0.00116	0.00589	
	0.04000	0.03290	0.00098	0.00270	0.00099	0.00505	
	0.04999	0.02743	0.00081	0.00225	0.00083	0.00421	
	10	0.00250	0.10879	0.00323	0.00893	0.00328	0.01671
10	0.00500	0.10740	0.00319	0.00882	0.00324	0.01650	
	0.01000	0.10465	0.00311	0.00859	0.00316	0.01608	
	0.02000	0.09917	0.00294	0.00814	0.00299	0.01524	
	0.03000	0.09372	0.00278	0.00769	0.00283	0.01440	
	0.03999	0.08824	0.00262	0.00724	0.00266	0.01356	
	0.04999	0.08276	0.00246	0.00679	0.00250	0.01271	
	15	0.00250	0.16467	0.00489	0.01352	0.00497	0.02531
	15	0.00500	0.16330	0.00485	0.01340	0.00493	0.02509
0.01000		0.16064	0.00477	0.01318	0.00484	0.02468	
0.02000		0.15508	0.00460	0.01273	0.00468	0.02383	
0.03000		0.14962	0.00444	0.01228	0.00451	0.02299	
0.04000		0.14414	0.00428	0.01183	0.00435	0.02215	
0.04999		0.13865	0.00411	0.01138	0.00418	0.02130	
20		0.00250	0.22113	0.00656	0.01816	0.00667	0.03398
20		0.00500	0.21978	0.00652	0.01804	0.00663	0.03377
	0.01000	0.21703	0.00644	0.01781	0.00655	0.03334	
	0.02000	0.21156	0.00628	0.01737	0.00638	0.03250	
	0.03000	0.20609	0.00611	0.01692	0.00622	0.03166	
	0.04000	0.20062	0.00595	0.01647	0.00605	0.03082	
	0.04999	0.19511	0.00579	0.01602	0.00588	0.02998	
	35	0.00250	0.42511	0.01058	0.02927	0.01075	0.05478
	35	0.00500	0.42265	0.01058	0.02927	0.01075	0.05478

Supplementary Material to:
pH Measurements in Brackish Waters:
Extending the Electrochemical pH_r Determination of TRIS buffers to Salinities 5 – 20

	0.01000	0.41760	0.01058	0.02927	0.01075	0.05478
	0.02000	0.40759	0.01058	0.02927	0.01075	0.05478
	0.02982	0.39517	0.01051	0.02909	0.01069	0.05444
	0.04000	0.38761	0.01058	0.02927	0.01075	0.05479
	0.05000	0.37761	0.01058	0.02927	0.01075	0.05478

Table S4: Overview of the molalities in mol·kg-H₂O⁻¹ of all equimolal TRIS buffered ASW solutions.

S	w_{H2O}	b_{HCl}	b_{NaCl}	b_{KCl}	b_{Na2SO4}	b_{CaCl2}	b_{MgCl2}	b_{TRIS}
5	0.99470	0.03997	0.03287	0.00098	0.00270	0.00099	0.00505	0.07995
	0.99470	0.02500	0.04111	0.00122	0.00337	0.00124	0.00632	0.05000
	0.99470	0.00999	0.04927	0.00146	0.00404	0.00149	0.00757	0.01998
10	0.98940	0.03998	0.08818	0.00262	0.00724	0.00266	0.01355	0.07995
	0.98941	0.02500	0.09644	0.00285	0.00792	0.00289	0.01475	0.05000
	0.98940	0.01000	0.10465	0.00311	0.00859	0.00316	0.01608	0.02000
15	0.98411	0.03998	0.14405	0.00427	0.01183	0.00435	0.02213	0.07995
	0.98412	0.02500	0.15234	0.00450	0.01251	0.00457	0.02329	0.05000
	0.98410	0.01000	0.16057	0.00476	0.01318	0.00484	0.02467	0.02000
20	0.97881	0.03998	0.20050	0.00595	0.01646	0.00605	0.03081	0.07996
	0.97880	0.02500	0.20882	0.00620	0.01714	0.00630	0.03209	0.05000
	0.97881	0.00999	0.21686	0.00644	0.01780	0.00654	0.03332	0.01998
35	0.96290	0.04000	0.38759	0.01058	0.02927	0.01075	0.05478	0.08000
	0.96295	0.01000	0.41761	0.01053	0.02927	0.01070	0.05451	0.02000

Harned cell measurements



Figure S1: Picture of a Harned cell utilized for the measurements performed in this work.

In this work, the utilized electrodes were in-house made. The platinum hydrogen electrode was prepared by welding a platinum plate to the free end of a glass covered platinum wire. The resulting platinum electrode was platinized for 9 minutes with $45 \text{ mA}\cdot\text{cm}^2$ in an aqueous solution of $\text{H}_2\text{PtCl}_6\cdot 6\text{H}_2\text{O}$ and $\text{Pb}(\text{CH}_3\text{COO})_2\cdot 3\text{H}_2\text{O}$ and afterwards cleaned in distilled water. Ag|AgCl electrodes have been prepared using the thermal-electrolytic method (Bates 1973).

The Harned cells were filled with the solution to be measured and placed into a thermostating bath controlled by two thermostating units (DLK 45 and PV 36 from Lauda).

The temperature inside the bath is measured at four positions using PT100 probes connected to a thermometer (ASL F250 MKII), switched by a Multi Switch module (ASL SB250). The air surrounding the cells is temperature-controlled using a thermostat (Lauda Proline RP 855) inside a temperation box. The temperature inside the thermostating bath is kept constant within ± 0.005 K. The cells are equipped with a hydrogen gas supply and two humidification units. The hydrogen gas used is of 6.0 purity. The cell voltage was measured using a digital voltmeter (Agilent A3458) after temperature stability was reached and corrected for the actual partial pressure of the hydrogen gas p_{H_2} according to equation (S1):

$$\Delta E = \frac{RT}{2F} \cdot \ln\left(\frac{p_{\text{H}_2}}{p^\circ}\right) \quad (\text{S1})$$

With R: gas constant ($8.314 \text{ J}\cdot\text{mol}^{-1}\cdot\text{K}^{-1}$), T: temperature (K), F: Faraday constant ($96485.333 \text{ A}\cdot\text{s}\cdot\text{mol}^{-1}$), p_{H_2} : partial pressure of hydrogen gas at the position of the electrode immersed into the measurement solution (Pa), p° : standard pressure (101325 Pa)

$$p_{\text{H}_2} = p_{\text{atm}} + p_{\text{hydrostatic}} - p_{\text{water}} \quad (\text{S2})$$

With p_{atm} : hydrogen gas pressure above the measurement solution measured with a barometer (Setra Systems),

$$p_{\text{hydrostatic}} = 0.42 \cdot \rho \cdot g \cdot h \quad (\text{S3})$$

with ρ : Density of the measurement solution, g: gravity constant, h: immersion depth of the platinum hydrogen electrode, and the empiric factor 0.42 for the correction of the hydrostatic pressure (Hills and Ives, 1951), and

p_{water} : saturated vapor pressure of water calculated from the Clausius-Clapeyron equation. The calculation of p_{water} performed in this study refers to pure water. In reality, p_{water} is decreased due to the decreased water activity in solutions containing salts. Actual values of p_{water} have to be calculated by multiplying the Clausius-Clapeyron expression with the activity of water. However, at salinity 35 and 298 K the water activity is around 0.98, hence the water vapour pressure decreases by around 2%. This results only in around $8 \mu\text{V}$ lower corrected measured Harned cell voltages and hence around $5\cdot 10^{-7}$ lower pH_T values, which is far below the limits of uncertainty. At lower salinities the effect is even lower.

Supplementary Material to:
pH Measurements in Brackish Waters:
Extending the Electrochemical pH_T Determination of TRIS buffers to Salinities 5 – 20

Measured potentials in ASW/TRIS-HCl and ASW/HCl solutions

Table S5.1: Overview of the electric potentials E/V of the TRIS (molality in mol·kg-H₂O⁻¹) buffered artificial seawater solutions measured with the Harned cell and corrected according to equation S1.

S	T	278.205	283.201	288.193	293.187	298.176	303.172	308.165	313.159	318.147
	b_{TRIS}									
5	0.04	0.784618	0.782839	0.780964	0.779008	0.776976	0.774869	0.772684	0.770424	0.768082
		0.784606	0.782831	0.780953	0.778996	0.776963	0.774855	0.772670	0.770411	0.768067
		0.784603	0.782839	0.780953	0.778998	0.776974	0.774872	0.772691	0.770436	0.768097
	0.025	0.785466	0.783672	0.781852	0.779915	0.777899	0.775804	0.773629	0.771377	0.769034
		0.785489	0.783741	0.781881	0.779937	0.777918	0.775822	0.773649	0.771398	0.769060
		0.785469	0.783715	0.781860	0.779924	0.777915	0.775826	0.773660	0.771410	0.769070
	0.01	0.786293	0.784548	0.782705	0.780780	0.778785	0.776721	0.774583	0.772378	0.770096
		0.786304	0.784573	0.782725	0.780802	0.778812	0.776753	0.774620	0.772420	0.770139
		0.786283	0.784546	0.782705	0.780780	0.778785	0.776720	0.774583	0.772379	0.770096
10	0.04	0.772368	0.770375	0.768299	0.766135	0.763903	0.761600	0.759220	0.756767	0.754231
		0.772397	0.770409	0.768322	0.766158	0.763927	0.761626	0.759247	0.756796	0.754266
		0.772372	0.770393	0.768316	0.766158	0.763934	0.761636	0.759261	0.756812	0.754285
	0.025	0.772781	0.770796	0.768714	0.766562	0.764342	0.762050	0.759683	0.757247	0.754734
		0.772778	0.770787	0.768705	0.766551	0.764330	0.762036	0.759666	0.757226	0.754708
		0.772756	0.770775	0.768685	0.766538	0.764322	0.762033	0.759670	0.757235	0.754723
	0.01	0.773104	0.771104	0.769059	0.766919	0.764708	0.762425	0.760065	0.757642	0.755146
		0.773196	0.771225	0.769153	0.767007	0.764791	0.762505	0.760142	0.757711	0.755207
		0.773080	0.771109	0.769043	0.766908	0.764703	0.762431	0.760081	0.757663	0.755173
15	0.04	0.764975	0.762856	0.760635	0.758346	0.755994	0.753573	0.751076	0.748507	0.745861

Supplementary Material to:
 pH Measurements in Brackish Waters:
 Extending the Electrochemical pH_T Determination of TRIS buffers to Salinities 5 – 20

		0.764971	0.762849	0.760626	0.758340	0.755989	0.753570	0.751076	0.748512	0.745867
		0.764970	0.762852	0.760634	0.758341	0.755982	0.753565	0.751070	0.748500	0.745850
	0.025	0.765243	0.763122	0.760906	0.758624	0.756274	0.753857	0.751367	0.748805	0.746167
		0.765251	0.763133	0.760915	0.758635	0.756289	0.753877	0.751392	0.748837	0.746204
		0.765246	0.763121	0.760909	0.758627	0.756278	0.753863	0.751374	0.748817	0.746184
	0.01	0.765292	0.763154	0.760964	0.758693	0.756352	0.753943	0.751468	0.748927	0.746316
		0.765352	0.763241	0.761036	0.758757	0.756415	0.754005	0.751530	0.748989	0.746376
		0.765321	0.763204	0.760999	0.758729	0.756395	0.753994	0.751521	0.748988	0.746379
20	0.04	0.759642	0.757414	0.755099	0.752720	0.750277	0.747767	0.745183	0.742532	0.739808
		0.759631	0.757408	0.755090	0.752708	0.750254	0.747747	0.745167	0.742515	0.739785
		0.759622	0.757409	0.755085	0.752702	0.750256	0.747753	0.745176	0.742530	0.739803
	0.025	0.759787	0.757569	0.755255	0.752883	0.750435	0.747927	0.745350	0.742709	0.739990
		0.759781	0.757556	0.755249	0.752871	0.750431	0.747920	0.745344	0.742704	0.739985
		0.759763	0.757538	0.755233	0.752860	0.750424	0.747920	0.745351	0.742718	0.740006
	0.01	0.759759	0.757514	0.755229	0.752858	0.750418	0.747917	0.745347	0.742714	0.740010
		0.759778	0.757559	0.755258	0.752882	0.750444	0.747944	0.745378	0.742749	0.740050
		0.759767	0.757544	0.755244	0.752875	0.750439	0.747945	0.745387	0.742765	0.740070
35	0.04	0.748673	0.746230	0.743708	0.741115	0.738476	0.735778	0.733009	0.730179	0.727279
		0.748665	0.746218	0.743696	0.741111	0.738455	0.735755	0.732983	0.730149	0.727243
		0.748658	0.746218	0.743688	0.741096	0.738461	0.735767	0.733000	0.730170	0.727270
	0.01	0.748304	0.745852	0.743327	0.740741	0.738101	0.735407	0.732647	0.729829	0.726950
		0.748372	0.745918	0.743394	0.740805	0.738156	0.735456	0.732694	0.729876	0.726996
		0.748306	0.745854	0.743331	0.740750	0.738118	0.735428	0.732672	0.729868	0.726999

Supplementary Material to:
pH Measurements in Brackish Waters:
Extending the Electrochemical pH_T Determination of TRIS buffers to Salinities 5 – 20

Table S5.2: Overview of the mean electric potentials E/V of the unbuffered artificial seawater solutions at different HCl molalities (in mol·kg-H₂O⁻¹) measured with the Harned cell and corrected according to equation S1.

S	T	278.205	283.201	288.193	293.187	298.176	303.172	308.165	313.159	318.147
	b_{HCl}									
5	0.0025	0.451591	0.453091	0.454465	0.455745	0.456939	0.458064	0.459138	0.460174	0.461173
	0.0050	0.434560	0.435739	0.436787	0.437730	0.438580	0.439350	0.440058	0.440713	0.441308
	0.0100	0.417419	0.418265	0.418964	0.419550	0.420028	0.420409	0.420706	0.420929	0.421067
	0.0200	0.399869	0.400355	0.400678	0.400881	0.400962	0.400928	0.400790	0.400550	0.400185
	0.0300	0.389236	0.389499	0.389604	0.389572	0.389410	0.389122	0.388718	0.388203	0.387562
	0.0400	0.381463	0.381579	0.381520	0.381322	0.380990	0.380527	0.379945	0.379245	0.378426
	0.0500	0.375289	0.375273	0.375095	0.374769	0.374306	0.373711	0.372992	0.372155	0.371195
10	0.0025	0.437718	0.439083	0.440352	0.441554	0.442699	0.443803	0.444888	0.445968	0.447043
	0.0050	0.420982	0.422034	0.422983	0.423858	0.424667	0.425427	0.426156	0.426864	0.427557
	0.0100	0.404004	0.404720	0.405325	0.405844	0.406283	0.406653	0.406971	0.407244	0.407475
	0.0200	0.386680	0.387043	0.387264	0.387390	0.387420	0.387359	0.387217	0.386999	0.386685
	0.0300	0.376389	0.376524	0.376520	0.376402	0.376173	0.375838	0.375406	0.374875	0.374235
	0.0400	0.368959	0.368932	0.368758	0.368460	0.368048	0.367521	0.366888	0.366146	0.365288
	0.0500	0.363055	0.362905	0.362603	0.362167	0.361610	0.360933	0.360143	0.359238	0.358209
15	0.0025	0.429361	0.430666	0.431892	0.433069	0.434206	0.435320	0.436432	0.437558	0.438703
	0.0050	0.412798	0.413797	0.414702	0.415555	0.416361	0.417137	0.417906	0.418677	0.419449
	0.0100	0.395811	0.396467	0.397033	0.397532	0.397967	0.398355	0.398716	0.399058	0.399377
	0.0200	0.378710	0.379017	0.379203	0.379313	0.379341	0.379299	0.379196	0.379035	0.378809
	0.0300	0.368534	0.368620	0.368572	0.368429	0.368189	0.367859	0.367451	0.366967	0.366392
	0.0400	0.361165	0.361078	0.360860	0.360532	0.360098	0.359566	0.358943	0.358227	0.357406

Supplementary Material to:
 pH Measurements in Brackish Waters:
 Extending the Electrochemical pH_T Determination of TRIS buffers to Salinities 5 – 20

	0.0500	0.355354	0.355135	0.354785	0.354312	0.353726	0.353030	0.352230	0.351334	0.350333
20	0.0025	0.423596	0.424865	0.426074	0.427246	0.428392	0.429527	0.430681	0.431862	0.433073
	0.0050	0.406806	0.407762	0.408652	0.409498	0.410306	0.411108	0.411913	0.412738	0.413592
	0.0100	0.389938	0.390561	0.391109	0.391605	0.392046	0.392466	0.392875	0.393284	0.393693
	0.0200	0.372888	0.373162	0.373332	0.373440	0.373480	0.373468	0.373414	0.373322	0.373192
	0.0300	0.362702	0.362743	0.362682	0.362533	0.362300	0.361997	0.361631	0.361197	0.360694
	0.0400	0.355362	0.355238	0.354996	0.354658	0.354229	0.353713	0.353118	0.352448	0.351696
	0.0500	0.349661	0.349401	0.349024	0.348538	0.347948	0.347262	0.346485	0.345623	0.344664
35	0.0025	0.409902	0.411049	0.412156	0.413246	0.414336	0.415449	0.416597	0.417794	0.419046
	0.0050	0.393204	0.394044	0.394835	0.395603	0.396372	0.397160	0.397975	0.398826	0.399720
	0.0100	0.376519	0.377032	0.377498	0.377929	0.378351	0.378780	0.379220	0.379679	0.380161
	0.0200	0.359653	0.359825	0.359935	0.359995	0.360027	0.360041	0.360043	0.360040	0.360032
	0.0300	0.350022	0.349987	0.349878	0.349708	0.349484	0.349231	0.348944	0.348629	0.348284
	0.0400	0.342674	0.342430	0.342190	0.341832	0.341409	0.340946	0.340436	0.339879	0.339280
	0.0500	0.337104	0.336779	0.336364	0.335867	0.335293	0.334657	0.333962	0.333209	0.332394

Supplementary Material to:
pH Measurements in Brackish Waters:
Extending the Electrochemical pH_T Determination of TRIS buffers to Salinities 5 – 20

pH_T values

Table S6: Measured pH_T values and corresponding standard measurement uncertainties of equimolar TRIS/TRIS·H⁺ (in mol·kg-H₂O⁻¹) buffered artificial seawater solutions at salinities 5, 10, 15, 20 and 35. Actual measurement temperatures between 278.205 and 318.147 K are indicated in the first row.

S	T	278.205	283.201	288.193	293.187	298.176	303.172	308.165	313.159	318.147
	b_{TRIS}									
5	0.040	8.6938 ± 0.0013	8.5304 ± 0.0013	8.3733 ± 0.0013	8.2223 ± 0.0013	8.0769 ± 0.0014	7.9364 ± 0.0015	7.8006 ± 0.0016	7.6689 ± 0.0018	7.5412 ± 0.0021
	0.025	8.6877 ± 0.0013	8.5236 ± 0.0013	8.3662 ± 0.0013	8.2143 ± 0.0013	8.0680 ± 0.0014	7.9264 ± 0.0015	7.7892 ± 0.0016	7.6559 ± 0.0018	7.5264 ± 0.0021
	0.010	8.6793 ± 0.0013	8.5149 ± 0.0013	8.3565 ± 0.0013	8.2039 ± 0.0014	8.0568 ± 0.0014	7.9144 ± 0.0015	7.7764 ± 0.0016	7.6422 ± 0.0018	7.5118 ± 0.0021
10	0.040	8.6975 ± 0.0011	8.5316 ± 0.0011	8.3718 ± 0.0011	8.2172 ± 0.0011	8.0679 ± 0.0011	7.9231 ± 0.0011	7.7821 ± 0.0011	7.6448 ± 0.0012	7.5107 ± 0.0013
	0.025	8.6923 ± 0.0011	8.5260 ± 0.0011	8.3654 ± 0.0011	8.2104 ± 0.0011	8.0606 ± 0.0011	7.9151 ± 0.0011	7.7735 ± 0.0011	7.6353 ± 0.0012	7.5004 ± 0.0013
	0.010	8.6870 ± 0.0011	8.5203 ± 0.0011	8.3596 ± 0.0011	8.2042 ± 0.0011	8.0538 ± 0.0011	7.9077 ± 0.0011	7.7653 ± 0.0011	7.6265 ± 0.0012	7.4908 ± 0.0013
15	0.040	8.7074 ± 0.0014	8.5397 ± 0.0014	8.3777 ± 0.0013	8.2209 ± 0.0013	8.0691 ± 0.0013	7.9215 ± 0.0013	7.7775 ± 0.0013	7.6367 ± 0.0014	7.4989 ± 0.0014
	0.025	8.7036 ± 0.0014	8.5356 ± 0.0014	8.3731 ± 0.0013	8.2160 ± 0.0013	8.0637 ± 0.0013	7.9156 ± 0.0013	7.7711 ± 0.0013	7.6297 ± 0.0014	7.4913 ± 0.0014
	0.010	8.6971 ± 0.0014	8.5287 ± 0.0014	8.3662 ± 0.0013	8.2087 ± 0.0013	8.0561 ± 0.0013	7.9076 ± 0.0013	7.7627 ± 0.0013	7.6210 ± 0.0014	7.4822 ± 0.0014

Measurement uncertainty of pH_T :

The uncertainties of the measured pH_T values were determined for all temperatures, salinities and TRIS/TRIS·H⁺ molalities according to the Guide to the expression of uncertainty in measurement (GUM) using a Monte Carlo method in Mathematica.

If input quantities are correlated, these correlations should be taken into account in the calculation of the measurement uncertainty in order to meet the requirements of the GUM strictly. In this work, however, correlations between input quantities were not taken into account due to the complexity of the dataset and due to the fact that correlation data were not available in most of the cases.

An example measurement uncertainty budget is given in table S7. An illustrative representation for the determination of the standard potential, $E^{*\circ}$ is shown in Fig. S2. Standard measurement uncertainties (covariance factor $k=1$) are given with mean pH_T values in Tab. S6. Extended measurement uncertainties (covariance factor $k=2$) are displayed in Fig. S3. The salinity dependence of the two largest contributions to the measurement uncertainty are shown in Fig. S4.

Table S7: Details of pH_T uncertainty analysis for TRIS 0.04 M buffered artificial seawater of salinity 10 and 318 K.

Input quantity	Estimate x_i	$u(x_i)$	unit	Distribution	sensitivity coefficient $ c_i $	unit	$u(\text{pH}_T)$
$E^{*\circ}$	0.2320172	0.0000712	V	Gaussian	16	V ⁻¹	$11 \cdot 10^{-4}$
E	0.7529549	0.0000335	V	Gaussian	16	V ⁻¹	$5.3 \cdot 10^{-4}$
T	318.147	0.0060	K	Gaussian	0.025	K ⁻¹	$1.5 \cdot 10^{-4}$
X_{HCl}	0.20050	0.00007	mol·kg-H ₂ O ⁻¹	Gaussian	0.54	kg-H ₂ O · mol ⁻¹	$0.38 \cdot 10^{-4}$
X_{NaCl}	2.54464	0.00152	mol·kg-H ₂ O ⁻¹	Gaussian	0.094	kg-H ₂ O · mol ⁻¹	$1.4 \cdot 10^{-4}$
X_{MgCl_2}	0.71603	0.00149	mol·kg-H ₂ O ⁻¹	Gaussian	0.10	kg-H ₂ O · mol ⁻¹	$1.5 \cdot 10^{-4}$
Combined standard uncertainty of pH_T							0.0011

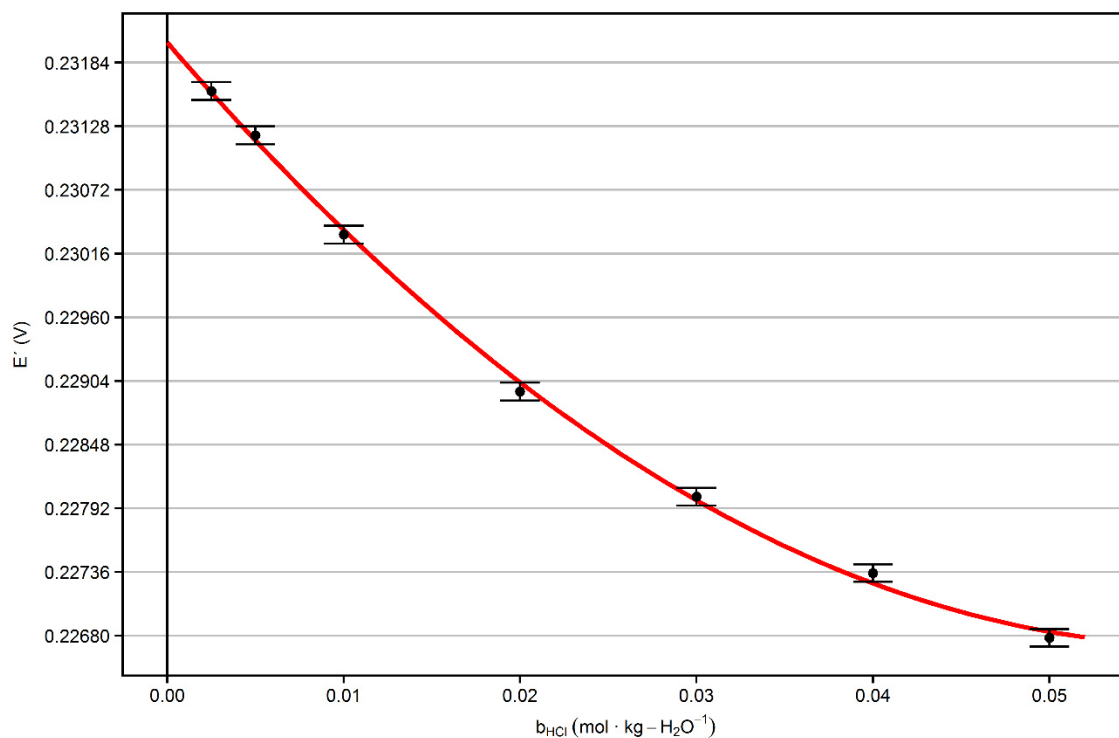


Figure S2: Determination of the standard potential of the Ag|AgCl electrodes E° by extrapolation E' values according to eq. 4 (see manuscript) to zero HCl molality for salinity 10 and 318 K. Error bars denote the standard measurement uncertainties of the functional values according to eq. 4. The vertical distance between grey lines is 560 μV , which corresponds to 0.01 in terms of pH.

Supplementary Material to:
pH Measurements in Brackish Waters:
Extending the Electrochemical pH_T Determination of TRIS buffers to Salinities 5 – 20

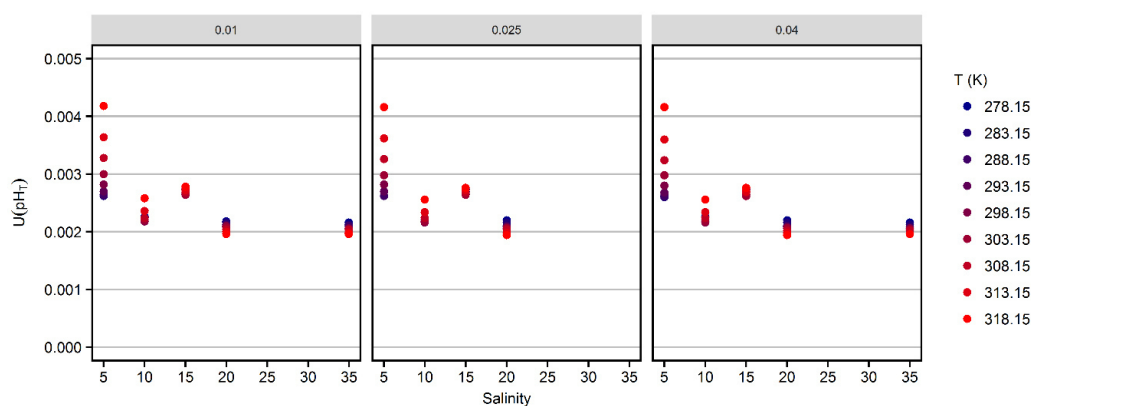


Figure S3: Extended measurement uncertainty, $U(pH_T)$, of pH_T measurements performed in this study as a function of salinity (x-axis), temperatures (color) and TRIS/TRIS·H⁺ molalities (in mol·kg-H₂O⁻¹) indicated at the top of the panels).

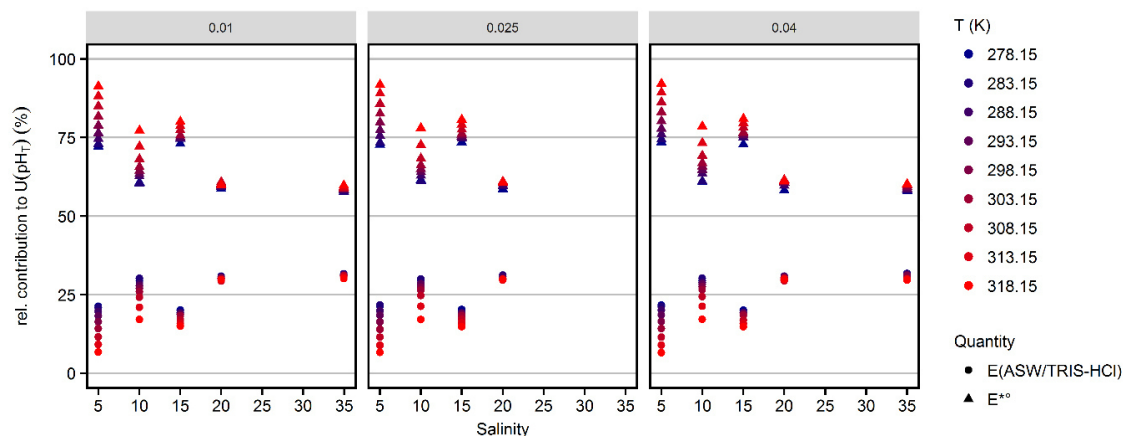


Figure S4: Relative contributions to the pH_T measurement uncertainty (Fig. S3) by the determination of the standard potential of the silver-silver chloride electrodes, E° , and the cell potential measured in the buffer solutions, $E_{ASW/TRIS-HCl}$. Results are displayed as a function of salinity (x-axis), temperatures (color) and TRIS/TRIS·H⁺ molalities (in mol·kg-H₂O⁻¹) indicated at the top of the panels).

pH_T model comparison to previous results

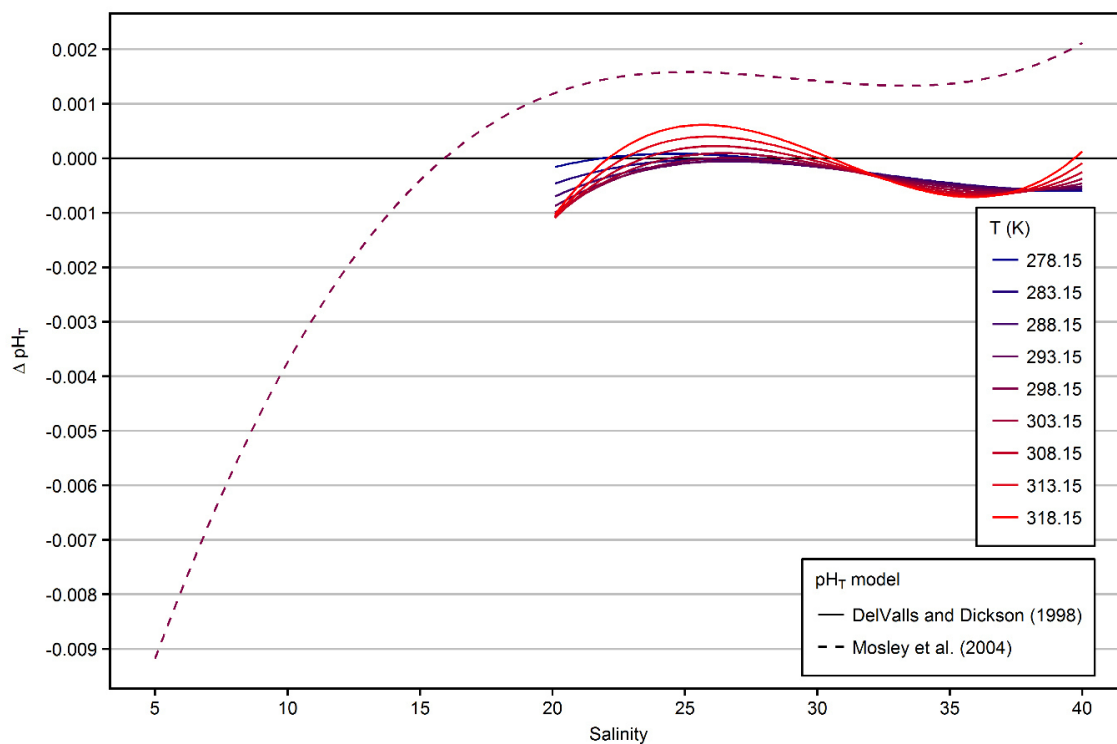


Figure S5: Deviation of the pH_T model fitted in this study (eq. 10, Tab. 2) from the models published by DeValls and Dickson (1998) and at 298.15 K by Mosley et al. (2004). Results are displayed at TRIS/TRIS \cdot H $^+$ molalities of 0.04 mol \cdot kg-H $_2$ O $^{-1}$

pH Measurements in Brackish Waters:

Experimental Characterization of Purified m-Cresol Purple for Spectrophotometric pH_T Measurements

J.D. Müller^{1*} and G. Rehder¹

¹Department of Marine Chemistry, Leibniz Institute for Baltic Sea Research Warnemünde, Rostock, Germany

*corresponding author: Jens Daniel Müller, Jens.Mueller@io-warnemuende.de

Abstract

Spectrophotometric pH measurements allow for an accurate quantification of acid-base equilibria in natural waters, provided that the physico-chemical properties of the indicator dye are well known. Here we present the first characterization of purified m-Cresol Purple (mCP) directly linked to a primary pH standard in the salinity range 5-20. Results were obtained from mCP absorption measurements in TRIS buffer solutions. The pH_T of identical buffer solutions was previously determined by Harned cell measurements in a coordinated series of experiments. The contribution of the TRIS/HCl component to the ionic strength of the buffer solutions increases towards lower salinity: This was taken into account by extrapolating the determined pK_{2e_2} to zero buffer concentration, thereby establishing access to a true hydrogen ion concentration scale for the first time. The results of this study were extended with previous determinations of pK_{2e_2} at higher and lower salinity and a pK_{2e_2} model was fitted to the combined data set. For future investigations that include measurements in the salinity range 5-20, pH_T should be calculated according to this pK_{2e_2} model, which can also be used without shortcomings for salinities 0-40 and temperatures from 278.15 – 308.15 K. It should be noted that conceptual limitations and methodical uncertainties are not yet adequately addressed for pH_T determinations at very low ionic strength.

Keywords: m-Cresol Purple, brackish water, estuaries, spectrophotometric pH measurements, traceability, primary standard, TRIS buffer

Introduction

pH is a master variable of seawater analysis. It allows the tracking of numerous biogeochemical processes, including organic matter production and mineralization, and is the most direct measure for ocean acidification (Byrne, 2014; Byrne et al., 2010). Several methods were developed to determine pH, ranging from glass electrodes (Easley and Byrne, 2012), to ISFET sensors (Martz et al., 2010) and to pH optodes (Clarke et al., 2015).

However, spectrophotometric pH measurements have proven to be the most precise and accurate method and are often considered to be a reference method (Byrne, 2014; Liu et al., 2011). Mueller et al. (2017) recently demonstrated that the method works reliably in the presence of high concentrations of dissolved organic matter and hydrogen sulfide and therefore supports full CO₂ system characterizations even under challenging conditions typical for brackish waters.

Spectrophotometric pH measurements rely on the addition of pH-sensitive indicator dyes, like m-Cresol Purple (mCP), to a water sample. The dye changes its color with sample pH. Those color changes are reflected in the absorbance spectra of the dye as changes in the peak absorbance ratio R , which depends on physico-chemical properties of the dye molecule (Clayton and Byrne, 1993; Liu et al., 2011). The accurate determination of acid-base equilibria in seawater – including the speciation of the CO₂ system – and the determination of long-term acidification trends require knowledge of the dye's dissociation constant and absorbance behavior. In order to ensure comparability of pH measurement results, the determination of the dissociation constant should be traceable to a fully characterized primary pH standard, e.g., by Harned cell measurements (Buck et al., 2002; Dickson et al., 2015).

In previous studies, reliable determinations of the dissociation and absorption behavior of mCP have been established in the salinity range 20-40 (Liu et al., 2011) and for river water conditions (Lai et al., 2016, 2017). The characterization experiments involved measurements of buffer solutions with pH assigned by Harned cell measurements (e.g., DelValls and Dickson, 1998) to determine the dissociation constant. Such buffer solutions were previously not available for salinities between 0 and 20. Mosley et al. (2004) provided an interim solution for this brackish water gap and characterized mCP for the full salinity range. However, the uncertainty of this characterization remained large, mainly due to (i) the interpolation of unknown TRIS buffer pH values between salinity 5 and 20, (ii) the lack of seawater salts in the salinity range 0.06-2, and (iii) the use of non-purified mCP. Further, the characterization was restricted to 298.15 K. Douglas and Byrne (2017b) combined the previous characterizations of purified mCP (Lai et al., 2016, 2017; Liu et al., 2011) with the results of Mosley et al. (2004) and modelled mCP properties over the full salinity and temperature range after correcting for dye impurities (Douglas and Byrne, 2017a). Nevertheless, a direct experimental characterization of purified mCP in brackish waters traceable to a primary pH standard was still missing, making it impossible to quantify the accuracy of spectrophotometric pH measurements in brackish waters. Uncertainties remained especially large at temperatures different from 298.15 K, due to the absence of experimental data.

To overcome these limitations, a concerted series of experiments was performed, which included two work packages:

1. Preceding Harned cell measurements of TRIS buffered artificial seawater (ASW) solutions to determine pH values on the total scale (pH_T) at salinities ranging from 5-20, temperatures from 278.15 – 318.15 K and equimolar TRIS/TRIS·H⁺ molalities of 0.01, 0.025, and 0.04 mol·kg-H₂O⁻¹ (Müller et al, *subm.*).
2. Determination of the mCP dissociation behavior in brackish waters based on spectrophotometric measurements performed with the newly available TRIS buffers (this study).

The obtained characterization of mCP in the salinity range 5-20 was combined with previous results at higher and lower salinity, to derive a model for the dissociation behavior covering the full salinity and temperature range. This model was evaluated in comparison to previous characterizations, with special emphasizes to remaining uncertainties for spectrophotometric pH measurements at very low ionic strength.

Material and methods

Theory

The basic principles of spectrophotometric pH measurements have been described extensively before (Clayton and Byrne, 1993; Liu et al., 2011; Mosley et al., 2004). In brief, the measurements are based on the addition of a pH-sensitive indicator dye to a water sample. The second dissociation constant, pK₂, of the diprotic dye mCP lies in the pH range typical for seawater. In this case, the solution pH can be expressed as:

$$pH = pK_2 + \log_{10} \left(\frac{[I^{2-}]}{[HI^-]} \right) \quad (1)$$

where [HI⁻] and [I²⁻] are the concentrations of the monoprotonated and deprotonated species of the indicator dye, respectively. The concentration ratio [HI⁻] / [I²⁻] can be determined by absorbance (A) measurements, because HI⁻ and I²⁻ have two clearly distinguishable absorbance maxima (Fig. 1) at wavelength λ₁ = 434 nm and λ₂ = 578 nm, respectively (Clayton and Byrne, 1993). However, the absorbance spectra of both indicator species overlap. Therefore, at both wavelength λ₁ and λ₂ the absorbance A_λ needs to be expressed by the Lambert-Beer-law describing the additive absorbance contribution, A_λ(I²⁻) + A_λ(HI⁻), of both species as:

$$A_\lambda = (\varepsilon_\lambda(HI^-) \cdot [HI^-] + \varepsilon_\lambda(I^{2-}) \cdot [I^{2-}]) \cdot d \quad (2)$$

where $\epsilon_{\lambda}(X)$ are the molar extinction coefficients of the indicator species X at wavelength λ , and d is the cuvette length.

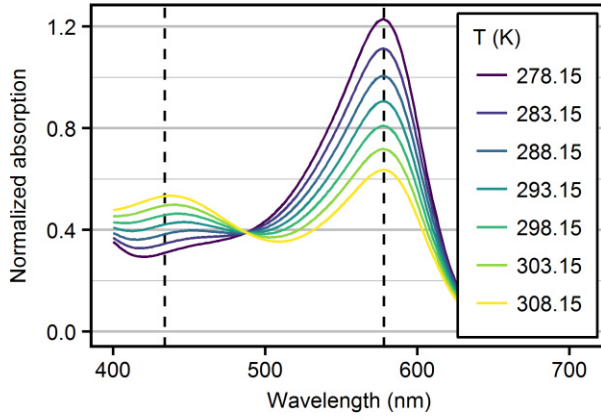


Fig. 1: Absorbance spectra of mCP recorded in TRIS ASW solutions ($S=10$, $b_{\text{TRIS}/\text{TRIS-H}^+} = 0.04 \text{ mol}\cdot\text{kg}\cdot\text{H}_2\text{O}^{-1}$) as a function of temperature. Spectra are normalized to the absorption at the isosbestic wavelength at 488nm. Dashed lines mark the wavelengths of HI^- and I^{2-} peak absorbances.

After combining equations (1) and (2), and with algebraic manipulation, the pH of the solution can be expressed as:

$$pH = pK_2 + \log_{10} \left(\frac{R - e_1}{e_2 - e_3 \cdot R} \right) \quad (3)$$

where $R = A_{578} / A_{434}$ is the ratio of the absorbance measured at the two peak wavelengths (dashed lines in Fig. 1) and $e_1 = \epsilon_{578}(\text{HI}^-) / \epsilon_{434}(\text{HI}^-)$, $e_2 = \epsilon_{578}(\text{I}^{2-}) / \epsilon_{434}(\text{HI}^-)$ and $e_3 = \epsilon_{434}(\text{I}^{2-}) / \epsilon_{434}(\text{HI}^-)$ are the molar absorptivity ratios (Clayton and Byrne, 1993; Mosley et al., 2004).

The molar absorptivity ratio e_2 includes molar extinction coefficients of both mCP species, HI^- and I^{2-} . Therefore, the separate determination of e_2 and e_3 would require the combination of measurements obtained in high and low pH solutions. Liu et al. (2011) avoided this by rearranging equation (3) to:

$$pH = pK_2 e_2 + \log_{10} \left(\frac{R - e_1}{1 - \frac{e_3}{e_2} \cdot R} \right) \quad (4)$$

The salinity and temperature dependence of the term $pK_2 e_2$ can be determined from measurements in buffer solutions with a known pH, provided that e_1 and e_3/e_2 are known. Previously, the required seawater buffer solutions with pH values assigned on the total scale were only available at salinities ≥ 20 (DeValls and Dickson, 1998).

Buffer solutions

TRIS buffered ASW solutions were prepared at salinities 5, 10, 15, 20, and at 35 for consistency assessments with previous results, according to Müller et al. (subm.). At each salinity, three buffer solutions contained equimolar TRIS/TRISH⁺ molalities ($b_{\text{TRIS/TRISH}^+}$) of 0.01, 0.025, 0.04 mol·kg-H₂O⁻¹. This allows the impact of the solution composition on the pH_T of the buffers and on the dissociation behavior of the dye to be corrected by extrapolation the determined pK_{2e2} values to zero TRIS/TRISH⁺ molality. The preparation and bottling of the buffer solutions was performed by the national metrological institute of Germany, Physikalisch-Technische Bundesanstalt (PTB), in parallel (same lab, day, stock solutions, and person, but separate weighings) to the preparation of identical buffer solutions for Harned cell pH_T measurements (Müller et al., subm.). Solutions prepared at PTB were stored in 500 mL glass bottles (Schott DURAN, GL 45 polypropylene screw caps). The headspace was filled with humidified Argon gas in order to avoid CO₂ uptake from the atmosphere. Solutions were shipped to the Leibniz-Institute for Baltic Sea Research in Warnemünde (IOW) for spectrophotometric measurement. The headspace was refilled with humidified Argon whenever bottles were opened to take subsamples.

Spectrophotometric measurements

In the buffer solutions described above, absorbance spectra of mCP were recorded at seven temperatures from 278.15 – 308.15 K in intervals of 5 K. Measurements were performed with an instrument set-up as described by Carter et al. (2013). The system consisted of an Agilent 8453 diode array spectrophotometer (Santa Clara, US) and a 10-cm, cylindrical, jacketed, flow-through cuvette (custom made by Hellma Analytics, Müllheim, Germany). The mantle of the cuvette was permanently flushed with water from a Julabo F30 heating circulator (Seelbach, Germany). Temperature was measured with a Pt resistance thermometer (Burster Kelvimat 4306 equipped with needle probe 42905, Gernsbach, Germany) calibrated at IOW's calibration lab with an uncertainty of 0.02 K. The needle probe was inserted in the water stream just behind the cuvette. Measured temperatures were within ±0.05 K of the target values. Before analysis, buffer solutions were brought to within 1 K of the analysis temperature in a separate temperature bath. The cuvette was filled and emptied with a computer-controlled syringe pump. The Agilent 8453 spectrometer was operated with both the tungsten- and the deuterium lamp switched on. More details on the measurement procedure are given in Carter et al., (2013).

All measurements were performed with purified mCP (Liu et al., 2011) kindly provided by the lab of Robert H. Byrne, Univ. of South Florida. A 2 mM stock solution of the dye was prepared by dissolving 0.08 g mCP in 100 mL deionized water. For better dissolution and

pH adjustment, the stock solution was sonicated and 3.25 mL of 0.1 M NaOH were added to achieve a pH of around 8.

Spectrometers are known to behave non-linearly at high and low absorbances. For mCP absorbance spectra, this is critical for the strong absorbance of I²⁻ at 578 nm (Fig. 1), especially at high pH in cold TRIS buffer solutions. To avoid non-linear behavior, absorbances at 578 nm were limited to values around 1 by adjusting the added amount of mCP. However, this may result in low absorbance at 434 nm. The most critical conditions were encountered at salinity 35 and 278.15 K with an absorbance ratio around 5 (Supplementary information Fig. S1).

The spectrometer performance was verified by running the self-test of the instrument (deuterium lines test for wavelength accuracy and reproducibility; as well as noise-, baseline flatness-, and stability tests). Wavelength accuracy was further verified by measurements of Holmium oxide standards. Furthermore, spectrophotometric comparison measurements were performed under conditions with well-defined solution pH and dye characteristics. This refers to measurements of TRIS buffer solutions (batch T27 and T30) and CRM standards (batch #146) provided by the lab of Andrew G. Dickson (Univ. of California) at 298.15 K. Further, measurements performed on own TRIS buffer solutions at salinity 20 and 35 were compared with previous results of Liu et al. (2011), who performed identical experiments, at temperatures from 278.15 – 303.15 K.

Determination of pK₂e₂

pH_T values of TRIS buffer solutions used in this study to calculate pK₂e₂ were assigned by Harned cell measurement (Table S1) and according to Müller et al. (subm.). The determination of pK₂e₂ from known pH_T values and corresponding R ratios according to:

$$pK_2e_2 = pH_T - \log_{10} \left(\frac{R - e_1}{1 - \frac{e_3}{e_2} \cdot R} \right) \quad (5)$$

requires knowledge of the absorptivity ratios e₁ and e₂/e₃. As proposed by Douglas and Byrne (2017b), the absorptivity ratios by Liu et al. (2011) according to equations (6) and (7):

$$e_1 = -0.007762 + 4.5174 \cdot 10^{-5} \cdot T \quad (6)$$

$$\frac{e_3}{e_2} = -0.020813 + 2.60262 \cdot 10^{-4} \cdot T + 1.0436 \cdot 10^{-4} \cdot (S - 35) \quad (7)$$

, were applied for the salinity range 5-20, although originally determined for salinities >20. Deviations between the salinity-dependent e₂/e₃ of Liu et al. (2011) extrapolated to S=0,

and e_2/e_3 determined by Lai et al. (2016) for freshwater conditions are presumably related to differences in the determination procedure. Only Liu et al. (2011) applied an iterative process to derive e_3/e_2 values that account for all absorbing species in solution, (R.H. Byrne, pers. comm.).

pK_{2e_2} values were determined from measured R and pH_T data for all buffer solutions described above. At each combination of salinity and temperature, the change of pK_{2e_2} with TRIS/TRISH⁺ molality was determined by linear regression analysis. The determined slope was used to correct individual pK_{2e_2} values to zero TRIS/TRIS·H⁺ molality (Fig. S2 in supplemental information).

Fitting a pK_{2e_2} model to a combined data set including previously published results

pK_{2e_2} results determined in this study at salinities 5-20 were combined with previously published results to derive a complete characterization of mCP from ocean to river water. In order to include the measurement uncertainty of previous work, we calculated pK_{2e_2} values from individual data rather than fitted equations given in the respective publications. The following data were included:

- For salinities 20, 30, 35, and 40 and temperatures from 278.15 – 308.15 K, pK_{2e_2} values were calculated from Table S4 in the supporting information of Liu et al. (2011).
- For salinities between 0.06 and 4.03 and 298.15 K, impurity-corrected results based on Mosley et al., (2004) were taken from Table 1 in Douglas and Byrne (2017b). An offset of +0.0065 pH units was observed at S=5 between the results of Douglas and Byrne (2017b) and this study. This offset was added to all pK_{2e_2} values at salinities from 0.06 to 4.03. This correction is smaller than the uncertainty in the data (see discussion) and allows for a pK_{2e_2} fit without a discontinuity.
- For salinity 0 and temperatures from 281.2 – 303.2 K, pK_{2e_2} was calculated from the measured dissociation constant at infinite dilution, pK_1^0 (Chun-Ze Lai and Michael DeGrandpre, pers. comm.), and e_2 (Table 2 in Lai et al. (2016)) as $pK_1^0 - \log_{10}(e_2)$.

The following full model, expressing pK_{2e_2} as a function (f) of S, T, was fitted to the combined data set:

$$pK_{2e_2} = f \left\{ (1 + S^{0.5} + S + S^{1.5} + S^2 + S^{2.5}) \cdot \left(1 + T + \ln(T) + \frac{1}{T} \right) \right\} \quad (8)$$

Equation (8) includes 24 terms representing all combinations of the terms of a fifth order $S^{0.5}$ polynomial and the terms of the physico-chemical expression of the temperature dependence of dissociation constants. The salinity polynomial in equation (8) is identical to that fitted by Douglas and Byrne (2017). Expressions with identical temperature dependence were previously fitted to pK_{2e_2} results (Liu et al., 2011) and TRIS buffer pH_T data (DeValls and Dickson, 1998).

The fit was obtained by generalized linear modeling with the “stats” package of the statistical programming language “R” (R Core Team, 2014). After fitting the full model (eq. 8), insignificant terms were removed by stepwise variable selection in both directions based on the Akaike information criterion. The removal of terms was performed with the “stepAIC” function from the R package “MASS” and resulted in a pK_{2e_2} model with 19 terms (eq. 9).

Results

Extrapolation of pK_{2e_2} to zero buffer concentration

At each combination of temperature and salinity, pK_{2e_2} was determined at three different TRIS/TRISH⁺ molalities, 0.01, 0.025 and 0.04 mol·kg-H₂O⁻¹. The pK_{2e_2} values were extrapolated linearly to zero TRIS/TRISH⁺ molality (Fig. S2). The mean slope of this extrapolation ranged from 0.3 to -0.07 mol⁻¹·kg-H₂O at salinities 5 and 35, respectively. For a TRIS/TRISH⁺ molality of 0.04 mol·kg-H₂O⁻¹, this slope corresponds to a mean pK_{2e_2} correction ranging from 0.012 to -0.003 at salinities 5 and 35, respectively (Fig. S3). The standard deviation of the residuals from the linear extrapolation fit was <0.001 for all combinations of temperature and salinity. The pK_{2e_2} value determined at S=20 and a TRIS/TRISH⁺ molality of 0.025 mol·kg-H₂O⁻¹ deviated from the value interpolated between the results at TRIS/TRISH⁺ molalities of 0.01 and 0.04 mol·kg-H₂O⁻¹ by more than three times the standard deviation of all measurements, and was removed for further analysis without knowing the source of error.

pK_{2e_2} results and model

The extrapolated pK_{2e_2} values of mCP determined in this study for salinities 5-20 ranged from 7.57 to 8.08 (Fig. 2A). The salinity-dependence of pK_{2e_2} increases towards lower salinity. The dependence on temperature is almost linear at constant salinity. The pK_{2e_2} model fitted to the combined data set, including results from this study and from that of Douglas and Byrne (2017b), Lai et al. (2016, 2017), and Liu et al. (2011) is given in equation (9) with respective coefficients given in Table 1.

$$\begin{aligned}
 \text{pK}_{2e_2} = & a + b_1 \cdot S^{0.5} + b_2 \cdot S^{1.5} + b_3 \cdot S^2 + b_4 \cdot S^{2.5} \\
 & + c_1 \cdot T^{-1} + c_2 \cdot S^{1.5} \cdot T^{-1} + c_3 \cdot S^2 \cdot T^{-1} + c_4 \cdot S^{2.5} \cdot T^{-1} \\
 & + d_1 \cdot \ln(T) + d_2 \cdot S^{1.5} \cdot \ln(T) + d_3 \cdot S^2 \cdot \ln(T) + d_4 \cdot S^{2.5} \cdot \ln(T) \\
 & + e_1 \cdot T + e_2 \cdot S^{0.5} \cdot T + e_3 \cdot S \cdot T + e_4 \cdot S^{1.5} \cdot T + e_5 \cdot S^2 \cdot T + e_6 \cdot S^{2.5} \cdot T
 \end{aligned} \tag{9}$$

Table 1: Coefficients of equation 9 fitted to the combined data set displayed in Fig. 2A. Control value for pK_{2e_2} at $S=20$ and $T=298.15$ K is 7.6920.

Coefficient	Value
a	$1.08071477 \cdot 10^3$
b ₁	$-1.35394946 \cdot 10^{-1}$
b ₂	$-1.98063716 \cdot 10^2$
b ₃	$6.31924397 \cdot 10^1$
b ₄	-5.18141866
c ₁	$-2.66457425 \cdot 10^4$
c ₂	$5.08796578 \cdot 10^3$
c ₃	$-1.62454827 \cdot 10^3$
c ₄	$1.33276788 \cdot 10^2$
d ₁	$-1.89671212 \cdot 10^2$
d ₂	$3.49038762 \cdot 10^1$
d ₃	$-1.11336508 \cdot 10^1$
d ₄	$9.12761930 \cdot 10^{-1}$
e ₁	$3.27430677 \cdot 10^{-1}$
e ₂	$-7.51448528 \cdot 10^{-4}$
e ₃	$3.94838229 \cdot 10^{-4}$
e ₄	$-6.00237876 \cdot 10^{-2}$
e ₅	$1.90997693 \cdot 10^{-2}$
e ₆	$-1.56396488 \cdot 10^{-3}$

Residuals from the fitted pK_{2e_2} model (Fig. 2B) are within ± 0.005 for the entire salinity and temperature range.

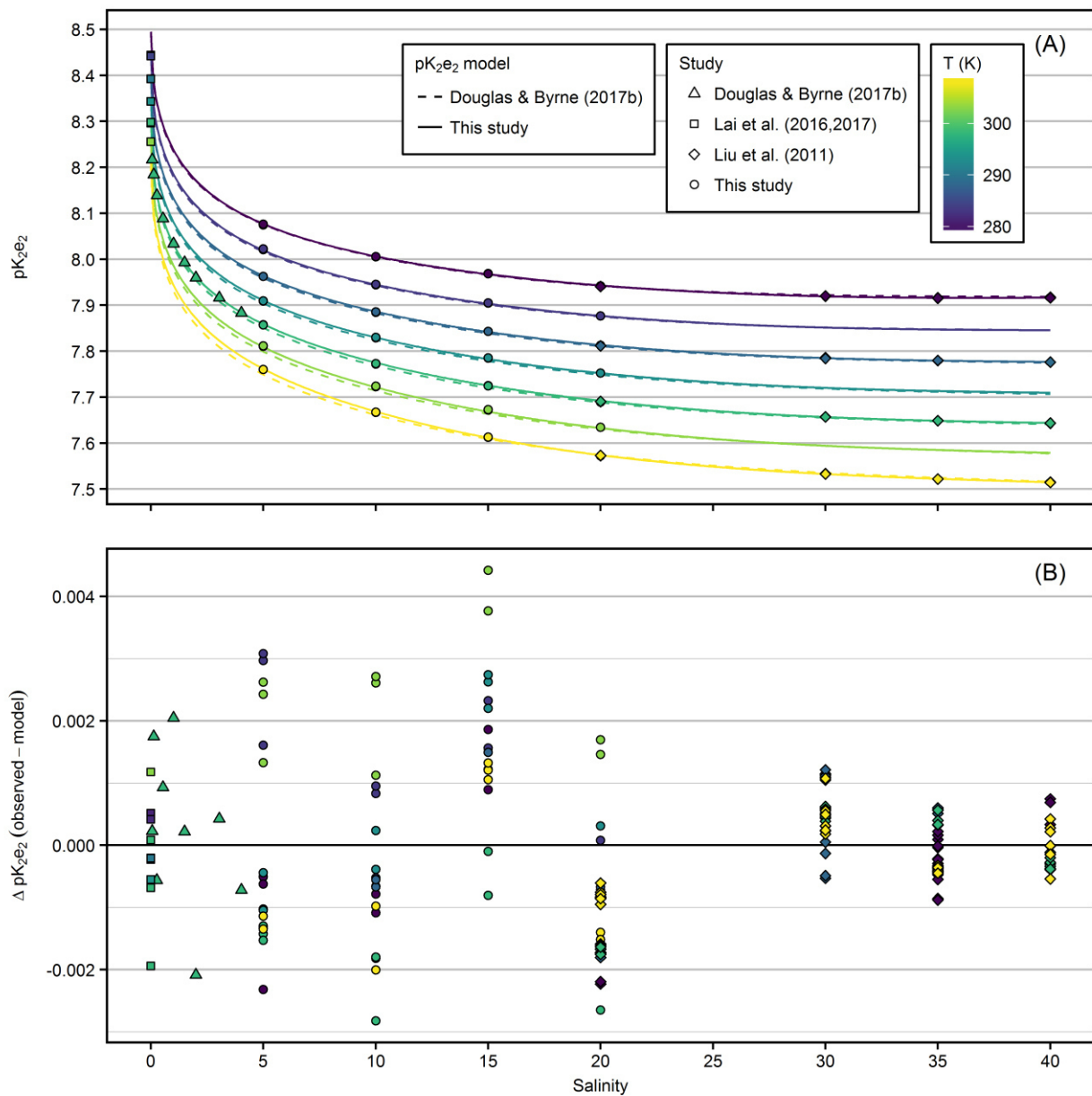


Fig. 2: (A) pK_{2e_2} of mCP as a function of salinity and temperature. Results from this study (salinity range 5-20) were combined with previous results and fitted to a common pK_{2e_2} model (solid lines). Dashed lines represent the pK_{2e_2} model by Douglas and Byrne (2017b). (B) Residuals from the model fitted in this study.

Agreement with previous studies

In the salinity range 5-20, the pK_{2e_2} model of Douglas and Byrne, (2017b) agrees with the new model presented in this study within 0.008 at 298.15 K (Fig. S4). At salinity 20, deviations are within 0.004. At salinity 5 and 308.15 K, the largest offset between both

models was observed with 0.013 higher pK_{2e_2} values predicted by the model fitted in this study.

In the salinity range 20-40, the pK_{2e_2} model of Liu et al., (2011) agrees with the model presented in this study within 0.002 across all temperatures (Fig. S4). At freshwater conditions, pK_{2e_2} calculated according to Lai et al. (2017) agrees with the model presented in this study within 0.006 across all temperatures (Fig. S4).

The residuals from the model (Fig. 2B) are larger at salinities ≤ 20 , compared to the residuals at salinities > 20 . However, the precision achieved within each group of salinity, temperature and TRIS/TRISH⁺ is < 0.001 and comparable for the results of this study and those of Liu et al. (2011). The higher residuals at lower salinities reflect the uncertainty in the pH_T determination by Harned cell measurements (compare residuals in Fig. 5 of Müller et al., *subm.*), which was not included in previous studies when pH_T values of buffer solutions were calculated from fitted models.

For a direct comparison to previous results, spectrophotometric pH_T values calculated according to Liu et al. (2011) were determined in TRIS buffer solutions (batch T27 and T30) and CRM standards (batch #146) purchased from the laboratory of Andrew G. Dickson (Scripps Institution of Oceanography). Results were highly reproducible and consistently 0.005-0.006 pH units lower than theoretical values (TRIS pH_T calculated according to DelValls and Dickson (1998); CRM pH_T calculated from certified C_T and A_T according to Lueker et al. (2000)). For own TRIS buffer solutions at salinity 20 and 35, spectrophotometric pH_T values calculated according to Liu et al. (2011) were 0.002 to 0.008 pH units lower than pH_T values determined by Harned cell measurements over the temperature range from 278.15-308.15 K.

Discussion

Advantages of a coordinated experimental concept

The experiments presented here were part of a coordinated measurement program covering the preparation of TRIS buffered ASW solutions, pH_T determination by Harned cell measurements and subsequent recording of mCP absorption spectra. This reduces uncertainties included in all previous experiments, in which the required analysis of the buffer solutions (e.g., DelValls and Dickson 1998) and subsequent mCP characterizations (e.g., Liu et al. 2011) were performed in separate experiments. Nemzer and Dickson (2005) found TRIS buffer pH to vary by up to 0.0034, even when carefully prepared in the same laboratory, and argued that an error of only 0.23% in the TRIS/TRISH⁺ ratio will result in an error of 0.001 in pH. Müller et al. (*subm.*) and this study reduced this uncertainty

by titrating the TRIS- against the HCl- stock solution and subsequently preparing all buffers from the same stock solution. Further, in this study we determined pK_{2e_2} based on pH_T values individually assigned by Harned cell measurements to the same batch of buffer solution, whereas previous studies had to rely on pH_T values calculated from fitted models.

Correcting the contribution of TRIS and HCl to the ionic composition of the buffer solutions

The ionic composition of buffered ASW solutions differs from that of pure ASW solutions, due to the replacement of seawater salts by TRIS and HCl at a given ionic strength. The relative contribution of the buffer components increases towards lower salinity. This can only to a certain degree be circumvented by lower buffer concentrations, because solutions with lower buffer concentrations are less stable and reproducible. The inevitable difference in solution composition has two effects: (i) The pH_T of the buffer solution changes with the concentration of the buffer and assigned pH_T values do not exactly correspond to the total hydrogen ion concentration scale (see discussion in Dickson et al., 2015; Nemzer and Dickson, 2005; Müller et al., *subm.*). (ii) The difference in solution composition affects the pK_{2e_2} of mCP. However, both effects (i) and (ii) are corrected when calibration results are extrapolated to zero buffer concentration, as done in this study for the first time.

At salinity 35, we found the pK_{2e_2} correction to be <0.005 for a $0.04 \text{ mol}\cdot\text{kg}\cdot\text{H}_2\text{O}^{-1}$ TRIS/TRISH⁺ molality. Although this effect might be small in comparison to other sources of uncertainty, similar extrapolation experiments as performed in this study are required to accurately determine pH_T at salinities 20-40. More pronounced pK_{2e_2} corrections need to be applied at lower salinity and amounted up to 0.02 for a TRIS/TRISH⁺ molality of $0.04 \text{ mol}\cdot\text{kg}^{-1}$ (Fig. S3).

Performing the required extrapolation, this study presents the first attempt to determine pK_{2e_2} values that allow the measurements of pH on a true hydrogen ion concentration scale referring to the reference ASW composition in the salinity range 5-20. In contrast, the mCP characterization by Mosley et al. (2004) did not account for the ionic strength contribution of TRIS/TRISH⁺, despite covering salinities as low as 0.06. Furthermore, at salinities below 2, TRIS/TRISH⁺ represented the only contribution to ionic strength but was still interpreted in terms of salinity, based on the results of Bates and Hetzer (1961). In view of these uncertainties, the currently available characterization of pK_{2e_2} is strictly valid only for salinities as low as 5 and the ASW solutions composition reported in this study. For salinities below 5, the pK_{2e_2} models reported in this study and that of Douglas and Byrne (2017) are associated with similar uncertainties, going back to the limitations in the study of Mosley et al. (2004).

Spectrophotometric pH measurements at very low ionic strength

Similar to the pK_{2e_2} extrapolation performed in this study, Lai et al. (2016) determined changes of the dissociation constant of mCP of ~ 0.02 when decreasing the phosphate buffer concentration by only $\sim 0.005 \text{ mol}\cdot\text{kg}^{-1}$ under freshwater conditions. This highlights the strong sensitivity of the dissociation behavior of mCP on the ionic composition of the sample at low ionic strength. It remains to be studied, whether the dissociation behavior of mCP is controlled only by the ionic strength of the solution or whether the ionic composition plays a significant role. If the latter is the case, it would be questionable, whether an accuracy in the order of a few thousandths of pH units can ever be achieved at very low ionic strength, without knowing the ionic composition of the sample. This is a consequence of the more general problem to determine salinity from conductivity measurements in low-saline water with variable composition (Feistel et al., 2009; Wright et al., 2011).

Lai et al. (2016) compared spectrophotometric pH measurements with two different indicator dyes, phenol red and mCP, on seven different freshwater samples and found pH results that agreed within ± 0.01 . Those results indicate same ionic interactions of both dyes, i.e., similar activity coefficients in similar media, but do not allow for an independent assessment of the accuracy of the results. Accordingly, more comprehensive mCP characterizations are required to unravel the impact of ionic composition. Potential approaches to improve the understanding of mCP behavior in very low-saline and river water conditions include: (i) traceable characterization experiments at variable buffer concentrations and ionic composition of the salt matrix, and (ii) estimation of the effects of solution composition changes on the dyes dissociation behavior with Pitzer models (Turner et al., 2016).

Observed offsets in pH_T comparison measurements

Performing comparison measurements with TRIS buffers and certified reference materials, our pH_T values calculated according to Liu et al. (2011) were consistently lower by 0.005 at 298.15 K. Over the full temperature range, pH_T values determined in own TRIS buffer solutions were 0.002 to 0.008 lower. Similar offsets were reported by Carter et al. (2013), but the reason for this offset could not be determined so far. Lower determined pH_T values result from a lower R-dependent log-term in equation (4). Vice versa, lower log-terms in equation (5) lead to slightly higher determined pK_{2e_2} values compared to previous results (Liu et al., 2011), when identical pH_T values are assigned to the buffer solutions. Interestingly, our extrapolation to zero TRIS/TRISH⁺ molality compensates for this offset to the results of Liu et al. (2011) at salinity 20. In contrast, at salinity 35 the correction has

an opposite sign and observed pH_T differences do not cancel out. Due to the scarce amount of data at salinities >20 obtained in this study, we included only the results by Liu et al. (2011) into our combined data set.

Model evaluation and recommendation

The pK_{2e2} model by Douglas and Byrne (2017) agrees surprisingly well with the results presented in this study, although previous experimental data in the salinity range 5-20, going back to the results of Mosley et al. (2004), were limited to 298.15 K and associated to several uncertainties. However, differences between both models (>0.01) are larger than the measurement uncertainty of the method (Carter et al., 2013). In addition, the pK_{2e2} model presented in this study fits the results of Liu et al. (2011) almost as well as the original model (residuals within ±0.002), and therefore better than the model of Douglas and Byrne (2017), who found residuals >0.003.

Therefore, we recommend to use the pK_{2e2} model presented in this study for all spectrophotometric pH measurements in brackish water that cover salinities below 20. Due to the excellent agreement with the results of Liu et al. (2011), the pK_{2e2} model presented in this study can also be applied for pH calculations at salinities >20 without constraints. However, the uncertainty of this model is as large as that of (Douglas and Byrne, 2017b) for salinities well below 5.

Conclusion

In this study, we provided the experimental basis to directly link spectrophotometric pH_T measurements in the salinity range 5-20 to Harned cell pH_T determinations of TRIS buffered artificial seawater solutions. We combined the derived pK_{2e2} estimates of mCP with the results from previous studies and fitted a pK_{2e2} model as a function of temperature and salinity to the combined data set. We recommend using the new pK_{2e2} model for all measurements in brackish waters that include samples with salinities below 20. Measurements under fully marine conditions can be performed without compromise compared to previous pK_{2e2} models. For S < 5, the model faces the same problems as in previous work, but is potentially better suited for pH measurements near 5. For near river water conditions, the impact of ionic composition on spectrophotometric pH determination remains to be studied to answer the question whether spectrophotometric measurements can produce accurate pH results without knowledge of the exact ionic composition of the sample.

Acknowledgement

The quality of this paper gained from scientific discussions with Bernd Schneider, Robert H. Byrne, and Michael DeGrandpre.

The research leading to this manuscript has received funding from BONUS, the joint Baltic Sea research and development programme (Art 185), funded jointly from the European Union's Seventh Programme for research, technological development and demonstration and from the German Federal Ministry of Education and Research through Grant No. 03F0689A (BONUS PINBAL).

References

- Bates, R. G., and Hetzer, H. B. (1961). DISSOCIATION CONSTANT OF THE PROTONATED ACID FORM OF 2-AMINO-2-(HYDROXYMETHYL)- 1, 3-PROPANEDIOL [TRIS- HYDROXYMETHYL) - AMINOMETHANE] AND RELATED THERMODYNAMIC QUANTITIES FROM 0 TO 50°. *J. Phys. Chem.* 65, 667–671.
- Buck, R. P., Rondinini, S., Covington, A. K., Baucke, F. G. K., Brett, C. M. A., Camoes, M. F., et al. (2002). Measurement of pH. Definition, standards, and procedures (IUPAC Recommendations 2002). *Pure Appl. Chem.* 74, 2169–2200. Available at: <http://www.degruyter.com/view/j/pac.2002.74.issue-11/pac200274112169/pac200274112169.xml> [Accessed October 2, 2014].
- Byrne, R. H. (2014). Measuring ocean acidification: new technology for a new era of ocean chemistry. *Environ. Sci. Technol.* 48, 5352–60. doi:10.1021/es405819p.
- Byrne, R. H., Mecking, S., Feely, R. a., and Liu, X. (2010). Direct observations of basin-wide acidification of the North Pacific Ocean. *Geophys. Res. Lett.* 37. doi:10.1029/2009GL040999.
- Carter, B. R., Radich, J. a., Doyle, H. L., and Dickson, a. G. (2013). An automated system for spectrophotometric seawater pH measurements. *Limnol. Oceanogr. Methods* 11, 16–27. doi:10.4319/lom.2013.11.16.
- Clarke, J. S., Achterberg, E. P., Rérolle, V. M. C., Abi Kaed Bey, S., Floquet, C. F. A., and Mowlem, M. C. (2015). Characterisation and deployment of an immobilised pH sensor spot towards surface ocean pH measurements. *Anal. Chim. Acta* 897, 69–80. doi:10.1016/j.aca.2015.09.026.
- Clayton, T. D., and Byrne, R. H. (1993). Spectrophotometric seawater pH measurements : total hydrogen results. *Deep Sea Res. Part I Oceanogr. Res. Pap.* 40, 2115–2129.
- DelValls, T. A., and Dickson, A. G. (1998). The pH of buffers based on 2-amino-2-hydroxymethyl-1,3-propanediol (“tris”) in synthetic sea water. *Deep Sea Res. Part I Oceanogr. Res. Pap.* 45, 1541–1554. doi:10.1016/S0967-0637(98)00019-3.
- Dickson, A. G., Cam, M. F., Spitzer, P., Fiscaro, P., Stoica, D., Pawlowicz, R., et al. (2015). Metrological challenges for measurements of key climatological observables . Part 3 : seawater pH. *Metrologica*.
- Douglas, N. K., and Byrne, R. H. (2017a). Achieving accurate spectrophotometric pH measurements using unpurified meta-cresol purple. *Mar. Chem.* 190, 66–72. doi:10.1016/j.marchem.2017.02.004.

- Douglas, N. K., and Byrne, R. H. (2017b). Spectrophotometric pH measurements from river to sea: Calibration of mCP for $0 \leq S \leq 40$ and $278.15 \leq T \leq 308.15$ K. *Mar. Chem.*, 1–6. doi:10.1016/j.marchem.2017.10.001.
- Easley, R. A., and Byrne, R. H. (2012). Spectrophotometric Calibration of pH Electrodes in Seawater Using Purified m-Cresol Purple.
- Feistel, R., Weinreben, S., Wolf, H., Seitz, S., Spitzer, P., Adel, B., et al. (2009). Density and Absolute Salinity of the Baltic Sea 2006–2009. *Ocean Sci.* 6, 3–24. doi:10.5194/osd-6-1757-2009.
- Lai, C., DeGrandpre, M. D., Wasser, B. D., Brandon, T. A., Clucas, D. S., Jaqueth, E. J., et al. (2016). Spectrophotometric measurement of freshwater pH with purified meta-cresol purple and phenol red. *Limnol. Oceanogr. Methods* 14, 864–873. doi:10.1002/lom3.10137.
- Lai, C. Z., DeGrandpre, M. D., Wasser, B. D., Brandon, T. A., Clucas, D. S., Jaqueth, E. J., et al. (2017). Corrigendum to: Spectrophotometric measurement of freshwater pH with purified meta-cresol purple and phenol red: Freshwater pH with purified indicators (*Limnology and Oceanography: Methods*, (2016), 14, 12, (864-873), 10.1002/lom3.10137). *Limnol. Oceanogr. Methods* 15, 903. doi:10.1002/lom3.10210.
- Liu, X., Patsavas, M. C., and Byrne, R. H. (2011). Purification and characterization of meta-cresol purple for spectrophotometric seawater pH measurements. *Environ. Sci. Technol.* 45, 4862–8. doi:10.1021/es200665d.
- Lueker, T. J., Dickson, A. G., and Keeling, C. D. (2000). Ocean pCO₂ calculated from dissolved inorganic carbon, alkalinity, and equations for K₁ and K₂: validation based on laboratory measurements of CO₂ in gas and seawater at equilibrium. *Mar. Chem.* 70, 105–119.
- Martz, T. R., Connery, J. G., and Johnson, K. S. (2010). Testing the Honeywell Durafet for seawater pH applications. *Limnol. Oceanogr. Methods* 8, 172–184. doi:10.4319/lom.2010.8.172.
- Mosley, L. M., Husheer, S. L. G., and Hunter, K. a. (2004). Spectrophotometric pH measurement in estuaries using thymol blue and m-cresol purple. *Mar. Chem.* 91, 175–186. doi:10.1016/j.marchem.2004.06.008.
- Nemzer, B. V., and Dickson, A. G. (2005). The stability and reproducibility of Tris buffers in synthetic seawater. *Mar. Chem.* 96, 237–242. doi:10.1016/j.marchem.2005.01.004.
- Turner, D. R., Achterberg, E. P., Chen, C.-T. A., Clegg, S. L., Hatje, V., Maldonado, M. T., et al. (2016). Toward a Quality-Controlled and Accessible Pitzer Model for Seawater and Related Systems. *Front. Mar. Sci.* 3, 139. doi:10.3389/fmars.2016.00139.
- Wright, D. G., Pawlowicz, R., McDougall, T. J., Feistel, R., and Marion, G. M. (2011). Absolute salinity, “density salinity” and the reference-composition salinity scale: Present and future use in the seawater standard TEOS-10. *Ocean Sci.* 7, 1–26. doi:10.5194/os-7-1-2011.

Supplementary Material to: pH measurements in brackish waters: Experimental Characterization of Purified m-Cresol Purple for Spectrophotometric pH_T Measurements

Jens Daniel Müller and Gregor Rehder

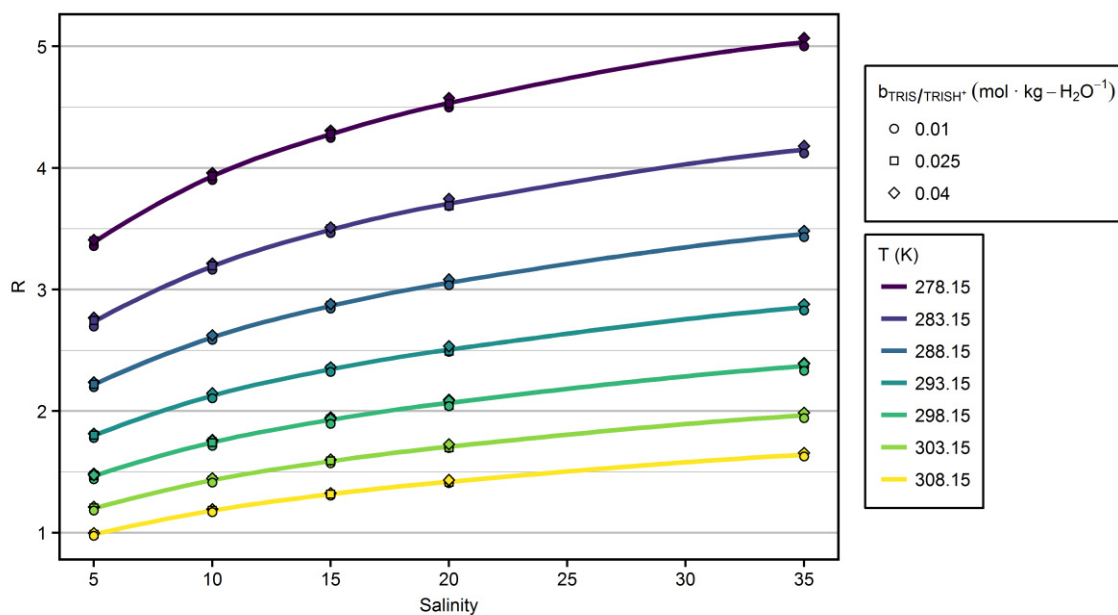


Figure S1: mCP absorbance ratios R in TRIS buffered artificial seawater solutions as function of salinity, temperature and TRIS/TRISH⁺ molality.

Supplementary Material
pH Measurements in Brackish Waters:
Experimental Characterization of Purified m-Cresol Purple for Spectrophotometric pH_T Measurements

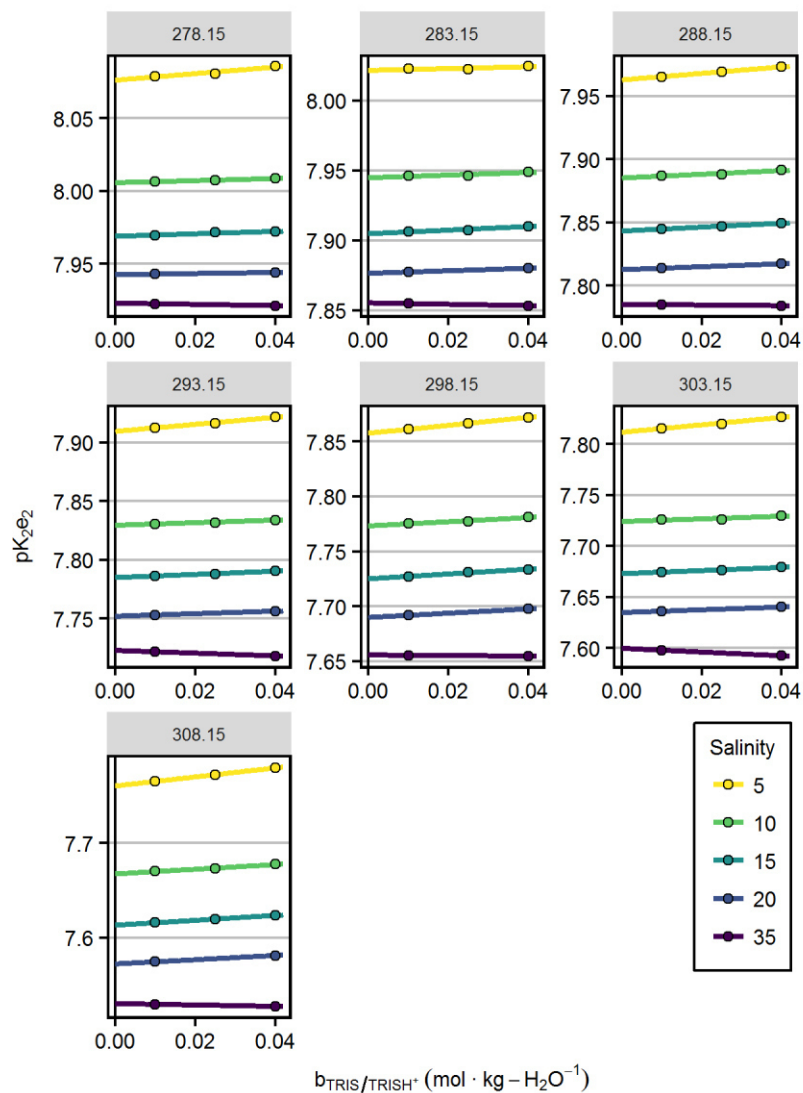


Figure S2: pK_{2e2} values as a function of TRIS/TRISH⁺ molalities for all salinities (color) and temperatures in K (indicated at the top of the panels). Lines indicate results of linear regression analysis that are used to correct pK_{2e2} values to zero TRIS/TRISH⁺ molality, corresponding mean slopes are shown in Fig. S3

Supplementary Material
pH Measurements in Brackish Waters:
Experimental Characterization of Purified m-Cresol Purple for Spectrophotometric pH_T Measurements

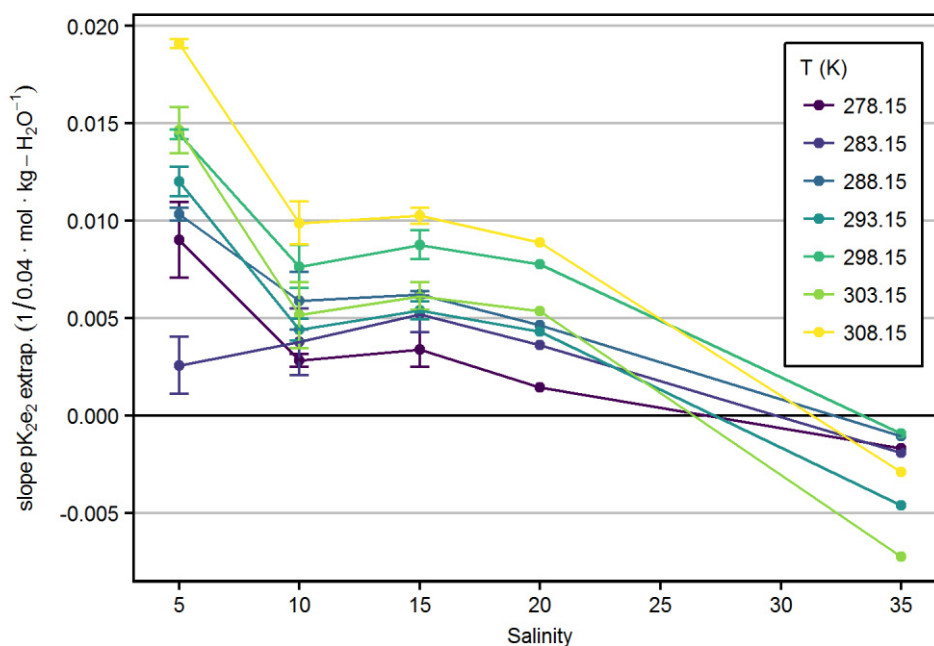


Figure S3: Linear regression slope of pK_{ze2} extrapolation to zero TRIS/TRISH⁺ molality (shown in Fig. S2) as a function of salinity and temperatures (color). Error bars indicate the standard error of the regression intercept. Note that the absolute values on the y-axis correspond to the correction applied to pK_{ze2} values determined in $0.04 \text{ mol}\cdot\text{kg}\cdot\text{H}_2\text{O}^{-1}$ TRIS buffers.

Supplementary Material
pH Measurements in Brackish Waters:
Experimental Characterization of Purified m-Cresol Purple for Spectrophotometric pH_T Measurements

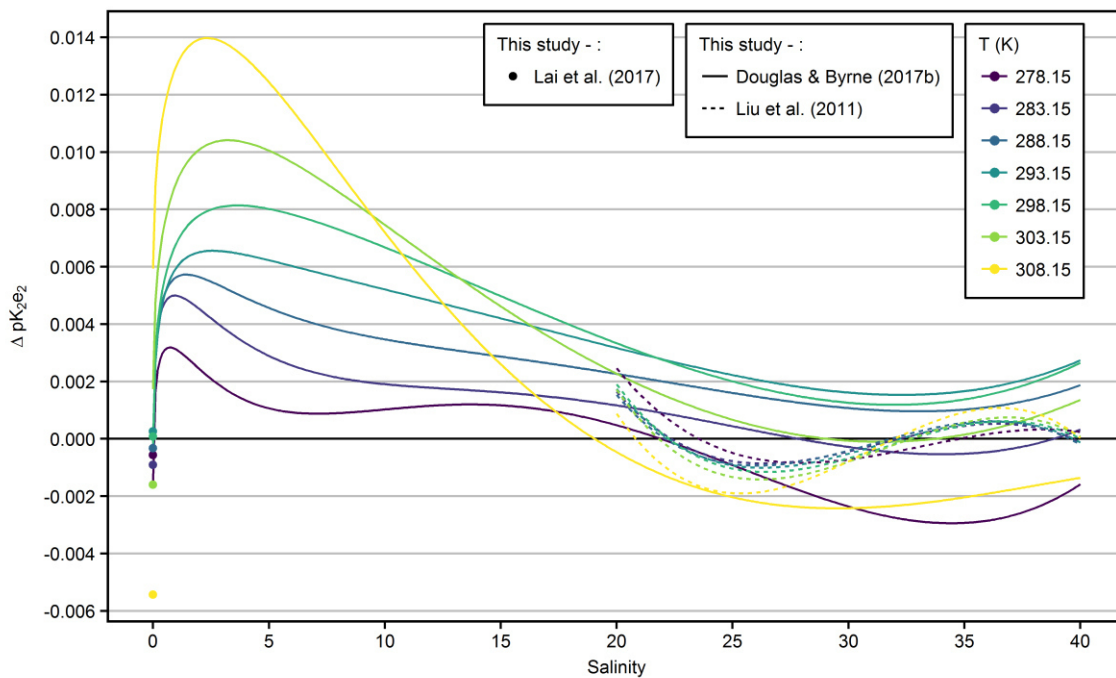


Figure S4. Deviations between the pK_{2e2} model of this study and those of Lai et al. (2016, 2017); Liu et al. (2011), and Douglas and Byrne (2017b).

Supplementary Material
pH Measurements in Brackish Waters:
Experimental Characterization of Purified m-Cresol Purple for Spectrophotometric pH_T Measurements

Table S1. Experimental results of this study: Nominal salinities and TRIS molalities ($b_{\text{TRIS}/\text{TRIS}\cdot\text{H}^+}$) of the buffers solutions prepared according to Müller et al. (subm.). Temperature recorded during spectrophotometric measurements. pH_T values of TRIS buffers, corrected for minor difference (<0.1 K) between the measurement temperature during Harned cell measurements (Tab. S6 in Müller et al. (subm.)) and the temperature recorded during spectrophotometric measurements. R values determined by spectrophotometric measurements.

Salinity	$b_{\text{TRIS}/\text{TRIS}\cdot\text{H}^+}$ mol·kg-H ₂ O ⁻¹	Temperature K	pH _T	R
5	0.01	278.14	8.6813	3.357315
5	0.025	278.14	8.6897	3.401491
5	0.04	278.13	8.6960	3.409187
5	0.01	283.19	8.5152	2.696398
5	0.025	283.19	8.5239	2.745707
5	0.04	283.2	8.5305	2.768608
5	0.01	288.16	8.3576	2.196929
5	0.025	288.16	8.3672	2.221552
5	0.04	288.16	8.3743	2.237790
5	0.01	293.18	8.2041	1.779782
5	0.025	293.19	8.2142	1.803389
5	0.04	293.18	8.2225	1.814800
5	0.01	298.13	8.0582	1.456799
5	0.025	298.12	8.0697	1.474943
5	0.04	298.12	8.0785	1.486515
5	0.01	303.13	7.9156	1.183075
5	0.025	303.11	7.9282	1.204038
5	0.04	303.11	7.9382	1.212915
5	0.01	308.17	7.7762	0.975945
5	0.025	308.17	7.7890	0.988495
5	0.04	308.17	7.8004	0.997054
10	0.01	278.14	8.6891	3.900920
10	0.025	278.14	8.6943	3.933452
10	0.04	278.15	8.6991	3.958607
10	0.01	283.18	8.5210	3.163536
10	0.025	283.2	8.5260	3.195515
10	0.04	283.19	8.5319	3.213577
10	0.01	288.15	8.3610	2.586284
10	0.025	288.17	8.3661	2.608743
10	0.04	288.16	8.3727	2.624376
10	0.01	293.19	8.2041	2.105310
10	0.025	293.18	8.2107	2.128686
10	0.04	293.19	8.2171	2.147315
10	0.01	298.13	8.0552	1.731753
10	0.025	298.13	8.0620	1.749701
10	0.04	298.13	8.0693	1.762160
10	0.01	303.1	7.9099	1.413715
10	0.025	303.11	7.9170	1.433998
10	0.04	303.11	7.9249	1.447479

Supplementary Material
 pH Measurements in Brackish Waters:
 Experimental Characterization of Purified m-Cresol Purple for Spectrophotometric pH_T Measurements

10	0.01	308.16	7.7655	1.169369
10	0.025	308.16	7.7736	1.183034
10	0.04	308.16	7.7823	1.193039
15	0.01	278.13	8.6995	4.247623
15	0.025	278.14	8.7056	4.279102
15	0.04	278.13	8.7096	4.306907
15	0.01	283.18	8.5293	3.464424
15	0.025	283.19	8.5359	3.500540
15	0.04	283.18	8.5403	3.511220
15	0.01	288.16	8.3672	2.842487
15	0.025	288.15	8.3745	2.871055
15	0.04	288.16	8.3787	2.880670
15	0.01	293.18	8.2089	2.322994
15	0.025	293.18	8.2162	2.349730
15	0.04	293.19	8.2208	2.359748
15	0.01	298.12	8.0578	1.922835
15	0.025	298.12	8.0654	1.937263
15	0.04	298.12	8.0708	1.948240
15	0.01	303.12	7.9091	1.570804
15	0.025	303.12	7.9172	1.591972
15	0.04	303.12	7.9231	1.601744
15	0.01	308.13	7.7637	1.306756
15	0.025	308.15	7.7715	1.318853
15	0.04	308.14	7.7783	1.325910
20	0.01	278.12	8.7060	4.498299
20	0.04	278.12	8.7166	4.574945
20	0.01	283.18	8.5343	3.685731
20	0.04	283.18	8.5456	3.745668
20	0.01	288.16	8.3707	3.034941
20	0.04	288.16	8.3823	3.083136
20	0.01	293.18	8.2107	2.489037
20	0.04	293.18	8.2230	2.534067
20	0.01	298.12	8.0578	2.064414
20	0.04	298.12	8.0708	2.094459
20	0.01	303.1	7.9079	1.696082
20	0.04	303.12	7.9210	1.728344
20	0.01	308.17	7.7584	1.409458
20	0.04	308.16	7.7732	1.433810
35	0.01	278.12	8.7505	5.000099
35	0.04	278.12	8.7571	5.067886
35	0.01	283.19	8.5757	4.119820
35	0.04	283.19	8.5825	4.180463
35	0.01	288.17	8.4091	3.432154
35	0.04	288.16	8.4160	3.481869
35	0.01	293.18	8.2464	2.828156
35	0.04	293.2	8.2522	2.878979

Supplementary Material
pH Measurements in Brackish Waters:
Experimental Characterization of Purified m-Cresol Purple for Spectrophotometric pH_T Measurements

35	0.01	298.12	8.0904	2.363981
35	0.04	298.13	8.0963	2.395338
35	0.01	303.1	7.9369	1.942415
35	0.04	303.11	7.9427	1.987336
35	0.01	308.18	7.7834	1.627207
35	0.04	308.17	7.7896	1.655656

Spectrophotometric pH measurements in the presence of dissolved organic matter and hydrogen sulfide

Jens Daniel Müller ^{1*}, Bernd Schneider,¹ Steffen Aßmann,² Gregor Rehder¹

¹Department of Marine Chemistry, Leibniz Institute for Baltic Sea Research, Warnemünde, Germany

²Kongsberg Maritime Contros GmbH, Kiel, Germany

Abstract

Spectrophotometric pH measurements were first introduced for oceanic environments and they facilitated the determination of the marine CO₂ system, including the direct observation of Ocean Acidification. Extended characterizations of the indicator dye m-Cresol purple over the past two decades enabled the application of this method to natural waters ranging from brines to freshwaters. However, the required determination of the dye's dissociation constants and absorbance properties were exclusively performed in buffer solutions prepared with artificial seawater. Potential perturbations by substances that occur in natural waters, but are not included in the buffer solutions, have never been tested. Therefore, we studied the impact of elevated amounts of dissolved organic matter (DOM) and hydrogen sulfide (H₂S) on spectrophotometric pH measurements. We did not observe an impact on spectrophotometric pH measurements by H₂S concentrations up to 400 μmol kg⁻¹, which reflect high levels such as those reported from the Black Sea. Likewise, natural DOM did not interfere with the spectrophotometric measurements at concentrations typical for oceanic environments and large estuarine systems. However, strongly colored river waters can cause spectral disturbances resulting in calculated pH values that are up to tenths of pH units too low. To circumvent such disturbances, we recommend using intense light sources, a shorter cuvette length or spectrophotometrically calibrated glass electrodes when performing spectrophotometric measurements under critical conditions.

The need to understand the oceans' role in the global CO₂ system (Le Quéré et al. 2015) and the aim to track the ongoing process of Ocean Acidification (Doney et al. 2009) stimulated the development of high-quality pH measurement techniques. Spectrophotometric measurements have proven to be the most reliable method to determine seawater pH. The analytical procedure is based on the addition of a pH-sensitive indicator dye to the water sample. The calculation of pH from recorded absorbance spectra requires the knowledge of the dissociation constants and absorbance properties of the dye. More than two decades ago Clayton and Byrne (1993) first determined these properties of the dye m-Cresol purple (mCP) for oceanic measurements. The authors introduced the method stating that “the relative constancy of seawater composition throughout the world's ocean basins, plus low concentrations of reactive trace elements, produce only small medium-induced changes

in the physical-chemical characteristics of the indicator dyes.” Accordingly, the theoretically predicted Ocean Acidification processes could be directly observed by spectrophotometric pH measurements in open ocean surface waters (Byrne et al. 2010).

The rising awareness that understanding Coastal Acidification (Waldbusser and Salisbury 2014) requires more detailed knowledge about the processes affecting pH (Hofmann et al. 2011; Duarte et al. 2013), stimulated extended characterizations of mCP for the application first in brackish (Mosley et al. 2004) and most recently in freshwaters (Lai et al. 2016). Currently, spectrophotometric measurements are the most reliable method to measure pH across the entire spectrum from ground to ocean waters, achieving uncertainty levels below 0.01 pH units (Degrandpre et al. 2014; Dickson et al. 2015). However, the extended characterization of mCP was exclusively based on experiments performed in buffered artificial sea- or freshwater solutions. These solutions have a stable and defined pH, controlled by comparably high concentrations of a buffering substance like TRIS (DeValls and Dickson 1998), and contain the major salt components of seawater. However, for the broad spectrum of natural waters over which spectrophotometric pH measurement can in principle be applied, the requirement of “low concentrations

*Correspondence: Jens.Mueller@io-warnemuende.de

Additional Supporting Information may be found in the online version of this article.

This is an open access article under the terms of the Creative Commons Attribution License, which permits use, distribution and reproduction in any medium, provided the original work is properly cited.

of reactive trace elements” originally expressed by Clayton and Byrne (1993) is not always fulfilled. In contrast, natural waters contain several substances that are not included in the artificial buffer solutions but potentially impact spectrophotometric pH measurements. Two important and widespread chemical components of natural waters are dissolved organic matter (DOM) and hydrogen sulfide (H_2S).

DOM occurs ubiquitously in natural waters typically with increasing concentrations from oceanic toward freshwater environments: open ocean DOM concentrations in terms of moles carbon per volume are typically $< 100 \mu\text{mol-C L}^{-1}$ (Nelson et al. 1998), whereas higher DOM concentrations were reported from large estuaries like the Baltic Sea ($300\text{--}400 \mu\text{mol-C L}^{-1}$, Kuliński et al. 2014) and the Chesapeake Bay (around $250 \mu\text{mol-C L}^{-1}$ toward the freshwater end-member, Rochelle-Newall and Fisher 2002). The weighted worldwide river DOM concentration was estimated at $500 \mu\text{mol-C L}^{-1}$ (Ertel et al. 1986), but many rivers like the Rio Negro in the Amazon basin ($\sim 1000 \mu\text{mol-C L}^{-1}$, Ertel et al. 1986) and the Suwannee river in Florida ($> 2000 \mu\text{mol-C L}^{-1}$, Averett et al. 1994) feature much higher concentrations.

In contrast to the ubiquitous presence of DOM, hydrogen sulfide occurs regionally in areas where the hydrographical conditions favor anoxic conditions. Examples include extended stratified basins like the Black Sea, the Baltic Sea, and the Cariaco basin with H_2S concentrations up to $400 \mu\text{mol kg}^{-1}$ (Luther et al. 1991), $100 \mu\text{mol kg}^{-1}$ (Fonselius and Valderrama 2003; Gustafsson et al. 2014), and $75 \mu\text{mol kg}^{-1}$ (Scranton et al. 2001), respectively. Smaller estuarine systems like silled fjords with restricted water exchange can temporarily develop even higher H_2S concentrations. Apart from stagnant water masses, hydrogen sulfide can also be formed in coastal-reinforced oxygen minimum zones (e.g., anoxic events on the Peruvian and Namibian shelf), but typically at lower concentrations (Canfield 2006; Schunck et al. 2013).

In open ocean surface waters, an overdetermination of the CO_2 system—by determining more than two out of the four measurable parameters alkalinity (A_T), dissolved inorganic carbon (DIC), pH, and CO_2 partial pressure (pCO_2)—allows researchers to evaluate the analytical performance by internal consistency checks (Byrne 2014). However, this evaluation becomes ambiguous in the presence of DOM and H_2S because both contribute to A_T (Kuliński et al. 2014; Yang et al. 2015) and this contribution is not accounted for in the available software for CO_2 -system calculations, e.g., CO_2sys (Pierrot et al. 2006). In addition, analytical techniques to determine the pCO_2 of discrete samples are not well developed and optical pCO_2 sensors are prone to poisoning by H_2S (Atamanchuk et al. 2014; Fritzsche et al. 2017). Consequently, A_T and pCO_2 are often not accessible for an overdetermination of the CO_2 system. Under such conditions, it is even more important that the remaining parameters (DIC and pH) are determined with low uncertainty.

The impact of DOM and H_2S on the acid-base system of natural waters needs to be clearly distinguished from potential methodological interferences with spectrophotometric pH measurements. Such perturbations could for example be induced by spectral disturbances or molecular interactions with the dye and would lead to incorrect pH readings. In regard to H_2S and DOM, spectral disturbances need to be expected from chromophoric dissolved organic matter (CDOM), the fraction of DOM that absorbs light in the UV and visible spectrum (Bricaud et al. 1981; Green and Blough 1994; Stedmon et al. 2000). Concerning the characterization of mCP for freshwater conditions, it was already pointed out by Lai et al. (2016) that the effect of “colored dissolved organic matter on measurements needs to be more systematically studied in the future.” Furthermore, it was shown that DOM enhances the water solubility of nonionic organic solutes (Averett et al. 1994). Although mCP has different molecular properties than the organic solutes studied by Averett et al. (1994), comparable molecular interactions between DOM and mCP could alter the dissociation constants and/or extinction coefficients of the dye, both of which would cause erroneous pH readings. Likewise, molecular interactions with H_2S , or rather its dissociation products HS^- and S^{2-} that are present under typical pH conditions in seawater, cannot be excluded. In particular the formation of polysulfides (Kremling 1983) could alter the chemical properties of the seawater matrix and impact the dye properties through molecular interactions.

Keeping in mind the importance of high quality pH measurements for the characterization of natural waters and being aware of the risk of disturbances that spectrophotometric pH measurements face in waters that deviate from oceanic standard conditions, this study aims for a systematic evaluation of potential perturbations on mCP-based spectrophotometric pH measurements caused by DOM and H_2S , covering the entire concentration range encountered in natural waters.

Material and procedures

Approach

DOM and H_2S impact the pH of natural waters by interacting with a complex set of other acid-base equilibrium reactions (*see* Introduction). Here we investigated only potential perturbations of spectrophotometric pH measurements, which we distinguished from actual pH effects of DOM and H_2S by the following two approaches:

- Buffer solutions prepared in artificial seawater (Dickson 1993; Millero et al. 1993) were used to investigate whether increasing amounts of DOM impact the pH value obtained from absorbance measurements with mCP. The advantage of using buffered solutions is a stable pH that remains unaffected even when adding relative small amounts of a DOM stock solution. However, the disadvantage of buffered solutions is that their chemical composition differs from

that of natural waters, which could change potential molecular interactions between DOM and the dye.

- Artificial seawater (ASW) solutions and natural water samples were used to study the impact of DOM and H₂S on spectrophotometric pH measurements. As the pH of these weakly buffered solutions is sensitive to changes in the DOM/H₂S content, this approach requires potentiometric comparison measurements and therefore relies on the assumption that the selected glass electrodes are not affected by the presence of DOM/H₂S. In a first series of measurements the glass electrodes were calibrated against the spectrophotometric method (Easley and Byrne 2012). Thereafter, parallel potentiometric and spectrophotometric measurements were performed at increasing concentrations of the potentially perturbing substance. At each DOM/H₂S level, the pH-dependence of the perturbation was investigated by manipulating the CO₂ content of the solution.

Spectrophotometric measurements

The basic principles of spectrophotometric pH measurements were described extensively in the existing literature (Clayton and Byrne 1993; Mosley et al. 2004; Liu et al. 2011) and will only be briefly summarized here. The measurements are based on the addition of a pH-sensitive indicator dye to a water sample. The second dissociation constant pK_2 of the diprotic dye mCP is in the pH range typical for seawater and in this case the pH of the solution can be expressed as:

$$\text{pH} = pK_2 + \log_{10} \left(\frac{[I^{2-}]}{[HI^-]} \right) \quad (1)$$

where $[HI^-]$ and $[I^{2-}]$ are the concentrations of the monoprotonated and deprotonated species of the indicator dye, respectively. The concentration ratio $[HI^-]/[I^{2-}]$ is determined by absorbance (A) measurements, which in general relate the light intensity recorded for the blank (I_0) to the light intensities recorded for the sample solution (I):

$$A = -\log_{10} \left(\frac{I}{I_0} \right) \quad (2)$$

HI^- and I^{2-} have two clearly distinguishable absorbance maxima at wavelength $\lambda_1 = 434$ nm and $\lambda_2 = 578$ nm, respectively (Clayton and Byrne 1993). However, the absorbance spectra of both indicator species overlap. Therefore, at both wavelength λ_1 and λ_2 the absorbance A_λ needs to be expressed by the Lambert-Beer-law describing the additive absorbance contribution of both indicator species as:

$$A_\lambda = A_\lambda(I^{2-}) + A_\lambda(HI^-) = (\epsilon_\lambda(HI^-) \times [HI^-] + \epsilon_\lambda(I^{2-}) \times [I^{2-}]) \times d \quad (3)$$

where $\epsilon_\lambda(X)$ are the molar extinction coefficients of the indicator species X at wavelength λ , and d is the cuvette length.

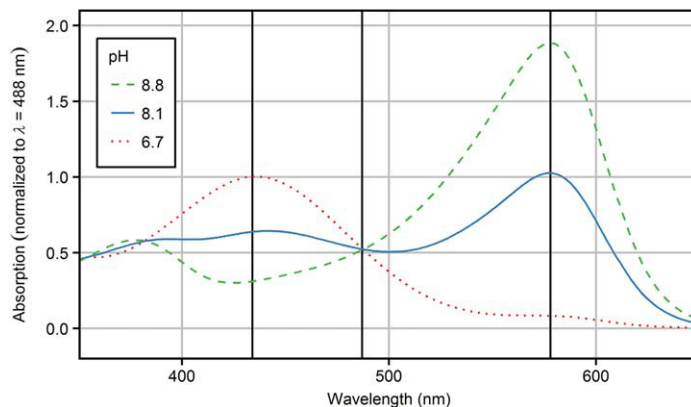


Fig. 1. Absorbance spectra of mCP in buffered artificial seawater solution. In TRIS (pH 8.1, solid blue line) both indicator species contribute significantly to the total absorbance, which results in a typical spectrum with two peaks and reflects the ideal pH level for measurements with mCP. Toward high and low pH the spectra are dominated by the basic (dashed green line) and acidic (dotted red line) form of the dye, respectively.

Illustrative absorbance spectra of mCP at high, low, and intermediate pH are displayed in Fig. 1.

After combining the Eqs. 1 and 3 and with algebraic manipulation, the pH of the solution can be expressed as:

$$\text{pH} = pK_2 + \log_{10} \left(\frac{R - e_1}{e_2 - e_3 \times R} \right) \quad (4)$$

where $R = A_{578}/A_{434}$ is the ratio of the absorbance measured at the two peak wavelengths and $e_1 = \epsilon_{578}(HI^-)/\epsilon_{434}(HI^-)$, $e_2 = \epsilon_{578}(I^{2-})/\epsilon_{434}(HI^-)$, and $e_3 = \epsilon_{434}(I^{2-})/\epsilon_{434}(HI^-)$ are the molar absorptivity ratios (Clayton and Byrne 1993).

In this study, pH values were calculated on the total scale based on the pK_2 , e_1 , e_2 , and e_3 values reported by Mosley et al. (2004). This bears minor uncertainties in the calculated absolute pH values because the coefficients were determined with nonpurified mCP, whereas all experiments reported here were performed with mCP purified according to Liu et al. (2011) and kindly provided by the lab of Robert H. Byrne, Univ. of South Florida. However, error propagation analysis revealed that uncertainties in the coefficients do not significantly alter relative pH changes, which are reported in this study and interpreted as perturbations by DOM and H₂S. The stock solution of the purified dye was prepared by dissolving 0.08 g of the purified dye in 100 mL of deionized water. For better dissolution and pH adjustment, the stock solution was sonicated and 2.75 mL of 0.1 M NaOH were added.

The majority of spectrophotometric pH measurements were executed with an instrumental set-up as described by Carter et al. (2013), which consists of an Agilent 8453 diode array spectrophotometer (Santa Clara, U.S.) and a 10-cm, cylindrical, jacketed, flow-through cuvette (custom made by Hellma Analytics, Müllheim, Germany). The mantle of the cuvette was permanently flushed with water from a Julabo

F30 heating circulator (Seelbach, Germany), and the temperature ($25 \pm 0.05^\circ\text{C}$) was controlled with a Burster Kelvimat 4306 + needle probe 42905 (Gernsbach, Germany) inserted into the water stream just behind the cuvette. The cuvette was filled/emptied with a computer-controlled syringe pump (Supporting Information Fig. S1a). The performance of the instrument was routinely verified by running the self-test of the instrument (covering wavelength accuracy and reproducibility through deuterium lines test, as well as noise-, baseline flatness-, and stability tests) and measuring TRIS buffer solutions and CRM standards provided by the lab of Andrew G. Dickson, Univ. of California (deviation < 0.005 pH units from assigned value).

The routine measurement sequence as reported by Carter et al. (2013) determines the mCP absorption spectra from two intensity spectra (Eq. 2): the sample (I_0) and the sample with mCP added (I). For the purpose of this study we also aimed at recording the DOM self-absorption of the spiked ASW solutions against a clean blank. Accordingly, for each measurement sequence intensity spectra were recorded for three types of solutions: blank solution (subscript: ASW), spiked solution (subscript: DOM), and spiked solution with dye addition (subscript: mCP). From those three intensity spectra two absorption spectra were derived, which we refer to as:

1. The self-absorption spectra were derived from the spiked solution (I_{DOM}) vs. the blank solution ($I_{0,\text{ASW}}$).
2. The mCP-absorption spectra were derived from the spiked solution with mCP (I_{mCP}) vs. the spiked sample ($I_{0,\text{DOM}}$). This second step corresponds to the routine measurement procedure and was used to calculate the spectrophotometric pH of the solution according to Eq. 4.

The mCP-absorption spectra in the second step were taken in replicates of six from a single filling of the cuvette, except for the first series of measurements performed in TRIS buffered solutions.

A critical point for the examination of potential spectral disturbances is the light source used for the absorbance measurements. The Agilent spectrometer is equipped with a tungsten- and a deuterium lamp that can be run independently. The intensity spectra of only the tungsten lamp and the spectra of both lamps operating in parallel are displayed in the Supporting Information (Fig. S2). The tungsten lamp emits light in the visible range, with higher intensities at 578 nm ($\sim 60,000$ counts) than at 434 nm ($\sim 10,000$ counts). The deuterium lamp primarily emits light in the UV range. Operating both lamps in parallel increases the intensity of the emitted light slightly at 578 nm ($\sim 90,000$ counts) and more than doubles the intensity at 434 nm ($\sim 30,000$ counts). Carter et al. (2013) performed their experiments with both lamps operating together. However, to avoid the degradation of the dye or organic matter, the authors recommended operating the instrument with the deuterium lamp

off and compensating for the added noise by averaging six successively recorded spectra. As the change in the light source intensity could impact the characteristics of spectral disturbances by DOM, both approaches were tested in this study (deuterium lamp on and no averaging vs. deuterium lamp off and averaging six spectra).

In addition to the experiments with the spectrophotometric pH measurement setup (Carter et al. 2013) described above, we performed comparison measurement with a CONTROS HydroFIA[®] pH measurements system currently under development within the framework of the EU BONUS project PINBAL (see Acknowledgments). The system is a continued development of the flow injection analysis (FIA) approach described by Aßmann et al. (2011). The overall measurement principle of the instrument is based on the injection of a mCP stock solution into a continuous sample flow. After the injection of the dye, a concentration peak passes through the cuvette. The backward flank of the dilution curve is continuously recorded, resulting in more than 100 absorbance spectra per single pH measurement. The pH-perturbation caused by the dye addition can be corrected by extrapolating the pH values calculated from each spectrum to zero absorbance at the isosbestic wavelength, which is directly related to the dye concentration. The absorbance measurements are performed with a VIS broadband LED as light source and a CCD spectrometer as detector (see Aßmann et al. 2011 for details). The HydroFIA[®] operates with a 1-cm cuvette, and a nonpurified indicator dye stock solution provided by Kongsberg Maritime Contros GmbH.

DOM experiments

Equimolar ($m = 0.04 \text{ mol kg}^{-1}$) buffer solutions of 2-amino-2-hydroxymethyl-1.3-propanediol (TRIS, Amresco, Solon, U.S.), 2-aminopyridine (AMP, Acros Organics, New Jersey, US), and 2-amino-2-methyl-1.3-propanediol (BIS, Alfa Aesar, Karlsruhe, Germany) were prepared in an artificial seawater (ASW) matrix with a salinity of 7. Furthermore, an ASW solution with a carbonate alkalinity ($1650 \mu\text{mol kg}^{-1}$) and salinity (7) typical for Central Baltic Sea surface water was produced. All solutions were produced with the ionic composition as recommended by Dickson et al. (2007) and the salts used were of analytical grade.

Well-characterized humic (HA) and fulvic acid (FA) extracts from the Suwannee River (International Humic Substances Society (IHSS), catalogue numbers: 2S101H and 2S101F) were used to produce high concentrated DOM stock solutions. Hundred milligrams of each acid extract was dissolved in 50 mL of the ASW solution described above, and the pH was adjusted to 8 with the addition of 0.1 M NaOH solution. Both stock solutions were sonicated for 15 min and subsequently filtered through $0.2 \mu\text{m}$ polyethersulfone filters (Sartorius, Göttingen, Germany) to ensure the absence of particles and colloids. The stock solution DOM concentration was diluted and analyzed with a HTOCO Shimadzu TOC analyzer (Sugimura and Suzuki

1988) as 64,600 and 75,400 $\mu\text{mol-C L}^{-1}$ for HA and FA, respectively.

As described above, two types of solutions (buffered solution and ASW) were spiked with the DOM stock solutions and analyzed independently:

- Subsamples (110 mL) of three buffer solutions (AMP, TRIS, and BIS) were spiked with the HA and FA stock solutions to achieve HA concentrations of 0, 500, 1000, and 1500 $\mu\text{mol-C L}^{-1}$ and FA concentrations of 0, 500, 1500, and 2500 $\mu\text{mol-C L}^{-1}$ (see Supporting Information Fig. S1b for a series of spiked buffer solutions). The pH of the buffered solutions did not change by the addition of the DOM stock solutions, which was verified by potentiometric measurements.
- As an alternative approach, ASW solution subsamples (1 L) were spiked with the HA stock solution to achieve HA concentrations of 0, 300, and 1300 $\mu\text{mol-C L}^{-1}$. This HA addition changes the pH of the solution. Therefore, the impact of DOM on spectrophotometric measurements was traced by comparisons measurements with glass electrodes, which are described below.

For the DOM spike-experiments in ASW, a glass electrode (Sentix 980, WTW, Weilheim, Germany) was calibrated with comparison measurements using the spectrophotometric method as proposed by Easley and Byrne (2012). Potentiometric and spectrophotometric measurements were performed in parallel with non-spiked ASW water stirred in a double-walled, temperature-controlled, gastight glass container, which is in the following referred to as the *mini ocean* (Supporting Information Fig. S1a). The sample compartment of the mini ocean had a volume of 1 L that could be accessed from three sealable openings. In contrast to Easley and Byrne (2012), we achieved different pH levels for the calibration by manipulating the DIC content of the ASW solution, rather than by adding hydrochloric acid. This procedure lets the alkalinity of the solution remain unaffected and mimics the natural processes of CO_2 addition and removal. The DIC manipulation was achieved by flushing with nitrogen gas prior to the calibration run (highest pH ~ 8.7), followed by the successive addition (6–8 steps) of a CO_2 -enriched subsample of the same ASW solution (lowest pH ~ 6.5). The added subsample was enriched beforehand with CO_2 by dissolving 20 mL of pure CO_2 gas in 40 mL of the solution in a syringe. For the established range of pH levels, the relation between the electromotive force (emf) reading from the glass electrode and the spectrophotometric pH was analyzed by linear regression analysis. The subsequent spike experiments were performed on the same day and exactly like the calibration run described above, except that the mini ocean container was filled with the DOM-spiked ASW solutions. The previously obtained linear regression coefficients were used to convert emf readings of the glass electrode to pH units, which were finally compared to the spectrophotometric pH readings.

Hydrogen sulfide experiments

Hydrogen sulfide spike experiments were performed in natural seawater sampled from Landsort Deep (salinity = 11, depth = 110 m) in the Baltic Sea, which regularly becomes anoxic during stagnation periods (Fonselius and Valderrama 2003). The water sample contained H_2S on the day of sampling but was oxidized during transport to the laboratory. The water sample was filtered through 0.2 μm polyethersulfone filters prior to the experiment and filled into the *mini ocean* container described above. A H_2S -resistant glass electrode with a split ring diaphragm (Sentix HWS, WTW, Weilheim, Germany) was calibrated in the Landsort Deep water as described above for the DOM experiments. The initial flushing with nitrogen gas ensured that the solution was fully deoxygenated. After calibration of the glass electrode, the DIC content of the sample was adjusted to achieve a pH of around 7, which reflects the typical pH level present when the Landsort Deep becomes anoxic during a stagnation period (SMHI, monitoring data). This solution was then spiked stepwise with a highly concentrated H_2S stock solution (“ H_2S ” in the following represents the sum of H_2S , HS^- , and of S^{2-}). This stock solution was produced by dissolving 0.57 g sodium sulfide nonahydrate ($\text{Na}_2\text{S}\cdot 9\text{H}_2\text{O}$) in 100 mL deoxygenated Landsort Deep water. The pH of the H_2S stock solution was adjusted to 7 by adding a CO_2 -enriched subsample. This CO_2 -enrichment of the H_2S stock solution reduced pH changes during the spike experiment and reflected the natural process of sulfate reduction coupled to organic matter oxidation and CO_2 production. The H_2S concentration of the solution was measured with the standard procedure of methylene blue formation (Fonselius 1962) after each stepwise addition of the H_2S stock solution. Spectrophotometric and potentiometric pH measurements were performed in parallel to the sampling for H_2S measurements, which was followed by the immediate addition of reagents.

Assessment

DOM self-absorption

For a wide range of concentration levels, self-absorption spectra of humic (HA) and fulvic acids (FA) dissolved in buffered artificial seawater (ASW) solutions were recorded against the non-spiked solution as a blank (see Material and Methods: “Approach” and “Spectrophotometric measurements”). Figure 2 shows illustrative self-absorption spectra of TRIS buffer solution spiked with HA at concentrations of 0–1500 $\mu\text{mol-C L}^{-1}$ and with the deuterium lamp (UV light) off. In general, the self-absorption spectra of DOM reveal a typical exponential increase of the absorbance toward lower wavelength. With respect to the subsequently recorded mCP- absorption spectra (Fig. 1), this implies that the peak absorbance of the monoprotonated species of the indicator (HI^-) at 434 nm, is more likely to be affected by spectral disturbances than the peak absorbance of the deprotonated species

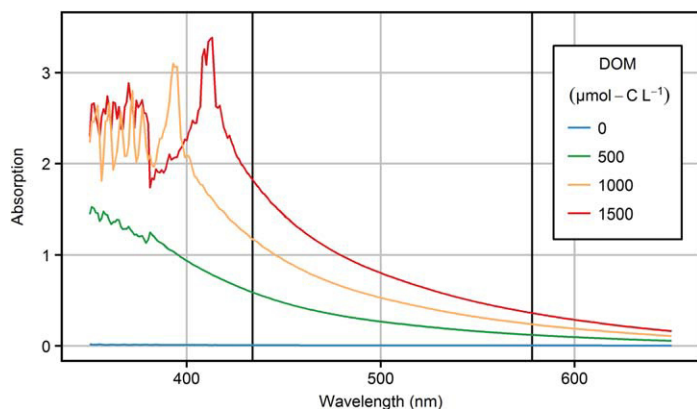


Fig. 2. DOM self-absorption spectra of TRIS buffer solutions (pH 8.1) with humic acid concentrations of 0–1500 $\mu\text{mol-C L}^{-1}$. The vertical black lines at 434 nm and 578 nm indicate the wavelength of the m-Cresol purple (mCP) HI^- and I^{2-} peak absorbances. The spectra were obtained with the deuterium lamp (UV light) off. The self-absorption spectra of all other experiments are shown in the Supporting Information Fig S3.

I^{2-} at 578 nm. A complete overview of all self-absorption spectra recorded for three buffer solutions, AMP (pH 6.7), TRIS (pH 8.1), and BIS (pH 8.8), each separately spiked with HA and FA, and with the deuterium lamp on/off is given in the Supporting Information (Fig. S3).

The DOM self-absorbance at $\lambda = 434$ nm is linearly correlated to the concentration of dissolved humic- or fulvic acids (Fig. 3). However, at the same DOM concentration (in units of moles carbon per volume) the absorbance of humic acids is roughly twice as strong as the absorbance of fulvic acids. In addition, the DOM self-absorbance slightly decreases with decreasing pH at a constant HA or FA concentration (Fig. 3). The measured DOM self-absorbance is independent of the deuterium lamp being on or off, except when the self-absorbance is > 1.5 (HA at 1500 $\mu\text{mol-C L}^{-1}$). In this case, the measured DOM self-absorbance is slightly higher with the deuterium lamp off (Light: vis), which is an indication of the spectrometers tendency to overestimate the absorbance when the light intensity at the detector is low.

Impact of high DOM concentrations on spectrophotometric pH measurements

After the addition of the indicator dye, the mCP-absorption spectra (measured against the same DOM-spiked solution without mCP as blank) reveal disturbances in the low wavelength range, which impact the absorbance reading at $\lambda = 434$ nm. The spectral disturbances increase with increasing HA and FA concentration and are considerably less pronounced with the deuterium lamp (UV light) on. Disturbed mCP-absorption spectra are shown in Fig. 4 for TRIS buffer solutions spiked with humic acids. The presented spectra are normalized to the undisturbed absorbance at 578 nm (A_{578}) according to the following equation:

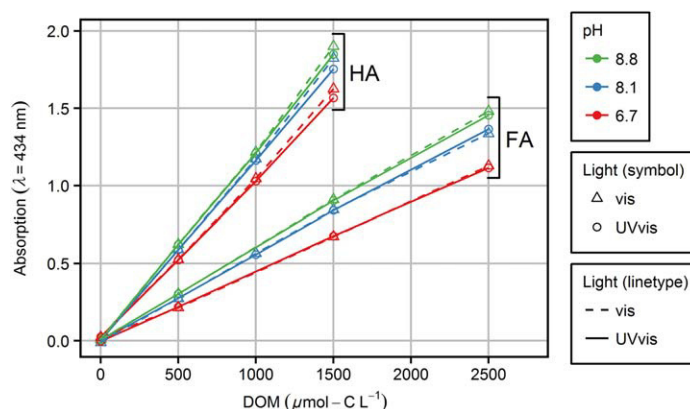


Fig. 3. DOM self-absorption at $\lambda = 434$ nm of buffered artificial seawater solutions spiked with different amounts of humic (HA) and fulvic (FA) acids. The buffered solutions are TRIS (pH 8.1), 2-aminopyridine (AMP, pH 6.7), and BIS (pH 8.8). The self-absorbance at 434 nm was measured with the deuterium lamp on (UVvis) and off (vis).

$$A_{\lambda, \text{norm}} = \frac{A_{\lambda}}{A_{578}} \times \overline{A_{578}} \quad (5)$$

where $A_{\lambda, \text{norm}}$ is the normalized absorbance at wavelength λ , A_{λ} is the absorbance at wavelength λ as measured, and $\overline{A_{578}}$ is the mean absorbance at 578 nm of all displayed spectra. This normalization procedure eliminates slight spectral differences caused by variations in the amount of dye added, but does not change the absolute absorbance significantly.

Figure 4 shows that the mCP-absorption spectra are not disturbed at wavelength > 500 nm. However, at $\lambda = 434$ nm the absorbance of the HI^- species of the indicator is increasingly overestimated toward higher HA concentrations. With the deuterium lamp off (Fig. 4, right panel), the normalized absorbance at $\lambda = 434$ nm increases from 0.61 at zero DOM to 0.77 at a DOM concentration of 1500 $\mu\text{mol-C L}^{-1}$. In contrast, the disturbance is reduced with the deuterium lamp on and the normalized absorbance does not exceed 0.64 (Fig. 4, left panel). It should be noted that the observed disturbances appear when very low amounts of light reach the detector, e.g., at $\lambda = 434$ nm and a HA concentration of 1000 $\mu\text{mol-C L}^{-1}$ the DOM self-absorption amounts to ~ 1.2 absorption units (Fig. 2) to which ~ 0.7 absorption units are added by the mCP-absorption (Fig. 4). Thus, the observed disturbances occur under conditions known as the performance limits of the Agilent spectrometer (~ 1.3 absorption units, pers. comm. R.H. Byrne). The overestimation of the absorbance at $\lambda = 434$ nm was also observed in the other buffer solutions (AMP, TRIS, BIS) and when the solutions were spiked with fulvic acid. A complete overview of all mCP-absorption spectra is given in the Supporting Information (Fig. S4). The clear dependence of the spectral disturbance on the light source (vis vs. UVvis) indicates that this spectral disturbance might reflect instrument-specific limitations, rather than being caused by direct interactions between the dye and DOM.

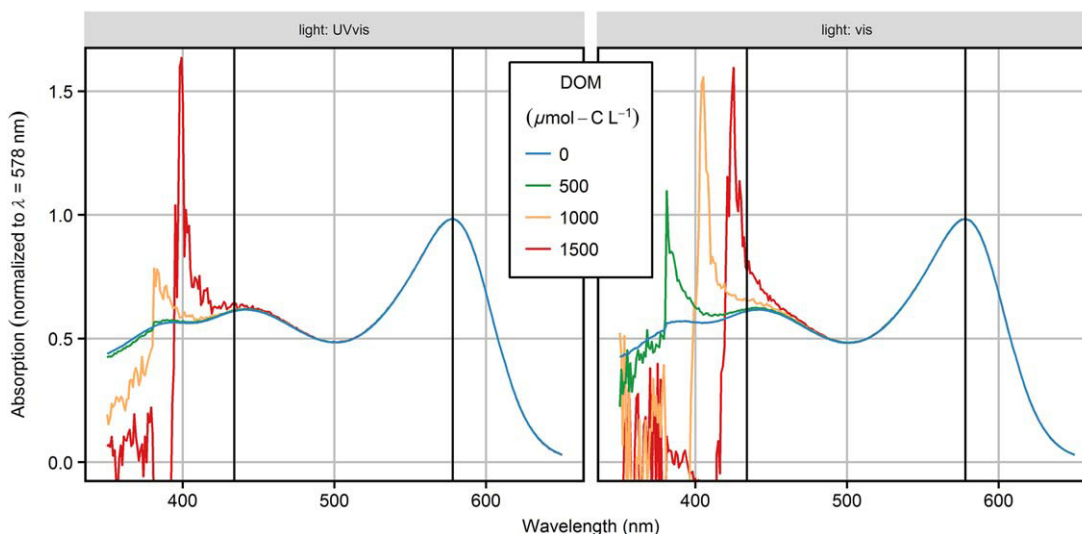


Fig. 4. Normalized absorption spectra of m-Cresol purple (mCP) in TRIS buffer solutions spiked with variable amounts of humic acids in the range of 0–1500 $\mu\text{mol-C L}^{-1}$. Shown are spectra recorded with the deuterium lamp on (light: UVvis, left panel) and off (light: vis, right panel).

The mCP-absorption spectra (Fig. 4) show a disturbance maximum in the low wavelength range. The disturbance maxima shift toward higher wavelength with increasing self-absorbance of the solution (DOM concentration) and with the deuterium lamp off. This indicates that the disturbance maxima are not regular absorption peaks, but rather spectral artefacts that mark the wavelengths at which an overestimation of the absorption signal (associated to low light intensity at the detector) turns into noise. The pH error is not directly affected by this change of the disturbance maximum position, as only the absorbance measured at $\lambda = 434$ nm is included in the pH calculation.

As a consequence of the overestimated HI^- absorbance at $\lambda = 434$ nm, the absorbance ratios (R) and the resulting pH values calculated from the disturbed spectra (Fig. 4) are underestimated. Figure 5 presents the pH values calculated from the disturbed absorbance spectra as a function of the self-absorbance of the solution at $\lambda = 434$ nm before adding the indicator dye. The true pH value of the solutions corresponds to the pH measured at zero self-absorbance. The addition of the DOM stock solution does not change the pH significantly (< 0.005 pH units), which was controlled by potentiometric measurements. For spectrophotometric pH measurements in solutions with a DOM self-absorbance at $\lambda = 434$ nm of around 0.3, no significant deviation (< 0.002 pH units) between the spectrophotometrically obtained pH and the true pH was observed (Fig. 4). In contrast, when the self-absorbance of the solutions is in the range 1.0–1.5 the calculated pH values are around 0.01–0.1 pH units below the true value with the deuterium lamp off. With the deuterium lamp on, the differences remain within the uncertainty range of the method (~ 0.01 pH units in the pH range 7–8). When the self-absorbance is > 1.5 the calculated pH values

are > 0.01 pH units below the true value, even with the deuterium light on. Without the UV light source, the deviations increase to levels > 0.1 pH units. The deviations appear to be more pronounced toward high (BIS buffer, pH 8.8) and low (AMP buffer, pH 6.7) pH of the solution, compared to the optimum working range of mCP around pH 8.1 (TRIS buffer). The observed pH error correlates well with the self-absorbance of the spiked solutions, independent of the nature of the DOM (HA vs. FA). This is a further indication that the disturbances are instrument-specific and arise when low light levels reach the detector, rather than being caused by a direct interaction between the dye and the DOM.

The DOM spike-experiments performed in unbuffered artificial seawater (Fig. 6, corresponding spectra in Supporting Information Fig. S6) reveal very similar deviations in the spectrophotometric pH values as observed in the buffered solutions (Fig. 5, corresponding spectra in Supporting Information Fig. S4). The calibration of the glass electrode against the spectrophotometric method revealed an almost exact linear relationship between the emf signal and spectrophotometric pH (deviations < 0.01 pH units from the linear regression are represented by the blue symbols and line in Fig. 6). At a humic acid concentration of $300 \mu\text{mol-C L}^{-1}$, which corresponds to a self-absorbance of the solution between 0.32 and 0.38, no significant deviation between the spectrophotometric and potentiometric pH exists, regardless whether the deuterium lamp was running or not. At a humic acid concentration of $1300 \mu\text{mol-C L}^{-1}$ (corresponding to a self-absorbance between 1.38 and 1.67) and with the deuterium lamp off, the deviations between the spectrophotometric and potentiometric pH reading are in the order of 0.06–0.17 pH units. Running the deuterium lamp reduces the

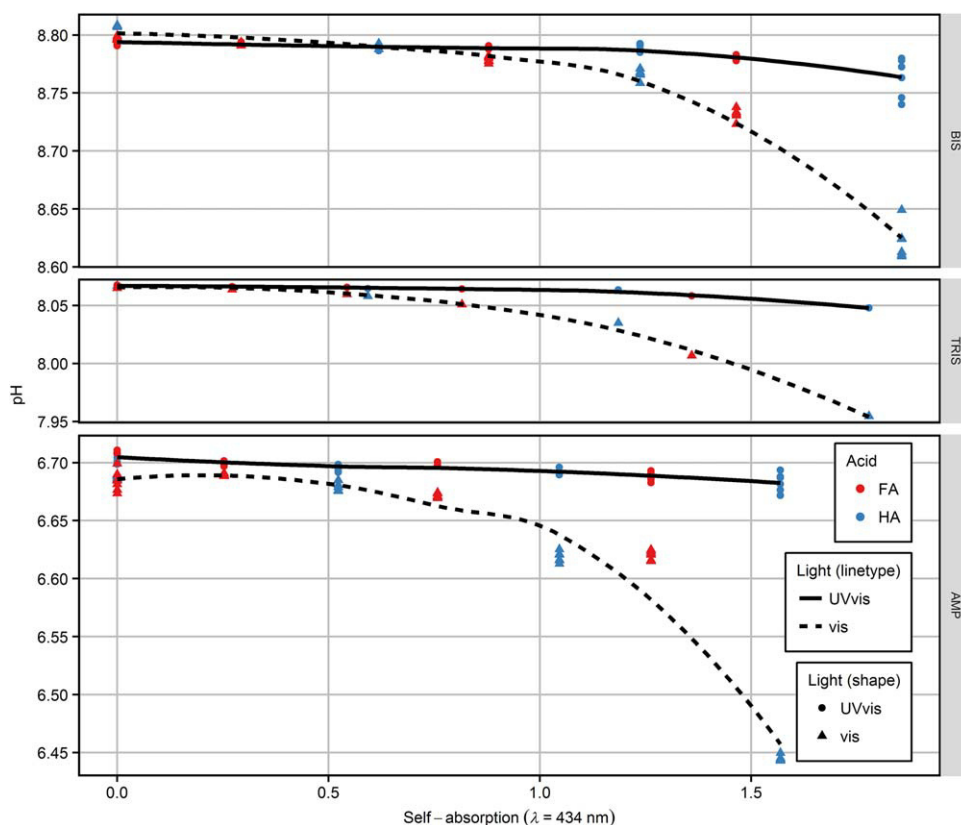


Fig. 5. Spectrophotometric pH values of buffered artificial seawater solutions spiked with variable amounts of humic (HA) and fulvic (FA) acids that cause the self-absorbance (yellowish color) of the solution. The true pH of the strongly buffered solutions TRIS, AMP, and BIS did not change from the value at zero self-absorbance by the addition of DOM, which was verified by potentiometric measurements. Lower pH values toward higher self-absorbance of the solution are caused by the spectral disturbances displayed in Fig. 4 and Supporting Information Fig. S4. Separate smooth curves are fitted to the measurements performed with the deuterium lamp turned off/on (Light vis/UVvis).

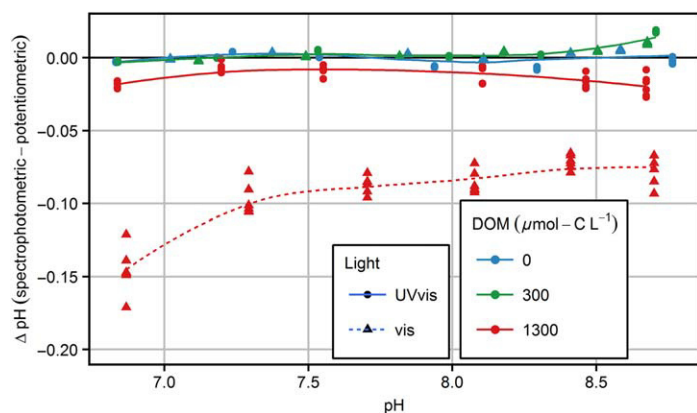


Fig. 6. Deviations between spectrophotometric and potentiometric pH in artificial seawater solutions spiked with three different levels of humic acids. Only for the highest DOM concentration a smooth curve is fitted separately for the measurements performed with the deuterium lamp turned off (dashed line) and on (solid line).

deviations significantly to levels below 0.03 pH units. The deviations increase slightly toward low pH at the highest DOM concentration and with the deuterium lamp off. The

agreement of the pH deviations observed in strongly buffered solutions (Fig. 5) in which the ionic composition is dominated by the buffer substance and in artificial seawater solutions (Fig. 6) containing only carbonate alkalinity, again indicates that the disturbances are presumably related to technical aspects of the absorbance measurement, rather than being caused by dye-DOM interactions, as the latter would not necessarily be independent of the matrix.

In both experimental approaches (buffer vs. ASW solution), we observed significantly higher pH-errors at high DOM concentrations with the deuterium lamp off. However, Carter et al. (2013) reported that running the deuterium lamp decreases the pH by 0.00025 pH units per absorbance measurement (exposure to UV radiation) at a sample pH of 7.95 and attributed this to the degradation of the dye or organic matter contained in the sample. We observed pH changes in the same order of magnitude when doing repeated measurements (Supporting Information Fig. S10). These pH changes are more pronounced at high pH, but rather independent from the amount of DOM in the sample. However, the pH change caused by a single exposure to the UV beam is well below 0.001 pH units and therefore

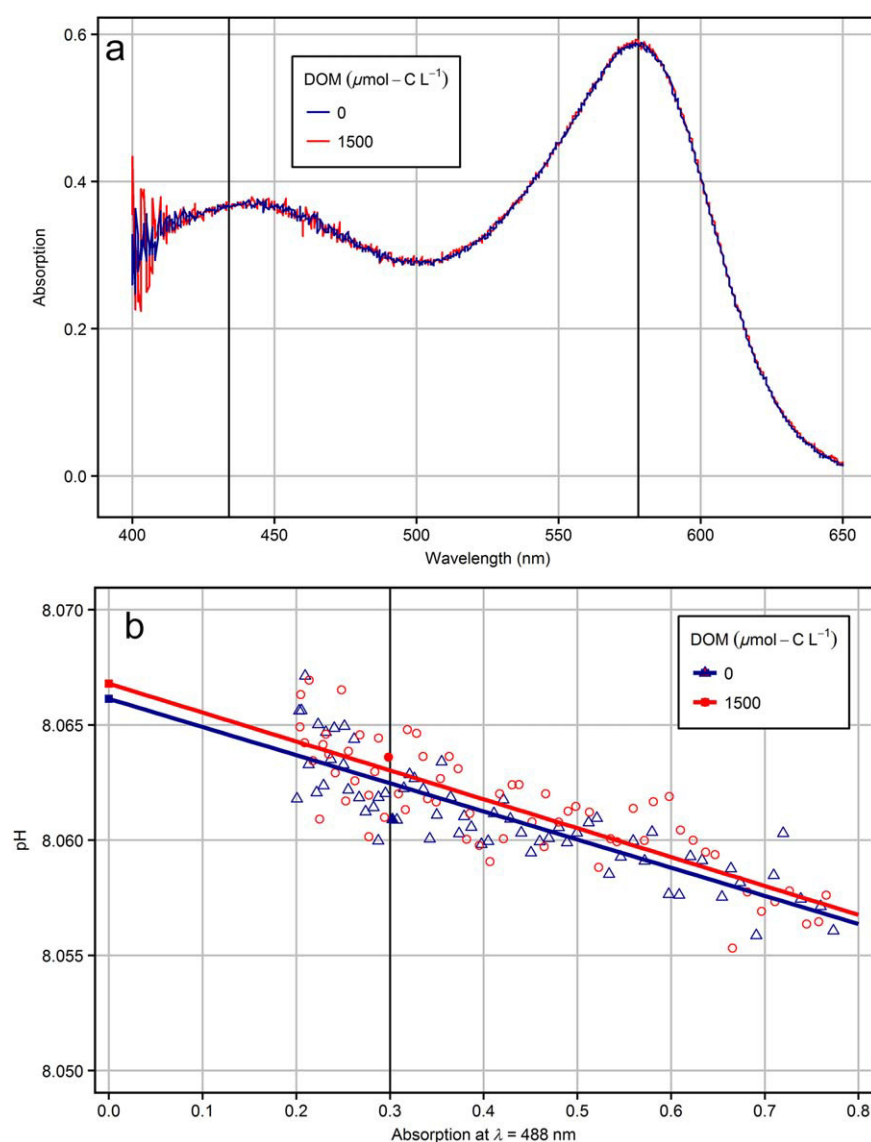


Fig. 7. HydroFIA[®] mCP-absorption spectra (a) and pH extrapolation plots (b) obtained from measurements of TRIS buffers (blue lines and symbols) and TRIS buffers spiked with humic acid extracts (HA) to achieve a DOM concentration of 1500 $\mu\text{mol-C L}^{-1}$ (red lines and symbols, same solutions as analyzed in Fig. 5). Squares at the left indicate the pH values extrapolated to zero dye concentration.

significantly lower than the potential pH error associated to measurements in strongly self-absorbing solutions when relying only on the tungsten lamp. We therefore recommend to run the deuterium lamps when analyzing strongly colored samples (*see* Recommendations section).

In contrast to the absorption spectra obtained with the Agilent 8453 spectrometer and a 10-cm cuvette (Fig. 4, Supporting Information S3, S5), the absorption spectra measured with the CONTROS HydroFIA[®] pH system (1-cm cuvette) do not show a significant disturbance (Fig. 7a). Only a slight increase of the noise in the low wavelength range was observed in the presence of DOM. However, the high concentration of DOM does not impact the extrapolated pH values

significantly (deviation < 0.001 pH unit, Fig. 7b). This can be attributed to the shorter cuvette length and proportionally higher indicator concentrations, which are directly related to the ratio of DOM self-absorbance to mCP-absorbance. The disadvantage of a high indicator concentration is the increased pH perturbation induced by the indicator addition (Chierici et al. 1999), which is especially critical for low alkalinity samples (Hammer et al. 2014). For oceanic waters and low dye concentrations, this perturbation is commonly corrected by adding a second aliquot of dye and linearly extrapolating to zero dye concentration (Carter et al. 2013). However, this approach was not yet tested for more challenging conditions (high dye concentrations, low-alkalinity

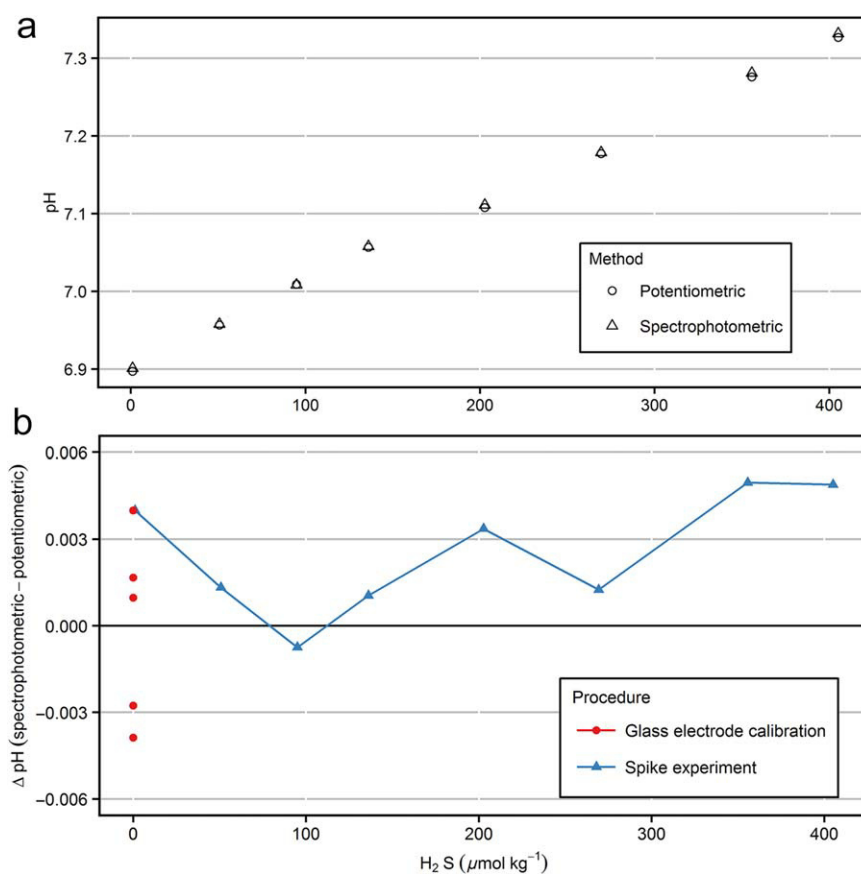


Fig. 8. Hydrogen Sulfide (H_2S) perturbation experiment. **(a)** Adding the H_2S stock solution increases the pH of the solution from 6.9 to slightly above 7.3. **(b)** The deviations between spectrophotometric and potentiometric pH measurements are within 0.005 pH units for the calibration of the glass electrode (red points) as well as during the H_2S addition (blue triangles). The deviations do not show any dependence on the H_2S concentration indicating that the spectrophotometric method works robustly even under the highest H_2S concentration.

samples). Measurements performed with a FIA (flow injection analysis) approach can help to investigate this problem, as they allow extrapolating the pH to zero indicator concentration based on a high number of recorded spectra (Aßmann et al. 2011 and Fig. 7b).

Robustness of spectrophotometric pH measurements to hydrogen sulfide

Potential perturbations of spectrophotometric pH measurements by the presence of hydrogen sulfide (H_2S) were tested through comparison measurements with H_2S -resistant glass electrodes in a natural water sample. Applying linear regression analysis to the 5-point spectrophotometric calibration (see Materials and Procedures) of the glass electrode revealed only minor deviations (< 0.005 pH units) from a strict linear relationship (red points in Fig. 8b). The subsequent spiking of the sample with up to 400 $\mu\text{mol kg}^{-1}$ H_2S (including HS^- and S^{2-}) increased the pH of the solution from initially 6.9 to slightly above 7.3 (Fig. 8a), which indicates that the H_2S stock solution had a higher pH than the sample solution in the *mini ocean* container despite the CO_2 enrichment. However, the

addition of H_2S did not cause deviations between the spectrophotometrically and the potentiometrically determined pH larger than 0.005 pH units (blue points in Fig. 8b). Furthermore, no trend of the pH deviations as a function of H_2S concentration was observed. Repeated measurements of the pH from a single filling of the cuvette resulted in a decrease of the pH in the range of 0.00055–0.0007 pH units per measurement (Supporting Information Fig. S7). This is higher than the pH change that Carter et al. (2013) attributed to the degradation of the dye by UV light. Currently, it cannot be determined, whether this observation is related to the degradation of the dye or whether the pH decrease is related to a potential oxidation of H_2S , which would correspond to a loss of alkalinity. The mCP-absorption spectra did not show any significant disturbances (Supporting Information, Fig. S8).

Discussion

Dissolved organic matter perturbations

Significant spectrophotometric pH measurement errors were observed at the highest DOM concentrations (> 1000

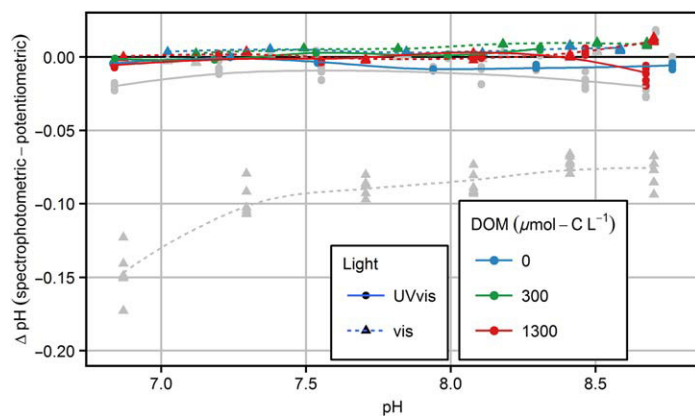


Fig. 9. Recalculated deviations between spectrophotometric and potentiometric pH in artificial seawater solutions spiked with three different levels of humic acids. The spectrophotometric pH values were calculated from the modified $R^* = A_{578}/A_{488}$ (colored symbols and lines), instead of the classical $R = A_{578}/A_{434}$ (gray symbols and lines, reproduced from Fig. 6 for comparison). This avoids using the absorbance measurement disturbed by the strong self-absorbance of the solution at $\lambda = 434$ nm (Fig. 4).

$\mu\text{mol-C L}^{-1}$) for measurements with an Agilent 8453 spectrophotometer (Carter et al. 2013) equipped with a 10-cm cuvette. Determined pH values are tenths of pH units too low with the deuterium lamp off, and hundredths of pH units too low with the deuterium lamp on, which increases the light intensity at low wavelengths. Strong evidence was found that these deviations are caused by spectral disturbances related to the instrument performance, rather than molecular interactions that impact the dissociation or absorbance behavior of the dye. The following observations support this conclusion: First, the pH deviations correlate well to the self-absorbance of the solution at $\lambda = 434$ nm (Fig. 5). Second, the deviations are very similar in strongly buffered solutions (Fig. 5) and in artificial seawater solutions that contain only carbonate alkalinity (Fig. 6). Third, the light source (deuterium lamp on/off) clearly impacts the pH deviations. Fourth: No deviations were observed when performing measurements with the CONTROS HydroFIA[®] pH measurements system, which has a short cuvette length and a proportionally higher dye concentration (Fig. 7).

The underlying problem for the pH errors observed with the Agilent 8453 spectrophotometer seems to be an overestimation of the absorbance when the light intensity at the detector is low (Figs. 3, 4). This overestimation impacts only the absorbance reading at $\lambda = 434$ nm in the mCP-absorption spectra, because the DOM self-absorbance is much more pronounced at this wavelength than at $\lambda = 578$ nm (Fig. 2). Since only the mCP-absorbance at $\lambda = 434$ nm is overestimated the pH readings are too low. A low light intensity threshold cannot be determined because this quantity is not accessible from the instrument. Likewise, relating our findings to recommended operation ranges in terms of absorption units, which refer to measurements against a colorless blank, is not

meaningful, because the measurements presented here were made against colored DOM blank solutions.

In order to confirm the hypothesis that the observed pH errors are attributed to an overestimation of the absorbance reading at $\lambda = 434$ nm and that significant molecular DOM-mCP interactions, which would alter the dissociation constant and/or the absorptivity ratios of mCP, can be ruled out, an alternative pH calculation was applied to the mCP-absorption spectra. To avoid relying on the absorbance of the HI^- peak at $\lambda = 434$ nm, an alternative absorbance ratio $R^* = A_{578}/A_{488}$ was used, where the HI^- absorbance is replaced by the absorbance at the isosbestic wavelength $\lambda = 488$ nm. The latter is linearly related to the indicator concentration, irrespective of the solution pH. Therefore, R^* relates $[\text{I}^{2-}]$ to the total indicator concentration, instead of relating $[\text{I}^{2-}]$ to $[\text{HI}^-]$ (Eq. 1). Using R^* reduces the precision of the method, but in principle allows for equally accurate results. The calculation of pH from R^* requires modified molar absorptivity ratios $e_1^* = \epsilon_{578}(\text{HI}^-)/\epsilon_{488}(\text{HI}^-)$, $e_2^* = \epsilon_{578}(\text{I}^{2-})/\epsilon_{488}(\text{HI}^-)$, and $e_3^* = \epsilon_{488}(\text{I}^{2-})/\epsilon_{488}(\text{HI}^-) = 1$ (compare Eq. 4). We roughly estimated these modified absorptivity ratios from preliminary experiments (for details see Supporting Information S11), however, application of the R^* approach for environmental pH analysis would require a more rigorous e^* determination. The reanalysis of the measurements performed with DOM-spiked ASW solutions are shown in Fig. 9, which displays the exact same results as Fig. 6, except that the spectrophotometric pH was calculated from R^* instead of R . The pH disturbance even at the highest DOM concentration is eliminated. Likewise, recalculating the pH of the spiked buffer solutions (Fig. 5) with R^* eliminates the pH disturbances (Supporting Information Fig. S12). As expected, toward high pH, where the absorbance at $\lambda = 578$ nm increases, pH values calculated from R^* reveal to be less precise. However, the absence of significant directional pH errors when applying R^* supports the finding that (i) no spectral disturbances impact the absorbance readings at $\lambda = 488$ nm and 578 nm and (ii) molecular interactions between mCP and DOM do not significantly alter the dissociation constant or absorption properties of the dye.

Exploring the reasons for the overestimation of the absorbance at low light intensities is beyond the scope of this study. However, it should be noted that this overestimation occurs when the combined DOM- and mCP-absorbance reaches the limits of the application range of the Agilent 8453 spectrometer. Other instruments will presumably show similar effects, which, however, might differ in strength and direction. In this respect, we consider our results instrument-specific and a procedure to correct the observed errors cannot be introduced. However, the described spectral perturbations, occurring primarily in the low wavelength range, are related to the patterns of the DOM self-absorption spectra and should thus be universal in nature.

The investigated DOM concentration range was designed to cover the concentrations reported from natural waters (see

Introduction). However, it was found that interferences with spectrophotometric pH measurements are rather related to the self-absorbance of the sample than to the DOM concentration. In addition, the absorbance per carbon unit of natural DOM is typically lower than that of the isolated humic and fulvic acids we used (Alberts and Takács 2004). Thus, the following assessment of potential pH errors that might be associated to the analysis of natural samples refers to estimated self-absorbance properties of various waters rather than to reported DOM concentrations. Based on the typically exponential dependence of DOM-absorbance on wavelength (Fig. 1; Bricaud et al. 1981; Coble 2007), we calculated the self-absorbance at $\lambda = 434$ nm of various natural waters from the reported absorbance coefficients at other wavelength and converted it to a 10-cm cuvette length as used for our experiments (details in the Supporting Information Table S9). Accordingly, open-ocean waters have very low self-absorbance (< 0.005) at $\lambda = 434$ nm (Bricaud et al. 1981; Nelson et al. 1998). The Baltic Sea, a semi-enclosed brackish water system, has higher amounts of DOM (Bricaud et al. 1981), resulting in self-absorbances at $\lambda = 434$ nm ranging from 0.01 to 0.03 (Ferrari et al. (1996) and IOW, unpubl. data). Similar levels were reported from the Chesapeake Bay (Rochelle-Newall and Fisher 2002). Relating this to the observed pH deviations, spectrophotometric pH measurements should work without restrictions at the DOM self-absorbance levels typical for ocean waters and large estuaries. The self-absorbance at $\lambda = 434$ nm of rivers entering the Baltic Sea are typically below 0.1 (Ferrari et al. 1996; Stedmon et al. 2000; IOW, unpubl. data). Even under these conditions reliable spectrophotometric pH measurements should be possible with errors < 0.01 pH units (Figs. 4, 5). However, river waters can also have significantly higher DOM self-absorbances, for example Rio Orinoco with self-absorbances at $\lambda = 434$ nm around 0.4 in the main river and above 1 in its minor tributaries (Battin 1998), as well as the Suwannee River with self-absorbances around 0.5 (Yacobi et al. 2003). Even higher levels can be encountered in pore or ground waters (own observations). In the case of such high self-absorbance levels the water samples appear colored to the human eye. Under such conditions, the measurement quality can be improved by following the instructions given in the section Recommendations.

Robustness of spectrophotometric pH measurement to hydrogen sulfide

Over a wide range of H_2S concentrations from $0 \mu\text{mol kg}^{-1}$ to $400 \mu\text{mol kg}^{-1}$ the deviations between spectrophotometric and potentiometric pH measurements were below 0.005 pH units, which is within the expected uncertainty range for this kind of comparison measurement (Easley and Byrne 2012). The investigated H_2S range covers the naturally occurring concentrations in highly euxinic environments such as the Cariaco Basin, the Baltic Sea, and the Black Sea (see Introduction). Only local extreme values, as they may emerge in fjords

or salt marshes, are not covered by our study. Since there is no trend in the observed pH deviations we conclude that spectrophotometric pH measurements are not impacted by the presence of H_2S , which is further supported by the spectra that show the expected shape (Supporting Information Fig. S8).

Recommendations

For the vast majority of natural DOM concentrations, as typical for ocean waters and large estuaries, no perturbations of spectrophotometric pH measurements were detected. Therefore, neither re-evaluation of previous measurements, nor modifications of the method for future investigations are required under these conditions.

However, in strongly colored river waters we recommend examining the mCP-absorption spectra for any sign of disturbances. In addition, the self-absorbance of the sample at $\lambda = 434$ nm should be measured, as performed in this study. If it exceeds 0.3 absorbance units (threshold identified for an Agilent 8453 with 10-cm cuvette, potentially different for other instrumentation), we propose the following actions to improve the quality of the measurements:

1. The light intensity should be high at both wavelengths. For measurements with an Agilent 8453 spectrophotometer this can be achieved by running the deuterium lamp.
2. A shorter cuvette length and proportionally higher indicator concentrations help to reduce the spectral disturbances caused by DOM, as both decrease the ratio of solution self-absorbance to mCP-absorbance. However, at higher indicator concentrations the pH perturbation induced by the indicator addition is more pronounced, especially for samples with low alkalinities (Hammer et al. 2014). Measurement systems with a FIA (flow injection analysis) approach could help to circumvent this problem, as they allow to extrapolate to zero indicator concentration (Aßmann et al. 2011).
3. When direct spectrophotometric pH measurements are impossible due to very strong DOM-absorbance, glass electrodes that are carefully calibrated against the spectrophotometric method can in principle be used to obtain accurate values on the total scale (Easley and Byrne 2012). However, a rigorous control of experimental conditions (e.g., temperature, stirring, and gas exchange) is critical.

For a wide range of naturally occurring H_2S concentrations of up to $400 \mu\text{mol kg}^{-1}$, our results do not indicate interferences with spectrophotometric pH measurements. Accordingly, there is no need for a change of the method in this respect, nor is a re-evaluation of previous data required. Nevertheless, H_2S containing samples need to be handled with care to avoid gas exchange with the atmosphere, which could

impact the sample pH by two processes: (i) Oxygen uptake could cause the oxidation of H₂S components, which corresponds to an alkalinity loss, and thus a decrease in pH. (ii) H₂S containing samples are typically characterized by high pCO₂ and an outgassing of CO₂ leads to an increase in pH. Though both effects will partially cancel out, the net effects will still cause erroneous pH measurements.

Conclusion

Spectrophotometric pH measurements with the indicator dye mCP work robustly and produce correct pH values over a wide range of DOM and H₂S concentrations as typical for the vast majority of marine and brackish waters. We did not observe any impact on the characteristics of mCP due to molecular interactions with DOM or H₂S. However, strongly colored, self-absorbing river, ground or pore waters can impact the optical method. We propose three recommendations (strong light source, shorter cuvette length and spectrophotometrically calibrated glass electrodes) that allow to apply spectrophotometric measurements even under such challenging conditions. We conclude that spectrophotometric pH measurements in the presence of DOM and H₂S are a valuable method to support a full characterization of the CO₂ system in aqueous solutions, which is especially important when the carbonate alkalinity is not accessible due to organic alkalinity contributions by significant amounts of DOM.

References

- Abmann, S., C. Frank, and A. Körtzinger. 2011. Spectrophotometric high-precision seawater pH determination for use in underway measuring systems. *Ocean Sci.* **7**: 597–607. doi:10.5194/os-7-597-2011
- Alberts, J. J., and M. Takács. 2004. Total luminescence spectra of IHSS standard and reference fulvic acids, humic acids and natural organic matter: Comparison of aquatic and terrestrial source terms. *Org. Geochem.* **35**: 243–256. doi:10.1016/j.orggeochem.2003.11.007
- Atamanchuk, D., A. Tengberg, P. J. Thomas, J. Hovdenes, A. Apostolidis, C. Huber, and P. O. J. Hall. 2014. Performance of a lifetime-based optode for measuring partial pressure of carbon dioxide in natural waters. *Limnol. Oceanogr.: Methods* **12**: 63–73. doi:10.4319/lom.2014.12.63
- Averett, R. C., J. A. Leenheer, D. M. McKnight, and K. A. Thorn. 1994. Humic substances in the Suwannee River, Georgia: Interactions, properties and proposed structures. US Geological Survey Open-File Report. 87–557.
- Battin, T. J. 1998. Dissolved organic matter and its optical properties in a blackwater tributary of the upper Orinoco river, Venezuela. *Org. Geochem.* **28**: 561–569. doi:10.1016/S0146-6380(98)00028-X
- Bricaud, A., A. Morel, and L. Prieur. 1981. Absorption by dissolved organic matter of the sea (yellow substances) in the UV and visible domains. *Limnol. Oceanogr.* **26**: 43–53. doi:10.4319/lo.1981.26.1.0043
- Byrne, R. H. 2014. Measuring ocean acidification: New technology for a new era of ocean chemistry. *Environ. Sci. Technol.* **48**: 5352–5360. doi:10.1021/es405819p
- Byrne, R. H., S. Mecking, R. A. Feely, and X. Liu. 2010. Direct observations of basin-wide acidification of the North Pacific Ocean. *Geophys. Res. Lett.* **37**: L02601. doi:10.1029/2009GL040999
- Canfield, D. E. 2006. Models of oxic respiration, denitrification and sulfate reduction in zones of coastal upwelling. *Geochim. Cosmochim. Acta* **70**: 5753–5765. doi:10.1016/j.gca.2006.07.023
- Carter, B. R., J. A. Radich, H. L. Doyle, and A. G. Dickson. 2013. An automated system for spectrophotometric seawater pH measurements. *Limnol. Oceanogr.: Methods* **11**: 16–27. doi:10.4319/lom.2013.11.16
- Chierici, M., A. Fransson, and L. G. Anderson. 1999. Influence of m-cresol purple indicator additions on the pH of seawater samples: Correction factors evaluated from a chemical speciation model. *Mar. Chem.* **65**: 281–290. doi:10.1016/S0304-4203(99)00020-1
- Clayton, T. D., and R. H. Byrne. 1993. Spectrophotometric seawater pH measurements: Total hydrogen results. *Deep-Sea Res. Part I Oceanogr. Res. Pap.* **40**: 2115–2129. doi:10.1016/0967-0637(93)90048-8
- Coble, P. G. 2007. Marine optical biogeochemistry: The chemistry of ocean color. *Chem. Rev.* **107**: 402–418. doi:10.1021/cr050350+
- Degrandpre, M. D., R. S. Spaulding, J. O. Newton, E. J. Jaqueth, S. E. Hamblock, A. A. Umansky, and K. E. Harris. 2014. Considerations for the measurement of spectrophotometric pH for ocean acidification and other studies. *Limnol. Oceanogr.: Methods* **12**: 830–839. doi:10.4319/lom.2014.12.830
- DelValls, T. A., and A. G. Dickson. 1998. The pH of buffers based on 2-amino-2-hydroxymethyl-1,3-propanediol (“tris”) in synthetic sea water. *Deep-Sea Res. Part I Oceanogr. Res. Pap.* **45**: 1541–1554. doi:10.1016/S0967-0637(98)00019-3
- Dickson, A. G. 1993. The measurement of sea water pH. *Mar. Chem.* **44**: 131–142. doi:10.1016/0304-4203(93)90198-W
- Dickson, A. G., C. L. Sabine, and J. R. Christian. 2007. Guide to best practices for ocean CO₂ measurements. PICES Special Publication 3.
- Dickson, A. G., M. F. Cam, P. Spitzer, P. Fiscaro, D. Stoica, R. Pawlowicz, and R. Feistel. 2015. Metrological challenges for measurements of key climatological observables. Part 3: Seawater pH. *Metrologica*.

- Doney, S. C., V. J. Fabry, R. A. Feely, and J. A. Kleypas. 2009. Ocean acidification: The other CO₂ problem. *Ann. Rev. Mar. Sci.* **1**: 169–192. doi:10.1146/annurev.marine.010908.163834
- Duarte, C. M., and others. 2013. Is ocean acidification an open-ocean syndrome? Understanding anthropogenic impacts on seawater pH. *Estuaries Coasts* **36**: 221–236. doi:10.1007/s12237-013-9594-3
- Easley, R. A., and R. H. Byrne. 2012. Spectrophotometric calibration of pH electrodes in seawater using purified m-cresol purple. *Environ. Sci. Technol.* **46**: 5018–5024. doi:10.1021/es300491s
- Ertel, J. R., J. I. Hedges, A. H. Devol, J. E. Richey, and M. de Nazare Beoes Ribeiro. 1986. Dissolved humic substances of the Amazon River system. *Limnol. Oceanogr.* **31**: 739–754. doi:10.4319/lo.1986.31.4.0739
- Ferrari, G. M., M. D. Dowell, S. Grossi, and C. Targa. 1996. Relationship between the optical properties of chromophoric dissolved organic matter and total concentration of dissolved organic carbon in the southern Baltic Sea region. *Mar. Chem.* **55**: 299–316. doi:10.1016/S0304-4203(96)00061-8
- Fonselius, S. 1962. Hydrography of the Baltic deep basins. *Fish. Board Swed. Ser. Hydrogr. Rep.* **13**: 1–41.
- Fonselius, S., and J. Valderrama. 2003. One hundred years of hydrographic measurements in the Baltic Sea. *J. Sea Res.* **49**: 229–241. doi:10.1016/S1385-1101(03)00035-2
- Fritzsche, E., P. Gruber, S. Schutting, J. P. Fischer, M. Strobl, J. D. Müller, S. M. Borisov, and I. Klimant. 2017. Highly sensitive poisoning-resistant optical carbon dioxide sensors for environmental monitoring. *Anal. Methods* **9**: 55–65. doi:10.1039/C6AY02949C
- Green, S. A., and N. V. Blough. 1994. Optical absorption and fluorescence properties of chromophoric dissolved organic matter in natural waters. *Limnol. Oceanogr.* **39**: 1903–1916. doi:10.4319/lo.1994.39.8.1903
- Gustafsson, E., T. Wällstedt, C. Humborg, M. Mörth, and B. G. Gustafsson. 2014. External total alkalinity loads versus internal generation: The influence of nonriverine alkalinity sources in the Baltic Sea. *Global Biogeochem. Cycles* **28**: 1358–1370. doi:10.1002/2014GB004888
- Hammer, K., B. Schneider, K. Kuliński, and D. E. Schulz-Bull. 2014. Precision and accuracy of spectrophotometric pH measurements at environmental conditions in the Baltic Sea. *Estuar. Coast. Shelf Sci.* **146**: 24–32. doi:10.1016/j.ecss.2014.05.003
- Hofmann, G. E., and others. 2011. High-frequency dynamics of ocean pH: A multi-ecosystem comparison. *PLoS One* **6**: e28983. doi:10.1371/journal.pone.0028983
- Kremling, K. 1983. The behavior of Zn, Cd, Cu, Ni, Co, Fe, and Mn in anoxic baltic waters. *Mar. Chem.* **13**: 87–108. doi:10.1016/0304-4203(83)90019-1
- Kuliński, K., B. Schneider, K. Hammer, U. Machulik, and D. Schulz-Bull. 2014. The influence of dissolved organic matter on the acid–base system of the Baltic Sea. *J. Mar. Syst.* **132**: 106–115. doi:10.1016/j.jmarsys.2014.01.011
- Lai, C.-Z., and others. 2016. Spectrophotometric measurement of freshwater pH with purified meta-cresol purple and phenol red. *Limnol. Oceanogr.: Methods* **14**: 864–873. doi:10.1002/lom3.10137
- Liu, X., M. C. Patsavas, and R. H. Byrne. 2011. Purification and characterization of meta-cresol purple for spectrophotometric seawater pH measurements. *Environ. Sci. Technol.* **45**: 4862–4868. doi:10.1021/es200665d
- Luther, G. W., T. M. Church, and D. Powell. 1991. Sulfur speciation and sulfide oxidation in the water column of the Black Sea. *Deep-Sea Res. Part A Oceanogr. Res. Pap.* **38**: S1121–S1137. doi:10.1016/S0198-0149(10)80027-5
- Millero, F. J., J. Z. Zhang, S. Fiol, S. Sotolongo, R. N. Roy, K. Lee, and S. Mane. 1993. The use of buffers to measure the pH of seawater. *Mar. Chem.* **44**: 143–152. doi:10.1016/0304-4203(93)90199-X
- Mosley, L. M., S. L. G. Husheer, and K. A. Hunter. 2004. Spectrophotometric pH measurement in estuaries using thymol blue and m-cresol purple. *Mar. Chem.* **91**: 175–186. doi:10.1016/j.marchem.2004.06.008
- Nelson, N. B., D. A. Siegel, and A. F. Michaels. 1998. Seasonal dynamics of colored dissolved material in the Sargasso Sea. *Deep-Sea Res. Part I* **45**: 931–957. doi:10.1016/S0967-0637(97)00106-4
- Pierrot, D., E. Lewis, and D. W. R. Wallace. 2006. MS Excel Program Developed for CO₂ System Calculations. ORNL/CDIAC-105a. Carbon Dioxide Information Analysis Center, Oak Ridge National Laboratory, U.S. Department of Energy, Oak Ridge, Tennessee. doi:10.3334/CDIAC/otg.CO2SYS_XLS_CDIAC105a
- Le Quéré, C., and others. 2015. Global carbon budget 2015. *Earth Syst. Sci. Data* **7**: 349–396. doi:10.5194/essd-7-349-2015
- Rochelle-Newall, E., and T. Fisher. 2002. Chromophoric dissolved organic matter and dissolved organic carbon in Chesapeake Bay. *Mar. Chem.* **77**: 23–41. doi:10.1016/S0304-4203(01)00073-1
- Schunck, H., and others. 2013. Giant hydrogen sulfide plume in the oxygen minimum zone off Peru supports chemolithoautotrophy. *PLoS One* **8**: e68661. doi:10.1371/journal.pone.0068661
- Scranton, M. I., Y. Astor, R. Bohrer, T. Y. Ho, and F. Muller-Karger. 2001. Controls on temporal variability of the geochemistry of the deep Cariaco Basin. *Deep-Sea Res. Part I* **48**: 1605–1625. doi:10.1016/S0967-0637(00)00087-X
- Stedmon, C. A., S. Markager, and H. Kaas. 2000. Optical properties and signatures of chromophoric dissolved organic matter (CDOM) in Danish coastal waters. *Estuar. Coast. Shelf Sci.* **51**: 267–278. doi:10.1006/ecss.2000.0645
- Sugimura, Y., and Y. Suzuki. 1988. A high-temperature catalytic oxidation method for the determination of non-

- volatile dissolved organic carbon in seawater by direct injection of a liquid sample. *Mar. Chem.* **24**: 105–131. doi:[10.1016/0304-4203\(88\)90043-6](https://doi.org/10.1016/0304-4203(88)90043-6)
- Waldbusser, G. G., and J. E. Salisbury. 2014. Ocean acidification in the coastal zone from an organism's perspective: Multiple system parameters, frequency domains, and habitats. *Ann. Rev. Mar. Sci.* **6**: 221–247. doi:[10.1146/annurev-marine-121211-172238](https://doi.org/10.1146/annurev-marine-121211-172238)
- Yacobi, Y. Z., J. J. Alberts, M. Takács, and M. McElvaine. 2003. Absorption spectroscopy of colored dissolved organic carbon in Georgia (USA) rivers: The impact of molecular size distribution. *J. Limnol.* **62**: 41–46. doi:[10.4081/jlimnol.2003.41](https://doi.org/10.4081/jlimnol.2003.41)
- Yang, B., R. H. Byrne, and M. Lindemuth. 2015. Contributions of organic alkalinity to total alkalinity in coastal waters: A spectrophotometric approach. *Mar. Chem.* **176**: 199–207. doi:[10.1016/j.marchem.2015.09.008](https://doi.org/10.1016/j.marchem.2015.09.008)
- solution. We acknowledge Karoline Hammer for supporting the preparation and handling of DOM stock solutions, as well as Jenny Jeschek for analyzing the DOM concentration. We thank Karol Kuliński for a scientific revision and Charlotte Westhoven for linguistic revision of the manuscript. We also acknowledge supporting discussions with Andrew Dickson, Robert Byrne, and Michael DeGrandpre. The research leading to this manuscript has received funding from BONUS, the joint Baltic Sea research and development programme (Art 185), funded jointly from the European Union's Seventh Programme for research, technological development and demonstration and from the German Federal Ministry of Education and Research through Grant No. 03F0689A and 03F0689B (BONUS PINBAL).

Conflict of Interest

None declared.

Submitted 06 January 2017

Revised 06 October 2017

Accepted 10 November 2017

Acknowledgments

We would like to thank Robert Byrne and Nora Douglas for providing us with purified indicator dye and advice for the preparation of the indicator stock

Associate editor: Gregory Cutter

Macroalgae may mitigate ocean acidification effects on mussel calcification by increasing pH and its fluctuations

M. Wahl ^{1,*} S. Schneider Covachã,¹ V. Saderne,^{1,2} C. Hiebenthal,¹
J. D. Müller ³ C. Pansch,¹ Y. Sawall^{1,4}

¹GEOMAR Helmholtz Centre for Ocean research, Kiel, Germany

²King Abdullah University of Science and Technology (KAUST), Thuwal, Saudi Arabia

³Leibniz Institute for Baltic Sea Research, Warnemuende, Germany

⁴Bermuda Institute of Ocean Sciences (BIOS), St. George's, Bermuda

Abstract

Ocean acidification (OA) is generally assumed to negatively impact calcification rates of marine organisms. At a local scale however, biological activity of macrophytes may generate pH fluctuations with rates of change that are orders of magnitude larger than the long-term trend predicted for the open ocean. These fluctuations may in turn impact benthic calcifiers in the vicinity. Combining laboratory, mesocosm and field studies, such interactions between OA, the brown alga *Fucus vesiculosus*, the sea grass *Zostera marina* and the blue mussel *Mytilus edulis* were investigated at spatial scales from decimetres to 100s of meters in the western Baltic. Macrophytes increased the overall mean pH of the habitat by up to 0.3 units relative to macrophyte-free, but otherwise similar, habitats and imposed diurnal pH fluctuations with amplitudes ranging from 0.3 to more than 1 pH unit. These amplitudes and their impact on mussel calcification tended to increase with increasing macrophyte biomass to bulk water ratio. At the laboratory and mesocosm scales, biogenic pH fluctuations allowed mussels to maintain calcification even under acidified conditions by shifting most of their calcification activity into the daytime when biogenic fluctuations caused by macrophyte activity offered temporal refuge from OA stress. In natural habitats with a low biomass to water body ratio, the impact of biogenic pH fluctuations on mean calcification rates of *M. edulis* was less pronounced. Thus, in dense algae or seagrass habitats, macrophytes may mitigate OA impact on mussel calcification by raising mean pH and providing temporal refuge from acidification stress.

The uptake of rising anthropogenic CO₂ by the ocean is leading to substantial shifts in seawater carbonate chemistry: concentrations of CO₂, H⁺ and HCO₃⁻ are increasing, whereas CO₃²⁻ concentration and the saturation states of calcite (Ω_{Ca}) and aragonite (Ω_{Ar}) are decreasing (e.g., Feely et al. 2004). This on-going process called ocean acidification (OA) is expected to reduce surface open ocean pH by 0.3–0.4 units until the end of the century (Orr et al. 2005; Doney et al. 2009; IPCC 2013). However, these modeling projections for the open ocean are not always applicable to near-shore environments (Duarte et al. 2013; Müller et al. 2016). Coastal

ecosystems, especially when shallow and sheltered, are often subject to large fluctuations of the carbonate system caused by hydrodynamics and/or biological activity (Duarte et al. 2013; Waldbusser and Salisbury 2014). Continuous time series at various sites revealed that pH fluctuations in coastal waters can exceed those in the open ocean by an order of magnitude or more (e.g., Hofmann et al. 2011). In addition to seasonal pH fluctuations (e.g., Thomsen et al. 2013), a number of studies have reported substantial diurnal oscillations of pH and pCO₂ in productive coastal communities driven by biological photosynthesis/respiration cycles in, e.g., tide or rock pools (Truchot and Duhamel-Jouve 1980; Bjork et al. 2004; Beer et al. 2006; Wootton et al. 2008), coral reefs (Shamberger et al. 2011; Gray et al. 2012; Price et al. 2012; Smith et al. 2013), seagrass meadows (Invers et al. 1997; Semesi et al. 2009; Unsworth et al. 2012; Buapet et al. 2013; Hendriks et al. 2014) and macroalgal habitats (e.g., Middelboe and Hansen 2007; Krause-Jensen et al. 2015; Krause-Jensen and Duarte 2016). For shallow stands of *Fucus*

*Correspondence: mwahl@geomar.de

Additional Supporting Information may be found in the online version of this article.

This is an open access article under the terms of the Creative Commons Attribution License, which permits use, distribution and reproduction in any medium, provided the original work is properly cited.

vesiculosus, the most important macroalgal species in the Baltic Sea, diurnal amplitudes of about one pH unit can typically be observed during summer months (Middelboe and Hansen 2007; Saderne and Wahl 2013). Generally, the rate and amplitude of pH changes are inversely proportional to the spatial scale considered, i.e., small scale pH fluctuations can be fast (sec-min) and dramatic (1–3 units) in the diffusive boundary layer of macroalgal thalli whereas large-scale seasonal pH fluctuations in coastal waters are much slower (weeks-months) and less strong (< 1 unit) (Wahl et al. 2016). In addition, macroalgal photosynthesis may raise the mean pH in their vicinity, an effect which increases with increasing daily photoperiod (Krause-Jensen et al. 2016).

OA may represent a threat, in particular to calcifying taxa (e.g., Orr et al. 2005; Fabry et al. 2008; Hofmann et al. 2010; Clark and Gobler 2016; Ramajo et al. 2016), and numerous studies revealed negative impacts of OA on their growth and survival (reviewed by Kroeker et al. 2010; Harvey et al. 2013). The dominance of negative effects reported in numerous OA studies (e.g., Kroeker et al. 2010; Harvey et al. 2013; Nagelkerken et al. 2016), may in part be attributable to the fact that the great majority of these investigations were conducted under non-fluctuating (and mono-factorial) treatments and in the absence of species interactions. Both, fluctuations and biotic interactions, have a substantial potential to modulate OA impacts (e.g., Boyd et al. 2016; Gunderson et al. 2016; Wahl et al. 2016). If not buffered by physiological plasticity (e.g., Hofmann and Todgham 2010), natural fluctuations of the carbonate system may either enhance OA impact such as reported for reef calcification (Shaw et al. 2012) or mitigate it as found for various calcifiers living in algal boundary layers (Hurd et al. 2011; Cornwall et al. 2013, 2014, 2015; Hurd 2015). Such apparently contradictory effects of pH fluctuations on calcification were found even within the group of bivalves where fluctuations were reported to mitigate (Frieder et al. 2014) or not to mitigate the impact of OA on larval calcification (Clark and Gobler 2016). In consequence, understanding whether and when pH fluctuations enhance or mitigate the impact of progressing acidification on calcifying biota is crucial. Apart from the immediate effect of fluctuations, sparse available evidence suggests that strong spatial and temporal variability in near-shore coastal habitats (such as large portions of the Baltic Sea) may indeed select for populations more tolerant to extreme pH situations (Melzner et al. 2009; Johannesson et al. 2011; Thomsen et al. 2013; Frieder et al. 2014; Pansch et al. 2014).

In the Baltic Sea, “anthropogenic” eutrophication in combination with warming-enhanced stratification and intense benthic remineralization promotes the occurrence of oxygen-poor, CO₂-enriched bottom waters in late summer, which regularly reaches the surface by wind-driven upwelling (Myrberg and Andrejev 2003; Melzner et al. 2013; Thomsen et al. 2013). During such upwelling events, peak *p*CO₂-values of up to 2300 μatm are common in this region,

corresponding to pH values as low as 7.4 (Thomsen et al. 2010; Saderne et al. 2013). With respect to mussels (*Mytilus edulis*), the resulting acidification stress may, however, be compensated to some degree by elevated food (phytoplankton) supply in nutrient-rich waters (Thomsen et al. 2013; Ramajo et al. 2016). Whether biogenic fluctuations of O₂ and the carbonate system driven by macrophytes also helps compensating acidification stress impacts on calcifiers, remains to be verified. Biogenic fluctuations around a potentially stressful mean will only be beneficial for calcifying organisms if the benefit of low-stress phases outweighs the harm suffered during enhanced-stress phases. Calcifiers could benefit from pH fluctuations if they were capable of maintaining overall rates by shifting acidification-sensitive processes toward time windows of high pH (Thomsen et al. 2015). Since macrophytes, when photosynthesizing, can temporarily raise Ω_{Ca} and Ω_{Ar} (saturation state of calcite and aragonite, respectively) considerably, they may create a refuge for calcifiers during daylight hours as observed in various habitats (e.g., Manzello et al. 2012; Duarte et al. 2013; Hendriks et al. 2014). The strength of the modification of local seawater carbonate chemistry by primary production depends on light regime, salinity, macrophyte abundance, and density (Binzer and Sand-Jensen 2002; Buapet et al. 2013), as well as on the residence time of the water within the macrophyte habitat (e.g., Truchot and Duhamel-Jouve 1980; Perez-Llorens et al. 2004). The potential of such fluctuating conditions to reduce acidification stress and, thus, enhance local calcification rates has been claimed repeatedly (Semesi et al. 2009; Price et al. 2012; Unsworth et al. 2012; Findlay et al. 2013; Saderne and Wahl 2013), experimental evidence, however, is scarce.

Here, we present a comprehensive study on calcification and growth of the blue mussel *M. edulis*, an ecologically and economically important calcifier in the Baltic Sea, under various pH settings (fluctuating or constant, high and low) - with or without the putatively protective neighborhood of macrophytes. In a laboratory experiment, we examined the extent of changes in seawater carbonate chemistry by photosynthetic activity of a macrophyte (the bladder wrack *F. vesiculosus*), and how this modulates OA impacts on calcification rates in *M. edulis*, during net photosynthesis (day) and net respiration (night) of the macrophyte. In a second approach, we investigated interactive effects of acidification and warming on mussel calcification in simulated mussel-macrophyte communities in the Kiel Outdoor Benthocosms (Wahl et al. 2015a). These experiments featuring controlled conditions were complemented by two field studies on a meso-scale level (10–100 m), where we (1) compared in situ growth rates of mussels in small (1–2 m diameter) patches of *Fucus*, seagrass or sand, and (2) assessed calcification rates of *M. edulis* incubated in seawater taken at different spots along a transect into a large *Fucus* bed.

We hypothesized that (1) the activity of macrophytes imposes substantial fluctuations on oxygen and carbonate system conditions in their vicinity, that (2) such macrophyte-

driven fluctuations of the carbonate system may facilitate the calcification of *M. edulis* under acidified conditions and that (3) this effect increases with macrophyte biomass to water ratio, e.g., from periphery to the center of a macrophyte habitat.

Materials and methods

An overview of the experiments, the experimental parameters modulated, their replication and all measurements taken is given in Supporting Information Table 1.

Study organisms

In the Baltic Sea, the bladder wrack *F. vesiculosus* is the most widespread canopy forming macroalga (Kautsky and Kautsky 2000; Torn et al. 2006). It provides habitat, substratum and food for a large number of invertebrates (e.g., Kautsky et al. 1992). Another important habitat-forming primary producer in the Baltic ecosystems is the eelgrass *Zostera marina*, which—like *Fucus* sp.—contributes significantly to high local biodiversity, especially due to the associated epifaunal assemblages (Bostrom and Bonsdorff 1997, 2000). The blue mussel *M. edulis* tends to dominate benthic fouling communities in the Baltic Sea (Durr and Wahl 2004; Enderlein and Wahl 2004) and is undoubtedly one of the most common calcifiers in the Baltic (Hiebenthal et al. 2013; Thomsen et al. 2013). Blue mussels often occur in close proximity to the macrophyte stands formed by *Fucus* sp. or *Z. marina* (Reusch et al. 1994; Bostrom and Bonsdorff 1997; Wikstrom and Kautsky 2007; Vinther et al. 2008). More than 95% of the shell's wet weight consist of bimineralic calcium carbonate (Yin et al. 2005) deposited as aragonite in the inner layer and calcite in the outer layer (Dalbeck et al. 2006).

Total alkalinity and pH measurements and estimation of calcification rates

Total alkalinity (TA) and pH measurements were used to estimate mussel calcification rates and derive other CO₂ system parameters, like *p*CO₂ and Ω_{Ca}. Water samples for TA were kept in polypropylene tubes (Falcon) at 4°C for 1–2 d until analysis. When longer storage was anticipated, seawater samples (50 mL) for TA measurements were poisoned with 50 μL saturated HgCl₂-solution to inhibit biological activity (following Dickson et al. 2007), and samples were stored at room temperature until analysis. TA was measured in duplicates via potentiometric titration with an automated open cell titrator (Titroline 7000, SI analytics, Germany) using 25 mL of the sample and 0.05 M HCl (precision ± 8 μmol kg⁻¹), followed by TA calculation using the Gran approximation by determining the second endpoint of the titration curve (Grasshoff 1983). The gained TA data were corrected based on repeated measurements of Dickson's certified reference material (CRM batch 103; Dickson et al. 2003). Net calcification rate (*G*) was then calculated as the difference in TA between the initial and final sample. Standardization of calcification was achieved by dividing *G* by soft tissue dry

weight (DW) of the mussel used in the experiment and by the duration (*h*) of the respective incubation. Calcification rates were calculated after the following equation, with *V* as the volume of the incubation chamber and with a water density ρ of 1.012 kg L⁻¹ (at a temperature of 15°C and a salinity of 17 PSU):

$$G \left[\frac{\mu\text{mol CaCO}_3}{\text{g DW} \times h} \right] = \frac{\frac{\Delta\text{TA}}{2} \left[\frac{\mu\text{mol}}{\text{kg}} \right] \times V [L] \times \rho_{\text{seawater}} \left[\frac{\text{kg}}{L} \right]}{\text{DW} [\text{g}] \times t_{\text{incubation}} [h]}$$

For all (potentiometric) pH measurements performed within this study, glass electrodes were calibrated with NBS-buffers (3-point calibration: pH 4, 7, 10) and results are given at the NBS scale, if not stated differently (pH values are expressed on the total scale for the macrophyte patches field survey.). Exact types of the glass electrodes used in this study are specified in the respective chapters below.

Further carbonate system parameters (*p*CO₂, Ω_{Ca}) for the laboratory experiment were calculated from TA, pH, salinity, and temperature using the CO2SYS macro (Pierrot et al. 2006 with *K*₁ and *K*₂ according to Millero et al. 2006 and KHSO₄ after Dickson 1990).

Laboratory experiment

We tested the interactive effects of the factors OA (2 levels), daytime (2 levels, i.e., light and dark) and amount of simulated density of *F. vesiculosus* (5 levels) on calcification rates of *M. edulis*.

Specimens of *F. vesiculosus* growing on cobbles and small boulders at depths of 0.3–1 m were collected in Kiel Fjord (Strande: N54°26'48" E10°11'2") on 17 October 2012. Only vegetative thalli of healthy individuals were chosen. Algae were transferred to GEOMAR, Kiel, and allowed to acclimatize to laboratory conditions for 48 h in large (39 L) tanks filled with filtered seawater from Kiel Fjord at a constant temperature of 15°C (corresponding to in situ temperature). The tanks received constant aeration (ambient *p*CO₂) and seawater flow-through (two tank volumes per 24 h). Artificial light (per aquarium: four neon tubes, Hobar T5HO 39W/10,000K) was provided with a 12-h day/night-cycle. Specimens of *M. edulis* were collected from a subtidal population in Kiel Fjord at GEOMAR pier (N54°19'48" E10°9'1") on 19 October 2012 and kept in aerated (ambient *p*CO₂) natural seawater until the start of the experiment.

Seawater from Kiel Fjord was filtered by a sand filter and pumped into two header tanks in which two different *p*CO₂ levels were established by direct aeration of the water body with compressed ambient *p*CO₂-air (ca 400 μatm, present conditions) and CO₂-enriched air (1120 μatm, prediction for 2100 under more severe scenarios in IPCC 2013), respectively, using an automatic CO₂ mixing facility (Linde Gas & HTK Hamburg, Germany; Bleich et al. 2008). Each header tank was connected in parallel to three replicate series of aquaria. In each series, five 5 L plastic aquaria were connected in-line with a height

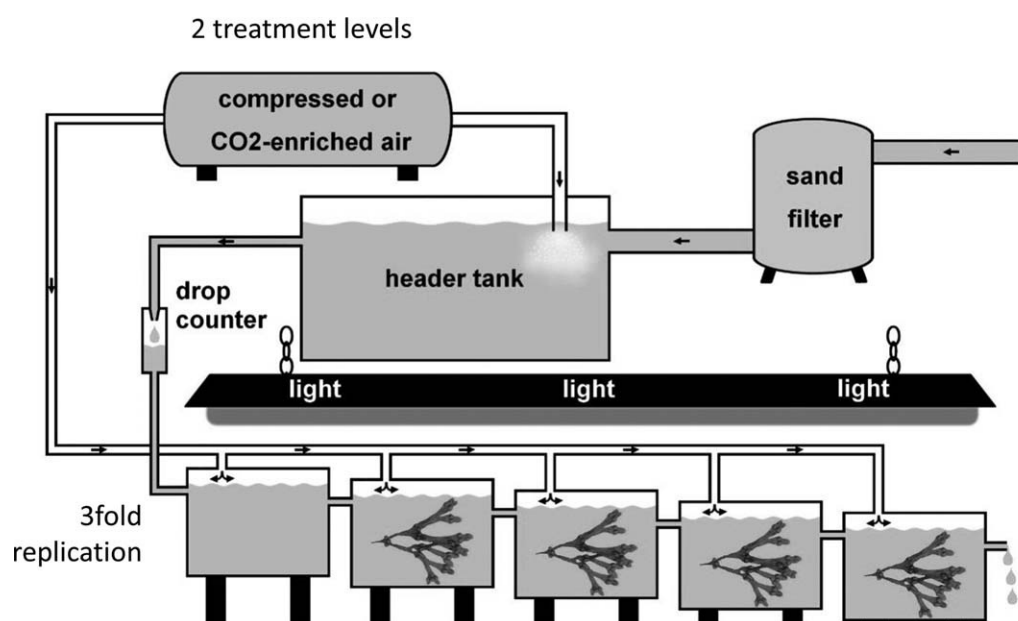


Fig. 1. Schematic illustration of the laboratory set-up. The graphic shows one header tank connected to one series of aquaria as an example for an acidification treatment (not to scale, replicates are not shown). Non-acidified units were bubbled with non-CO₂-enriched air. The pictured system was replicated thrice for each treatment level. Aquaria to the right (down-flow) represent a position closer to the center of an algal stand, aquaria to the left represent a position in the periphery.

difference of 1.2 cm between adjacent aquaria (Fig. 1) to ensure a steady directional flow (2.4 L h^{-1}) from the header tank downstream through aquaria #1 through #5. The aquaria were sealed with transparent plastic foil (permeable for photosynthetic active radiation) to minimize gas exchange with the atmosphere. The headspace between plastic covering and water surface in the aquaria was additionally aerated with ambient or CO₂-enriched air (see above). The experiment was started when the $p\text{CO}_2$ of the water in the header tanks reached equilibrium with the $p\text{CO}_2$ of the applied gas mixture and the pH had stabilized (Supporting Information Table 2).

F. vesiculosus thalli ($20 \pm 1 \text{ g}$ wet weight) were cut from the substratum and cleaned of all macroscopic epibionts the day before the experiment started. One thallus was placed into each aquarium of a series except the first. Thus, the conditioned water of the header tank was modulated by 0, 1, 2, 3, and 4 *Fucus* individuals (simulating an increasingly dense macroalgal stand or a position increasingly deep into a *F. vesiculosus* patch), from aquarium #1 to aquarium #5, respectively.

Temperature, salinity, oxygen concentration, total alkalinity (TA), and pH_{NBS} were measured before and immediately after each 12 h “daytime” treatment using a WTW Oxi 3315 analyser equipped with a WTW FDO925 optical sensor for oxygen measurements and a WTW Cond 315i salinometer with a WTW TETRACON 325 probe for temperature and salinity. Measurements of pH_{NBS} were performed using a WTW 3310 pH-meter with a WTW SenTix 81-electrode. The algae were incubated in two runs (“day”/“night”) for 12 h

each: under continuous illumination (four neon tubes, Hobar T5HO 39W/10,000K) and in the dark, respectively. At the end of each run, two 1 L plastic beakers were filled with water from each aquarium. Eight small mussels (shell length $24 \pm 3.8 \text{ mm}$ (mean \pm SD)) were placed in the first beaker containing the water from the various treatment combinations (daytime $\times p\text{CO}_2$ level $\times Fucus$ density) and incubated in the pre-treated seawater for 12 h in the dark. The second plastic beaker containing the same water but no mussels served as a reference to identify changes in seawater chemistry which were not caused by the mussels. Immediately after the end of the incubation, the second seawater sample for TA was taken (see above) from the plastic beaker. During the 24 h of incubation, no food was provided. Dry weight and calcification rates of the mussels as well as further carbonate system parameters were determined as described above. Replication in this experiment was threefold.

Benthocosm experiment

Calcification of mussels from Kiel Fjord was assessed under naturally fluctuating pH and temperature conditions of different means in the Kiel Outdoor Benthocosm infrastructure (details in Wahl et al. 2015a). The benthocosm facility consists of 12 experimental units of 1500 L each. The tanks are thermally insulated and were covered by a transparent hood, which allows for control of the headspace atmosphere composition. Each sub-unit is equipped with a water pump driving an internal circulation via a wave-generator. All sub-units are monitored by a set of four

sensors (temperature, salinity, oxygen und pH_{NBS}), the data of which are continuously logged. The crossed 2-factorial approach in this experiment consisted of warming and acidification: warming by 5°C relative to the temperature control tanks (ambient temperature in Kiel Fjord) was produced by three heaters (600 watt, Schego Titan, Schemel & Goetz, Offenbach am Main, Germany) per sub-unit. Acidification was obtained by increasing the pCO_2 of the headspace atmosphere to 1100 μatm . The intense mixing created by the wave-generators accelerates the air-sea gas exchange between headspace atmospheres (CO_2 treatment) and the water of the sub-units, enabling a rapid equilibration between atmospheric CO_2 and water carbonate chemistry. Both treatments caused add-ons to the natural fluctuations in temperature and pH which were driven by the season, weather, fjord hydrography, and biology with regard to the inflowing fjord water and, in addition to that, by the photosynthetic and respiratory activities of the organisms in the benthocosms.

During the experiment presented here (total duration 3 months), the community in the benthocosms consisted of bladder wrack (*F. vesiculosus*, wet weight biomass: 672 ± 103 (SE) g per 1500 L tank volume), mussels (*M. edulis*), sea stars (*Asterias rubens*), snails (*Littorina littorea*), isopods (*Idotea baltica*), amphipods (*Gammarus* spp.) and fishes (*Gasterosteus aculeatus*) in proportions typical for a bladder wrack community of the Kiel Fjord region (see Graiff et al. 2015a). Nutrients, plankton and microbes were provided by unfiltered through-flowing fjord water (ca 1.5 tank volumes per day).

In this near-natural setting of the benthocosms, calcification rates were assessed of “naïve” *M. edulis* specimen (2–3 cm long), collected at the GEOMAR pier in late June 2013. They were cleaned and placed in triplicates into each of twelve 300-mL glass jars, filled with water from one of the 12 benthocosm units, and left inside for 2–3 h for recovery and acclimatization. Subsequently, incubations were run for 3 h with 300 mL fresh water taken from the respective benthocosm unit. Before and after incubation, pH_{NBS} (Seven Multi + InLab Expert Pro, Mettler Toledo GmbH, Giessen, Germany) was measured and a 50 mL water sample was taken for TA measurements. Incubations with the same mussel individuals were conducted twice, at 15:00 h and at 09:00 h. Thus, the afternoon incubations took place in water conditioned by daytime activity (photosynthesis-dominated) and the morning incubations in water conditioned mainly by night activity (respiration-dominated) of the benthocosm community. Replication in this experiment was threefold.

Small macrophyte habitats - patches

A survey of O_2 concentration ($[\text{O}_2]$ TA, pH_T (total scale), seston and mussel growth was performed in three different components of a mosaic benthic habitat in Kiel Fjord (Kiel: N54°22'30", E10°9'34"): *F. vesiculosus* (40% of mosaic patches), *Z. marina* (15%) and sand patches (45%). In each of the patches the cover by *Fucus*, *Zostera* and sand,

was >90%. Five randomly arranged patches of each type with a size of 1–2 m^2 at a depth of 1–2 m were selected for the in situ exposure of mussels. Thus, replication in this experiment was fivefold.

At the center of each of the 15 patches, 5 mussels (pseudoreplicates) in a mesh bag were attached to a float at ~20 cm from the bottom. Prior to deployment, a mark was set on the edge of the mussel shells with a rotary tool grinder (Dremel Multi-pro, U.S.A.). After 5 weeks of deployment (19 August 2013 to 23 September 2013), the distance between the mark and the new shell edge was measured with a Vernier calliper. We refrained from assessing a change in wet weight here, since this metric is prone to changes unrelated to growth (gut content, mantle water content, gonad maturation, etc.).

During the deployment phase, seawater sampling in the 15 patches was performed by snorkelling twice a week, at dusk (11 events, between 19:00 and 20:30 h, depending on seasonal shift of sunset) and the following dawn (10 events, between 6:00 and 7:00 h, depending on seasonal shift of sunrise). Immediately after sampling, $[\text{O}_2]$ was measured with a WTW Oximeter ProfiLineOxi 3315 equipped with a FDO 925 sensor (WTW, Germany), salinity and voltage for pH_T assessment were measured using a Mettler-Toledo (USA) SG 7/8 equipped with the InLab 731 conductivity sensor and the Expert Pro pH sensor, and temperature was recorded from the thermistor integrated in the O_2 probe. Additionally, seston (food for mussels) was determined by taking a seawater sample of 200 mL at each patch and time point, filtering it through a pre-weighed GF/F filter and drying it at 60°C until constant weight. The filtered seawater was used for TA determination.

The voltage recorded by the pH sensor in the field was converted into pH_T after Dickson et al. (2007) by comparing the voltage of the sample at the field temperature with the voltage of a homemade TRIS pH_T buffer at salinity 15 measured in the same week at GEOMAR at the same temperature, and assuming Nernstian behavior (–59 mV/pH unit) of the electrode (Saderne and Wahl 2013).

Macrophyte habitat - transects

Water samples were collected along two 10 m transects from the outer rim to the center of a *Fucus* meadow in Kiel Fjord just north of Mönkeberg marina (N54°21'22" E10°10'43") on 30 May 2013 and 31 May 2013. The weather was calm and sunny with a gentle breeze from NNE (wind speed 4–5 m s^{-1}) and wavelets. Both transects started 12 m (ca. 0.7 m deep) and ended 2 m (ca. 0.3 m deep) from the shore. The distance between the two replicate transects was 20 m. On both days water samples were taken at 15:00 h and at 5:00 h (i.e., around the expected maximum and minimum peaks of pH, respectively, as driven by photosynthesis and respiration in the *Fucus* dominated community). Water samples were taken with glass jars 20–30 cm above the sea

floor at each meter along the transects. Jars were opened and closed underwater at the spot of sampling. Temperature and pH_{NBS} (Mettler Toledo Seven Multi + InLab Expert Pro) were measured in the jars within 15 min after sampling.

On 07 June 2013, calcification and respiration rates of *M. edulis* (in addition to temperature and pH_{NBS}) were measured in waters from five spots along the same two transects at 15:00 h. The day was sunny, however with substantially more water movement (along-shore wind NNE, 5–10 m s^{-1}) than on the day of the previous samplings (offshore wind SE, 2–7 m s^{-1}) and water exchange in the *Fucus* stand was presumably more intense. Water samples were collected as described above and five small mussels (ca 2 cm shell length) were placed in each jar and incubated for 1 h in 450 mL water. Before and after the incubation, in each jar oxygen and pH were measured and a 50 mL water sample was taken for TA measurements just before and after the calcification period.

Data analysis and statistics

In order to compare the effect of the alga-modulated seawater on mussel calcification, the differences between day and night calcification rates were transformed to Log Effect Ratios, i.e., Log (day calcification divided by night calcification). All data were checked for normal distribution and homogeneity of variance prior to testing.

The effects of acidification, its modulation by light (day, night) and of density of *Fucus* (position) in the laboratory experiment were analyzed in a 3-way-ANOVA followed by Tukeys HSD posthoc tests. The influence of increasing simulated *Fucus* density on the proportional partitioning of calcification between day and night calcification was analyzed by linear regression, separately for acidified and non-acidified conditions.

Calcification rates in the benthocosm experiment were analyzed in a 3-way-ANOVA including the factors headspace $p\text{CO}_2$ (ambient/high), temperature (ambient, high) and daytime (day, night). Growth of mussels in the field patch experiment were analyzed by an ANOVA with one factor (“habitat”) and three levels (Sand, *Zostera*, *Fucus*).

The calcification rate of mussels at different positions in the *Fucus* transects were not analyzed since these were not sufficiently replicated (2 transects only) for an ANOVA. We plotted the trend only.

Results

Across all laboratory experiments, mussel calcification, on average, increased by 40% ($1 \mu\text{mol CaCO}_3 \text{ g}^{-1} \text{ h}^{-1}$) when pH increases by half of a unit (e.g., from 7.8 to 8.3, Fig. 2, calcification rate = $2.12 * \text{pH} - 14.96$, $r^2 = 0.49$, $p < 0.0001$). In all experiments (laboratory, benthocosms, field) presented here, mean pH ranged from 7.73 (laboratory experiment, high CO_2 , without *Fucus*) to 9.03 (benthocosms, low $\text{CO}_2 \times$ low temperature, with *Fucus*), with day-night amplitudes ranging

from 0.1 (without *Fucus*) to more than 1 pH unit (inner zone of the in situ *Fucus* bed; Fig. 3). As a general trend across all experiments, mean pH and the amplitude of diurnal pH fluctuations increased with increasing *Fucus* biomass to water volume ratio (Figs. 2, 3). Additionally, in the benthocosms the diurnal amplitude of pH_{NBS} fluctuations driven by the biology of the macroalgae was larger by 24% under acidified conditions as compared to non-acidified conditions (Wilcoxon paired *t*-test, $n = 7$, $t = 3.72$, $p < 0.01$).

Laboratory experiment

The replicate sequence of the five aquaria connected in a flow through system (Fig. 1) in the laboratory experiment is henceforth referred to as aquarium #1 to #5 downstream beginning with the aquarium that contained no thallus (“aquarium #1”) and followed by four aquaria with one *Fucus* thallus each (“aquarium #2 - #5”). Both, pH and calcification varied between day and night, between low and high $p\text{CO}_2$ treatment and with upstream *Fucus* biomass (Fig. 2, Supporting Information Table 2a). After 12 h of light, pH_{NBS} increased from 7.74 ± 0.05 (mean \pm SD, aquarium #1) along the series of *Fucus* to 8.50 ± 0.05 (aquarium #5) in the high CO_2 treatment ($1120 \mu\text{atm } p\text{CO}_2$). In the ambient CO_2 treatment ($400 \mu\text{atm } p\text{CO}_2$) pH increased from 8.08 ± 0.04 (aquarium #1) to 8.54 ± 0.06 (aquarium #5) (Fig. 4). The pH_{NBS} values in the high and ambient CO_2 treatments were almost indistinguishable in aquaria #3 to #5 (Fig. 4). After 12 h of incubation in the dark, only a weak (not statistically significant) decrease in pH_{NBS} was observed along the series of *Fucus* (i.e., with increasing *Fucus* “patch size”) in both CO_2 treatments. Changes in $p\text{CO}_2$ and Ω_{Ca} (Fig. 4) mirrored, as usual, changes in pH across treatments, and undersaturation (< 1) with regard to Ω_{Ca} was only reached under high CO_2 treatments in the absence of *Fucus* (aquaria #1) and during night incubations in all high CO_2 aquaria. Remarkably, under high CO_2 in the light treatment, $p\text{CO}_2$ dropped below the aquarium #1 level of the ambient treatment already in aquarium #2 ($456 \pm 116 \mu\text{atm}$). After 12 h of “day” incubation, Ω_{Ca} increased from a slightly undersaturated level (0.97 ± 0.09) in aquarium #1 to a highly saturated level (4.71 ± 0.39) in aquarium #5, in the high CO_2 treatment. Oxygen concentration of the seawater increased under “day” conditions with increasing number of *Fucus* thalli conditioning the water, whereas measured values of the “night” incubation remained close to the start level.

Increasing *Fucus* biomass in the series of aquaria could have affected mussel calcification by two impacts on the CO_2 system: (1) under light conditions, it raised the mean pH_{NBS} (and Ω_{Ca}) from 8.1 (2.1) to 8.25 (5.5) in the ambient CO_2 treatment and from 7.7 (1.0) to 8.1 (5.2) in the high CO_2 treatment (Figs. 2, 4; aquarium #5), (2) it imposed circadian fluctuations of pH_{NBS} with amplitudes increasing from 0.14 (aquarium #1) to 0.63 (aquarium #5) in the series of non-acidified aquaria and from 0.1 (aquarium #1) to 0.9

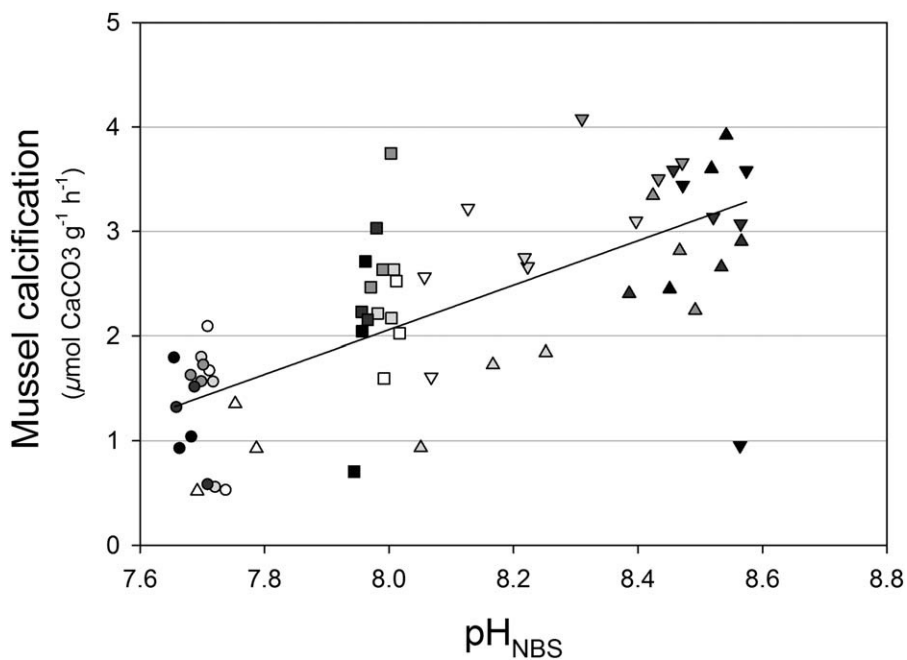


Fig. 2. Mussel calcification in response to pH_{NBS} . Represented are the calcification rates measured in the 30 laboratory aquaria subjected to the various treatment combinations (acidification \times daytime \times number of upstream *Fucus*). Triangle pointing upwards: hi pCO_2 at day time, triangles pointing downwards: lo pCO_2 at day time, dots: hi pCO_2 at night time, squares: lo pCO_2 at night time, filling: shading darkens with increasing algal biomass. Regression: $y = -15 + 2.13 \cdot x$, $R^2 = 0.49$, $p < 0.0001$).

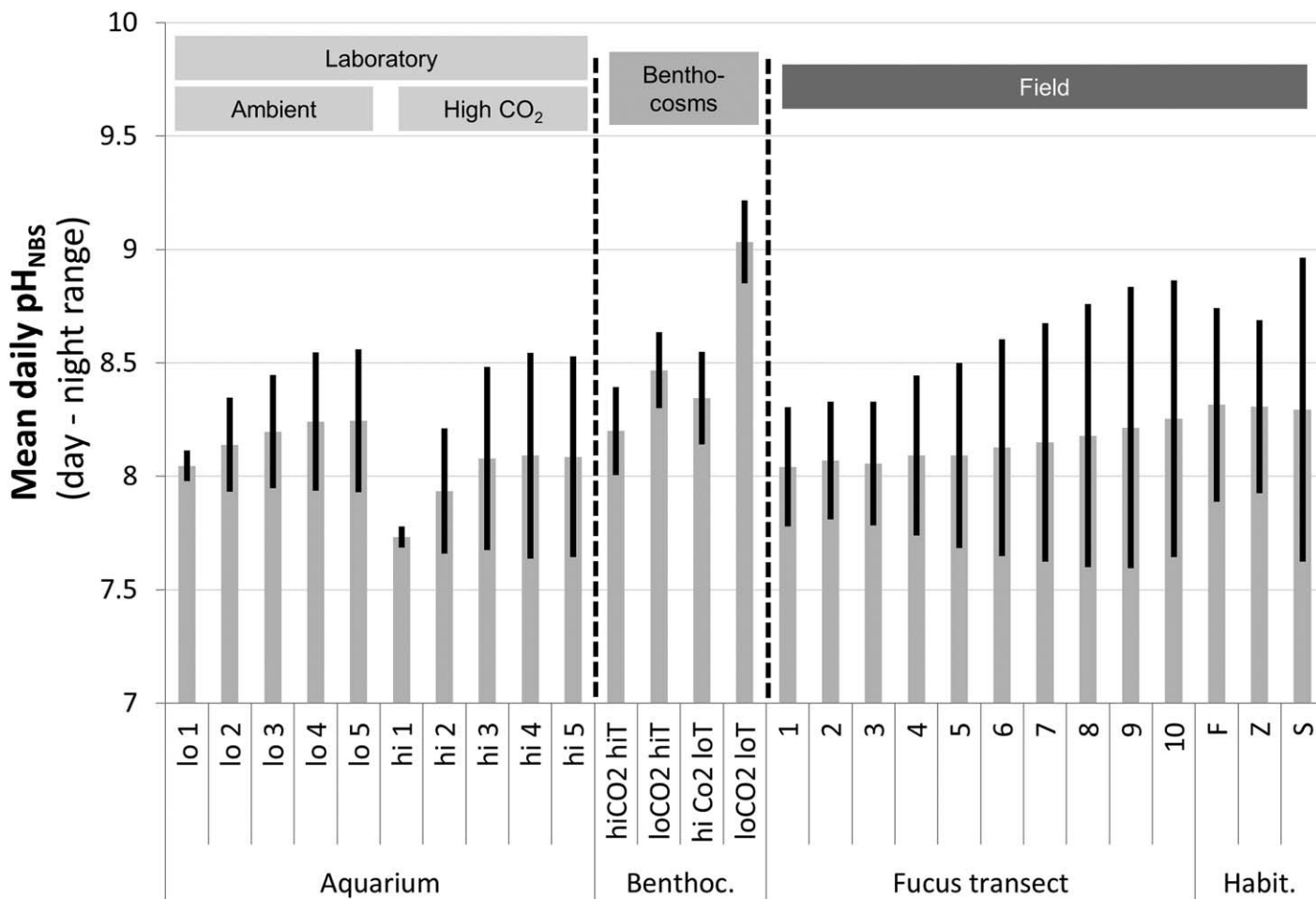


Fig. 3. pH_{NBS} conditions in the laboratory, benthocosm and field experiments. Depicted are the overall mean and the average day-night amplitude over the duration of the respective experiments (pH_T values measured for the habitats *Fucus* (F), *Zostera* (Z) and Sand (S) were converted to the NBS scale by adding 0.14 pH units).

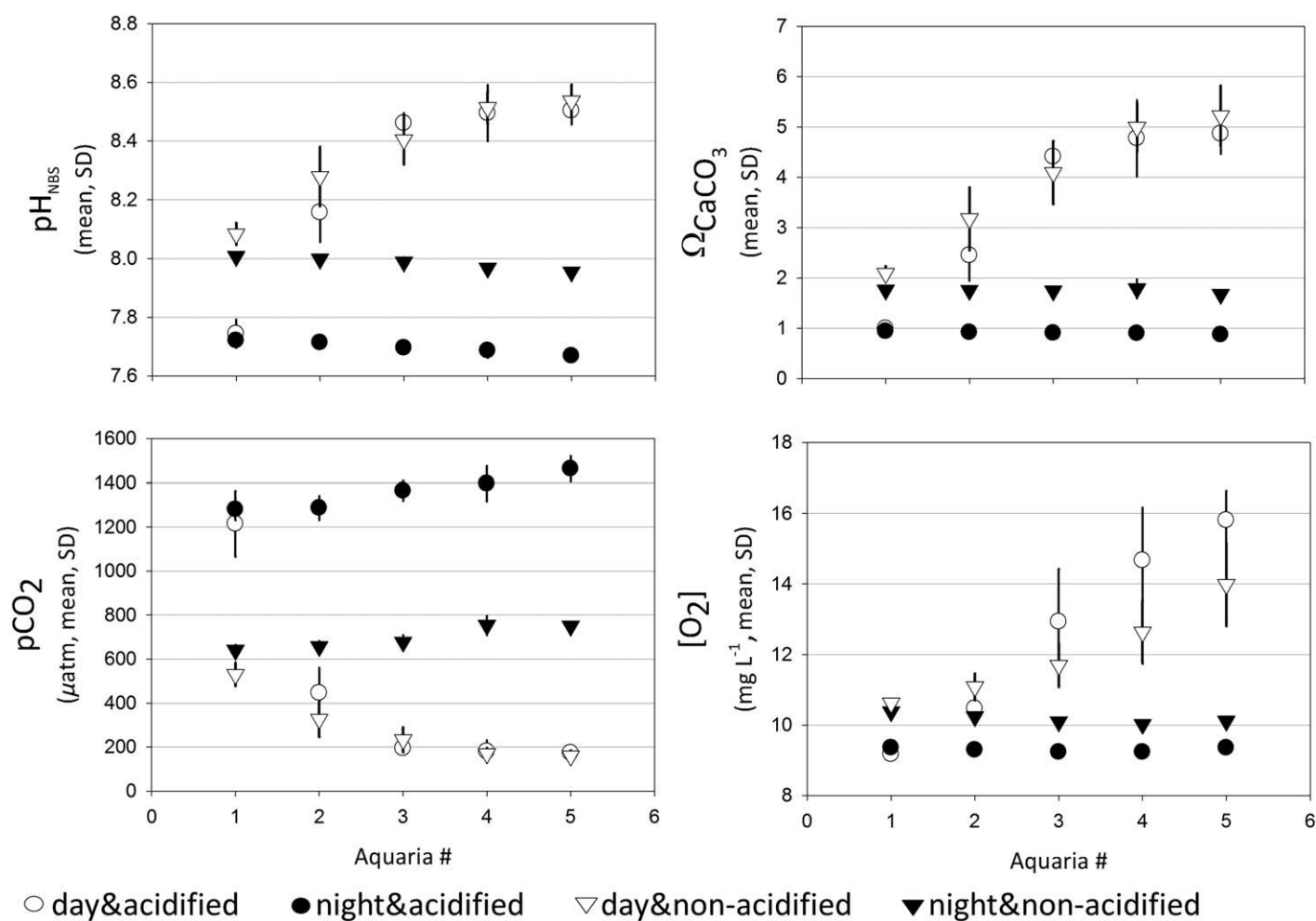


Fig. 4. Abiotic conditions regarding pH_{NBS} , pCO_2 , O_2 concentration and Ω_{Ca} in the series of aquaria subjected to acidified ($1120 \mu\text{atm pCO}_2$, dots) and non-acidified ($400 \mu\text{atm pCO}_2$, triangles) conditions during day time (light, white symbols) and night time (dark, black symbols). The serial aquaria at positions 2 through 5 contained one *Fucus* each so that the water in these aquaria were conditioned by 1, 2, 3, and 4 bladder wrack individuals, respectively, simulating a transect from outside into a *Fucus* stand.

(aquarium #5) in the acidified aquaria (Fig. 3). Mussel calcification was significantly lower under night conditions and under acidified conditions (Fig. 5; Table 1, Supporting Information Tables 2b, 3). At ambient conditions, calcification tended to peak at intermediate *Fucus* density (Fig. 5A), but this relation was not significant (polynomial regression; day: adj $R^2 = 0.64$, $p > 0.05$; night: adj. $R^2 = 0.73$, $p > 0.05$). At acidified conditions, in contrast, calcification increased linearly and significantly (linear regression, $R^2 = 0.91$, $p < 0.05$) with increasing *Fucus* density at daytime but not at night-time conditions (Fig. 5B). Likewise, the cumulated 24 h-calcification increased significantly with *Fucus* density (Fig. 5B). The presence of *Fucus* entirely compensated the impact of acidification from aquarium #3 onwards (overlapping CIs in Fig. 5, Supporting Information Table 3). Furthermore, time of day and the number of upstream *Fucus* interacted

significantly as compensation of the acidification was mainly visible during day time: In the high CO_2 treatment of the “day” incubation, net calcification increased significantly ca 3.5-fold from $0.93 \pm 0.42 \mu\text{mol CaCO}_3 \text{ gDW}^{-1} \text{ h}^{-1}$ in aquarium #1 to $3.32 \pm 0.77 \mu\text{mol CaCO}_3 \text{ gDW}^{-1} \text{ h}^{-1}$ in aquarium #5. During “night” incubation, net calcification was generally low, independent of the downstream position. Again, from aquarium #3 onwards, day calcification was significantly larger than night calcification under acidified conditions (non-overlap of CIs in Fig. 5B) whereas under non-acidified conditions only in aquarium #4 this difference was significant. Differences in calcification rates between day and night (displayed as Log Effect Ratios in Fig. 6) were larger in the high CO_2 treatment than under ambient CO_2 conditions in all but the first two positions and this difference increased along the series of increasing *Fucus* biomass substantially

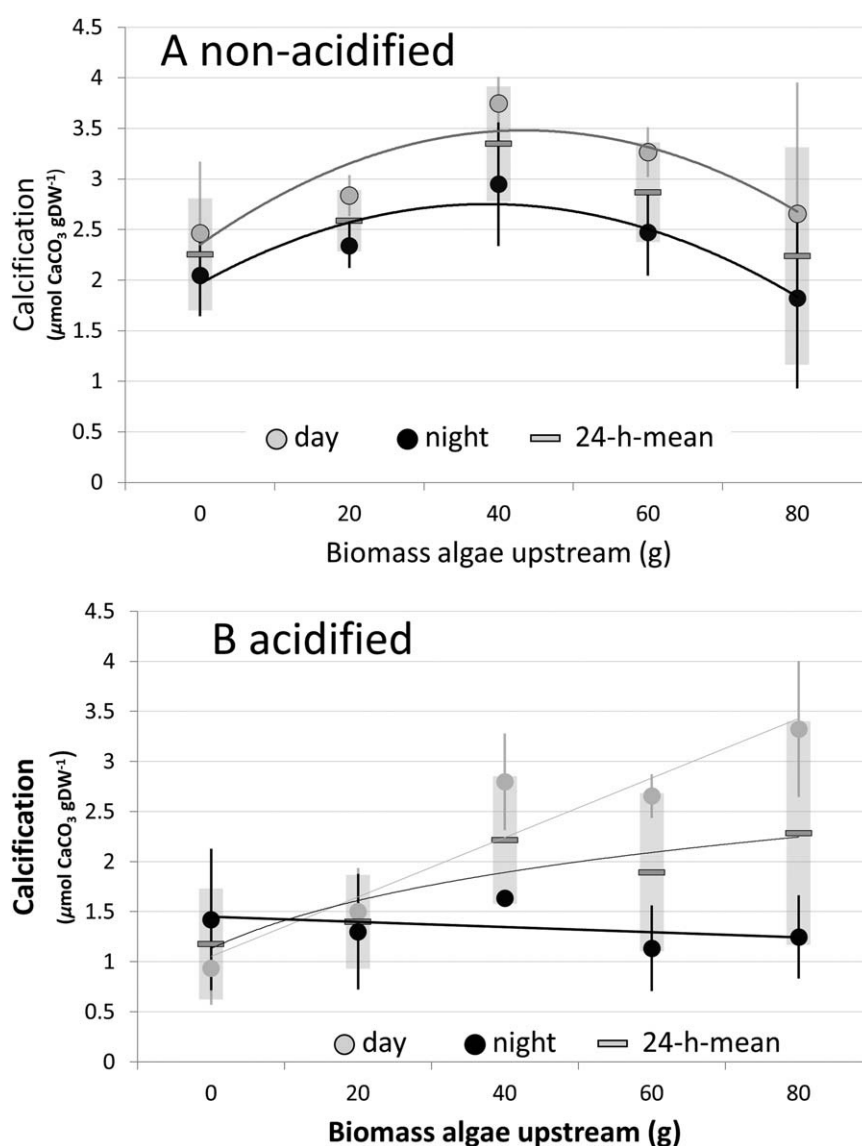


Fig. 5. Mussel calcification (means \pm CI) under non-acidified (**A**) and acidified (**B**) conditions during daytime (light gray dots and CIs), night time (black dots and CIs) and as daily mean (dark gray bars and transparent gray CIs). The serial aquaria at positions 2 through 5 contained one *Fucus* each so that the water in these aquaria were conditioned by 1, 2, 3, and 4 bladder wrack individuals, respectively, simulating a transect from outside into a *Fucus* stand. Regressions: Non-acidified day (panel **A**, gray line, $y = 2.34 + 0.052x - 0.0006x^2$, $R^2 = 0.76$, $p = 0.1$), non-acidified night (panel **A**, black line, $y = 1.965 + 0.41x - 0.0005x^2$, $R^2 = 0.86$, $p = 0.07$), acidified day (panel **B**, gray line, $y = 1.055 + 0.03x$, $R^2 = 0.9$, $p < 0.01$), acidified night (panel **B**, black line, $y = 1.45 - 0.003x$, $R^2 = 0.186$, $p = 0.47$), acidified 24-h-mean (panel **B**, dashed dark gray line, $y = -0.0135x + 1.253$, $R^2 = 0.76$, $p = 0.054$).

faster under acidified (slope of 0.15) than under non-acidified conditions (slope of 0.022) ($p < 0.05$, Fig. 6, Supporting Information Table 4).

Benthocosm experiment

During the Benthocosm experiment in June 2013 (details in Wahl et al. 2015a,b, monitored system data in Pangaea doi: 10.1594/PANGAEA.842739), temperature in the warm treatments ranged between 17°C and 23°C with typical day-night amplitudes of approximately 2°C (Supporting Information Fig. 1a). In the cold treatment temperature ranged between 12°C

and 17°C, again with day-night amplitudes of about 2°C. Under the CO₂ enriched headspace, water pH_{NBS} was consistently lower by 0.1 to 0.5 pH_{NBS} units compared to the ambient CO₂ treatment (Supporting Information Fig. 1b). The day-night amplitude of the pH_{NBS} fluctuations driven by photosynthesis-respiration cycles was larger under acidified (~ 0.6 pH_{NBS} units) than under non-acidified conditions (~ 0.4 pH_{NBS} units). Calcification (Fig. 7; Table 2) was significantly reduced by about 40% in the acidification treatment. In addition, calcification was significantly reduced by about 60% during the night as compared to daytime calcification rates.

Table 1. Three-factorial ANOVA on mussel calcification in the lab experiment in response to three factors, i.e., acidification level (“ $p\text{CO}_2$ ”, acidified, non-acidified), daytime (day, night) and position in the simulated transect into a *Fucus* belt (“Aqu#”1 through 5). All three factors affect calcification significantly with a significant interaction between daytime and position. Effects with p -values in bold are significant.

Effect	SS	Df	MS	F	p
Intercept	297.5272	1	297.5272	739.9119	0.000000
Day,night	9.1650	1	9.1650	22.7923	0.000024
$p\text{CO}_2$	11.2407	1	11.2407	27.9541	0.000005
Aqu #	7.7763	4	1.9441	4.8347	0.002822
Day,night* $p\text{CO}_2$	0.1915	1	0.1915	0.4763	0.494078
Day,night*Aqu #	4.4747	4	1.1187	2.7820	0.039503
$p\text{CO}_2$ *Aqu #	3.1959	4	0.7990	1.9869	0.115036
Day,night* $p\text{CO}_2$ *Aqu #	2.1329	4	0.5332	1.3261	0.276929
Error	16.0845	40	0.4021		

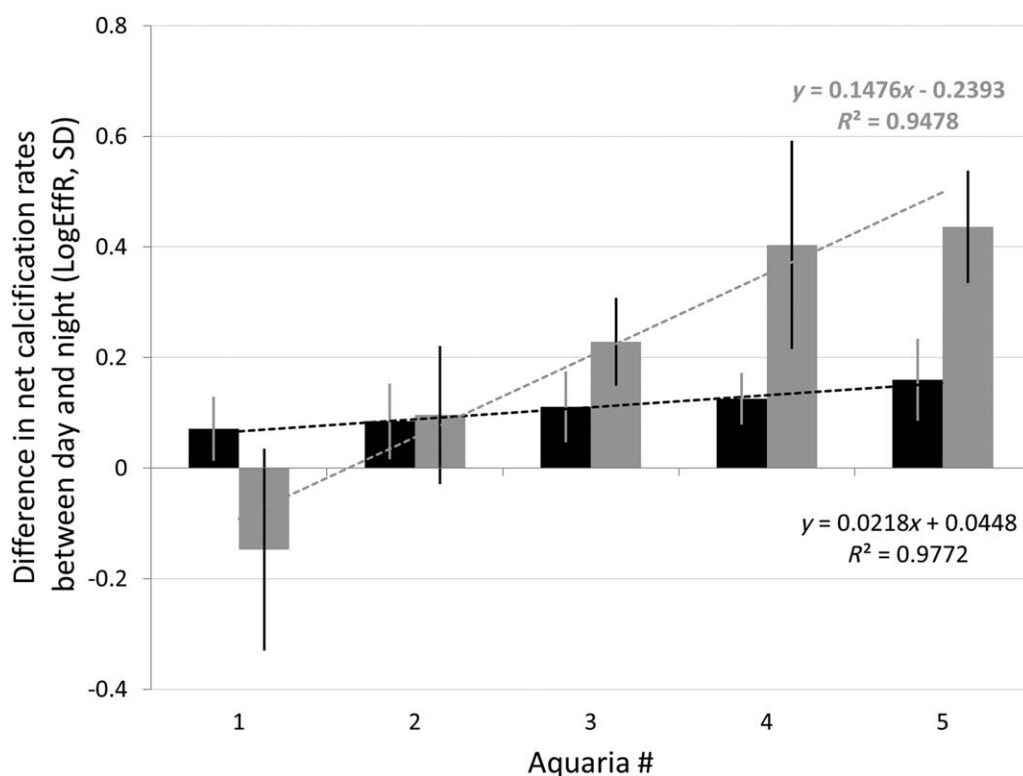


Fig. 6. Differences between calcification rates in day vs. night time under acidified (gray bars) and non-acidified (black bars) conditions. The ratio of day-to-night calcification is expressed as log response ration where a value of 1 means that calcification is 10 times stronger during daytime than during nighttime, a value of -1 means that the former is 10 times weaker. Under non-acidified conditions the increasing *Fucus* biomass does not affect the day-to-night ratio substantially. In contrast, under acidified conditions daytime calcification becomes increasingly important with increasing *Fucus* biomass.

Warming did not affect calcification and the three factors ($p\text{CO}_2$, temperature, day vs. night) did not significantly interact.

Field study

Macrophyte patches

The three habitat types (*Fucus* patches, *Zostera* patches, sand patches) turned out to be very similar considering seston, temperature, salinity, as well as with regard to daily mean and

day-night fluctuations of oxygen and pH (Fig. 8, Supporting Information Fig. 2). While temperature, salinity, and seston did not exhibit substantial day-night fluctuations, oxygen and pH were consistently higher during the day as compared to the night in all three habitat types. During the experimental run of 35 d, mussel length (mean, SD) increased by 2.2 ± 0.4 mm ($6.6\% \pm 0.7\%$) in the *Zostera* patches, by 2.8 ± 0.9 mm ($8.3\% \pm 1.0\%$) in the sand patches and by 2.6 ± 0.7 mm

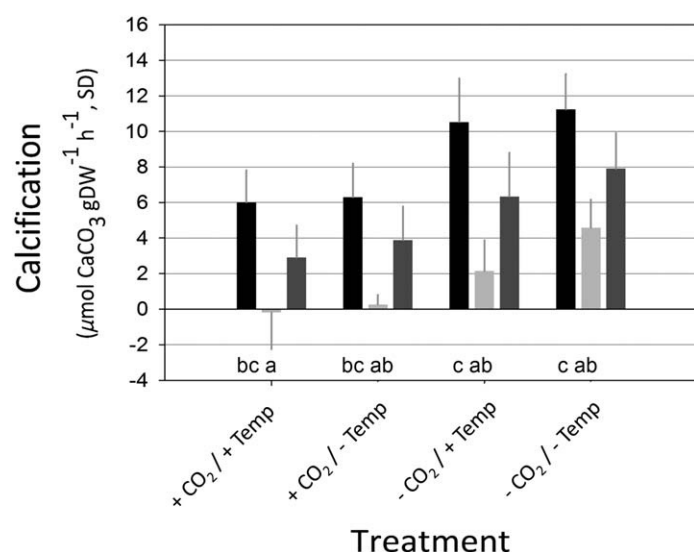


Fig. 7. Calcification rates in the benthocosms during daytime (black), night time (light gray) and averaged over 24 h (dark gray). Day and night calcification not sharing the same letters are significantly different. Error bars represent SD.

(7.7% ± 0.9%) in the *Fucus* patches (Fig. 8B). There was no significant effect of habitat type on mussel growth (ANOVA, $df = 2$, $F = 0.80$, $p = 0.475$).

Macrophyte transect

On the calm and sunny day along the transect from the outer rim (position #1) to the inner zone (position #9) of the *Fucus* belt, strong and opposite pH gradients were found during the day and night samplings, respectively. During day, pH_{NBS} increased from 8.30 outside to 8.83 10 m inside the *Fucus* belt (Fig. 9). During night, pH_{NBS} decreased from pH_{NBS} 7.78 outside to pH_{NBS} 7.59 10 m inside the belt. The amplitude of day-night pH_{NBS} fluctuations was 0.5 pH_{NBS} units outside the *Fucus* habitat, while in the inner part of the belt the pH_{NBS} reached an amplitude of 1.2 units. At the end of a sunny day, $[O_2]$ increased to 12 mg L⁻¹ at the outer edge and to 15 mg L⁻¹ in the inner part of the belt. After a calm night, $[O_2]$ had decreased to about 9 mg L⁻¹ (outside the belt) and to 6.5 mg L⁻¹ (at the inner part of the belt).

On the windy day of calcification measurements, the gradients in daylight pH_{NBS} along the transect were substantially less steep (Fig. 9). Nonetheless, changes in pH_{NBS} along the transect explained 52% of the variation in calcification rates but, due to large variation, this trend is not significant (Fig. 10; $df = 5$, $F = 3.27$, $p > 0.05$).

Discussion

Fluctuations in environmental variables have recently been suggested to alter the magnitude and/or direction of the effects caused by superimposed long-term changes (e.g., Cornwall et al. 2014; Gunderson et al. 2016; Wahl et al.

Table 2. Three-factorial ANOVA on mussel calcification in the benthocosm experiment with the factors acidification (“ pCO_2 ,” acidified, non-acidified), warming (“ T° ,” ambient, warmed by 5°C) and daytime (“night-day,” day, night). Acidification and daytime affect calcification significantly, without any interaction among the three factors. Effects with p -values in bold are significant.

Effect	SS	df	MS	F	p
Intercept	230517.7	1	230517.7	159.4726	<0.001
pCO_2	35803.1	1	35803.1	24.7687	0.000166
T°	2083.5	1	2083.5	1.4414	0.248531
Night-day	102346.7	1	102346.7	70.8037	<0.001
$pCO_2 * T^\circ$	785.2	1	785.2	0.5432	0.472484
$pCO_2 * \text{night-day}$	1113.4	1	1113.4	0.7703	0.393975
$T^\circ * \text{night-day}$	514.1	1	514.1	0.3557	0.559812
$pCO_2 * T^\circ * \text{night-day}$	342.8	1	342.8	0.2372	0.633295
Error	21682.5	15	1445.5		

2016). It is important to distinguish in this context between extreme events and fluctuations. The former are sporadic disturbances (e.g., Wernberg et al. 2013) which may have ecosystem-wide effects because they are unlikely to allow for acclimation or adaptation. The latter rather represent recurrent excursions from the mean with alternating phases of high stress and recovery which may alter global change effects at the organismic scale (e.g., Gunderson et al. 2016) and in the long run facilitate a “hardening” of populations (e.g., Pansch et al. 2014). The main goal of the investigations presented here was to investigate macrophyte-driven biogenic fluctuations of the seawater carbonate system at different scales, and to determine their influence on calcification rates and growth of the blue mussel *M. edulis*. We show that the diurnal photosynthesis/respiration cycles of macrophytes produce fluctuations of the carbonate system that, at least at small scales (dm to m), facilitated calcification even under acidified conditions, particularly so during daytime. The concurrently fluctuating $[O_2]$ may have contributed to beneficial daytime conditions since anti-stress mechanisms are supposed to be energy- and, thus, O_2 -demanding (e.g., Ramajo et al. 2016) but this effect was not in focus of this study.

Macrophytes modulate seawater carbonate chemistry

The metabolism (photosynthesis and respiration) of macrophytes cause diurnal DIC fluctuations together with fluctuations of other carbonate system parameters (e.g., pCO_2 , pH) in the surrounding seawater. Day-night amplitudes of such fluctuations may exceed one pH unit in dense macrophyte stands (Middelboe and Hansen 2007; Pajusalu et al. 2013; Saderne and Wahl 2013; Hurd 2015; all experiments here as shown in Fig. 3) but are strongly scale-dependent (Wahl et al. 2016 and references therein). The amplitude of biogenic diurnal pH fluctuations increases with algal biomass as evidenced along the aquaria series and along the in situ

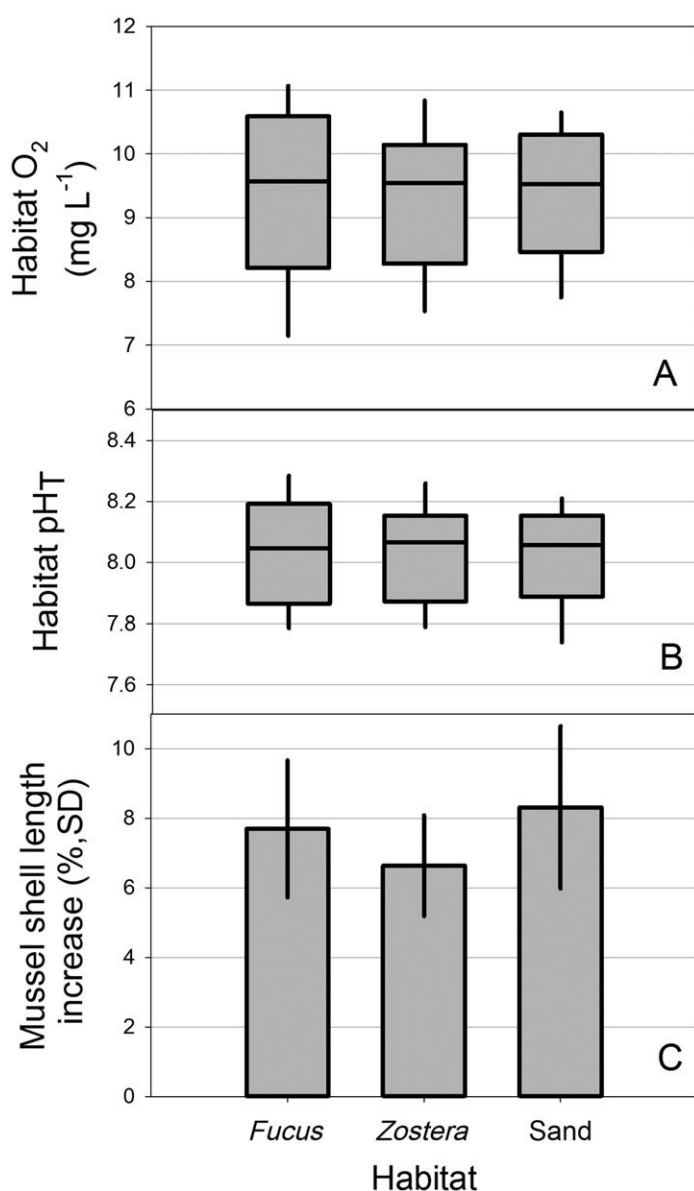


Fig. 8. Oxygen (A) and pH_T (B) conditions in the three microhabitats (as median, 25–75 percentiles, and 10–90 percentiles). The *Fucus*, *Zostera* and sand patches did not differ significantly in mean values but the *Fucus* habitats tends to vary most. Mussel growth (C) expressed as the increase in shell length (+SD) over the duration of the in situ experiment. Growth of mussel did not differ among the microhabitats.

transect into a *Fucus* belt (Fig. 3). We here demonstrate that biogenic activity may impact the carbonate system stronger than predicted future increase in pCO_2 means: Both in the laboratory tanks and in the benthocosm experiment, the amplitude of biogenic day-night fluctuations exceeded the (simulated) shift in seawater pH predicted for the end of the century (Fig. 3, Supporting Information Fig. 1b). The laboratory experiment illustrated how the pH drop caused by elevated pCO_2 levels was completely masked by only two *Fucus* individuals upstream of the mussel (i.e., in aquarium #3,

Fig. 4). Photosynthesis/respiration cycles of the macroalgae also incurred diurnal fluctuations in $[O_2]$ (e.g., by 7 mg L^{-1} in the large *Fucus* belt, Fig. 9) and an overall slight shift in mean pH (e.g., by 0.2 units along the aquaria series, Fig. 3). At this point, our data do not permit to clearly disentangle the impact of these aspects of macroalgal activity on mussel calcification.

Macrophytes may offer daytime refuge from OA

High levels of seawater pCO_2 associated with decreased pH can reduce mussel calcification (Gazeau et al. 2013; Thomsen et al. 2015 and Fig. 2). Reduced calcification may entail slower growth and/or higher predation risk jeopardizing mussel survival (Enderlein et al. 2003; Thomsen et al. 2013) if they do not adapt in time to the predicted acidification. When considering the results it should be noted that the experiments were too short to allow for any adaptation on the side of the mussels. Other recent transgenerational experiments suggest, however, that such an adaptation to OA could require numerous generations in *M. edulis* (Thomsen et al. 2017). In the present study, a decrease of the mean pH by half a unit (caused by a pCO_2 increase to $1120 \mu\text{atm}$, as predicted for the end of the century in some scenarios [IPCC 2013]), reduced mussel calcification by about 40% (Fig. 2). This effect was, however, partly mitigated by biogenic pH modulation in the system. In all of our experiments, from the laboratory to the field, the presence and activity of macrophytes increased the overall *mean* pH by 0.01 to 0.2 units (Figs. 3,4,9,10), which per se, should be beneficial to mean calcification of mussels (Gazeau et al. 2013; Thomsen et al. 2015) and other organisms (Kroeker et al. 2010; Cyronak et al. 2016). Similar beneficial effects by primary producers were reported by some tropical studies showing that photosynthesizing macrophytes could mitigate the negative impact of OA on marine calcifiers such as corals at the habitat scale (Kleypas et al. 2011; Manzello et al. 2012; Unsworth et al. 2012; Jokiel et al. 2014). In addition to the increase of the mean pH, the substantial diurnal fluctuations in pH, pCO_2 , and Ω_{Ca} represented phases favorable (daytime) or adverse (nighttime) to calcification. The mussels proved capable of benefitting from these temporal refuges from acidification stress and maintained high calcification by shifting a major portion of this process to the photosynthesis dominated periods (i.e., daytime: Fig. 6). Thus, the presence of *Fucus* enhanced mussel calcification, especially so under OA conditions, twofold to threefold (laboratory experiment, Fig. 5). Based on the numerical relation between pH and calcification rates (Fig. 2) the rise of *mean* pH_{NBS} along the series of aquaria by 0.35 pH_{NBS} units should increase calcification by $0.74 \mu\text{mol CaCO}_3 \text{ g DW}^{-1} \text{ h}^{-1}$. Instead it increased by $1.1 \mu\text{mol CaCO}_3 \text{ g DW}^{-1} \text{ h}^{-1}$ from aquarium 1 to aquarium 5. These additional 49% of calcification should be attributable to the biogenic fluctuations and the conspicuous increase of calcification under favorable

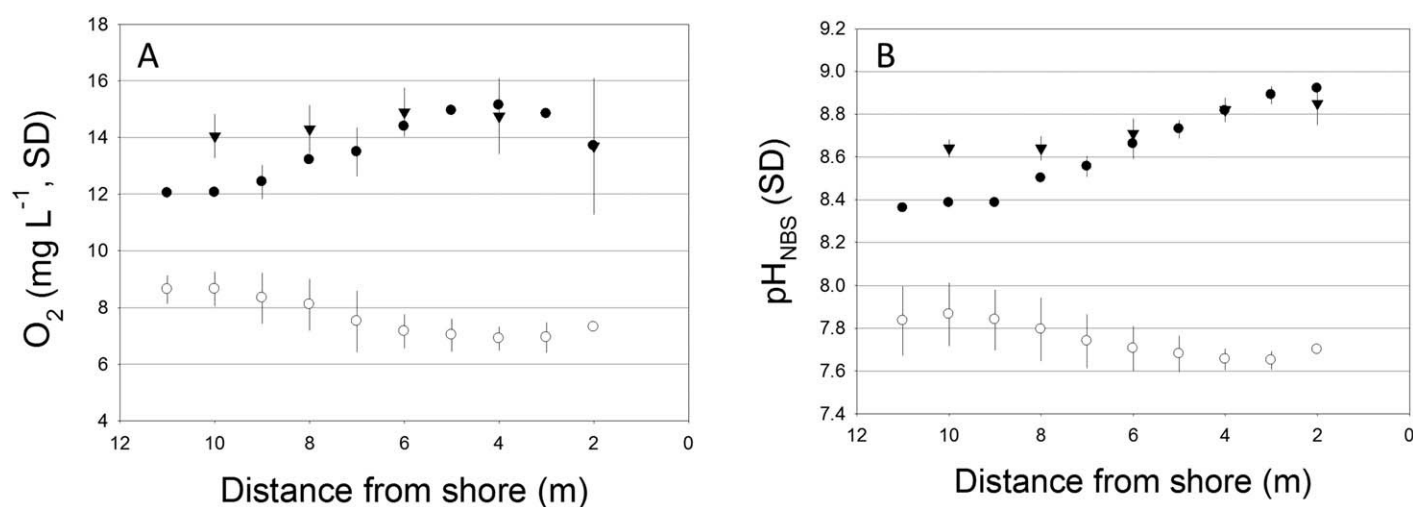


Fig. 9. Oxygen (A) and pH_{NBS} (B) profile through a *Fucus* belt from outside (12 m offshore) to deep into the belt (2 m offshore) under calm conditions daytime = black dots, night-time = white dots) and on a windy day (black triangles).

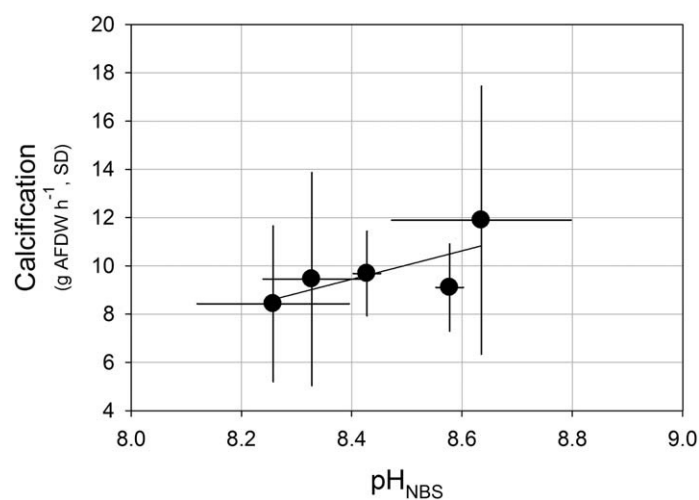


Fig. 10. Calcification of mussels under different pH_{NBS} conditions along the transect into a *Fucus* belt.

conditions produced by photosynthesis during daytime – especially so under acidification (Fig. 6). Under ambient $p\text{CO}_2$ conditions and in the absence of macrophyte-induced pH fluctuations, mussels calcified at similar rates during day- and night-time (laboratory experiment, Fig. 5), indicating that *M. edulis* does not feature an internal circadian rhythm in calcification. Why mussel calcification under non-acidified conditions peaked at intermediate algal density cannot be explained at present.

In a review article, Hofmann and Todgham (2010) emphasize the importance of physiological plasticity as a strategy of marine organisms to cope with changing environmental conditions such as acidification and heat stress. Regarding calcification, “physiological plasticity” means a reallocation of resources needed for biomineralization. This

should be facilitated if the available resources, e.g., food, are abundant as described for mussels in a eutrophied habitat (Thomsen et al. 2013). The already prevalent and in some regions still progressing nutrient enrichment in many coastal areas may increase phytoplankton density, thus mitigate the impact of ongoing acidification for plankton-feeding calcifiers (Ramajo et al. 2016). However, intensified plankton blooms may, in the course of sedimentation and remineralization, also lead to hypoxia of deeper water, which, when upwelled, may stress organisms by low [O₂], high $p\text{CO}_2$ and H₂S and low pH conditions (Melzner et al. 2013). Here, we did not quantify day-time vs. night-time concentrations of plankton since fluctuations at this high frequency are likely to be buffered by the mussel’s energy storage capacity. In the field, seston concentrations were similar in all microhabitats (Supporting Information Fig. 1).

Beneficial effects of macrophytes on calcifiers were described before. Semesi et al. (2009) demonstrated for the calcifying algae *Hydrolithon* sp., *Mesophyllum* sp. and *Halimeda* sp. that calcification was favored by the vicinity of seagrass driving substantial diurnal pH fluctuations with amplitudes of up to 1 pH unit. Also, the coralline alga *Arthrocardia corymbosa* calcified more and grew better at OA conditions when a thick diffusive boundary layer protected the alga’s surface at low-flow conditions, likely by enhancing daytime pH (Cornwall et al. 2014). In an acidification experiment, Saderne and Wahl (2013) showed that calcifying epibionts located in the thin (< 1 mm) diffusive boundary layer sheeting *Fucus serratus* thalli which displays strong diurnal pH and [O₂] fluctuations (e.g., Hurd 2015; Wahl et al. 2016), maintain growth and calcification even under high levels of $p\text{CO}_2$ (1200 μatm). In contrast to our observation, Cornwall et al. (2013) describe how pH fluctuations reduce growth and recruitment of a coralline alga both under acidified and

non-acidified conditions. In the Cornwall study, however, the pH changes were chemically (not biologically) induced and instantaneous (instead of gradual) and may not be comparable to the more sinusoidal fluctuations of pH (and $p\text{CO}_2$, $[\text{O}_2]$, Ω) imposed by biological processes in the field.

Macrophyte density and hydrodynamics mediate the biogenic refuge

In the relatively large *Fucus* belt (ca 20 m wide in an onshore-offshore direction and 200 m along shore), on calm and sunny days (field study, Fig. 9), biogenic fluctuations in pH were similar to or slightly larger than those found in the laboratory experiment (aquarium #5; Fig. 4) and in the benthocosm system (Supporting Information Fig. 1b). This is a result of the high biomass to seawater ratio, typical of shallow macroalgal habitats (Bjork et al. 2004; Middelboe and Hansen 2007; Pajusalu et al. 2013) in the absence of strong water movement. Fluctuations just outside the *Fucus* belt offshore were presumably caused by plankton activity mainly, whereas inside the *Fucus* habitat, both plankton and macrophytes contributed to the diurnal fluctuations. Overall, differences in pH between day and night ranged from 0.3 to 1.2 pH units (Fig. 3). This amplitude is similar to findings in field studies of Middelboe and Hansen (2007) and Pajusalu et al. (2013) who described diurnal amplitudes of about 1 pH unit for *Fucus* dominated macroalgal fields of the Baltic Sea, but higher than those of Saderne and Wahl (2013) who reported a mean diurnal amplitude in pH of 0.3 in a Baltic *Fucus* belt. Vertical gradients in pH already occur within the upper centimetres in a shallow macroalgae-dominated habitat (Middelboe and Hansen 2007; Krause-Jensen et al. 2015). Our study complements these observations by adding the factor of a horizontal pH gradient at the scale of meters (field study, Fig. 9). Comparing the $[\text{O}_2]$ and pH gradient into the belt on a calm (water movement estimated at 1 cm/s) and on a more windy day (water movement estimated at 3–5 cm/s, Fig. 9), illustrates how much the amplitude of the biogenic fluctuations depend on the biomass to water volume ratio. Such flow velocity dependency of a biogenic pH gradient was shown at a smaller scale, i.e., in the diffusive boundary layer of macrophytes, by Cornwall et al. (2014) and Wahl et al. (2016). In the small habitat patches of *Zostera* and *Fucus* ($\sim 1\text{--}2\text{ m}^2$), we did not detect a significant impact of the macrophytes on the carbonate chemistry (field study; Fig. 8A) and, consequently, with regard to mussel growth (field study; Fig. 8B). It is likely that the selected habitats were too small and the biomass to water volume ratio too little to substantially alter the carbonate system of the surrounding seawater. The high load of seston (i.e., mussel food; $\sim 8\text{ mg L}^{-1}$) during this field experiment could have contributed to the uniformly good growth of mussels in all habitat patches (Thomsen et al. 2013; Ramajo et al. 2016). Similarly to our findings, Middelboe and Hansen (2007) and Pajusalu et al. (2013) reported that fluctuations in CO_2 and

pH are less pronounced in a patchy habitat than in densely covered macrophyte meadows. Thus, both laboratory and field experiment illustrate how biogenic mitigation of acidification can be important at the m-scale while depending strongly on the macrophyte biomass to water volume ratio, i.e., water exchange in the macrophyte habitat.

Interacting effects of OA and warming

The human-induced shift in $p\text{CO}_2$ and oceanic mean pH is often superimposed by warming effects – the other (first known) side of the CO_2 problem (IPCC 2013). While the CO_2 treatment of the benthocosm experiment impacted calcification rates of *M. edulis*, temperature had no effect, neither alone nor in combination with the CO_2 treatment. Long-term experiments on *M. edulis* revealed that growth was not significantly affected by temperatures below 25°C and below seawater $p\text{CO}_2$ of $1600\ \mu\text{atm}$ in combined acidification and warming treatments (Hiebenthal et al. 2013; Keppel et al. 2015). In other studies, however, exposure to warming substantially reduced shell strength of the mussels (Mackenzie et al. 2014).

Macrophytes can increase their metabolic activity under elevated levels of CO_2 (Fig. 4; Falkenberg et al. 2013; Graiff et al. 2015a) but may suffer severely from ocean warming when passing a certain threshold temperature (Graiff et al. 2016). The performance of macrophytes under the combination of acidification, warming and eutrophication—probable future scenarios for many coastal regions—may be severely jeopardized by filamentous epiphytes thriving under these conditions (Werner et al. 2016a,b) and depriving their *Fucus* host of light and nutrients (Wahl 2008). Macrophyte decline would certainly reduce the calcification window of mussels. It seems likely, that the favorable effect of *Fucus* for mussel calcification and future acidification may be important in all seasons except summer when macroalgae tend to be increasingly stressed by warm temperatures and proliferating epiphytes (Werner and Matthiessen 2013; Graiff et al. 2015b).

Conclusions

The common macroalga *F. vesiculosus* has the capacity to raise mean pH in its vicinity and to provoke strong diurnal fluctuation of $[\text{O}_2]$, $p\text{CO}_2$, pH and Ω_{Ca} driven by its photosynthesis/respiration cycle. The calcification of the mussel *M. edulis* decreases with pH (and associated shifts in the carbonate system). Acidification impacts on mussel calcification may be neutralized by the alga-driven shifts and fluctuations of the carbonate system. Both traits of the carbonate system shifts, increased mean pH and enhanced amplitude of diurnal pH fluctuations contribute to the enhancement of calcification. The strength of this beneficial effect, however, relates to the ratio of algal biomass to water volume and in our series of experiments decreases from the laboratory over the benthocosms to the field.

Thus, *Mytilus*—and likely other calcifiers—can temporarily find refuge from future OA by increased mean pH and

pH variability already a few meters into a macrophyte belt. This ecological refuge offered by macrophyte habitats may, however, change in the course of future multifactorial change in two contrasting scenarios (see Graiff et al. 2015a; Werner et al. 2016a,b): (1) On-going CO₂ increase and progressing eutrophication in many coastal areas (but see Andersen et al. 2017 for recent signs of trend reversal in the Baltic Sea) fertilize macroalgae (Gutow et al. 2014; Graiff et al. 2015a,b), increase the biomass to water ratio at a local scale and, thus, benefit calcifiers (but see Britton et al. 2016). At the same time, eutrophication may lead to denser plankton. This may have two contrasting effects on the OA-macrophyte-calcifier interactions. The shading by plankton may reduce the beneficial effect on calcifiers of the macrophyte-driven diel fluctuations of pH and the slight rise of its mean. At the same time plankton blooms may indirectly enhance the prevalence of stressful hypoxic conditions in upwelling waters. On the other hand, the increased supply of suspended food renders calcifying filter feeders more robust to OA (e.g., Thomsen et al. 2013; Ramajo et al. 2016). (2) If *Fucus* benefits less from pCO₂ and nutrient increase than its epiphytes and/or consumption by mesograzers is strongly enhanced by ocean warming (e.g., Werner et al. 2016b) macroalgal biomass may decrease and progressive OA would continuously narrow the time window in which calcification by mussels is still possible. This capacity of macroalgae to mitigate stress such as hypoxia and low pH associated with summer upwelling events (Melzner et al. 2013), should be a further motivation for the protection of coastal macroalgal habitats which are increasingly endangered by various anthropogenic factors such as coastal construction, dredging, harvesting or eutrophication (Wahl et al. 2015b).

References

- Andersen, J. H., and others. 2017. Long-term temporal and spatial trends in eutrophication status of the Baltic sea. *Biol. Rev.* **92**: 135–149. doi:10.1111/brv.12221
- Beer, S., M. Mtolera, T. Lyimo, and M. Björk. 2006. The photosynthetic performance of the tropical seagrass *Halophila ovalis* in the upper intertidal. *Aquat. Bot.* **84**: 367–371. doi:10.1016/j.aquabot.2005.11.007
- Binzer, T., and K. Sand-Jensen. 2002. Importance of structure and density of macroalgae communities (*Fucus serratus*) for photosynthetic production and light utilisation. *Mar. Ecol. Prog. Ser.* **235**: 53–62. doi:10.3354/meps235053
- Björk, M., L. Axelsson, and S. Beer. 2004. Why is *Ulva intestinalis* the only macroalga inhabiting isolated rockpools along the Swedish atlantic coast? *Mar. Ecol. Prog. Ser.* **284**: 109–116. doi:10.3354/meps284109
- Bleich, M., and others. 2008. Kiel CO₂ manipulation experimental facility (KICO₂). Second Symposium on the Ocean in a High-CO₂ World.
- Bostrom, C., and E. Bonsdorff. 1997. Community structure and spatial variation of benthic invertebrates associated with *Zostera marina* (L) beds in the northern baltic sea. *J. Sea Res.* **37**: 153–166.
- Bostrom, C., and E. Bonsdorff. 2000. Zoobenthic community establishment and habitat complexity - the importance of seagrass shoot-density, morphology and physical disturbance for faunal recruitment. *Mar. Ecol. Prog. Ser.* **205**: 123–138. doi:10.3354/meps205123
- Boyd, P. W., C. E. Cornwall, A. Davison, S. C. Doney, M. Fourquez, C. L. Hurd, I. D. Lima, and A. McMinn. 2016. Biological responses to environmental heterogeneity under future ocean conditions. *Glob. Chang. Biol.* **22**: 2633–2650. doi:10.1111/gcb.13287
- Britton, D., C. E. Cornwall, A. T. Revill, C. L. Hurd, and C. R. Johnson. 2016. Ocean acidification reverses the positive effects of seawater pH fluctuations on growth and photosynthesis of the habitat-forming kelp, *Ecklonia radiata*. *Sci. Rep.* **6**: 26036, pp 1–10. doi:10.1038/srep26036
- Buapet, P., M. Gullström, and M. Björk. 2013. Photosynthetic activity of seagrasses and macroalgae in temperate shallow waters can alter seawater pH and total inorganic carbon content at the scale of a coastal embayment. *Mar. Freshw. Res.* **64**: 1040–1048. doi:10.1071/MF12124
- Clark, H. R., and C. J. Gobler. 2016. Diurnal fluctuations in CO₂ and dissolved oxygen concentrations do not provide a refuge from hypoxia and acidification for early-life-stage bivalves. *Mar. Ecol. Prog. Ser.* **558**: 1–14. doi:10.3354/meps11852
- Cornwall, C. E., C. D. Hepburn, C. M. McGraw, K. I. Currie, C. A. Pilditch, K. A. Hunter, P. W. Boyd, and C. L. Hurd. 2013. Diurnal fluctuations in seawater pH influence the response of a calcifying macroalga to ocean acidification. *Proc. R. Soc. B Biol. Sci.* **280**: 1–8. doi:10.1098/rspb.2013.2201
- Cornwall, C. E., P. W. Boyd, C. M. McGraw, C. D. Hepburn, C. A. Pilditch, J. N. Morris, A. M. Smith, and C. L. Hurd. 2014. Diffusion boundary layers ameliorate the negative effects of ocean acidification on the temperate coralline macroalga *Arthrocardia corymbosa*. *PLoS ONE* **9**: e97235. doi:10.1371/journal.pone.0097235
- Cornwall, C. E., C. A. Pilditch, C. D. Hepburn, and C. L. Hurd. 2015. Canopy macroalgae influence understory corallines' metabolic control of near-surface pH and oxygen concentration. *Mar. Ecol. Prog. Ser.* **525**: 81–95. doi:10.3354/meps11190
- Cyronak, T., K. G. Schulz, and P. L. Jokiel. 2016. The omega myth: What really drives lower calcification rates in an acidifying ocean. *ICES J. Mar. Sci.* **73**: 558–562. doi:10.1093/icesjms/fsv075
- Dalbeck, P., J. England, M. Cusack, M. R. Lee, and A. E. Fallick. 2006. Crystallography and chemistry of the calcium carbonate polymorph switch in *M. edulis* shells. *Eur. J. Mineral.* **18**: 601–609. doi:10.1127/0935-1221/2006/0018-0601

- Dickson, A. G. 1990. Standard potential of the reaction $\text{AgCl(s)} + 1/2\text{H}_2\text{(g)} = \text{Ag(s)} + \text{HCl(aq)}$ and the standard acidity constant of the ion HSO_4^- in synthetic sea-water from 273.15-k to 318.15-k. *J. Chem. Thermodyn.* **22**: 113–127. doi:10.1016/0021-9614(90)90074-Z
- Dickson, A. G., J. D. Afghan, and G. C. Anderson. 2003. Reference materials for oceanic CO_2 analysis: A method for the certification of total alkalinity. *Mar. Chem.* **80**: 185–197. doi:10.1016/S0304-4203(02)00133-0
- Dickson, A. G., C. L. Sabine, and J. R. Christian. (eds.). 2007. Guide to best practices for ocean CO_2 measurements. PICES Special Publication 3, 191 pp.
- Doney, S. C., V. J. Fabry, R. A. Feely, and J. A. Kleypas. 2009. Ocean acidification: The other CO_2 problem. *Ann. Rev. Mar. Sci.* **1**: 169–192. doi:10.1146/annurev.marine.010908.163834
- Duarte, C. M., and others. 2013. Is ocean acidification an open-ocean syndrome? Understanding anthropogenic impacts on seawater pH. *Estuaries Coast.* **36**: 221–236. doi:10.1007/s12237-013-9594-3
- Durr, S., and M. Wahl. 2004. Isolated and combined impacts of blue mussels (*Mytilus edulis*) and barnacles (*Balanus improvisus*) on structure and diversity of a fouling community. *J. Exp. Mar. Biol. Ecol.* **306**: 181–195. doi:10.1016/j.jembe.2004.01.006
- Enderlein, P., S. Moorthi, H. Rohrscheidt, and M. Wahl. 2003. Optimal foraging versus shared doom effects: Interactive influence of mussel size and epibiosis on predator preference. *J. Exp. Mar. Biol. Ecol.* **292**: 231–242. doi:10.1016/S0022-0981(03)00199-0
- Enderlein, P., and M. Wahl. 2004. Dominance of blue mussels versus consumer-mediated enhancement of benthic diversity. *J. Sea Res.* **51**: 145–155. doi:10.1016/j.seares.2003.05.006
- Fabry, V. J., B. A. Seibel, R. A. Feely, and J. C. Orr. 2008. Impacts of ocean acidification on marine fauna and ecosystem processes. *ICES J. Mar. Sci.* **65**: 414–432. doi:10.1093/icesjms/fsn048
- Falkenberg, L., D. R. Bayden, and S. D. Connell. 2013. Contrasting resource limitations of marine primary producers: Implications for competitive interactions under enriched CO_2 and nutrient regimes. *Oecologia* **172**: 575–583. doi:10.1007/s00442-012-2507-5
- Feely, R. A., C. L. Sabine, K. Lee, W. Berelson, J. Kleypas, V. J. Fabry, and F. J. Millero. 2004. Impact of anthropogenic CO_2 on the CaCO_3 system in the oceans. *Science* **305**: 362–366. doi:10.1126/science.1097329
- Findlay, H. S., Y. Artioli, J. Moreno Navas, S. J. Hennige, L. C. Wicks, V. A. Huvenne, E. M. Woodward, and J. M. Roberts. 2013. Tidal downwelling and implications for the carbon biogeochemistry of cold-water corals in relation to future ocean acidification and warming. *Glob. Chang. Biol.* **19**: 2708–2719. doi:10.1111/gcb.12256
- Frieder, C. A., J. P. Gonzalez, E. E. Bockmon, M. O. Navarro, and L. A. Levin. 2014. Can variable pH and low oxygen moderate ocean acidification outcomes for mussel larvae? *Glob. Chang. Biol.* **20**: 754–764. doi:10.1111/gcb.12485
- Gazeau, F., L. M. Parker, S. Comeau, J. P. Gattuso, W. A. O'Connor, S. Martin, H. O. Pörtner, and P. M. Ross. 2013. Impacts of ocean acidification on marine shelled molluscs. *Mar. Biol.* **160**: 2207–2245. doi:10.1007/s00227-013-2219-3
- Graiff, A., and others. 2015a. Effects of warming and acidification on a benthic community in the Baltic Sea - Kiel Benthocosms. *Eur. J. Phycol.* **50**: 89–90. doi:10.3389/fmars.2015.00112
- Graiff, A., D. Liesner, U. Karsten, and I. Bartsch. 2015b. Temperature tolerance of western baltic sea *Fucus vesiculosus* – growth, photosynthesis and survival. *J. Exp. Mar. Biol. Ecol.* **471**: 8–16. doi:10.1594/PANGAEA.842937
- Graiff, A., J. F. Pantoja, F. Tala, and M. Thiel. 2016. Epibiont load causes sinking of viable kelp rafts: Seasonal variation in floating persistence of giant kelp *Macrocystis pyrifera*. *Mar. Biol.* **163**: 191–205. doi:10.1007/s00227-016-2962-3
- Grasshoff, K. 1983. Methods of seawater analysis. Verlag Chemie GmbH, D-6940 Weinheim, doi:10.1002/iroh.19850700232
- Gray, S. E. C., M. D. Degrandpre, C. Langdon, and J. E. Corredor. 2012. Short-term and seasonal pH, pCO_2 and saturation state variability in a coral-reef ecosystem. *Global Biogeochem. Cycles* **26**: 1–13. doi:10.1029/2011GB004114
- Gunderson, A. R., E. J. Armstrong, and J. H. Stillman. 2016. Multiple stressors in a changing world: The need for an improved perspective on physiological responses to the dynamic marine environment. *Annu. Rev. Mar. Sci.* **8**: 357. doi:10.1146/annurev-marine-122414-033953
- Gutow, L., M. M. Rahman, K. Bartl, R. Saborowski, I. Bartsch, and C. Wiencke. 2014. Ocean acidification affects growth but not nutritional quality of the seaweed *Fucus vesiculosus* (Phaeophyceae, Fucales). *J. Exp. Mar. Biol. Ecol.* **453**: 84–90. doi:10.1016/j.jembe.2014.01.005
- Harvey, B. P., D. Gwynn-Jones, and P. J. Moore. 2013. Meta-analysis reveals complex marine biological responses to the interactive effects of ocean acidification and warming. *Ecol. Evol.* **3**: 1016–1030. doi:10.1002/ece3.516
- Hendriks, I. E., Y. S. Olsen, L. Ramajo, L. Basso, A. Steckbauer, T. S. Moore, J. Howard, and C. M. Duarte. 2014. Photosynthetic activity buffers ocean acidification in seagrass meadows. *Biogeosciences* **11**: 333–346. doi:10.5194/bg-11-333-2014
- Hiebenthal, C., E. E. R. Philipp, A. Eisenhauer, and M. Wahl. 2013. Effects of seawater pCO_2 and temperature on shell growth, shell stability, condition and cellular stress of western Baltic Sea *Mytilus edulis* (L.) and *Arctica islandica* (L.). *Mar. Biol.* **160**: 2073–2087. doi:10.1007/s00227-012-2080-9
- Hofmann, G. E., J. P. Barry, P. J. Edmunds, R. D. Gates, D. A. Hutchins, T. Klinger, and M. A. Sewell. 2010. The effect of ocean acidification on calcifying organisms in marine ecosystems: An organism-to-ecosystem perspective. *Annu. Rev. Ecol. Evol. Syst.* **41**: 127–147.
- Hofmann, G. E., and A. E. Todgham. 2010. Living in the now: Physiological mechanisms to tolerate a rapidly

- changing environment. *Annu. Rev. Physiol.* **72**: 127–145. doi:10.1146/annurev-physiol-021909-135900
- Hofmann, G. E., and others. 2011. High-frequency dynamics of ocean pH: A multi-ecosystem comparison. *PLoS ONE* **6**: e28983. doi:10.1371/journal.pone.0028983
- Hurd, C. L. 2015. Slow-flow habitats as refugia for coastal calcifiers from ocean acidification. *J. Phycol.* **51**: 599–605. doi:10.1111/jpy.12307
- Hurd, C. L., C. E. Cornwall, K. Currie, C. D. Hepburn, C. M. McGraw, K. A. Hunter, and P. W. Boyd. 2011. Metabolically induced pH fluctuations by some coastal calcifiers exceed projected 22nd century ocean acidification: A mechanism for differential susceptibility? *Glob. Chang. Biol.* **17**: 3254–3262. doi:10.1111/j.1365-2486.2011.02473.x
- Invers, O., J. Romero, and M. Perez. 1997. Effects of pH on sea-grass photosynthesis: A laboratory and field assessment. *Aquat. Bot.* **59**: 185–194. doi:10.1016/S0304-3770(97)00072-7
- IPCC. 2013. *Climate change 2013: The physical science basis.*
- Johannesson, K., K. Smolarz, M. Grahn, and C. Andre. 2011. The future of baltic sea populations: Local extinction or evolutionary rescue? *Ambio* **40**: 179–190. doi:10.1007/s13280-010-0129-x
- Jokiel, P. L., C. P. Jury, and S. R. Ku'ulei. 2014. Coral-algae metabolism and diurnal changes in the CO₂-carbonate system of bulk sea water. *PeerJ* **2**: e378. doi:10.7717/peerj.378x
- Kautsky, H., L. Kautsky, N. Kautsky, U. Kautsky, and C. Lindblad. 1992. Studies on the *Fucus vesiculosus* community in the Baltic sea. *Acta Phytogeogr. Suec.* **78**: 33–48.
- Kautsky, L., and N. Kautsky. 2000. The baltic sea, including Bothnian sea and Bothnian bay.
- Keppel, E. A., R. A. Scrosati, and S. C. Courtenay. 2015. Interactive effects of ocean acidification and warming on subtidal mussels and sea stars from atlantic Canada. *Mar. Biol. Res.* **11**: 337–348. doi:10.1080/17451000.2014.932914
- Kleypas, J. A., K. R. N. Anthony, and J. P. Gattuso. 2011. Coral reefs modify their seawater carbon chemistry - case study from a barrier reef (Moorea, French Polynesia). *Glob. Chang. Biol.* **17**: 3667–3678. doi:10.1111/j.1365-2486.2011.02530.x
- Krause-Jensen, D., C. M. Duarte, I. E. Hendriks, L. Meire, M. E. Blicher, N. Marbà, and M. K. Sejr. 2015. Macroalgae contribute to nested mosaics of pH variability in a subarctic fjord. *Biogeosciences* **12**: 4895–4911. doi:10.5194/bg-12-4895-2015
- Krause-Jensen, D., and C. M. Duarte. 2016. Substantial role of macroalgae in marine carbon sequestration. *Nat. Geosci.* **9**: 737–742.
- Krause-Jensen, D., N. Marbà, M. Sanz-Martin, I. E. Hendriks, J. Thyrring, J. Carstensen, M. K. Sejr, and C. M. Duarte. 2016. Long photoperiods sustain high pH in arctic kelp forests. *Sci. Adv.* **2**: e1501938. doi:10.1126/sciadv.1501938
- Kroeker, K. J., R. L. Kordas, R. N. Crim, and G. G. Singh. 2010. Meta-analysis reveals negative yet variable effects of ocean acidification on marine organisms. *Ecol. Lett.* **13**: 1419–1434. doi:10.1111/j.1461-0248.2010.01518.x
- Mackenzie, C. L., G. A. Ormondroyd, S. F. Curling, R. J. Ball, N. M. Whiteley, and S. K. Malham. 2014. Ocean warming, more than acidification, reduces shell strength in a commercial shellfish species during food limitation. *Plos One* **9**: e86764. doi:10.1371/journal.pone.0086764
- Manzello, D. P., I. C. Enochs, N. Melo, D. K. Gledhill, and E. M. Johns. 2012. Ocean acidification refugia of the Florida reef tract. *Plos One* **7**: e41715. doi:10.1371/journal.pone.0041715
- Melzner, F., M. A. Gutowska, M. Langenbuch, S. Dupont, M. Lucassen, M. C. Thorndyke, M. Bleich, and H.-O. Pörtner. 2009. Physiological basis for high CO₂ tolerance in marine ectothermic animals: Pre-adaptation through lifestyle and ontogeny? *Biogeosciences* **6**: 2313–2331. doi:10.5194/bg-6-2313-2009
- Melzner, F., J. Thomsen, W. Koeve, A. Oschlies, M. A. Gutowska, H. W. Bange, H. P. Hansen, and A. Körtzinger. 2013. Future ocean acidification will be amplified by hypoxia in coastal habitats. *Mar. Biol.* **160**: 1875–1888. doi:10.1007/s00227-012-1954-1
- Middelboe, A. L., and P. J. Hansen. 2007. High pH in shallow-water macroalgal habitats. *Mar. Ecol. Prog. Ser.* **338**: 107–117. doi:10.3354/meps338107
- Millero, F. J., T. B. Graham, F. Huang, H. Bustos-Serrano, and D. Pierrot. 2006. Dissociation constants of carbonic acid in seawater as a function of salinity and temperature. *Mar. Chem.* **100**: 80–94. doi:10.1016/j.marchem.2005.12.001
- Müller, J. D., B. Schneider, and G. Rehder. 2016. Long-term alkalinity trends in the Baltic sea and their implications for CO₂-induced acidification. *Limnol. Oceanogr.* **61**: 1984–2002. doi:10.1002/lno.10349
- Myrberg, K., and O. Andrejev. 2003. Main upwelling regions in the Baltic sea - a statistical analysis based on three-dimensional modelling. *Boreal Environ. Res.* **8**: 97–112.
- Nagelkerken, I., B. D. Russell, B. M. Gillanders, and S. D. Connell. 2016. Ocean acidification alters fish populations indirectly through habitat modification. *Nat. Clim. Chang.* **6**: 89. doi:10.1038/nclimate2757
- Orr, J. C., and others. 2005. Anthropogenic ocean acidification over the twenty-first century and its impact on calcifying organisms. *Nature* **437**: 681–686. doi:10.1038/nature04095
- Pajusalu, L., G. Martin, and A. Pollumae. 2013. Results of laboratory and field experiments of the direct effect of increasing CO₂ on net primary production of macroalgal species in brackish-water ecosystems. *Proc. Estonian Acad. Sci.* **62**: 148–154. doi:10.3176/proc.2013.2.09
- Pansch, C., I. Schaub, J. Havenhand, and M. Wahl. 2014. Habitat traits and food availability determine the response of marine invertebrates to ocean acidification. *Glob. Chang. Biol.* **20**: 765–777. doi:10.1111/gcb.12478
- Perez-Llorens, J. L., F. G. Brun, J. Andria, and J. J. Vergara. 2004. Seasonal and tidal variability of environmental

- carbon related physico-chemical variables and inorganic carbon acquisition in *Gracilaria longissima* and *Enteromorpha intestinalis* from Los Torufios salt marsh (Cadiz bay, Spain). *J. Exp. Mar. Biol. Ecol.* **304**: 183–201. doi:10.1016/j.jembe.2003.12.003
- Pierrot, D., E. Lewis, and D. Wallace. 2006. Ms excel program developed for CO₂ system calculations. Carbon Dioxide Information Analysis Center.
- Price, N. N., T. R. Martz, R. E. Brainard, and J. E. Smith. 2012. Diel variability in seawater pH relates to calcification and benthic community structure on coral reefs. *Plos One* **7**: e43843. doi:10.1371/journal.pone.0043843
- Ramajo, L., and others. 2016. Food supply confers calcifiers resistance to ocean acidification. *Sci. Rep.* **6**: 19374. doi:10.1038/srep19374
- Reusch, T. B. H., A. R. O. Chapman, and J. P. Groger. 1994. Blue mussels *Mytilus-edulis* do not interfere with eelgrass *Zostera-marina* but fertilize shoot growth through biodeposition. *Mar. Ecol. Prog. Ser.* **108**: 265–282. doi:10.3354/meps108265
- Saderne, V., P. Fietzek, and P. M. J. Herman. 2013. Extreme variations of pCO₂ and pH in a macrophyte meadow of the Baltic sea in summer: Evidence of the effect of photosynthesis and local upwelling. *Plos One* **8**: e62689. doi:10.1371/journal.pone.0062689
- Saderne, V., and M. Wahl. 2013. Differential responses of calcifying and non-calcifying epibionts of a brown macroalga to present-day and future upwelling pCO₂. *Plos One* **8**: e70455. doi:10.1371/journal.pone.0070455
- Semesi, I. S., S. Beer, and M. Björk. 2009. Seagrass photosynthesis controls rates of calcification and photosynthesis of calcareous macroalgae in a tropical seagrass meadow. *Mar. Ecol. Prog. Ser.* **382**: 41–47. doi:10.3354/meps07973
- Shamberger, K. E. F., R. A. Feely, C. L. Sabine, M. J. Atkinson, E. H. DeCarlo, F. T. Mackenzie, P. S. Drupp, and D. A. Butterfield. 2011. Calcification and organic production on a Hawaiian coral reef. *Mar. Chem.* **127**: 64–75. doi:10.1016/j.marchem.2011.08.003
- Shaw, E. C., B. I. McNeil, and B. Tilbrook. 2012. Impacts of ocean acidification in naturally variable coral reef flat ecosystems. *J. Geophys. Res.* **117**: C03038. doi:10.1029/2011JC007655
- Smith, J. E., N. N. Price, C. E. Nelson, and A. F. Haas. 2013. Coupled changes in oxygen concentration and pH caused by metabolism of benthic coral reef organisms. *Mar. Biol.* **160**: 2437–2447. doi:10.1007/s00227-013-2239-z
- Thomsen, J., and others. 2010. Calcifying invertebrates succeed in a naturally CO₂-rich coastal habitat but are threatened by high levels of future acidification. *Biogeosciences* **7**: 3879–3891. doi:10.5194/bg-7-3879-2010
- Thomsen, J., I. Casties, C. Pansch, A. Kortzinger, and F. Melzner. 2013. Food availability outweighs ocean acidification effects in juvenile *Mytilus edulis*: Laboratory and field experiments. *Glob. Chang. Biol.* **19**: 1017–1027. doi:10.1111/gcb.12109
- Thomsen, J., K. Haynert, K. M. Wegner, and F. Melzner. 2015. Impact of seawater carbonate chemistry on the calcification of marine bivalves. *Biogeosciences* **12**: 4209–4220. doi:10.5194/bg-12-4209-2015
- Thomsen, J., L. S. Stapp, K. Haynert, H. Schade, M. Danelli, G. Lannig, K. M. Wegner, and F. Melzner. 2017. Naturally acidified habitat selects for ocean acidification-tolerant mussels. *Sci. Adv.* **3**: e1602411. doi:10.1126/sciadv.1602411
- Torn, K., D. Krause-Jensen, and G. Martin. 2006. Present and past depth distribution of bladderwrack (*Fucus vesiculosus*) in the Baltic sea. *Aquat. Bot.* **84**: 53–62. doi:10.1016/j.aquabot.2005.07.011
- Truchot, J. P., and A. Duhamel-Jouve. 1980. Oxygen and carbon dioxide in the marine intertidal environment: Diurnal and tidal changes in rockpools. *Respir. Physiol.* **39**: 241–254. doi:10.1016/0034-5687(80)90056-0
- Unsworth, R. K. F., C. J. Collier, G. M. Henderson, and L. J. McKenzie. 2012. Tropical seagrass meadows modify seawater carbon chemistry: Implications for coral reefs impacted by ocean acidification. *Environ. Res. Lett.* **7**: 24026–24034. doi:10.1088/1748-9326/7/2/024026
- Vinther, H. F., J. S. Laursen, and M. Holmer. 2008. Negative effects of blue mussel (*Mytilus edulis*) presence in eelgrass (*Zostera marina*) beds in Flensborg fjord, Denmark. *Estuar. Coast. Shelf Sci.* **77**: 91–103. doi:10.1016/j.ecss.2007.09.007
- Wahl, M. 2008. Ecological lever and interface ecology: Epibiosis modulates the interactions between host and environment. *Biofouling* **24**: 427–438. doi:10.1080/08927010802339772
- Wahl, M., and others. 2015a. A mesocosm concept for the simulation of near-natural shallow underwater climates: The Kiel Outdoor Benthocosms (KOB). *Limnol. Oceanogr.: Methods* **13**: 651–663. doi:10.1002/lom3.10055
- Wahl, M., and others. 2015b. The responses of brown macroalgae to environmental change from local to global scales: Direct versus ecologically mediated effects. *Perspect. Phycol.* **2**: 11–30. doi:10.1127/pip/2015/0019
- Wahl, M., V. Saderne, and Y. Sawall. 2016. How good are we at assessing the impact of ocean acidification in coastal systems? Limitations, omissions and strengths of commonly used experimental approaches with special emphasis on the neglected role of fluctuations. *Mar. Freshw. Res.* **67**: 25–36. doi:10.1071/MF14154
- Waldbusser, G. G., and J. E. Salisbury. 2014. Ocean acidification in the coastal zone from an organism's perspective: Multiple system parameters, frequency domains, and habitats. *Annu. Rev. Mar. Sci.* **6**: 221–247. doi:10.1146/annurev-marine-121211-172238
- Wernberg, T., D. A. Smale, F. Tuya, M. S. Thomsen, T. J. Langlois, T. de Bettignies, S. Bennett, and C. S. Rousseaux. 2013. An extreme climatic event alters marine ecosystem structure in a global biodiversity hotspot. *Nat. Clim. Chang.* **3**: 78–82. doi:10.1038/nclimate1627

- Werner, F. J., and B. Matthiessen. 2013. Temperature indirectly affects benthic microalgal diversity by altering effects of top-down but not bottom-up control. *Oikos* **122**: 52–63. doi:10.1111/j.1600-0706.2012.19952.x
- Werner, F. J., A. Graiff, and B. Matthiessen. 2016a. Even moderate nutrient enrichment negatively adds up to global climate change effects on a habitat-forming seaweed system. *Limnol. Oceanogr.* **61**: 1891–1899. doi:10.1002/lno.10342
- Werner, F. J., A. Graiff, and B. Matthiessen. 2016b. Temperature effects on seaweed-sustaining top-down control vary with season. *Oecologia* **180**: 889–901. doi:10.1007/s00442-015-3489-x
- Wikstrom, S. A., and L. Kautsky. 2007. Structure and diversity of invertebrate communities in the presence and absence of canopy-forming *Fucus vesiculosus* in the Baltic sea. *Estuar. Coast. Shelf Sci.* **72**: 168–176. doi:10.1016/j.ecss.2006.10.009
- Wootton, J. T., C. A. Pfister, and J. D. Forester. 2008. Dynamic patterns and ecological impacts of declining ocean pH in a high-resolution multi-year dataset. *Proc. Natl. Acad. Sci. USA* **105**: 18848–18853. doi:10.1073/pnas.0810079105
- Yin, Y., J. Huang, M. L. Paine, V. N. Reinhold, and N. D. Chasteen. 2005. Structural characterization of the major extrapallial fluid protein of the mollusc *Mytilus edulis*: Implications for functions. *Biochemistry* **44**: 10720–10731. doi:10.1021/bi0505565

Acknowledgments

We wish to thank Björn Buchholz for technical support with the experimental set-up in the lab, Philipp Gremler for laboratory assistance and Jörn Thomsen for helpful advice in calcification issues. JDM received funding from the EU BONUS project PINBAL through Grant No. 03F0689A. Highly constructive comments and advice by two reviewers have substantially improved an earlier version of this article. We much appreciate this.

Conflict of Interest

None declared.

Submitted 05 December 2016

Revised 11 April 2017

Accepted 15 May 2017

Associate editor: Núria Marbà